Cop 1

ANALYSIS OF ION CYCLOTRON RESONANCE

by

MICHAEL THOMAS RIGGIN

B.Sc., University of Waterloo, 1969.
M.Sc., University of Waterloo, 1970.

A THESIS SUBMITTED IN PARTIAL FULFILMENT
OF THE REQUIREMENTS FOR THE DEGREE
OF DOCTOR OF PHILOSOPHY
IN THE DEPARTMENT OF PHYSICS

We accept this thesis as conforming
to the required standard

THE UNIVERSITY OF BRITISH COLUMBIA

MARCH, 1974

In presenting this thesis in partial fulfilment of the requirements for an advanced degree at the University of British Columbia, I agree that the Library shall make it freely available for reference and study. I further agree that permission for extensive copying of this thesis for scholarly purposes may be granted by the Head of my Department or by his representatives. It is understood that copying or publication of this thesis for financial gain shall not be allowed without my written permission.

Department of Physics

The University of British Columbia
Vancouver 8, Canada

Date May 3, 1974

Abstract

An analysis of the most commonly used type of Ion Cyclotron Resonance (ICR) spectrometer is given. Though the equations of motion of an isolated ion in the ICR geometry are extremely non-linear, it was found possible to decouple the longtitudinal oscillations due to the trapping potential from the cyclotron motion by exploiting the fact that the cyclotron frequency is very much greater than the trapping frequency. A previously unsuspected dependence of the cyclotron frequency and drift velocity of an ion on its spatial coordinates was discovered and experimentally investigated. The distribution of energies for ions at resonance with an applied r-f electric field is also discussed and improved techniques for the study of energy dependent cross-sections are proposed. Conventional ICR techniques were used to estimate collision frequencies of sodium and potassium ions in helium and argon gases. These experiments yield information about the d.c. drift mobility, in the zero field limit, of the alkali ions in inert gases and are discussed in terms of various models of the ion-atom interaction potential. A crossed beam arrangement was used to obtain preliminary estimates of low energy rate constants for both asymmetric and symmetric resonant charge transfer between alkali ion-atom pairs.

TABLE OF CONTENTS

Section		Page
	Preface	v
	Acknowledgements	vi
	List of Figures	vii
	List of Tables	xi
1.	Introduction	1
2.	Potentials and Fields in the ICR Cell, and Equations of Motion for an Isolated Ion.	8
3.	General Method of Solving the Equations of Motion and Finding the Quasi-Cyclotron Frequency	20
4.	Simple Expressions for x(t), y(t) and the Drift Velocity	31
5.	The Trap Oscillations	38
6.	Another Way to Express the Results	40
7.	Influence of the Trap Oscillations	42
8.	The ICR Line Shape	56
9.	Influence of the Cell Potentials on the Spatial Distribution of the Ions	64
10.	Ad Hoc. 'Average Ion Model' for Studying the Spatial Distribution of Ions in an ICR Cell	68
11.	Distribution of Ion Kinetic Energies in an ICR Cell	80
12.	Experimental Apparatus: Ionisation by Electron Bombardment	92
13.	Effect of the Electron Beam on ICR	97

Section Table of Contents (Continued) Page

Section	Title	Page
14.	Control of the Ions' Position in the Ioniser	111
15.	Determination of the Initial Distribution of Energies in the ICR System	123
16.	Experimental Apparatus: Surface Ionisation	134
17.	Non-Reactive Collisions: Discussion of Collision Frequencies and Ionic Energy Distribution Functions	147
18.	Discussion of Ion-Atom Interaction	170
19.	A Crossed Beam Experiment	177
20.	Summary	214
Appendix 1	Drift Between Different Regions of an ICR Cell	216
Appendix 2	Effect of Magnetic Field Modulation on ICR	220
Appendix 3	Bi-Particle Collisions	226
Appendix 4	Moments of Energy Distribution Function	238
Appendix 5	The Relative Velocity Distribution Function	240
	References	245
	Glossary of Symbols	249

PREFACE

Portions of this thesis are identical in content to manuscripts which have been accepted for publication in the Canadian Journal of Physics. These papers are entitled:

'Analysis of Ion Cyclotron Resonance': by T.F. Knott and M. Riggin.

'Theory of Ion Cyclotron Resonance': by M. Bloom and M. Riggin.

'Dependence of ICR on Electrostatic Potentials': by M. Riggin and I.B. Woods

Two sections (17 and 18) of the thesis have been submitted for publication under the title:

'ICR Collision Frequencies of Alkali Ions in Rare Gases': by M. Riggin.

The MKS system is used throughout this thesis except for quantities that are traditionally expressed in different units. Traditional symbols are used for most quantities, and this leads to some duplication. To avoid confusion a glossary of symbols is included at the end of the thesis.

ACKNOWLEDGEMENTS

The author is pleased to acknowledge the guidance of Myer Bloom who supervised this work. His infectious good nature made working in his lab a pleasure. The very capable tutoring of Tom Knott and Eric Enga was also of considerable benefit to the author. D.Ll.Williams was more than generous in sharing magnet facilities.

LIST OF FIGURES

Figure		Page
1.	A Schematic Diagram of the ICR Cell	3
2.	Electric Field; E_y (y,o) - E_y (o, o)	12
3.	Electric Field; E_y (o, z) - E_y (o, o)	14
4.	Electric Field; E_z (o, z)	16
5.	Contours of Constant Effective Magnetic Field	29
6.	Contours of Constant Drift Velocity	36
7.	A Plot of the Instantaneous Quasi-Cyclotron Frequency as a Function of Z(t)	44
8.	A Plot of the Quasi-Cyclotron Frequency as a Function of the Trapping Oscillation Amplitude	53
9.	A Plot of the Drift Velocity as a Function of the Trapping Oscillation Amplitude	55
10.	The r-f Electric Field as a Function of the Trapping Oscillation Amplitude	59
11.	The Low Pressure ICR Line Shape	63
12.	The Amplitude Averaged Potential	71
13.	Position Dependence of the Amplitude Averaged Electric Field Gradient	74
14.	Position Dependence of the Amplitude Averaged Electric Field	77
15.	Distribution of Energy of the Cyclotron Motion at Low Pressures	85
16.	Distribution of Energy of the Trapping Oscillation	90
17.	The Electron Beam Filament	95

Figure	List of Figures (Continued)	Page

18. The Dependence of Magnetic Field at Maximum Absorption on V_1-V_2 and the Electron Beam Current 99

19. The Dependence of the Magnetic Field at Maximum Absorption on V_T and the Electron Beam Current 101

20. The Dependence of the Line Width on V_1-V_2 107

21. Dependence of the Line Width on V_T [illegible] 109

22. The Dependence of the Magnetic Field at Maximum Absorption on V_1-V_2 in the Source Region of the Cell 114

23. The Effect of the Source Trapping Potential on the Line Width 117

24. The Variation of the Average Ion Position in the Analyser with the Source Trapping Potential 119

25. The Dependence of the Line Width on V_1+V_2 in the Source Region 121

26. Energy Distribution of Particles Formed by Molecular Dissociation 129

27. The Fraction of Ions Collected by the Trap 132

28. The Primary Alkali Oven and Its Mount 137

29. A Side View of the Alkali Oven and the ICR Cell 139

30. The Dependence of the Line Width on the Potential of the Surface Ioniser 142

31. A Comparison of $^{39}K^+$ and $^{40}Ar^+$ Resonances 146

32. A Pressure Broadened ICR Line 151

33. The ICR Collision Frequency of K^+ and Na^+ Ions as a Function of Helium Gas Pressure 153

Figure List of Figures (Continued) Page

34. The ICR Collision Frequency of K^+ and Na^+ Ions as a Function of Argon Gas Pressure 155

35. The Relative Intensity of the $^{39}K^+$ Signal as a Function of Argon Pressure 158

36. The Effect of Collisions on the Energy Distribution of the Cyclotron Motion 162

37. The Fractional Energy Spread of the Cyclotron Motion as a Function of Neutral Particle Pressure 165

38. The ICR Collision Frequency of Na^+ in Argon as a Function of the Ions' Average Energy 169

39. The Secondary Alkali Oven 178

40. A Fit of Theory and Experiment of a Collision Broadened $^{39}K^+$ Resonance 186

41. The Collision Frequencies of $^{41}K^+$ and $^{39}K^+$ Ions in Potassium Metal Vapour 188

42. The Collision Frequency of $^{23}Na^+$ in Potassium Metal Vapour 191

43. The Area Under the $^{23}Na^+$ Resonance as a Function of the Vapour Pressure Inside the Secondary Oven 194

44. Area of the $^{41}K^+$ Resonance as a Function of the Vapour Pressure Inside the Secondary Oven 201

45. Velocity Dependence for Charge Exchange Between $^{39}K^+$ and ^{39}K 206

46. Dependence of Double Resonance of $^{39}K^+$ and $^{41}K^+$ on Secondary Oscillator Frequency 209

47. The Double Resonance Signal as a Function of Magnetic Field 212

Figure | List of Figures (Continued) | Page

A2.1 The Effect of Magnetic Field Modulation Amplitude on the Apparent Line Width of the ICR Line 223
A2.2 The Effect of Magnetic Field Modulation Amplitude on the ICR Signal Intensity 225
A3.1 A Collision in Velocity Space 229
A3.2 The One Body Equivalent of a Bi-Particle Collision 237
A5.1 The Relative Velocity Vector 242

LIST OF TABLES

Table Page

1. Coefficients in the Power Series Expansion of the Electric Field, E (y, z) 18
2. Hierarchy of Frequencies in the ICR Spectrometer 46
3. Comparison of Experimental and Theoretical D.C. Drift Mobilities 174
4. D.C. Drift Mobilities of Alkali Ions in Rare Gases 176

1. Introduction

Ion Cyclotron Resonance spectroscopy (ICR) is a well established technique for the study of ion-neutral collisions [Wobscall et al., 1963] and other gas phase phenomena which require the retention of charged particles in a well defined region for relatively long periods of time. Briefly, the principle of ICR may be explained as follows. Ions, of mass m and charge q, orbit near a frequency $\omega_c = q/m\ B$ about a static magnetic field B. When an oscillating electric field with frequency near ω_c is applied in the plane of the cyclotron oscillation the ions absorb energy from the electric field. This resonant absorption of energy may be detected directly using techniques similar to those used in Nuclear Magnetic Resonance [Abragam, 1960].

A typical ICR apparatus [Baldeschwieler, 1968; Beauchamp, 1967] is shown in Fig. 1, together with the coordinate system (Insert Fig. 1) which we will adopt for this thesis. Ions, normally produced by electron bombardment of an ambient gas, are extracted from the region in which they are produced (the source region) by perpendicular electric and magnetic fields. The magnetic field is applied in the -z direction and an electric field, in the -y direction, results from potentials V_1 and V_2 applied to the upper and lower plates of the cell (Fig. 1) respectively. Since the ions' motion is unconstrained in the direction of the magnetic field, they must be trapped between two suitably biased electrodes (a positive bias V_T to trap positive ions, negative V_T for negative ions) oriented in the x-y plane. After production in the source region the ions drift in the x-direction under the combined influence of the static and magnetic fields into the analyser or resonance region where they are detected via a change in level of oscillation

Fig. 1: A schematic diagram of the ICR spectrometer. The insert in the right hand corner shows the co-ordinate system and the dimensions used in the text.

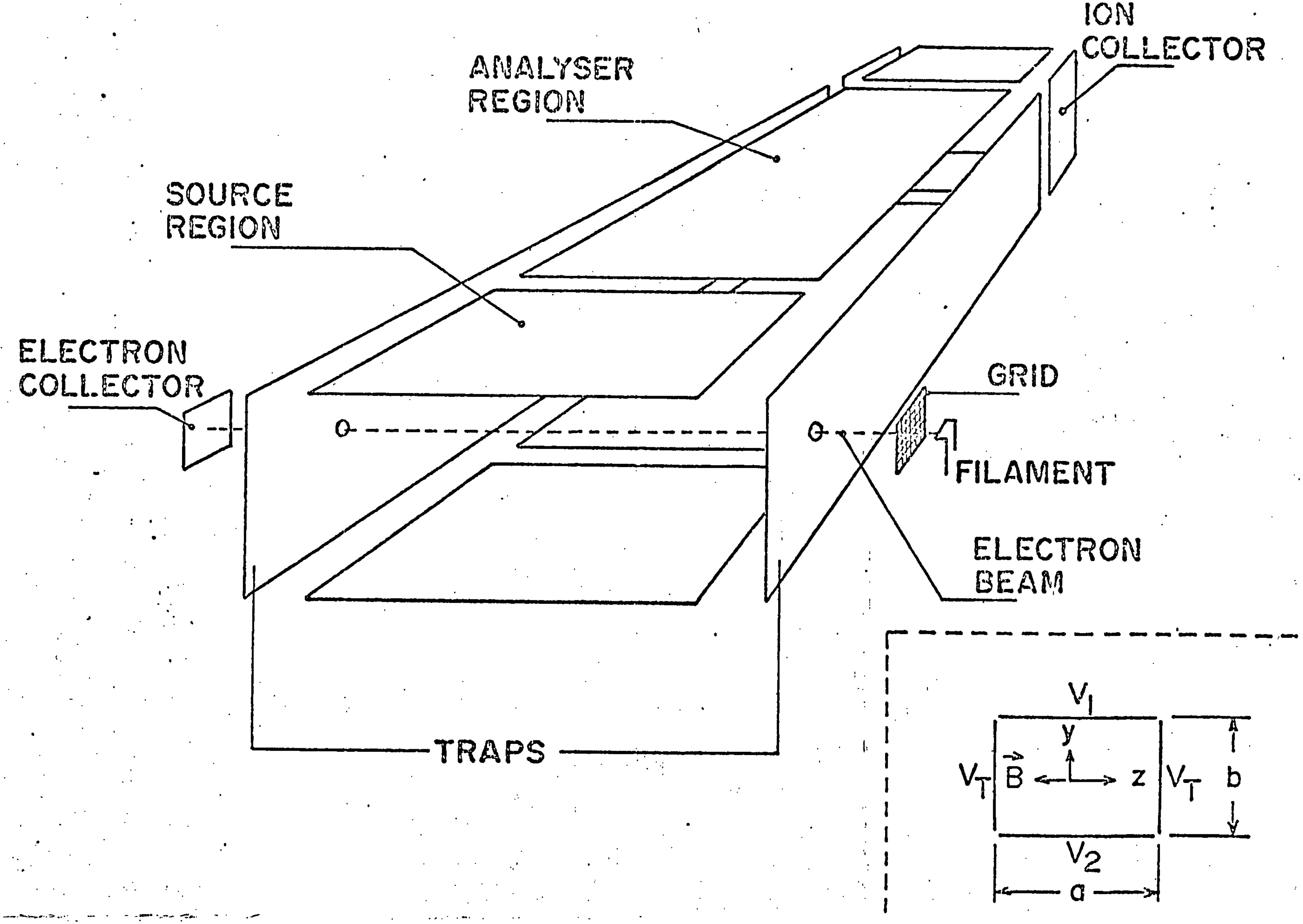
ION COLLECTOR
ANALYSER REGION
SOURCE REGION
ELECTRON COLLECTOR
GRID
FILAMENT
ELECTRON BEAM
TRAPS
V_1
y
V_T
$\vec{B}$
z
V_T
b
V_2
a

of an oscillator used to generate the electric field with which the ions are brought to resonance [Robinson, 1959]. Hence there are three motions of the ions, a rapid cyclotron oscillation in the x-y plane, a net drift with speed $|(\underline{E}\times\underline{B})|/B^2$ in the x direction and periodic oscillation in the potential well formed by the traps.

The ICR device then is a type of radio-frequency mass spectrometer of fairly good mass resolution at low pressures and sufficient sensitivity to detect 1 to 10 ions per cubic centimeter [Beauchamp, 1970]. When operated in a "trapping" mode, by placing electrodes at the ends of the drift regions of the cell [McIver, 1970], ions may be retained in the cell for several seconds. This feature, combined with the good sensitivity of ICR, allows measurements of cross sections for photodissociation of positive molecular ions [Dunbar, 1971], as well as for photodetachment of electrons from negative ions [Smyth and Brauman, 1972]. Of course, the ICR spectrometer may be used for more conventional types of mass spectrometry such as the determination of relative abundances of ionic species from electron ionisation of gases and relative yields of products from ion-molecule reactions. These attractive features of this device are enhanced by its ability to selectively accelerate different ionic species to greater than thermal energies. Thus it is possible to do double resonance experiments by monitoring the change in the ICR signal of one ion, say C^+, which results from excitation to non-equilibrium velocities of a different ion A^+. This type of experiment can be used, in principle, to measure the rate constants, k of reactions,

$$[1.1] \qquad A^+ + B \xrightarrow{k} C^+ + D$$

as a function of energy since the average energy of A^+ can be calculated in terms of the strength of the electric field applied at resonance with the cyclotron frequency of A^+ and the time duration for which this field is applied. In a given gaseous system a particular ion C^+ may have several different precursor ions such as A^+ so that monitoring the ICR signal strength of C^+ and sweeping a probing oscillator over a wide range of frequencies will reveal all of the parent ions of C^+ through a change in its population. This type of experiment may reveal the reaction channels in very complex ion-molecule systems.

The ICR method is potentially useful at ion energies sufficiently low ($\lesssim$tens of ev.) that the ions are contained in a cell of reasonable size (several cm.) at standard laboratory magnetic fields. The ICR apparatus is cheaper, more compact and easier to operate than other standard techniques such as merged beams, etc. used in this energy range. However, these advantages are offset by the fact that there are several general aspects of the operation of ICR devices that have not been fully investigated. For example, instrumental artifacts have hampered kinetic studies of ion molecules and charge transfer reactions at the low energies accessible to ICR. Loss of ions from the cell [Goode et al., 1970], ill-defined drift velocities [Smith and Futrell, 1973] and inhomogeneous electric fields [Huntress et al., 1971] are a few of the problems encountered. To overcome these problems, transient ICR experiments [Dunbar, 1971; Huntress, 1971], pulsed techniques for drift time measurement, [Smith and Futrell, 1973] and different ICR geometries [Clow and Futrell, 1971] have been developed. It seems to this author that these experimental attempts at improvement of the ICR device can benefit from a detailed analysis of the ion motion in the ICR field configuration.

In this thesis we wish to discuss as explicitly as possible the complicated features of the ICR experiment and to present an approximate analysis of some of the important properties of the ICR spectrometer. The analysis is based heavily on a well defined treatment of the non-linear equations of motion of an ion which are solved using an expansion of the cell potential to the fourth order in the y coordinate. Previous treatments of the equations of motion have included terms to y^2, at most, in which case the equations are linear and the cyclotron and trapping motions are rigorously decoupled. This is untrue when y^4 terms are considered. However, we will establish a procedure for obtaining approximate decoupled equations of motion which, though non-linear, may be solved in terms of Weierstrass elliptic functions. From this analysis it is found that both the frequency at which the ions orbit the magnetic field and the drift velocity are dependent on the ions' spatial coordinates. Using the analysis outlined in Sections 2 to 6 of this thesis we construct, in Sections 7 to 10, an ensemble appropriate to the mechanism of ion production and to the potential configuration of the ICR cell. Various predictions of our model of the ionic motions are experimentally investigated in Sections 12 to 16.

In non-resonant techniques of studying ion-neutral reactions energy selection is obtained by allowing the ions to pass across a well defined potential difference, in which case the final energy distribution is independent of the initial state. In Section 11 we find from an explicit energy distribution that this is not true when ions are prepared by cyclotron heating in the ICR geometry.

Various experimental techniques for improving the energy resolution are proposed in this thesis, but are in a preliminary stage of development.

Nevertheless we are able to report preliminary estimates of charge transfer rate constants for near thermal collisions of potassium and sodium ions with potassium atoms. Collision frequencies of potassium and sodium ions with helium and argon gases are also reported.

2. Potentials and Fields in the ICR Cell, and Equations of Motion for an Isolated Ion.

Ordinary methods of solving Laplace's equation in rectangular coordinates (Churchill, 1941, p. 114) give the two-dimensional potential inside the ICR cell shown in Fig. 1:

$$[2.1] \quad V(y,z) = V_T - \frac{2}{\pi} \sum_{k=o}^{\infty} \frac{(-)^k}{2k+1} \left\{ [2V_T - (V_1+V_2)] \frac{\cosh[(2k+1)(\pi y/a)]}{\cosh[(2k+1)(\pi b/2a)]} - (V_1-V_2) \frac{\sinh[(2k+1)(\pi y/a)]}{\sinh[(2k+1)(\pi b/2a)]} \right\} \cos[(2k+1)(\pi z/a)]$$

The electric field is easily obtained from $\underline{E} = -\nabla V$.

A power series expansion is the most useful form for $\underline{E}=(0,E_y,E_z)$ in the equations of motion. Written in this way, $E_y(y,z)$ is

$$[2.2] \quad E_y(y,z) = \sum_{m,n=o}^{\infty} e_{m,n}\, y^m z^{2n}$$

where

$$[2.3] \quad \begin{aligned} e_{m,n}(\text{m even}) &= 4\,\frac{(-)^{n+1}\,(V_d/a)}{m!\,(2n)!} \sum_k \frac{(-)^k[(2k+1)(\pi/a)]^{m+2n}}{\sinh[(2k+1)(\pi b/2a)]} \\ e_{m,n}(\text{m odd}) &= 4\,\frac{(-)^{n+1}(V_t/a)}{m!\,(2n)!} \sum_k \frac{(-)^k[(2k+1)(\pi/a)]^{m+2n}}{\cosh[(2k+1)(\pi b/2a)]} \end{aligned}$$

We have written $V_t = V_T - (V_1+V_2)/2$ and $V_d = (V_1-V_2)/2$ for the two combinations of the applied potentials that appear in eq. [2.1].

Using $\nabla \cdot \underline{E} = 0$ it is simple to show that

$$[2.4] \qquad E_z(y,z) = - \sum_{m,n=0}^{\infty} \frac{(m+1)}{(2n+1)} e_{m+1,n} y^m z^{2n+1}$$

A useful recursion relation for the coefficients follows from $\nabla x \underline{E} = 0$ (or directly from eqs. [2.3]):

$$[2.5] \qquad e_{m+2,n-1} = - \frac{2n(2n-1)}{(m+2)(m+1)} e_{m,n}.$$

With this, we can express all the $e_{m,n}$ in terms of $e_{m,o}$.

Finally, the potential can be written as a power series using the coefficients $e_{m,n}$:

$$[2.6] \qquad V(y,z) = V_C - \sum_{m,n=0}^{\infty} (\frac{1}{m+1}) e_{m,n} y^{m+1} z^{2n}$$

where V_c is the potential at the centre of the cell

$$[2.7] \qquad V_c = V_T - (4/\pi) V_t \sum_{k=0}^{\infty} [\frac{(-)^k}{(2k+1) \cosh [(2k+1)(\pi b/2a)]}.]$$

It is interesting to compare the electric field calculated from the first few terms of eqs. [2.2] and [2.4] with that given by Beauchamp and Armstrong (1968) for the cell geometry in Fig. 1. They would say that

$$[2.8] \qquad \begin{aligned} E_y &= - (2V_d/b) + 4V_T(y/a^2) \\ E_z &= - 4 V_T (z/a^2) \end{aligned}$$

This form is not really correct for a rectangular cell, but is more acceptable than the choice of McMahon and Beauchamp (1971), which does not satisfy Maxwell's equations. The results of both calculations are shown in Figs. 2, 3 and 4 for three cases of interest. The cell dimensions are a = 0.025 m, b = 0.014 m, and the applied potentials V_t = 0.5 volts, V_d = 0.5 volts, which are typical operating values in our experiments. (We will use these values in all numerical illustrations in this thesis.) Eqs. [2.8] do not give even the right qualitative z-dependence of E_y, which we will see is quite important in understanding the resonance condition in ICR cells. The difference between the correct $E_y(y,0)$ and $E_z(0,z)$, and eqs. [2.8] is also significant.

Values of this first six $e_{m,o}$ are shown in Table 1, for a variety of cell geometries. The first line gives the leading term in E_y from eqs. [2.8] for comparison--as one expects,it agrees well with the more complete calculation of $e_{o,o}$ for flat cells (b/a << 1).

Now that we have complete and useful expressions for the electric field inside an ICR cell, we can turn to the equations of motion for an isolated ion of mass m and charge q:

[2.9] $$\dot{\underline{p}} = q\ (\underline{E} + \underline{v} \times \underline{B})$$

$\underline{B}$ is a homogeneous magnetic field pointing in the negative z-direction, so that this becomes

[2.10] $$\ddot{x} = -\omega_c \dot{y}$$

[2.11] $$\ddot{y} = \omega_c \dot{x} + \kappa E_y(y,z)$$

[2.12] $$\ddot{z} = \kappa E_z(y,z)$$

Fig. 2: $E_y(y,0) - E_y(0,0)$ calculated from the first three terms in the power series for E_y (solid curve). For this and all other illustrative calculations, we take a = 0.025 m, b = 0.014 m and $V_t = V_d = 0.5$ volt. The dashed curve is the field used by Beauchamp and Armstrong (1968). The solid curve agrees well with fields calculated from eq. [2.1] to twenty-five terms over the region of the cell shown in the diagram.

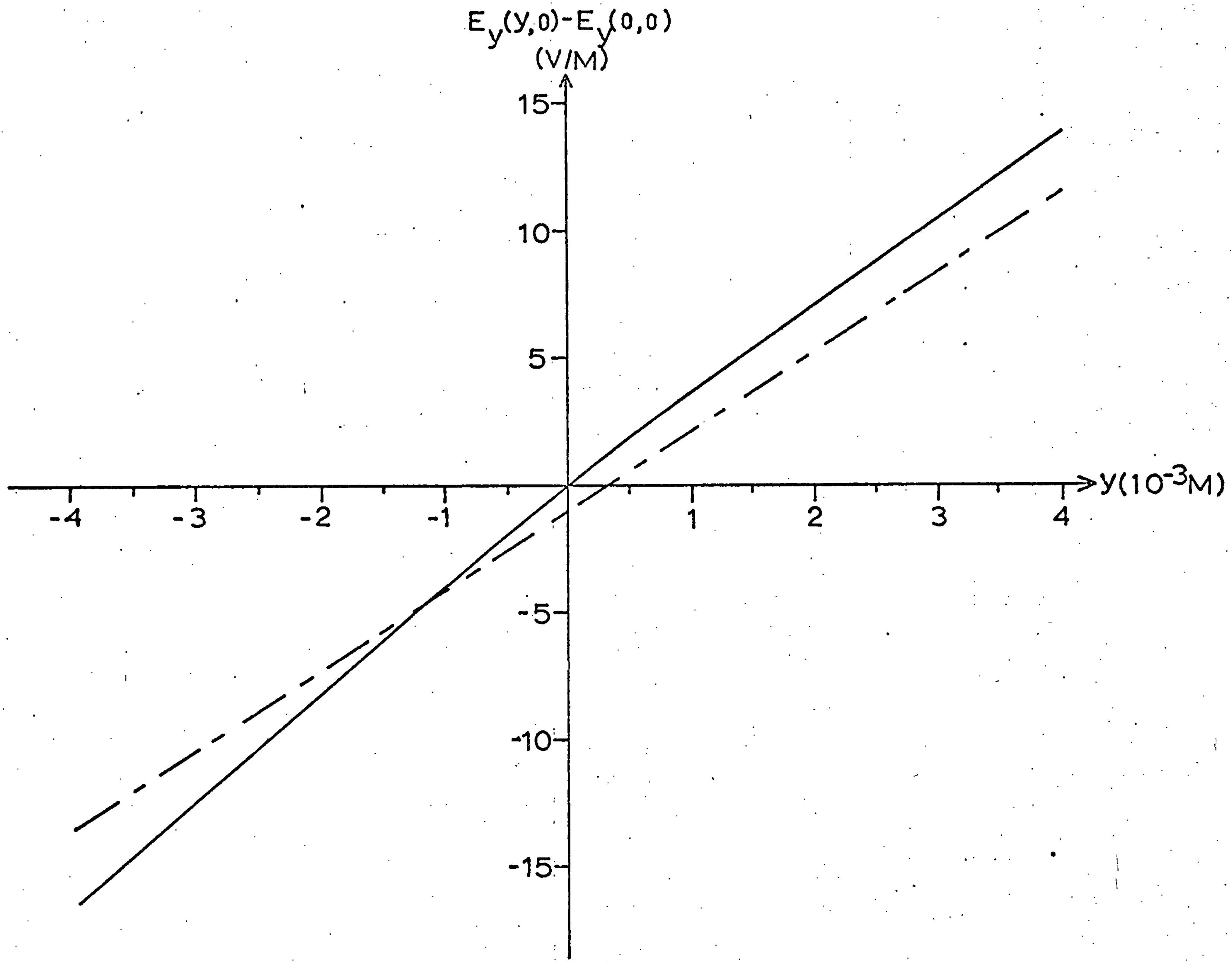
$E_y(y,0)-E_y(0,0)$
(V/M)
15
10
5
-5
-10
-15
-4
-3
-2
-1
1
2
3
4
$y(10^{-3}M)$

Fig. 3: $E_y(0,z) - E_y(0,0)$ calculated and compared as in Fig. 2.

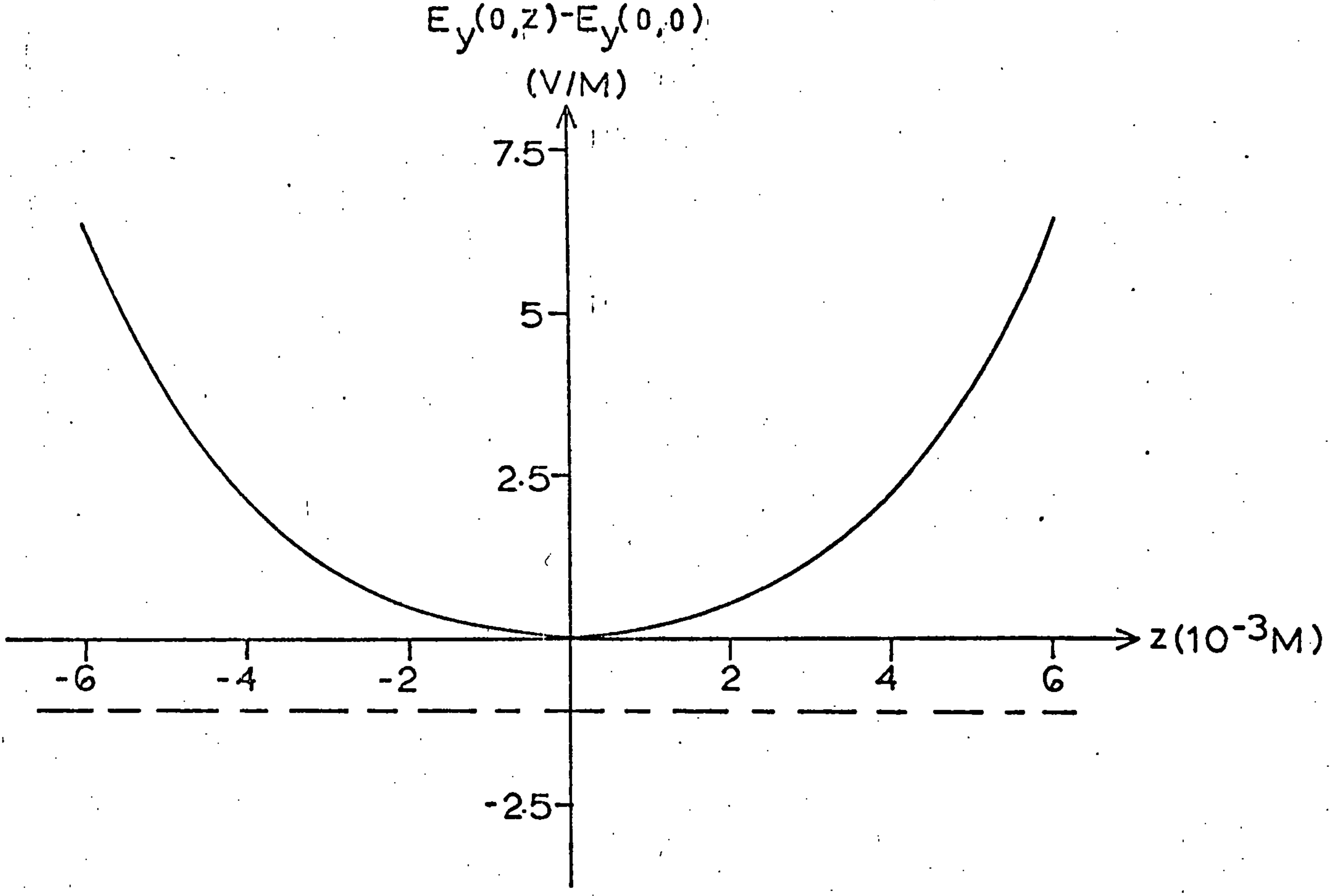
$E_y(0,z)-E_y(0,0)$
(V/M)
7.5
5
2.5
-2.5
$z(10^{-3}M)$
-6
-4
-2
2
4
6

Fig. 4: $E_z(0,z)$, calculated and compared as in Fig. 2.

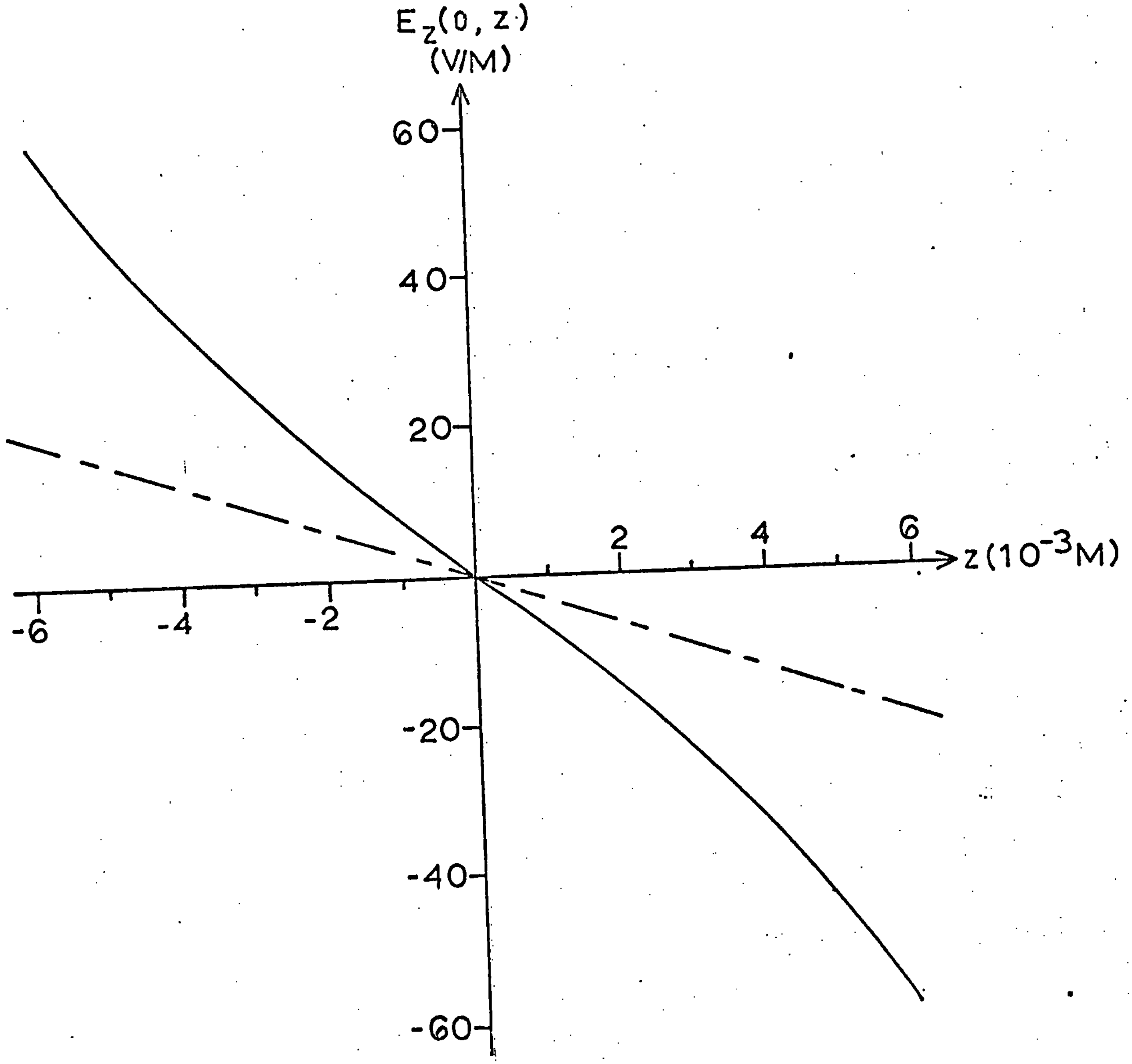
$E_z(0, z)$
(V/M)
60
40
20
-20
-40
-60
-6
-4
-2
2
4
6
$z(10^{-3}M)$

Table 1: Values of the coefficients $e_{m,o}$ in the power series expansion of $E_y(y,z)$ for a variety of cell geometries, expressed in dimensionless form, $(e_{mo}a^m/V)$. The illustrative calculations in this paper are based on $b/a = 0.56$. The recursion relation, eq. [2.5] can be used to generate other low-order $e_{m,n}$. For comparison, we include "parallel-plate capacitor" values for $2a/(V_d b)$ in the first line of the table.

TABLE 1

	$b/a = 0.1$	0.25	0.56	1	2
$2a/(bV_d)$	-20.0	-8.0	-3.57	-2.0	-1.0
$(e_{00}/V_d)a$	-20.0	-8.00	-3.52	-1.67	-0.35
$(e_{10}/V_t)a^2$	$+4.88\text{x}10^{-4}$	+0.75	+4.78	+4.38	+1.08
$(e_{20}/V_d)a^3$	$-2.36\text{x}10^{-3}$	-0.035	-3.24	-5.74	-1.68
$(e_{30}/V_t)a^4$	-0.049	-19.8	-22.87	0	+1.69
$(e_{40}/V_d)a^5$	-0.650	+1.85	+32.55	+9.86	-1.197
$(e_{50}/V_t)a^6$	+15.55	+155.9	+5.915	-20.69	-0.489

where we have abbreviated

$$[2.13]\qquad \begin{aligned} \omega_c &= q\,B/m \\ \kappa &= q/m \end{aligned}$$

for convenience. Eqs. [2.10] and [2.11] are combined by integration to give

$$[2.14]\qquad \ddot{y} + \omega_c^2\, y = \omega_c(\dot{x}_o + \omega_c\, y_o) + \kappa\, E_y(y,z)$$

The ion is initially at (x_o, y_o, z_o) where it has velocity $(\dot{x}_o, \dot{y}_o, \dot{z}_o)$.

These equations describe three types of superimposed motion, which are coupled by the complicated y and z dependence of $\underline{E}$:

1) A drift in the positive x-direction due to $\underline{B}$ and the non-zero average value of E_y.
2) Oscillation in the z-direction described by eq. [2.12] (trap oscillation)
3) Quasi-cyclotron motion about the drifting centre in the x-y plane (described by eqs. [2.14] and [2.10]).

The last of these is especially interesting because the frequency of this motion is detected in ICR experiments. The drift motion is also important, as it is involved in line-width computation, and in most rate constant measurements. The next job is to investigate the coupling of these motions, and simplify the equations so that we can solve them in closed (but approximate) form.

3. General Method of Solving the Equations of Motion and Finding the Quasi-cyclotron Frequency.

The really troublesome feature of the equations of motion for y and z (eqs. [2.14], [2.12]) is their coupling through $\underline{E}$ (y,z). If we keep only the leading term in E_z, however, the trap oscillation is harmonic, with frequency $\omega_T \cong (\kappa\, e_{10})^{\frac{1}{2}}$, while the frequency of the quasi-cyclotron oscillation is approximately ω_c. An ion with a mass of 40 amu has $\omega_T \sim 10^5$ sec^{-1}, while $\omega_c \sim 2 \times 10^6$ sec^{-1}, so that $\omega_T << \omega_c$. This means that the ion does not move very much in the trap (z-direction) while it goes through a complete period of its quasi-cyclotron motion in a plane perpendicular to $\underline{B}$. The electric field in which this high frequency motion takes place can therefore be parameterised by z, the trap coordinate, while the trapping field can be averaged (at each value of z) over the rapidly varying y-coordinate of the ion.

So, we can effectively uncouple the equations of motion given in the last section. Eq. [2.14] becomes, with the help of eq. [2.2] for $E_y(y,z)$,

$$[3.1] \qquad \ddot{y} + \omega_c^2 y = \omega_c(\dot{x}_o + \omega_c y_o) + \kappa \sum_{m=0}^{\infty} (m+1)\, e_m y^m$$

where

$$[3.2] \qquad e_m \doteq \left(\frac{1}{m+1}\right) \sum_{n=0}^{\infty} e_{mn}\, z^{2n}$$

The trap motion is described by

$$[3.3] \qquad \ddot{z} + 2\kappa \sum_{n=0}^{\infty} (n+1)\, t_n\, z^{2n+1} = 0$$

$$[3.4] \qquad t_n = \frac{1}{(2n+1)(2n+2)} \sum_{m=0}^{\infty} (m+1)\, e_{m+1,n} < y^m > .$$

The average, $< y^m >$, has to be calculated at each value of the trap coordinate, so that the t_n are functions of z.

Let us begin by solving eq. [3.1] for y(t). This is still an unpleasant-looking equation, since it contains terms which are not linear in the dependent variable. The anharmonic terms cannot be ignored, in general, because they may produce an amplitude and initial-position dependent frequency shift. Fortunately there is a general-- although little-known-- theory for the solution of equations with at most a cubic term in y.

The first step in finding the solution to eq. [3.1] is integration by the substitution $\ddot{y} = \dot{y}\,(d\dot{y}/dy)$ to get

$$[3.5] \qquad \dot{y}^2 = \dot{y}_o^2 + 2\omega_c (\dot{x}_o + \omega_c y_o)(y - y_o) - \omega_c^{\,2}(y^2 - y_o^2)$$

$$+ 2\kappa \sum_{m=0}^{\infty} e_m (y^{m+1} - y_o^{\,m+1})$$

Truncation of the series at m = 1 gives just the harmonic approximation used by Beauchamp and Armstrong (1968), although the form of the fields (and so the values of the coefficients) are different in their work.

It is possible to keep terms up to and including m = 3 if we are willing to have the solutions in terms of functions which are more complicated-looking and less familiar than the trigonometric functions used to solve the harmonic approximation. These are known as Weierstrass elliptic functions. Generally speaking, an elliptic function is any function of a single complex variable that is doubly periodic in that variable. It must be single-valued and analytic in the finite plane, except at poles (which are its only singularities). Just as a function for which $f(w + 2n\Omega) = f(w)$ (n an integer) is called singly periodic with half-period Ω, a doubly periodic function is one for which the relation $f(w + 2n\Omega + 2m\Omega') = f(w)$ holds for integer n and m. The double periodicity means that it is enough to know its behaviour inside a parallelogram in the complex plane. If this region has only a double pole at the origin, the elliptic function is called a Weierstrass elliptic function. Whittaker and Watson (1927) have an excellent discussion of elliptic functions (ch. XX), while Southard (1968) gives an extensive summary of their properties.

The solution of eq. [3.5] truncated at m = 3, as discussed by Whittaker and Watson (1927, p. 452f), is outlined below. Let $(ds/dw)^2=f(s)$ where f(s) is a quartic having no repeated factors;

$$f(s) = a_0s^4 + 4a_1s^3 + 6a_2s^2 + 4a_3s + a_4. \quad [3.6]$$

Then for $f(\alpha) = 0$,

$$[3.7] \qquad w = \int_{\alpha}^{s} d\xi\,[f(\xi)]^{-\frac{1}{2}}$$

may be inverted to express s as a function of w

$$[3.8] \qquad s = \alpha + \frac{1}{4} f'(\alpha)[\wp(w;\, g_2, g_3) - \frac{1}{24} f''(\alpha)]^{-1}$$

$\wp(w; g_2, g_3)$ is the Weierstrass elliptic function formed from the invariants of the quartic (eq. [3.6]):

$$[3.9] \qquad g_2 = 3a_2^{\,2} + a_o a_4 - 4a_1 a_3$$

$$[3.10] \qquad g_3 = -a_2^3 + 2a_1 a_2 a_3 + a_0 a_2 a_4 - a_0 a_3^{\,2} - a_1^2\, a_4.$$

The discriminant of the quartic

$$[3.11] \qquad \Delta = g_2^{\,3} - 27 g_3^{\,2}$$

turns out to be a useful guide to approximations for the solution and its real half-period, ω_2.

The direct integration of eq. [3.5] gives

$$[3.12] \qquad t = \int_{y_o}^{y} ds\,[f(s)]^{-\frac{1}{2}} ,$$

where f(s) is given by eq. [3.6] with

$$a_0 = 2\kappa e_3$$

$$a_1 = \kappa e_2/2$$

[3.13] $$a_2 = (-\omega_c^{\;2} + 2\kappa e_1)/6 \equiv -\omega_e^{\;2}/6$$

$$a_3 = [\kappa e_0 + \omega_c(\dot{x}_0 + \omega_c y_0)]/2$$

$$a_4 = \dot{y}_0^{\;2} - \omega_c^{\;2} y_0 - 2\,[\omega_c \dot{x}_0 y_0 + \kappa \sum_{m=0}^{3} e_m y_0^{\;m+1}]$$

We notice that $f(y_0) = \dot{y}_0^{\;2}$ ($\neq 0$ in general), so that eq. [3.12] must be rewritten

[3.14] $$t = {}_{\alpha}\!\int^{y} ds[f(s)]^{-\frac{1}{2}} - {}_{\alpha}\!\int^{y_0} ds[f(s)]^{-\frac{1}{2}}$$

with $f(\alpha) = 0$. The second integral is a constant which we call ϕ/ω, as it is related to the phase shift in the harmonic approximation.

Eq. [3.8] is the solution to the uncoupled, anharmonic approximation if we make the identification $w = t + \phi/\omega$ and use the invariants (g_2 and g_3) formed with the coefficients from eqs. [3.13]. The real half-period (ω_2) of the Weierstrass elliptic function is related to the angular frequency (ω) of the quasi-cyclotron motion by

[3.15] $$\omega = \pi/\omega_2.$$

In Southard (1969, p. 649) the invariants are expressed in terms of the real half-period and a complete elliptic integral of the first kind (we use μ for its modulus). If $\Delta < 0$ and $\mu << 1$, we find that

[3.16] $$g_2 = \frac{1}{12}\left(\frac{\pi}{\omega_2}\right)^4 (1 - 15\mu)$$

[3.17] $$g_3 = \frac{1}{216}\left(\frac{\pi}{\omega_2}\right)^6 \left(1 + \frac{63}{2}\mu\right)$$

and

[3.18] $$\Delta = -\frac{1}{16}\left(\frac{\pi}{\omega_2}\right)^{12} \mu$$

To find ω_2, which is the first goal, we have to express g_2, g_3 and Δ in terms of the coefficients of the quartic function. Using eqs. [3.9], [3.10] and [3.13], we have

[3.19] $$g_2 = \frac{1}{12}\omega_c^4 \left\{1 - 4\frac{\kappa}{\omega_c^2}[e_1 + 3e_2Y_o + 6e_3(Y_o^2 - R_o^2)]\right\}$$

[3.20] $$g_3 = \frac{1}{216}\omega_c^6 \left\{1 - 6\frac{\kappa}{\omega_c^2}[e_1 + 3e_2Y_o + 6e_3(Y_o^2 + 2R_o^2)]\right\}$$

and

[3.21] $$\Delta = \frac{1}{8}\kappa e_3(R_o/\omega_c)^2\omega_c^{12},$$

where

[3.22] $$Y_o = y_o + (\dot{x}_o/\omega_c)$$

and

[3.23] $$R_o = (\dot{x}_o^2 + \dot{y}_o^2)^{\frac{1}{2}}/\omega_c$$

R_o is the cyclotron radius of an ion in the magnetic field alone, where its frequency would be ω_c. We already know that $\omega_2 \gtrsim (\pi/\omega_c)$, so when the energy of the ion is expressed in electron volts and all other quantities in MKS units

[3.24] $$\mu = -(4/3)(e_3/\kappa^2B^4) \cdot (\text{K.E.})$$

For typical ions (mass = 40 amu, K.E. = (1/40) eV) in our ICR cell (with B = 0.78 tesla) we find that $\Delta < 0$, because $e_{30} < 0$. μ is small enough ($\sim 2 \times 10^{-7}$) that we can ignore it in the relations between the invariants and the real half period. Thus, from either eq. [3.19] or eq. [3.20], the frequency of the quasi-cyclotron motion is

[3.25] $$\omega = \omega_c[1 - (\kappa/\omega_c^2)(e_1 + 3e_2Y_o + 6e_3Y_o^2)]$$

The fractional error in the frequency shift, $\Delta\omega = \omega - \omega_c$, due to ignoring the term of order μ is less than 0.1% for the typical case considered above.

If $\Delta > 0$, which it will be for cells with $a < b$, a similar parameterisation in $\mu' = 4\mu^2$ leads to the same expression for the quasi-cyclotron frequency.

The frequency of the applied rf field in the analyser section of an ICR cell is usually fixed, for technical reasons, and the magnetic field varied instead. A lower resonance frequency at fixed field means a higher field at fixed frequency. Hence,

$$[3.26] \qquad \Delta B = (1/\omega_c)(e_1 + 3e_2Y_o + 6e_3Y_o{}^2)$$

is the change in resonance field for a given $\dot{x}_o$, y_o and z. Averaged over all (equally probable)values of $\dot{x}_o$, ΔB depends explicitly on the initial ion position (y_o) and implicitly on the trap coordinate (z) through eq. [3.2].

This result is quite different from the harmonic calculation, which gives ΔB independent of y_o and z. Ions are produced over an extended region of the ICR cell, usually along $y \sim 0$ for $(-a/2) \leq z \leq (a/2)$, and move toward the negative drift plate as they leave the negative space-charge region of the electron beam. In Fig. 5, we show contours of ΔB for isolated ions near the centre of the cell. It is obvious that there are large effects due to variation of y_o (for the analyser region) and z (the trap oscillation). The consequences of these are discussed in following sections.

The expression for ΔB is accurate as long as the last term in eq. [3.26] is small compared to the first, which means that

$$[3.27] \quad y_o << (e_{10}/3e_{30})^{\frac{1}{2}}$$

In our case, we are restricted to $y_o << 0.01$ m, approximately.

Fig. 5: Contours of ΔB = constant (units are 10^{-4} Tesla) in the (y_0,z) plane. The bold lines are given by the theory of section 3 (field expansion to 3rd order $y = 0$); the rest is from the theory of section 6, using terms up to $k = 25$ in eq. [2.1]. The cell parameters are the same as for Fig. 2; the ion mass is 40 amu, and $B = 0.780$ Tesla ($\omega_c = 1.867 \times 10^6$/sec.).

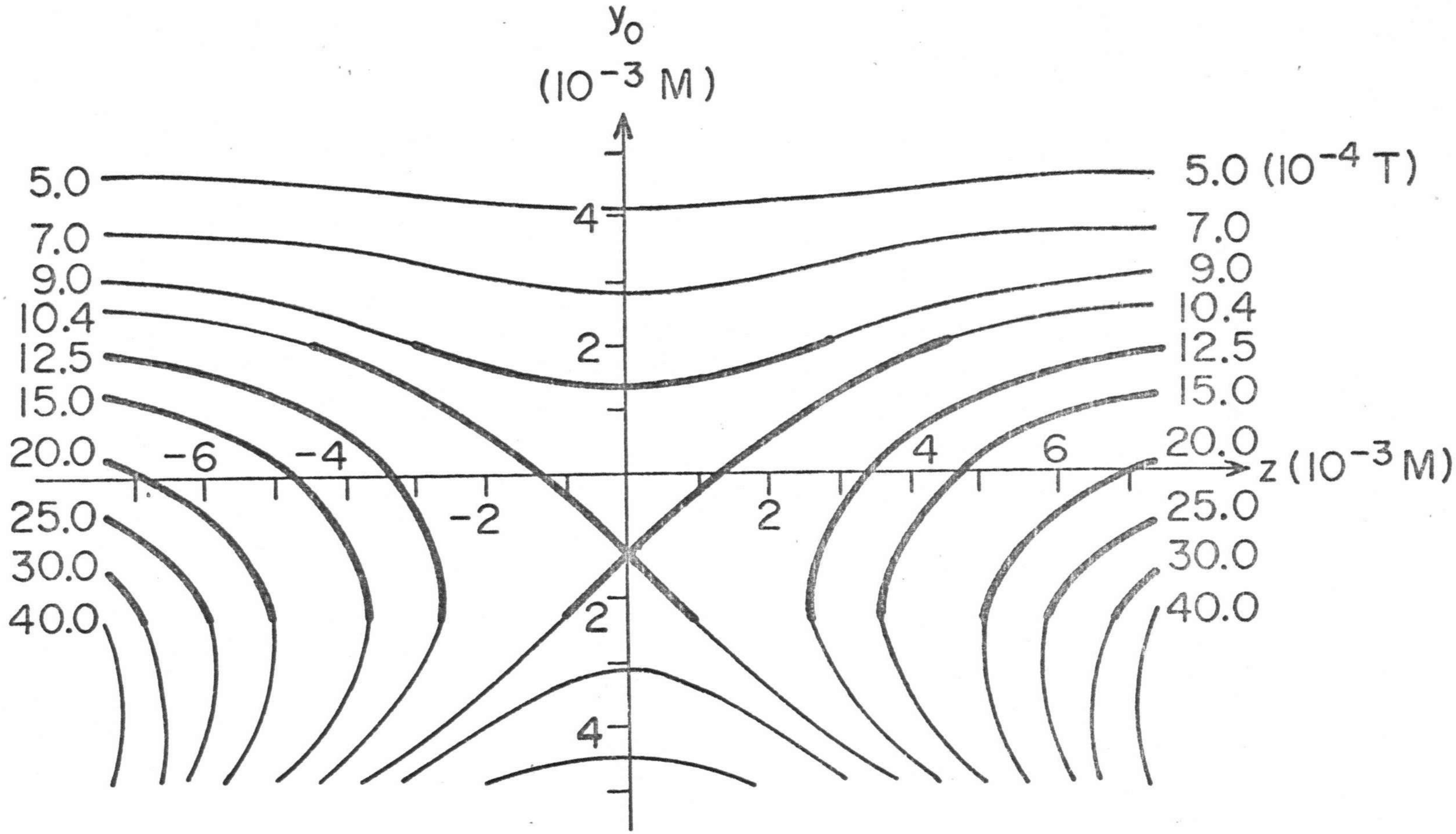

y_0
(10^{-3} M)
5.0
7.0
9.0
10.4
12.5
15.0
20.0
25.0
30.0
40.0
5.0 (10^{-4} T)
7.0
9.0
10.4
12.5
15.0
20.0
25.0
30.0
40.0
4
2
2
4
−6
−4
−2
2
4
6
z (10^{-3} M)

By using elliptic functions, we have solved the simplified equations of motion for the quasi-cyclotron frequency. This is possible because the y and z motions in an ICR cell have very different frequencies, which means that the more rapid component of motion in the complicated electric field can be considered as taking place at a constant value of the more slowly varying coordinate. As long as this is true, and the potential is well represented by a quartic in y, we have a trustworthy expression for the quasi-cyclotron frequency. In the next section, we tackle the problem of finding simple expressions for x(t) and y(t).

4. Simple Expressions for x(t), y(t) and the Drift Velocity.

We wish to find useful expressions for the quasi-cyclotron and drift motions of an ion in the ICR cell, for two reasons. The drift velocity is an important ingredient in line-width calculations, and a knowledge of the quasi-cyclotron motion figures into the averaging procedures used in the interpretation of resonance experiments. In the last section we saw that Weierstrass elliptic functions can be used to solve simplified equations of motion for the y-coordinate - but eq. [3.8] is not very useful for practical calculations.

Given the conditions under which we have solved for the quasi-cyclotron frequency, however, the motion in the x-y plane can be expressed in terms of trigonometric functions. The first step is to find the root of $f(y) = 0$ (given by eqs. [3.6] and [3.13]) near $y = y_o$. We find that

$$[4.1] \qquad \begin{aligned} f(y) = \dot{y}_o^{\,2} &+ 2\omega_c^{\,2} Y_o (y-y_o) - \omega_c^{\,2}(y^2-y_o^{\,2}) \\ &+ 2\kappa[e_o(y-y_o) + e_1(y^2-y_o^{\,2}) \\ &+ e_2(y^3-y_o^{\,3}) + e_3(y^4-y_o^{\,4})]. \end{aligned}$$

The root at $\alpha = y_o - \varepsilon$ is computed by setting the first three terms in the Taylor series expansion of f about y_o equal to zero: $f(y_o-\varepsilon) = 0$. Thus a bit of algebra yields

$$[4.2] \qquad \alpha = y_o - [f'(y_o) - f'(\alpha)]/\, f''(y_o)$$

with

[4.3] $f'(\alpha) = [(f'(y_o))^2 - 2f(y_o)\ f''(y_o)]^{\frac{1}{2}}$

Neglecting terms of order $(\Delta\omega/\omega_c) << 1$, we find that

[4.4] $f'(y_o) = 2\omega_c[\dot{x}_o + \kappa e_y(y_o)/\omega_c]$

[4.5] $f'(\alpha) = 2\omega_c\ \{[\dot{x}_o + \kappa e_y(y_o)/\omega_c]^2 + \dot{y}_o^{\ 2}\}^{\frac{1}{2}}$

and

[4.6] $f''(\alpha) = -\ 2\omega^2$

where we use the abbreviation

[4.7] $e_y(y_o) = e_o + 2e_1 y_o + 3e_2 y_o^2 + 4e_3 y_o^3$

for the y-component of the electric field calculated to third order in y_o, the ion's initial position.

Now, using the relation between Weierstrass functions and Jacobi elliptic functions given by Southard (1968, p. 649), we find that

[4.8] $\wp(w) = (\omega^2/6)[1 + \frac{3}{2}\ \frac{1 + \mathrm{cn}(\omega w|\mu)}{1 - \mathrm{cn}(\omega w|\mu)}]$

Terms of order μ can be ignored in ω, where we already know that they have small effect. Substituting from eqs [4.6] and [4.8] into the general solution, with $w = t + \phi/\omega$ gives us

[4.9] $y\ (w) = \alpha + (f'(\alpha)/2\omega^2)\,[1 - \mathrm{cn}(\omega w|\mu)]$

An approximate expression for $\mathrm{cn}(u|\mu)$, valid for small μ, is

$$[4.10] \qquad \mathrm{cn}(u|\mu) = \cos u + \frac{\mu}{4}(u - \sin u \cos u) \sin u.$$

The fractional error due to neglecting the term proportional to μ in $[1 - \mathrm{cn}(u|\mu)]$ is of order μ. We already have said that $\mu << 1$ is required for our approximations, so the very simple result is that

$$[4.11] \qquad \mathrm{cn}(u|\mu) \sim \cos u.$$

Using eqs. [4.2] and [4.3] for α and $f'(\alpha)$ in eq. [4.9], the final result is

$$[4.12] \qquad y(t) = y_o + \frac{1}{2\omega^2}[f'(y_o) - f'(\alpha) \cos(\omega t + \phi)].$$

The phase angle ϕ is chosen so that $y(o) = y_o$: $\cos \phi = f'(y_o)/f'(\alpha)$. Now it is simple to get $x(t)$ by integrating eq. [2.10],

$$[4.13] \qquad x(t) = x_o + \left\{(1 - \frac{\omega_c^2}{\omega^2})\, \dot{x}_o - \frac{\omega_c^2}{\omega^2} \cdot \frac{e_y(y_o)}{B}\right\} t$$

$$- \frac{f'(\alpha)}{2\omega^2} \left(\frac{\omega_c}{\omega}\right) [\sin(\omega t + \phi) - \sin \phi].$$

There are just four independent initial values of the coordinates (x_o, y_o) and their derivatives $(\dot{x}_o, \dot{y}_o)$ involved in the expressions for $x(t)$ and $y(t)$. Both $f'(\alpha)$ and ϕ are defined in terms of these. The value of the trap coordinate (z) that appears implicitly in $e_y(y_o)$ is a free parameter at this point, as is explained in section 3.

The motion described by eqs. [4.12] and [4.13] is similar to the motion of a charged particle in crossed $\underline{E}$ and $\underline{B}$ fields. However, the drift velocity, v_D, which is given by the term in curly brackets in eq. [4.13] is not just $(\underline{E} \times \underline{B})/|\underline{B}|^2$, although it is approximately that if we neglect terms of order $(\Delta\omega/\omega)$. Then

$$[4.14] \qquad v_D = - e_y(y_o)/B$$

shows that the electric field must be evaluated at the initial y-coordinate of the ion and the local value of the trap coordinate, z. Fig. 6 shows contours of constant v_D, in the same way that ΔB was plotted in Fig. 5. The quasi-cyclotron motion takes place about the drifting centre, which moves with velocity v_D. In this frame, it is elliptical (with the ratio of semi-axes equal to ω_c/ω). This is the same result as is obtained in the harmonic theory, although we must remember that ω is position-dependent when we take the higher order terms into account.

In this section, we have obtained solutions for the motion of an isolated ion in the plane perpendicular to the static magnetic field. While the main features of this motion are similar to the results of the harmonic treatment, they are different in subtle but significant detail. In particular we find a previously unsuspected dependence of the quasi-cyclotron frequency and drift velocity on the position of the ion in the cell. The assumptions needed to simplify the equations of motion and solve them in useful form are simple and well satisfied:

(1) The trap oscillation is much slower than the quasi-cyclotron oscillation.

(2) The y-component of the electric field is given accurately by cubic terms in y.

(3) The parameter $\mu = (1/48)(q/m)E_y'''(0)(R_o/\omega_c)^2$ is very small.

Fig. 6: Contours of v_D = constant (units are m/sec) for the same situation as in Fig. 5.

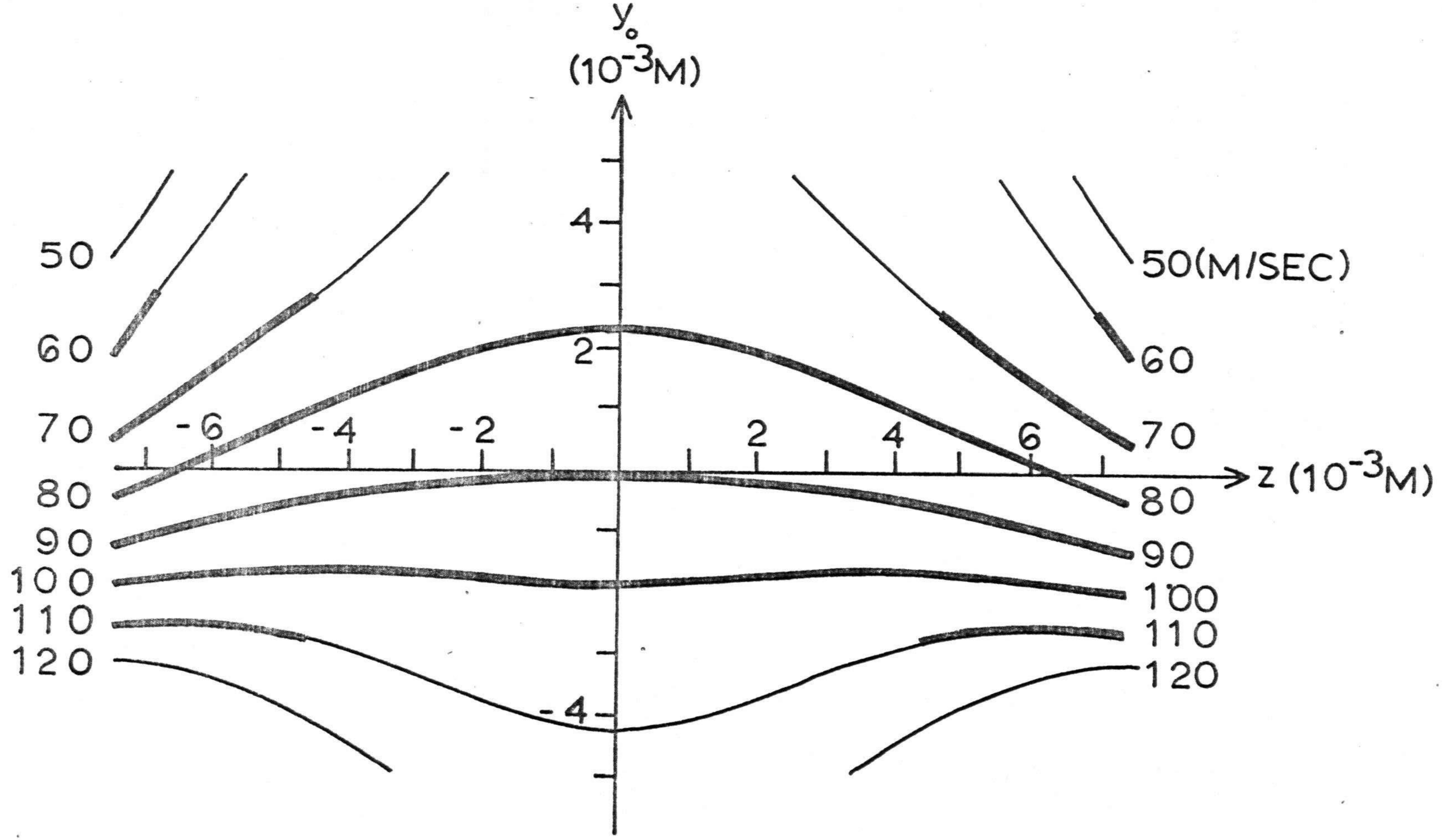

y_o $(10^{-3}M)$
z $(10^{-3}M)$
4
2
-4
-6
-4
-2
2
4
6
50(M/SEC)
60
70
80
90
100
110
120
50
60
70
80
90
100
110
120

Briefly, these conditions let us uncouple the equations of motion, terminate the power series expansion for the potential, and solve the resulting equations for the quasi-cyclotron motion in simple closed form.

As we have previously stressed, the drift velocity and quasi-cyclotron frequency depend on the coordinates of the ions. In order to relate the observed line width and resonance field to these quantities we must perform appropriate averages over all ions and their motions in the cell. In particular their z dependence must be averaged over the unobserved trap oscillation, which we examine in the next section.

5. The Trap Oscillations

The separation of variables in the equations of motion leads us to the equation for z:

$$[5.1] \qquad \dot{z}^2 - \dot{z}_o^2 + 2\kappa \sum_{n=0}^{\infty} t_n (z^{2n+2} - z_o^{2n+2}) = 0$$

where

$$[5.2] \qquad t_n = \frac{1}{(2n+1)(2n+2)} \sum_{m=0}^{\infty} (m+1)\, e_{m+1,n} < y^m >$$

The average of y^m has to be taken over one period of the quasi-cyclotron oscillation at a particular value of z, because its frequency and amplitude depend on z, by eqs. [3.25], [3.2] and [4.12]. Inspection shows us that $< y^m >$ is a function of z^2, so when eq. [5.1] is solved by the general method outlined in Section 3, we find the coefficients of the quartic to be

$$[5.3] \qquad \begin{aligned} a_o &\approx -\kappa e_{11}/6 \\ a_1 &= 0 \\ a_2 &\approx -\kappa(e_{10}+2e_{20}y_o+3e_{30}y_o^2)/6 \\ a_3 &= 0 \\ a_4 &= \dot{z}_o^2+2\kappa(t_o z_o^2+t_1 z_o^4) \end{aligned}$$

These lead to the solution for z(t) as in Section (3) and (4):

[5.4] $$z(t) = [z_o{}^2 + (\dot{z}_o/\omega_T)^2]^{\frac{1}{2}} \cos(\omega_T t + \psi)$$

where

[5.5] $$\omega_T{}^2 = \kappa[e_{10} + 2e_{20}y_o + 3e_{30}y_o{}^2]$$

ω_T is the frequency of oscillation of an isolated ion in the trapping field, which is shown in Fig. 4 for y = 0.

These expressions are correct if the parameter

[5.6] $$\mu'' = (\tfrac{1}{6})\, \kappa e_{11}\, \dot{z}_o{}^2/\omega_T{}^4)$$

is much less than one. Assuming that the ions form a thermal population, this may be related to the parameter (μ) governing the approximations made in understanding the y-motion of ions.

[5.7] $$\mu'' \simeq (\tfrac{1}{2})(\omega_c/\omega_T)^4\, \mu$$

Thus, $\mu'' \sim 2 \times 10^{-2}$, which is sufficiently small for us to accept the approximate expression for z(t).

6. Another Way to Express the Results

The equations of motion which we have worked with up to now use an expansion of the electric field about the origin. In the results for ω, ω_T and v_D, we found expressions for $E'_y(y_o)$ and $E_y(y_o)$, taken to second or third order in y_o. This fact makes it interesting to expand E_y about $y = y_o$ in a Taylor series , and use the same tactics to solve the equation of motion that follow when we truncate the series at the $(y-y_o)^3$ term. The results are

$$[6.1] \qquad \omega = \omega_c \left\{ 1 - \frac{\kappa}{2\omega_c^2} \left[E'_y(y_o,z) + (\dot{x}_o/\omega_c)E''_y(y_o,z) + \left(\frac{3\dot{x}_o^2 + 2\dot{y}_o^2}{2\omega_c^2}\right) E'''_y(y_o,z)\right]\right\}$$

for the frequency of the quasi-cyclotron oscillation. With the same assumptions that we made in section (3), and noting that $<\dot{x}_o> = 0$ for thermal ions, we have the very simple result that

$$[6.2] \qquad \Delta B = \frac{1}{2\omega_c} E'_y(y_o,z)$$

This supposes that

$$[6.3] \qquad \kappa E'''(y_o,z)(R_o^2/\omega_c^2) \ll 1,$$

which is essentially the criterion $\mu \ll 1$. Physically, this means that the second order part of the time-averaged variation in the energy associated with the electric field, $(\frac{1}{24})q\,E_y'''\,R_o^4$, is much less than the energy of the orbital motion, $\frac{1}{2}m\omega_c^{\,2}R_o^{\,2}$.

For the drift velocity, we find

$$[6.4] \qquad v_D = -\,E_y(y_o,z)/B.$$

The trap oscillation can, of course, be analysed in much the same way. The average of E_z over one quasi-cyclotron period is approximated by $E_z(y_o,z)$, and then expanded about $z = 0$. $\nabla\cdot\underline{E} = 0$ relates the first derivatives of E_y and E_z, so that

$$[6.5] \qquad \omega_T^2 = \kappa E_y'(y_o,0).$$

We see that the relation

$$[6.6] \qquad \omega_c^{\,2} = \omega^2 + \omega_T^{\,2}$$

which holds rigorously in the harmonic approximation (Beauchamp and Armstrong, 1968) is really true only when $\omega_T^{\,2} \ll \omega^2$ and $z = 0$. This is another example of the small but important differences between that approach and the more complete treatment given here.

7. Influence of the trap oscillations

The motion of ions in the ICR cell is conveniently described in terms of several characteristic frequencies. The ions may be pictured as precessing elliptically in the x-y plane ("quasi-cyclotron motion") about an instantaneous center, which oscillates along the z-axis ("trap oscillation") and drifts in the x-direction. Strictly speaking, the quasi-cyclotron frequency is expressed in terms of the initial value of y. Since the theory outlined previously implicitly assumes that the amplitude of the cyclotron motion is small, and since $\omega(y,z)$ is a slowly varying function of y and z, we may identify y with the centre of the cyclotron motion. This characteristic angular frequency $\omega(y,z)$ of the quasi-cyclotron motion, varies with z over a range of frequencies $\Delta\omega(y,z) << \omega_c$. That this inequality is very well satisfied may be seen from Fig. 7 in which $\omega(y,z)$ is plotted as a function of z for three different values of y for Ar^+ ions under typical operating conditions. The quasi-cyclotron frequency is modulated due to the trap oscillations at an angular frequency ω_T which usually satisfies the inequalities

$$[7.1] \qquad \Delta\omega(y,z) << \omega_T << \omega$$

as may be seen from Table 2. Finally, as a result of the drift of the ions through the resonance region of the ICR cell, the ions spend a finite time $\tau = \ell/v_D$ in a cell of length ℓ, giving rise to a resonance line width $\omega_{\frac{1}{2}}$ which usually falls between $\Delta\omega(y,z)$ and ω_T. In this section, we use the inequality [7.1] to derive an approximate expression for the ICR frequency for ions having a well-defined value of y and which oscillate between $z = \pm z_m$. The effect of a distribution of y and z_m is described in the next section.

For convenience of notation we re-write Eq. 2.1 in the form

Fig. 7: A plot of $\omega_c - \omega(y,z)$ as a function of z for three different values of y for Ar^+ ions. The cell parameters are a = 0.025 m., b = 0.014 m., $V_T = V_1 = 0.5$ volts, and $V_2 = -0.5$ volts. $\omega_c/2\pi$ is 300 kHz corresponding to a magnetic field of about 0.780 Tesla.

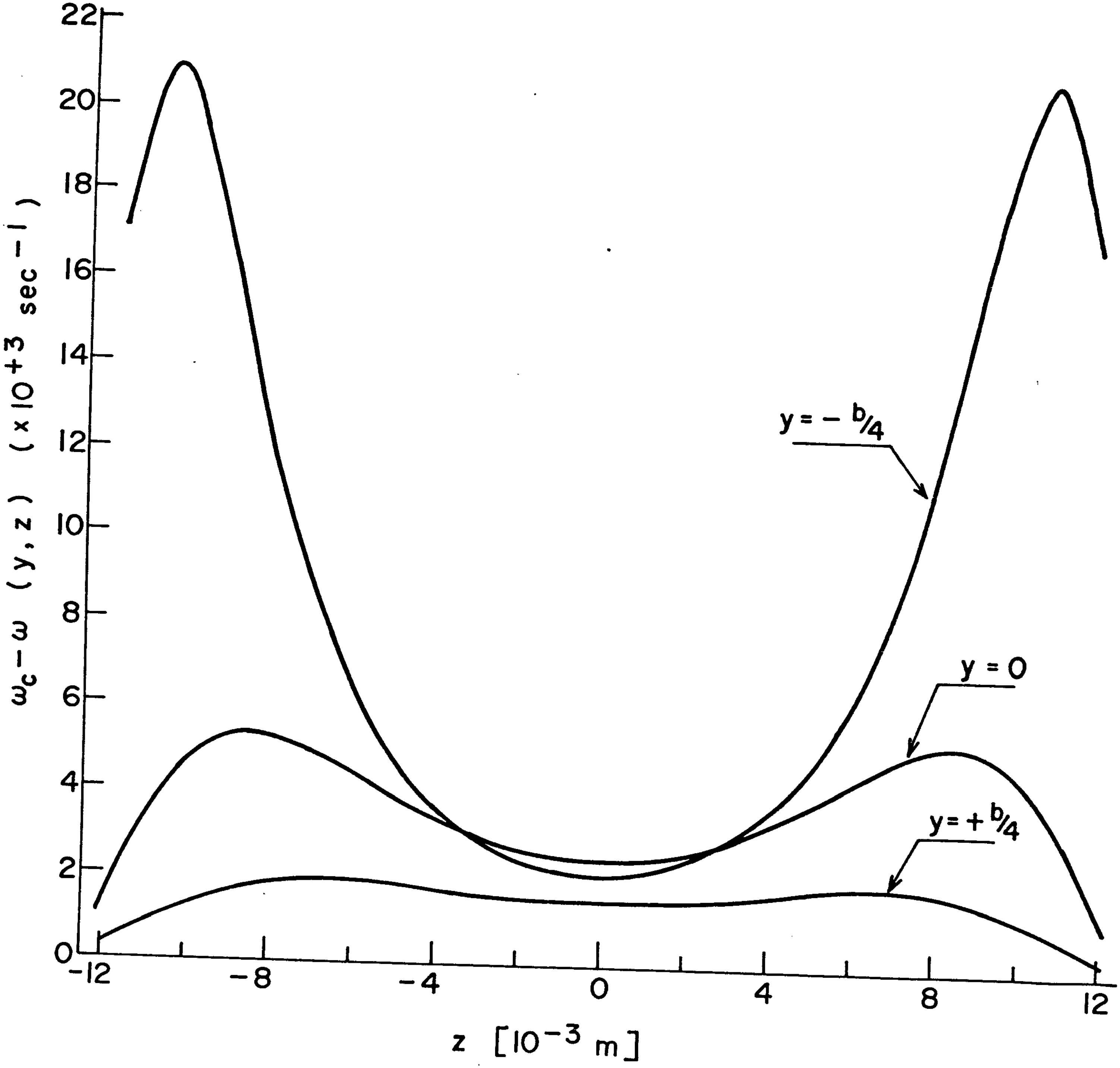
22
20
18
16
14
12
10
8
6
4
2
0
$\omega_c - \omega \; (y, z) \; (\times 10^{+3} \; \mathrm{sec}^{-1})$
-12
-8
-4
0
4
8
12
$z \; [10^{-3} \; \mathrm{m}]$
$y = -b/4$
$y = 0$
$y = +b/4$

Table 2. Values of characteristic frequencies of Ar^+ ions in an ICR cell under the operating conditions of Figure 5.

TABLE 2

Cyclotron Frequency	$\omega_c = \kappa B$	1.885×10^6 (sec.$^{-1}$)
Trapping Frequency	$\omega_T(0,0) = \sqrt{\frac{\kappa}{2} E_y'(0,0)}$	6.80×10^4 (sec.$^{-1}$)
Line Width (Full Width at half height)	$\omega_{\frac{1}{2}} = \dfrac{5.566\kappa \lvert E_y(0,0) \rvert}{\omega_c \ell}$	8.25×10^3 (sec.$^{-1}$)
Frequency Spread	$\omega(0,0) - \omega(0,0.35a) = \frac{\kappa}{2\omega_c} [E_y'(0,0.35a) - E_y'(0,0)]$	2.82×10^3 (sec^{-1})

[7.2] $$V(y,z) = V_T - \sum_{k=o}^{\infty} A_k(y) \cos\left[(2k+1)\frac{\pi z}{a}\right]$$

where

[7.3] $$A_k(y) = \frac{2}{\pi}\frac{(-1)^k}{2k+1}\left\{(2V_T - V_1 - V_2)\frac{\cosh[(2k+1)\frac{\pi y}{a}]}{\cosh[(2k+1)\frac{\pi b}{2a}]} - (V_1-V_2)\frac{\sinh[(2k+1)\frac{\pi y}{a}]}{\sinh[(2k+1)\frac{\pi b}{2a}]}\right\}.$$

When the condition $\omega_c >> \omega_T$ is satisfied, we can approximate the y-component of the ion motion over a time $t << 2\pi/\omega_T$ by the expression,

[7.4] $$y(t) = y_a + A\cos[\omega(y,z)t + \phi]$$

where the amplitudes y_a and A and the phase factor ϕ are determined by the initial conditions and $\omega(y,z)$ is defined by [6.1] in terms of the instantaneous center (y,z) of the quasi-cyclotron motion.

If an ICR experiment were carried out over a time much less than $2\pi/\omega_T$, the ICR spectrum would consist of a superposition of lines centered at frequencies distributed over a range $\Delta\omega$ corresponding to the spatial distribution of ions in the cell. However, each line would, under such conditions, have a width much greater than ω_T so that the frequency spread $\Delta\omega$ would be undetectable according to [7.1]. In practice, of course, ICR experiments are usually performed over a time much greater than $2\pi/\omega_T$ so that the effect of the trap oscillations must be taken into account.

The effect of the trap oscillations is to modulate $\omega(y,z(t))$ due to the time dependence of the z-co-ordinate. As mentioned earlier, the effect of the inhomogeneous electric field of the cell on the cyclotron motion is to change the circular cyclotron orbits into elliptical orbits. The ratio of the major and minor axes of the ellipse differs from unity only by an amount of order $\frac{\Delta\omega(y,z)}{\omega_c}$. Since $\Delta\omega << \omega_c$, we may neglect the small modulations of the amplitudes y_a and A to a good approximation and replace Eq. [7.4] by

$$[7.5] \qquad y(t) = y_a + A \cos[\int_o^t \omega(y,z(t'))\, dt' + \phi]$$

Eq. [7.5] is a good approximation for y(t) if the variation in the quasi-cyclotron frequency due to the trapping oscillation satisfies the adiabatic condition that

$$\omega_c^2 >> \frac{d\omega}{dz}\dot{z} ,$$

which is well met in the ICR apparatus. Using Eqs. [6.1], [7.2], [7.3] and $E'_y = -\frac{\partial^2 V}{\partial y^2}$,

$$[7.6] \qquad \int_o^t \omega(y,z(t'))dt' = \omega_c t - \frac{\kappa}{2\omega_c} \sum_{k=o}^{\infty} \frac{d^2 A_k(y)}{dy^2} \int_o^t \cos[(2k+1)\frac{\pi z(t')}{a}]dt'$$

Using Eq. [7.6] it is possible to define an average quasi-cyclotron frequency as a function of y and z_m by numerical methods. Firstly, the equation of motion for z(t) may be integrated for any given ICR cell potential parameters and the maximum amplitude of oscillation z_m. Then, if the integral in [7.6] is evaluated numerically at long times ($\omega_T t >> 1$) it will be well represented as a linear function of time plus small oscillations. The linear factor which multiplies t is the "average quasi-cyclotron frequency" for (y, z_m). Instead of presenting numerical results of such calculations, we choose to evaluate [7.6] in terms of a simplified description of the trap oscillations.

We now evaluate [7.5] and [7.6] in the harmonic approximation for the trap oscillations, i.e.

[7.7] $$z(t) = z_m \cos \omega_T t$$

This is quite a good approximation near y=o, where the decoupled equation of motion for z is almost linear. An accurate representation of z(t) for $y \lesssim -b/4$ would require the introduction of harmonics of ω_T. The generalization of the results to be derived below to include higher harmonics is straightforward, but tedious, and is not presented here. Substituting [7.7] into [7.6] and using the well known expression (Watson, 1962; page 22) involving Bessel functions

[7.8] $$\cos(\alpha \cos\beta) = J_o(\alpha) + 2 \sum_{n=1}^{\infty} (-1)^n J_{2n}(\alpha) \cos 2n\beta$$

we obtain

[7.9] $$\int_o^t \omega(y, z(t'))dt' = [\omega_c - \Omega_o(y, z_m)]t - \sum_{n=1}^{\infty} \frac{\Omega_{2n}(y, z_m)}{2n\omega_T} \sin(2n\omega_T t)$$

where

[7.10] $$\Omega_{2n}(y, z_m) = (-1)^n \frac{\kappa}{2\omega_c} \sum_{k=o}^{\infty} \frac{d^2 A_k(y)}{dy^2} J_{2n}\left[\frac{(2k+1)\pi z_m}{a}\right]$$

As may be seen from the definition of Ω_{2n} and Table 1,

$$\frac{\Omega_{2n}}{n\omega_T} \lesssim \frac{\Delta\omega}{\omega_T} << 1.$$

Therefore, substituting [7.9] into [7.5] and expanding to first order in these small quantities enables us to write

[7.11] $$y(t) \simeq y_a + A\{\cos[\omega_o(y,z_m)t+\phi] + \sin[\omega_o(y,z_m)t+\phi] \sum_{n=1}^{\infty} \frac{\Omega_{2n}}{n\omega_T} \sin(2n\omega_T t)\}.$$

where

[7.12] $$\omega_o(y,z_m) = \omega_c - \Omega_o(y,z_m)$$

We identify $\omega_o(y,z_m)$ with the average frequency of the quasi-cyclotron motion, the average being taken over the trap oscillation in the harmonic approximation. The ICR spectrum for ions having a vertical position y and an amplitude of oscillation in the trap z_m should consist of a main resonance line at $\omega_o(y,z_m)$ and small intensity satellite lines at the frequencies $\omega_o(y,z_m) \pm 2n\omega_T$, $n = 1,2, \ldots$.

We wish to emphasize that, though the harmonic approximation was used in treating z(t), the general expression for the potential was still used in calculating $\omega(y,z)$.

The drift velocity of the ions in the cell is given by Eq. [6.4], which may be treated in a manner similar to the quasi-cyclotron motion. The ions drift in the x-direction at an average velocity $v_D(y,z_m)$ which depends on y and z_m, with small oscillations at the frequencies $2n\omega_T$. The average velocity is given in the harmonic approximation by Eqs. [6.4], [7.2], [7.7] and [7.8] to be

$$[7.13] \qquad v_D(y,z_m) = -\frac{1}{B}\sum_{k=o}^{\infty}\frac{dA_k(y)}{dy}\,J_o[(2k+1)\frac{\pi z_m}{a}].$$

The variation of $\omega_o(y,z_m)$ and $v_{D.}(y,z_m)$ with y and z_m is shown, respectively, in Figures 8 and 9.

Fig. 8: A plot of $\omega_c - \omega_o(y,z_m)$ as a function of z_m, the maximum amplitude of oscillation in the z direction, for three different values of y. The harmonic approximation for the trapping oscillations has been used. All parameters are the same as in Fig. 5.

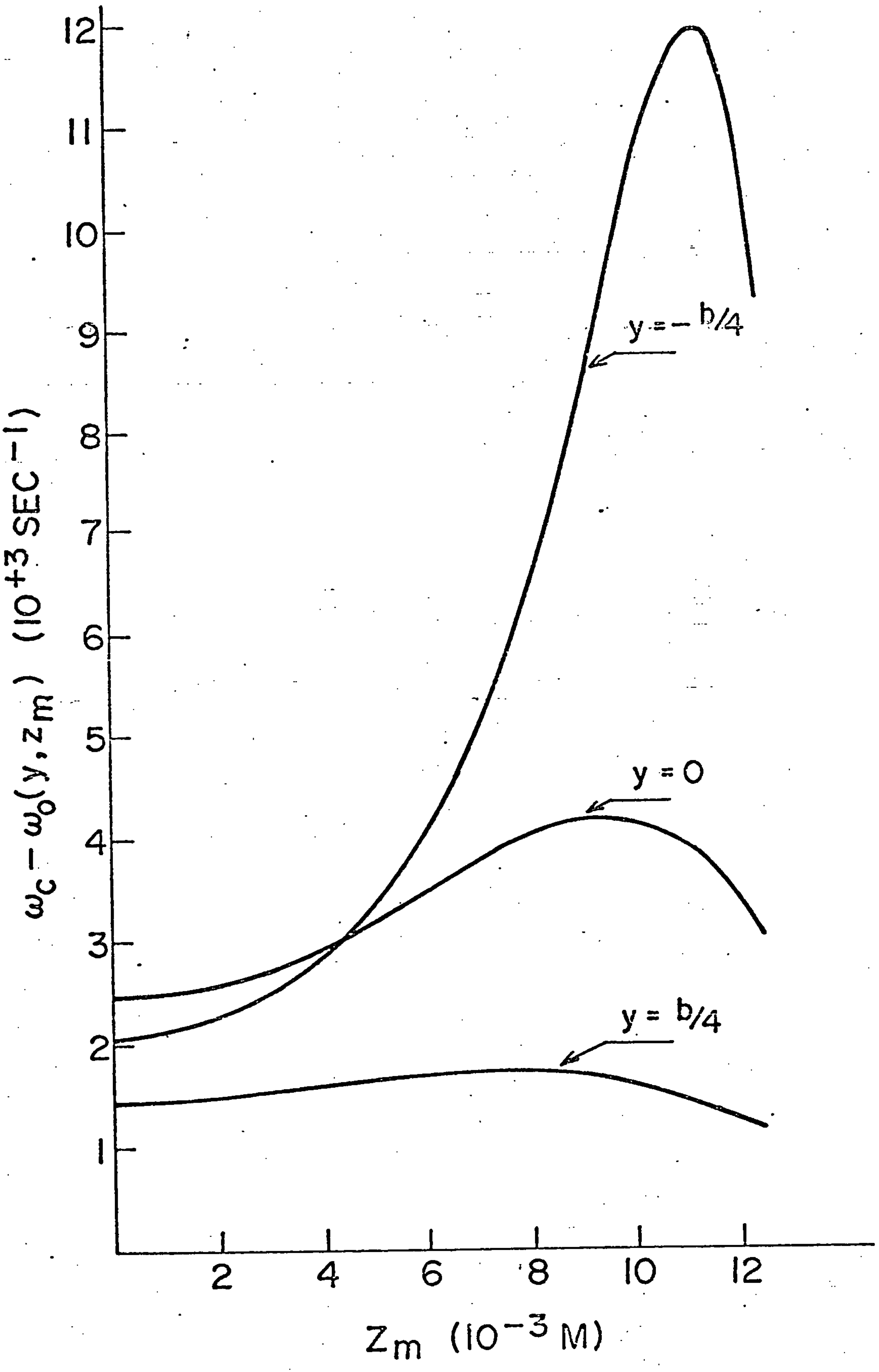
$\omega_c - \omega_0(y, z_m)$ $(10^{+3}\ \mathrm{SEC}^{-1})$
12
11
10
9
8
7
6
5
4
3
2
1
$y = -b/4$
$y = 0$
$y = b/4$
2
4
6
8
10
12
Z_m $(10^{-3}\ \mathrm{M})$

Fig. 9: A plot of the average drift velocity as a function of z_m for three values of y under the same conditions as in Figure 5.

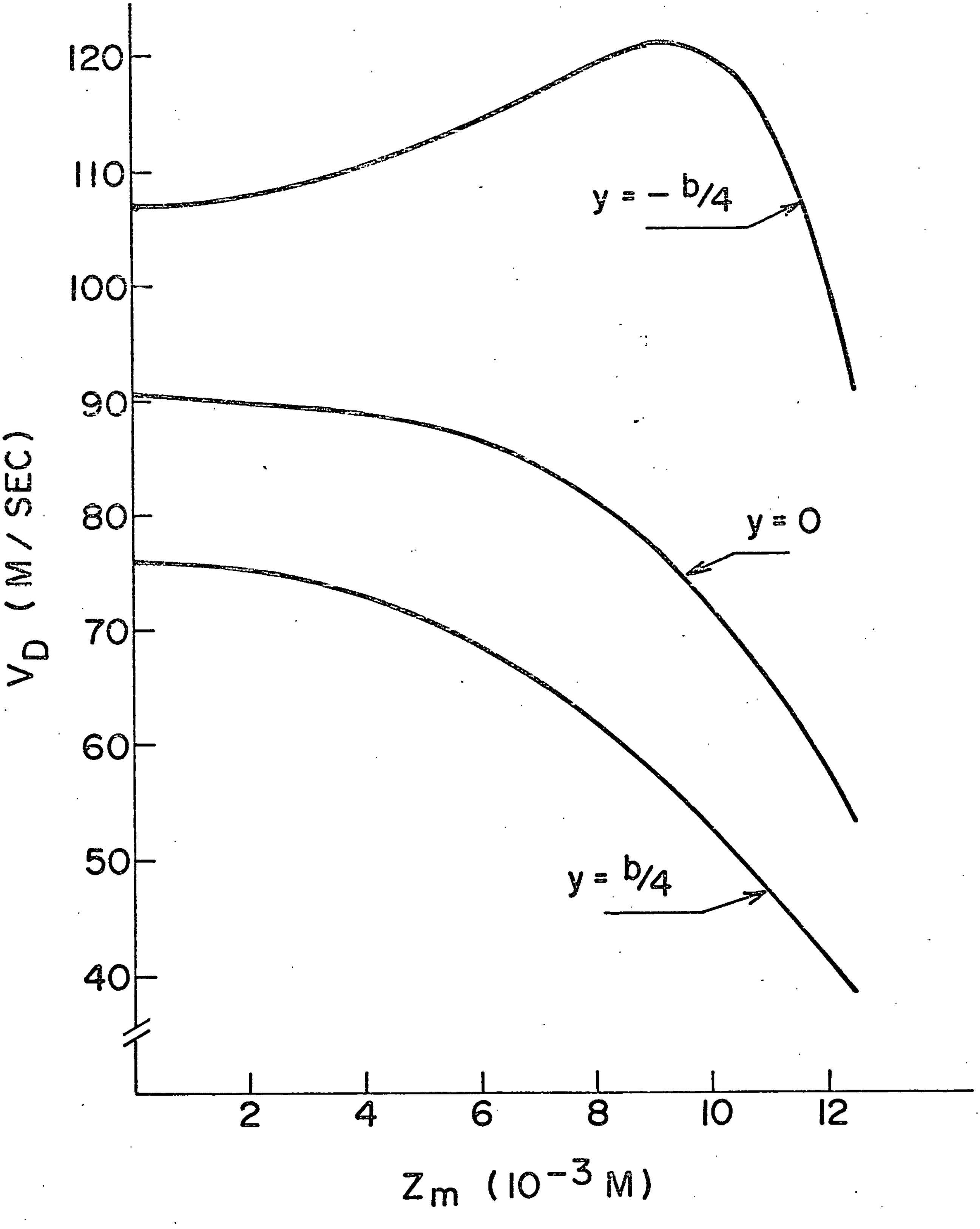
120
110
100
90
80
70
60
50
40
V_D (M / SEC)
2
4
6
8
10
12
Z_m (10^{-3} M)
y = – b/4
y = 0
y = b/4

8. Line Shapes

We have derived an expression for the ICR frequency $\omega_o(y,z_m)$ of an ion at a vertical position y and trap oscillation amplitude z_m. Suppose that N ions pass through the resonance region of the ICR cell per second and that a fraction

$$p(y,z_m)\ dydz_m$$

of these are between y and y+dy and have maximum oscillation amplitude between z_m and z_m+dz_m. Then the power absorption in the ICR cell for an oscillating field at a frequency ω_1 is given by

$$[8.1] \qquad I(\omega_1) = N \int_{-\frac{b}{2}}^{+\frac{b}{2}} dy \int_o^{a/2} dz_m\ p(y,z_m)\ \varepsilon(\omega_1;y,z_m)$$

where $\varepsilon(\omega_1;y,z_m)$ is the energy absorbed by a single ion characterized by (y,z_m) in passing through the cell in a time $\tau = \ell/v_D(y,z_m)$. The ensemble averaged line shape $I(\omega_1)$ should not be confused with the line shape of an ion having a well-defined (y,z_m), which is proportional to $\varepsilon(\omega_1;y,z_m)$. It is convenient to write

$$[8.2] \qquad \varepsilon(\omega_1;y,z_m) = \varepsilon_{res.}(y,z_m)\ G\{\omega_1-\omega_o(y,z_m)\}$$

where $\varepsilon_{res.}(y,z_m)$ is the energy absorbed by an ion at resonance as it traverses the cell and $G\{\omega_1-\omega_o(y,z_m)\}$ is an unnormalized line shape function which satisfies G(o) = 1. In our discussion we have assumed thus far that each ion has a constant (y,z_m) throughout its passage through the cell.

This implies that the time between collisions of the ions with the molecules of the background gas is much greater than τ. In this low density, collisionless regime, it is easy to show that (Butrill, 1969)

$$[8.3] \qquad \varepsilon_{\text{res.}}(y,z_m) = \frac{q^2 \langle E_{1y}\rangle^2 \tau^2}{8m}$$

and

$$[8.4] \qquad G(\delta\omega') = \frac{\text{Sin}^2\left(\frac{\delta\omega'\tau}{2}\right)}{\left(\frac{\delta\omega'\tau}{2}\right)^2}, \quad \delta\omega' = \omega_1 - \omega_o\,(y,z_m)$$

where $\langle E_{1y}\rangle$ is the average magnitude of the y-component of the r-f field for an ion characterized by (y,z_m), the average being taken over the trap oscillations. Thus, $\delta\omega'$, $\langle E_{1y}\rangle$ and τ all depend on y and z_m in [8.3] and [8.4].

In order to calculate $\langle E_{1y}\rangle$, the effective radio-frequency electrical circuit must be specified. Usually, the trap potential is at r-f ground, i.e. $(V_T)_{r-f} = 0$. Experiments could be performed with $(V_1)_{r-f}(t) = -(V_2)_{r-f}(t) = V_{r-f} \cos \omega_1 t$, but it seems to be more customary to put $(V_1)_{r-f}$ or $(V_2)_{r-f}$ equal to zero. In any case, once the r-f potentials are specified, the co-efficients $[A_k(y)]_{r-f}$ analogous to the d-c co-efficients of [7.3] may be calculated and the value of $\langle E_{1y}\rangle$ for a given (y,z_m) computed in terms of $d\,[A_k(y)]_{r-f}/dy$ in analogy with [7.13]. The dependence of $\langle E_{1y}\rangle$ on y and z_m for some typical operating conditions is shown in Fig. 10.

It is of interest to examine the line shape $I(\omega_1)$ for some special cases of experimental importance. When the ions are produced by electron bombardment, the electron beam traverses the cell over a very small range of y near $y = y'$, and the ions are produced with roughly equal probability at

Fig. 10: A plot of $<E_{1y}>$ versus z_m for two values of y and three different rf voltage configurations. The values of E_{rf}/V_{rf} are given for $a = 0.025$ m. and $b = 0.014$ m.

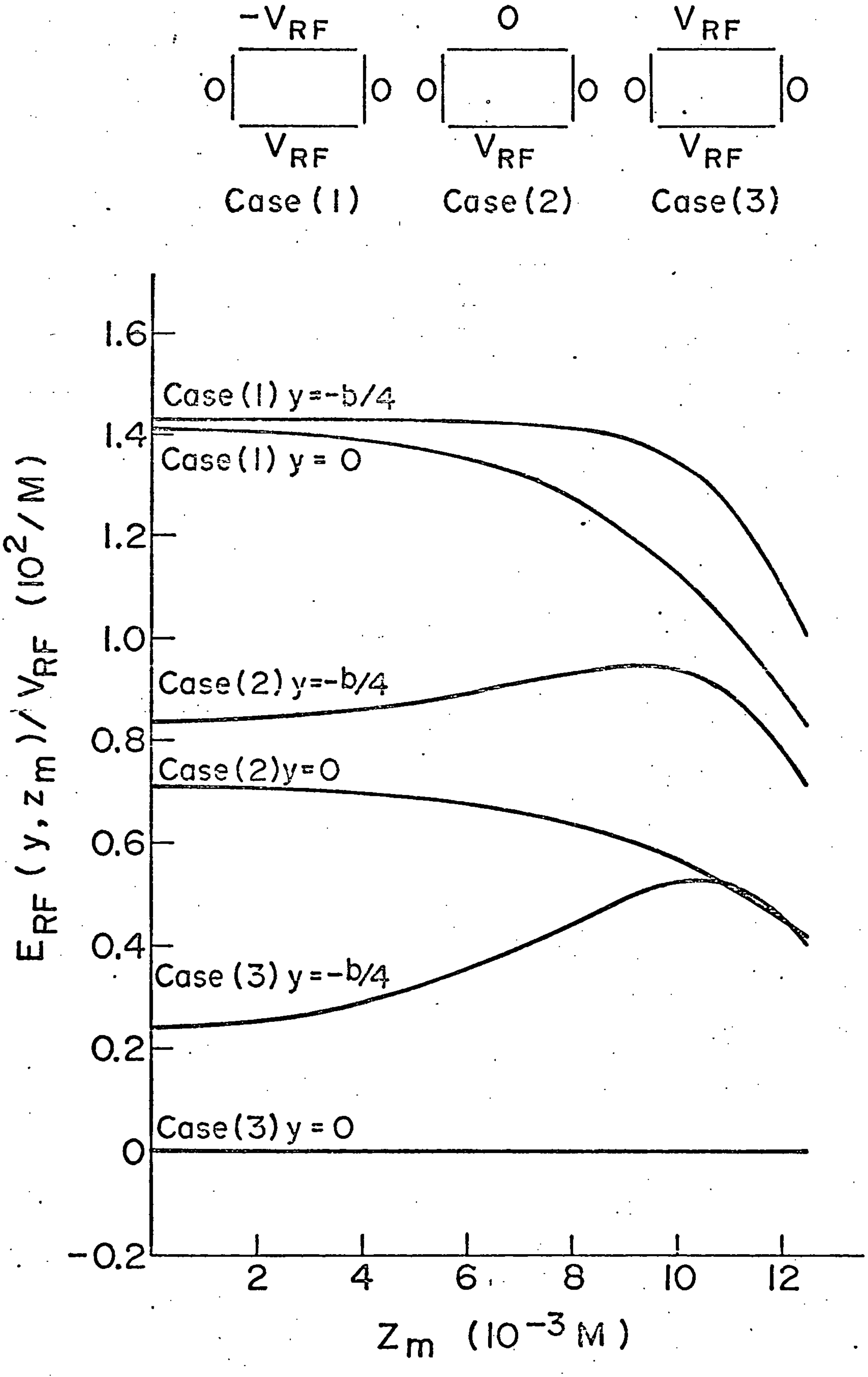
−V_RF
0
V_RF
0 0 0 0 0 0
V_RF
V_RF
V_RF
Case (1)
Case (2)
Case (3)
Case (1) y=−b/4
Case (1) y = 0
Case (2) y=−b/4
Case (2) y=0
Case (3) y=−b/4
Case (3) y = 0
1.6
1.4
1.2
1.0
0.8
0.6
0.4
0.2
0
−0.2
2
4
6
8
10
12
E_RF (y, z_m)/V_RF (10^2/M)
Z_m (10^−3 M)

each value of z. If the average recoil energy of the ions and the thermal energy of the background gas atoms or molecules from which the ions are produced are much less than qV_T, the ensemble of ions produced is well approximated by

$$[8.5] \qquad p_o(y,z_m) = \frac{2}{a}\,\delta(y-y')$$

where $\delta(y-y')$ is a Dirac δ-function. As we shall discuss in Section 9, this spatial distribution of ions will be preserved as the ions drift from the source to the resonance region only if certain stringent experimental conditions are met. Under these conditions, the line shape is given by

$$[8.6] \qquad I(\omega_1) = \frac{2N}{a}\int_o^{a/2} dz_m\ \varepsilon(\omega_1;y',z_m)$$

It is easy to see that [8.1] and [8.6] are each convolutions of two line shape functions. One of these shape functions is $G(\omega)$ given by [8.4]. The other is the distribution of frequencies $\omega_o(y',z_m)$, each weighted in [8.6] by $2N\varepsilon_{res}(y',z_m)\,\frac{dz_m}{a}$, which would be obtained from the ions in the small region between z_m and z_m+dz_m for very long cells. In a long cell the condition

$$\Delta\omega_o(y',z_m)\ \tau >> 1$$

is satisfied, where $\Delta\omega_o(y',z_m)$ is the spread of frequencies associated with the distribution of z_m.

Our numerical calculations indicate that under typical operating conditions, the width $1/\tau$ due to finite transit time of the ions in the cell is somewhat larger than the spread due to the spatial distribution of the ions, i.e.

$$\Delta\omega_o(y',z_m)\ \tau << 1.$$

Some typical line shapes predicted by [8.6] are shown in Fig. 11, but comparison with experiment is left to Section 16. The most striking features of the theoretical absorption spectra of Figure 11 are:

1. The frequency of maximum absorption and the line width are functions of y'. A detailed discussion of the properties will be given in Section 10 in terms of a simplified "average ion" model.
2. The lines are not symmetric, the degree of asymmetry being dependent on y'_o. Such asymmetric lines have been observed by many experimenters, though they have not been discussed extensively in the literature. We find that the sign and nature of the asymmetry are well explained by our theory. In Figure 11, the absorption sideband in the high frequency (low field) side of the resonance is noticeably larger than that on the opposite side for y' = -b/4. When V_T is decreased to smaller values the asymmetry decreases. It is common practice in many laboratories to eliminate the asymmetry empirically by using small trapping voltages. The origin of the asymmetry lies in the asymmetric distribution of frequencies associated with the distribution of trap oscillation amplitudes. However, the asymmetry is sometimes enhanced by the fact that the average drift velocity is also a function of z_m. The plots of Figure 11 include both of these effects as well as the variation of $<E_{1y}>$ with z_m. All these influences are included in Eqs. [8.2] - [8.6]. Calculations show, however, that the influence of $<E_{1y}>$ on the asymmetry is generally less important than the other factors.

Fig. 11: The ICR line shape as given by Eq. 8.6, for three different values of y' and the same parameters as in Fig. 5. The bottom scale shows a sweep of frequency, ω_1, with $\omega_c = 1.885 \times 10^6$ sec.$^{-1}$ while the top scale shows a sweep of ω_c (or field, B) with $\omega_1 = 1.885 \times 10^6$ sec.$^{-1}$.

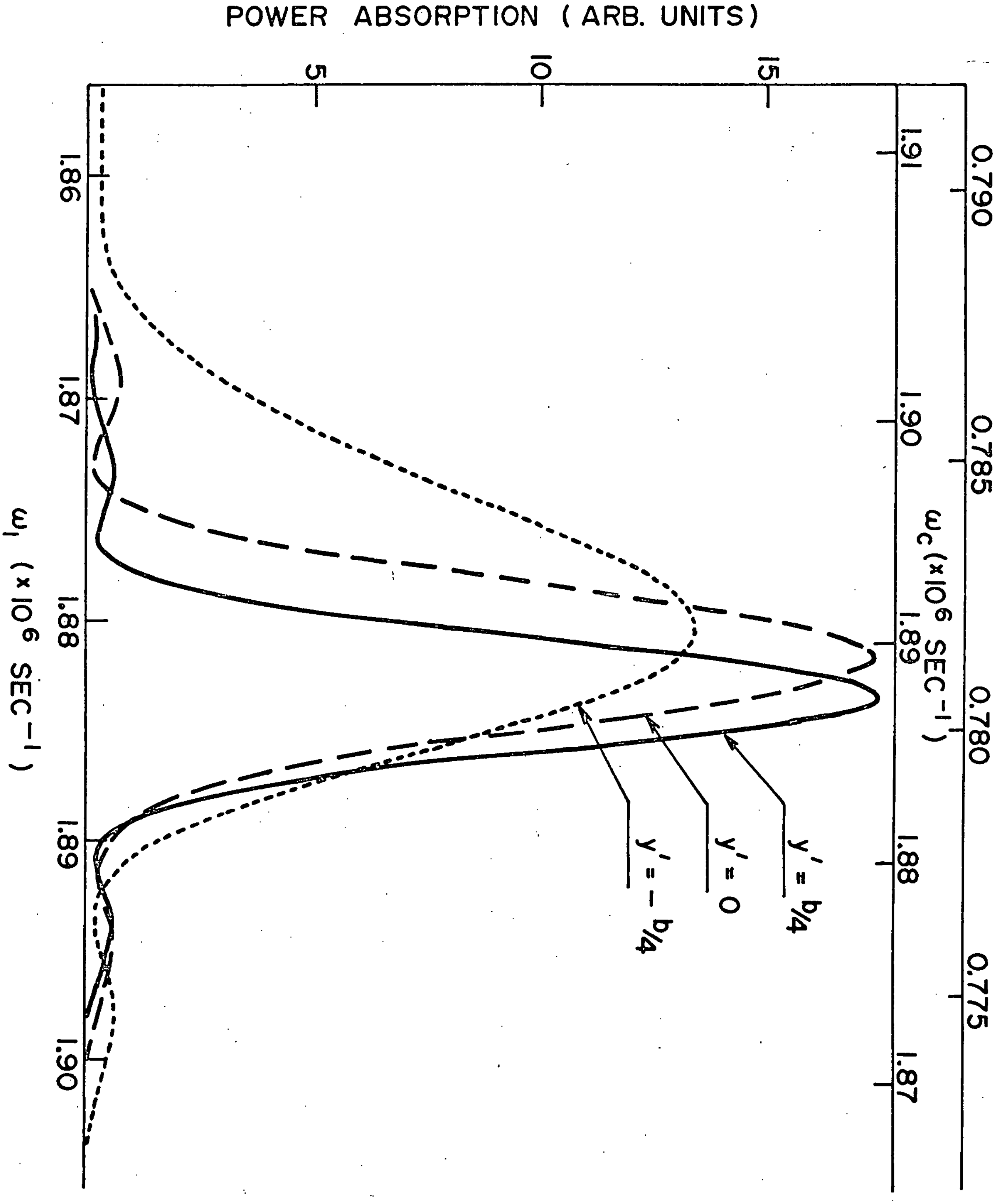
POWER ABSORPTION (ARB. UNITS)
5
10
15
B (TESLA)
0.790
0.785
0.780
0.775
ωc (×10⁶ SEC⁻¹)
1.91
1.90
1.89
1.88
1.87
1.86
1.87
1.88
1.89
1.90
ω1 (×10⁶ SEC⁻¹)
y′ = b/4
y′ = 0
y′ = −b/4

9. Influence of the Cell Potential on the Spatial Distribution of the Ions

As discussed in Section 8, the ICR characteristics are influenced by the spatial distribution function of the ions in the resonance region, denoted by $p(y,z_m)$ in [8.1]. Usually, the ions are produced in a source region by an electron beam and then drift slowly into the resonance region. The electron beam, if it is sufficiently intense, gives rise to an inhomogeneous electric field which may contribute appreciably to the potential energy of the ions when they are produced. The ions then drift far enough away from the electron beam, while still in the source, that the electron beam contribution to the potential can be neglected. One can then define a two-dimensional source spatial distribution function $p_s(y_s,z_{ms})$. For sufficiently weak electron beams that its contribution to the cell potential is everywhere negligible, $p_s(y_s,z_{ms})$ can be adequately approximated by [8.5], but more generally it is necessary to take into account the motion of the ions in the potential of the electron beam to estimate $p_s(y_s,z_{ms})$.

In some experiments, it has been found desirable to use different drift potentials (V_1,V_2) and/or trapping potentials (V_T) in the source and analyzer or other regions of the ICR cell. For example, Clow and Futrell (1970) introduced a reaction region between the source and analyzer. Primary ions were first excited by applying a resonant electric field in the form of a pulse in the source region and the effects of charge exchange reactions were monitored in the analyzer or resonance region. By using a drift field in the reaction region of magnitude much smaller than those in the source and detector regions, the probability of charge exchange reactions in the source and detector regions was minimized. In order to obtain the resonance region spatial probability distribution $p(y,z_m)$ from $p_s(y_s,z_{ms})$, it is necessary to integrate the equations of motion of the ions in the inhomogeneous electric field between the source and resonance regions to obtain $y(y_s,z_{ms})$ and $z_m(y_s,z_{ms})$. Then, we can write a formal expression for $p(y,z_m)$ in terms of $p_s(y_s,z_{ms})$ as follows

$$[9.1] \qquad p(y,z_m) = \int_{-\frac{b}{2}}^{+\frac{b}{2}} dy_s \int_0^{a/2} dz_{ms}\ \delta(y-y(y_s,z_{ms}))\ \delta(z_m-z_m(y_s,z_{ms}))\ p_s(y_s,z_{ms})$$

In a similar way, one can generate $p_s(y_s,z_{ms})$ from the initial spatial distribution function of the ions in the ionising electron beam if the potential of the electron beam is known.

The problem of integrating the equations of motion of the ions as they drift from one part (region 1) of the cell to another part (region 2) is complicated for the general case. It is possible to give simple solutions for two special limiting cases of experimental interest. We shall call these cases the fast drift and the adiabatic drift limits, respectively. Expressed in terms of the separation s, of the two regions, the average angular trapping frequency ω_T and average drift velocity between the regions, these limits can be defined by inequalities $\omega_T s/v_D << 1$ and $\omega_T s/v_D >> 1$, respectively, i.e. in the fast drift limit, the time to drift from one region to the other is much less than a single trapping oscillation, while the opposite is true in the adiabatic drift limit. In each case, we assume that many quasi-cyclotron oscillations occur during the time of drift between regions 1 and 2, i.e. $\omega_o s/v_D >> 1$. The implication of the last approximation is that the drift always occurs along equipotential surfaces. The particular path along these surfaces is different for the fast drift and slow drift limits, while the paths for drift speeds intermediate to these limits should lie between the paths for the limiting cases. In the following discussion, we denote the values of (y,z_m) by (y_1,z_{m1}) and (y_2,z_{m2}) for regions 1 and 2, respectively.

The fast drift limit: From the preceding discussion, it is clear that

[9.2] $$z_{m1} = z_{m2}$$

and

[9.3] $$V(y_1,z_{m1}) = V(y_2,z_{m2})$$

which, for this case, are sufficient to determine $y_2(y_1,z_{m1})$ and $z_{m2}(y_1,z_{m1})$.

The adiabatic drift limit: The well-known condition satisfied by adiabatic mechanical processes is that the action integrals remain constant (Born, 1969). Assuming, that the trap oscillations are decoupled from the quasi-cyclotron motions, this condition gives

[9.4] $$\int_o^{z_{m1}} \dot{z}_1 dz_1 = \int_o^{z_{m2}} \dot{z}_2 dz_2 \ ,$$

or equivalently

[9.5] $$\int_o^{z_{m1}} [V(y_1,z_{m1}) - V(y_1,z_1)]^{\frac{1}{2}} dz_1 = \int_o^{z_{m2}} [V(y_2,z_{m2}) - V(y_2,z_2)]^{\frac{1}{2}} dz_2$$

which, combined with the energy conservation equation [9.3], is sufficient to determine $y_2(y_1,z_{m1})$ and $z_{m2}(y_1,z_{m1})$.

Practical considerations: Under typical operating conditions $v_D \simeq 10^2$ m./sec. and $\omega_T \simeq 10^5 \text{sec.}^{-1}$ as may be seen from Table 1. Thus, the characteristic distance which defines the two limiting cases is $s_o = v_D/\omega_T \simeq 10^{-3}$m. In experiments such as those of Clow and Futrell (1970) in which different trapping and drift voltages are used in different regions of the cell, the distance over which the potential varies appreciably is determined by "end effects". The cell geometry dictates then that this distance is of the order of the smaller of a or b, i.e. typically, of the order of 10^{-2} m. Thus, the adiabatic drift limit should normally be applicable in this type of situation. On the other hand, in taking into account the influence of the potential due to the ionising electron beam on the drift of the ions, it would appear that for typical electron beams (diameter $\simeq 10^{-3}$ m.), the drift rate may be intermediate between the fast and adiabatic limits.

A calculation of the effect of drift between two regions in the adiabatic drift limit has been carried out in Appendix 1 for the harmonic potential approximation. It would be straightforward to carry out numerical calculations of the influence of drift on the spatial distribution of the ions for more realistic potentials, but the available experimental results do not seem to warrant such an effort at this time. In the next section, we shall develop a simplified, ad-hoc model which we have found useful in taking into account the effect of ICR potentials on the spatial distribution of the ions. It should be noted, however, that the calculation in Appendix 1 indicates a considerable dispersion of the ions in the y-direction.

10. Ad-Hoc "Average Ion Model" for Studying the Spatial Distribution of Ions in an ICR Cell

We have shown in previous sections that the ICR properties of an ensemble of ions depend on their spatial distribution. The ions are usually produced in the source with the relatively simple distribution of Eq. [8.5] corresponding to a well defined vertical position y in the cell and a uniform distribution of trap oscillation amplitudes z_m. It seems, from the considerations of Section 9 and Appendix 1, that as the ions drift from the source into the resonance region of the cell, an appreciable dispersion of the ions in the y-direction may result. Even for the simple distribution [8.5], however, the line shapes are not simple in the collisionless regime. For example, a marked asymmetry of the ICR line shape was predicted in Section 8.

In view of the complexity of numerical calculations of the ICR line shapes, we have looked for a simplified, but realistic model with which to probe the spatial distribution of the ions in the cell. The two most easily measured line shape parameters are the frequency of maximum power absorption $\overline{\omega}_1$ and the line width $\omega_{\frac{1}{2}}$ defined in Section 7. Both of these parameters, as well as the line shape, are influenced by changes in the cell potentials V_T, V_1, and V_2 in a manner which depends on the spatial distribution of the ions. Thus, study of the dependence of $\overline{\omega}_1$ and $\omega_{\frac{1}{2}}$ on the cell potentials can give information on the positions of the ions in the cell, thus serving as a useful diagnostic tool for ICR spectrometers.

In our model, we replace the ensemble of ions described by the distribution function $p(y,z_m)$ by an "average ion" at a vertical position y having a potential energy corresponding to the average potential energy of the simplified distribution function [8.5]. The average potential energy is given by

$$[10.1] \qquad \langle V\rangle = \int_{-\frac{b}{2}}^{+\frac{b}{2}} dy' \int_{o}^{a/2} dz_m \, p_o(y',z_m)\, V(y',z_m)$$

and $V(y',z_m)$ is the average potential energy of an ion characterized by (y',z_m) in the harmonic approximation as is given by [7.2], [7.7] and [7.8] to be

$$[10.2] \qquad V(y',z_m) = V_T - \sum_{k=o}^{\infty} A_k(y')\, J_o[(2k+1)\frac{\pi z_m}{a}]$$

Substituting [10.2] into [10.1], we obtain

$$[10.3] \qquad \langle V\rangle = V_T - \sum_{k=o}^{\infty} \alpha_k \hat{A}_k(y)$$

where

$$[10.4] \qquad \alpha_k = \frac{2}{\pi(2k+1)} \int_{o}^{(k+\frac{1}{2})\pi} J_o(p)dp$$

<V> is shown as a function of y in Fig. 12 for several different potential configurations.

It is convenient for our purposes to express <V> explicitly in terms of the cell potentials and the position y of the "average ion".

$$[10.5] \qquad \langle V\rangle = V_T + f_1(y)V_d + f_2(y)(V_T-V_a) \; ; \quad V_d = \frac{V_1-V_2}{2}\,, \quad V_a = \frac{V_1+V_2}{2}$$

Fig. 12: The position dependence of the averaged potential $\langle V(y) \rangle$ for five different values of $V_1 - V_2$ with $V_T = 0.5$ volt and $V_1 + V_2 = 0$. Similar curves for arbitrary V_1, V_2 and V_T may be obtained from Eq. [10.3].

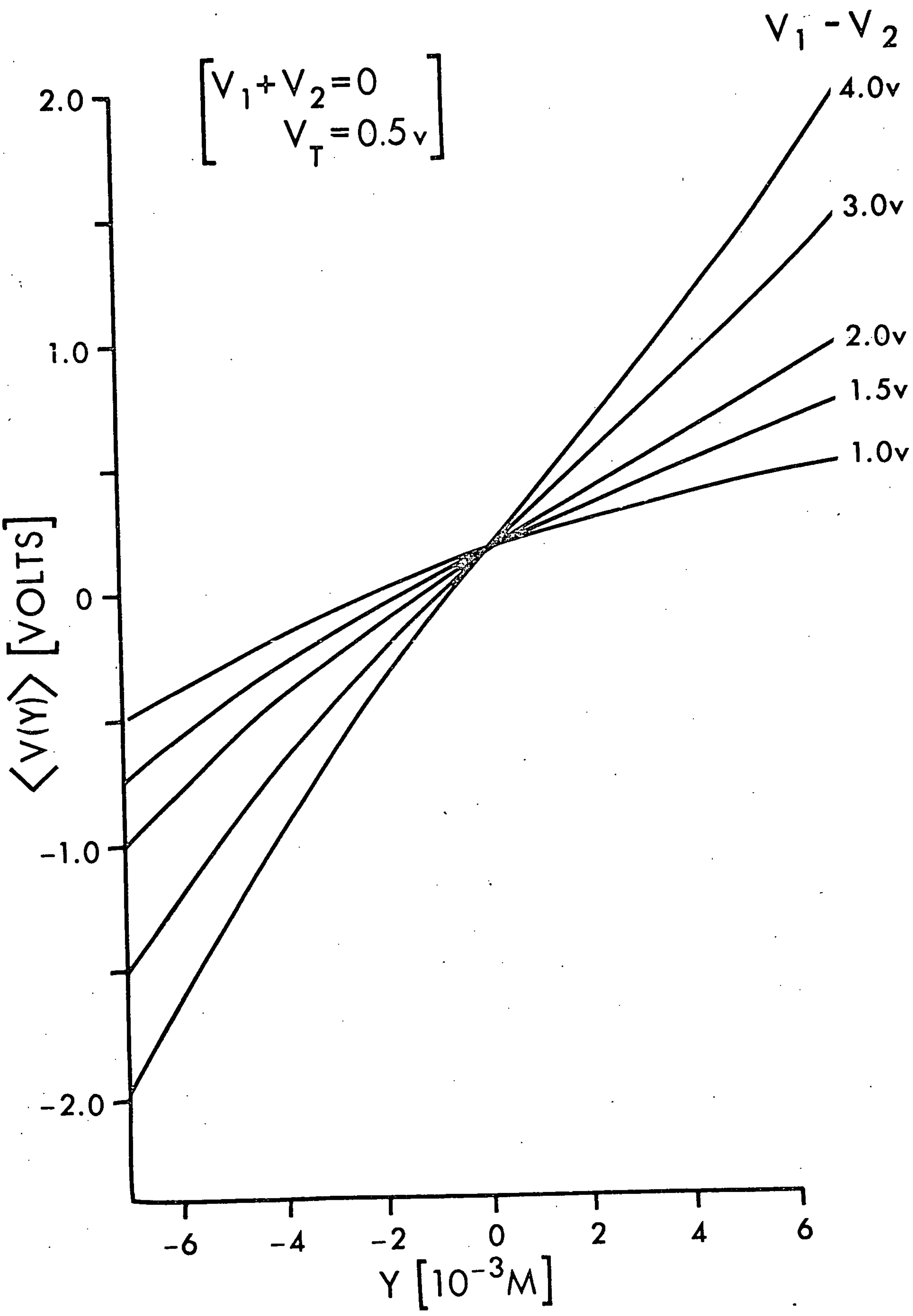

$V_1 - V_2$
$\left[V_1 + V_2 = 0 \quad V_T = 0.5\,v \right]$
4.0v
3.0v
2.0v
1.5v
1.0v
2.0
1.0
0
-1.0
-2.0
⟨V(Y)⟩ [VOLTS]
-6
-4
-2
0
2
4
6
Y [10^{-3}M]

where, using [7.2] and [10.3]

[10.6] $$f_1(y) = + \frac{4}{\pi} \sum_{k=o}^{\infty} \frac{(-1)^k \alpha_k}{2k+1} \frac{\sinh[(2k+1)\frac{\pi y}{a}]}{\sinh[(2k+1)\frac{\pi b}{2a}]}$$

and

[10.7] $$f_2(y) = - \frac{4}{\pi} \sum_{k=o}^{\infty} \frac{(-1)^k \alpha_k}{2k+1} \frac{\cosh[(2k+1)\frac{\pi y}{a}]}{\cosh[(2k+1)\frac{\pi b}{2a}]}$$

Similarly, the average quasi-cyclotron resonance frequency $<\omega_o(y,z_m)>$ is given by

[10.8] $$\begin{aligned} <\omega_o> &= \omega_c - \frac{\kappa}{2\omega_c} \sum_{k=o}^{\infty} \alpha_k \frac{d^2 A_k(y)}{dy^2} \\ &= \omega_c - \kappa[g_1(y)V_d + g_2(y)(V_T-V_a)] \\ &= \omega_c - \frac{\kappa}{2\omega_c} <\frac{\partial E_y}{\partial y}> \end{aligned}$$

Clearly,

[10.9] $$g_i = - \frac{1}{2\omega_c} \frac{d^2 f_i}{dy^2}, \qquad i = 1,2$$

The amplitude averaged electric field gradient $<E_y'(y)>$ is shown in Fig. 13.

Often, the resonance magnetic field is measured keeping the frequency fixed. This is given by

[10.10] $$B_{eff} = B + g_1(y)V_d + g_2(y)(V_T-V_a)$$

where B_{eff} is identified with the magnetic field corresponding to maximum ICR absorption intensity.

Following the same procedure for the drift velocity [2.13], which enters into the calculation of $<\omega_{\frac{1}{2}}>$,

Fig. 13: Position dependence of the averaged electric field gradient, $\langle \partial E_y/\partial y \rangle$. As in Figs. 5 and 6, $V_T = 0.5$ v and $V_1+V_2 = 0$.

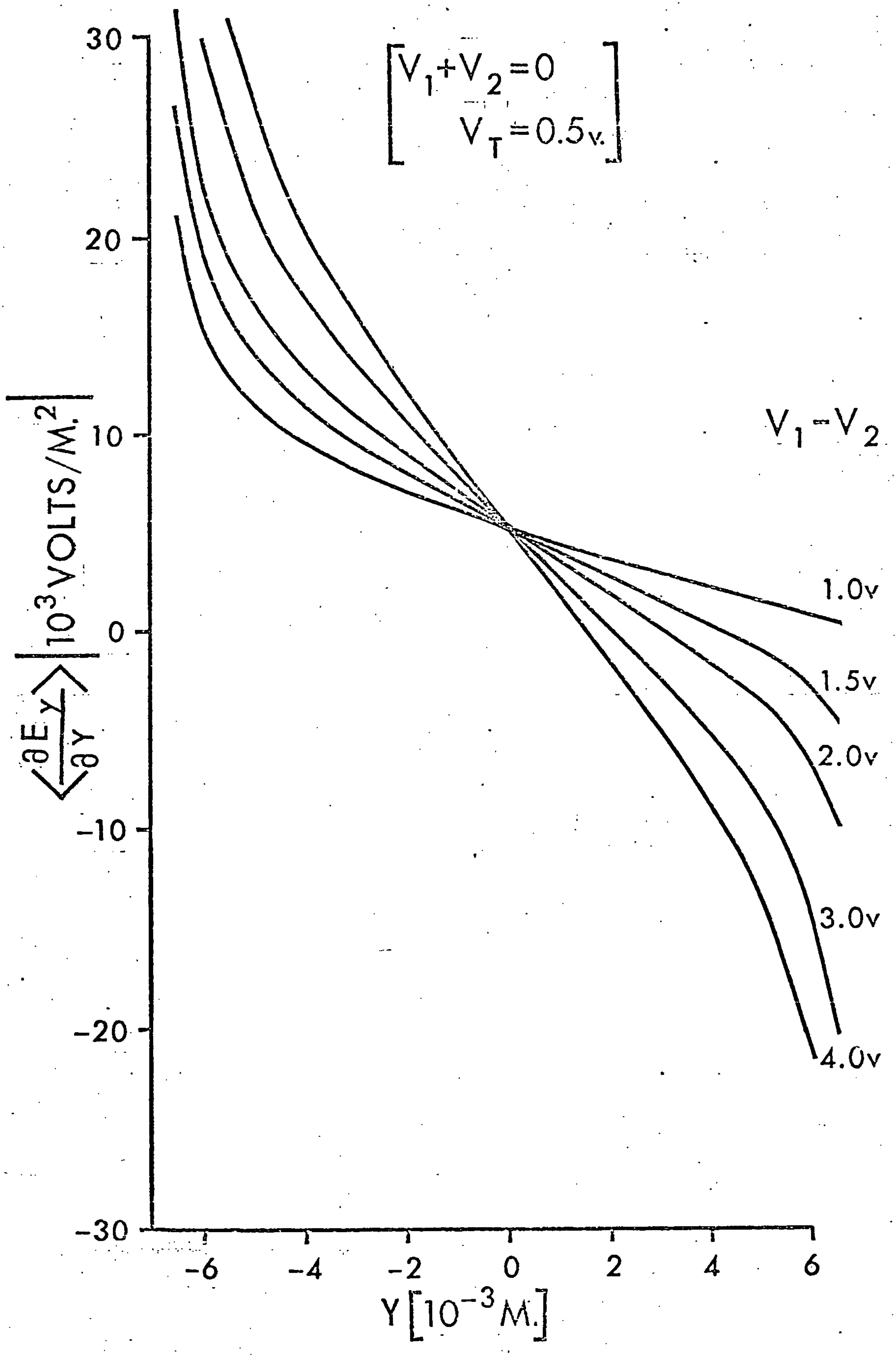
$V_1 + V_2 = 0$
$V_T = 0.5$v.
$V_1 - V_2$
1.0v
1.5v
2.0v
3.0v
4.0v
$\left\langle \frac{\partial E_Y}{\partial Y} \right\rangle \left| 10^3 \text{ VOLTS/M.}^2 \right|$
30
20
10
0
−10
−20
−30
−6
−4
−2
0
2
4
6
$Y \left[10^{-3} \text{M.} \right]$

[10.11] $$\langle V_d\rangle = \frac{1}{B}\left[\frac{df_1(y)}{dy} V_d + \frac{df_2(y)}{dy}(V_T - V_a)\right]$$
$$= \frac{1}{B}\langle E_y(y)\rangle$$

The amplitude averaged electric field $\langle E_y(y)\rangle$ is shown in Fig. 14.

Effect of a change in the cell potential

We now consider the effect of a change in an ICR cell voltage parameter on the resonance characteristics of the "average ion". Suppose, for example, that a small change ΔV_T is made in the V_T keeping V_d and V_a constant. Then, the ratio of the change in resonance field ΔB_{eff} to V_T is given, in the limit $\Delta V_T \to 0$, by

[10.12] $$\left(\frac{\partial B_{eff}}{\partial V_T}\right)_{V_a,V_d} = g_2(y) + \left[V_d\frac{dg_1}{dy} + (V_T - V_a)\frac{dg_2}{dy}\right]\left(\frac{\partial y}{\partial V_T}\right)_{V_a,V_d}$$

The first term in [10.12] is associated with the change in B_{eff} due to the local change in $\frac{\partial E_y}{\partial y}$ produced by ΔV_T, while the second term is due to the shift in B_{eff} resulting from the displacement of the ions as they follow the changed equipotentials due to ΔV_T. Since the ions drift along equipotentials (see Section 9), the "average ion" satisfies the condition that $\langle V\rangle$ is a constant for different parts of the cell. Thus, $\left(\frac{\partial y}{\partial V_T}\right)_{V_d,V_a}$ can be obtained from [10.5]. In order to do so, however, it is necessary to specify the manner in which the change in V_T changes $\langle V\rangle$ in the source and resonance region. Let us illustrate this remark by calculating $\left(\frac{\partial y}{\partial V_T}\right)_{V_d,V_a}$ for two different voltage configurations in the ICR cell.

Case 1. The potentials V_T, V_d, V_a are taken to be identical in the source and resonance region. Assume that the ions are produced in the source at y=0 by an electron beam which perturbs the potential in the immediate vicinity

Fig. 14: Position dependence of the averaged drift electric field. As in Fig. 5 $V_T = 0.5$ v, and $V_1+V_2 = 0$.

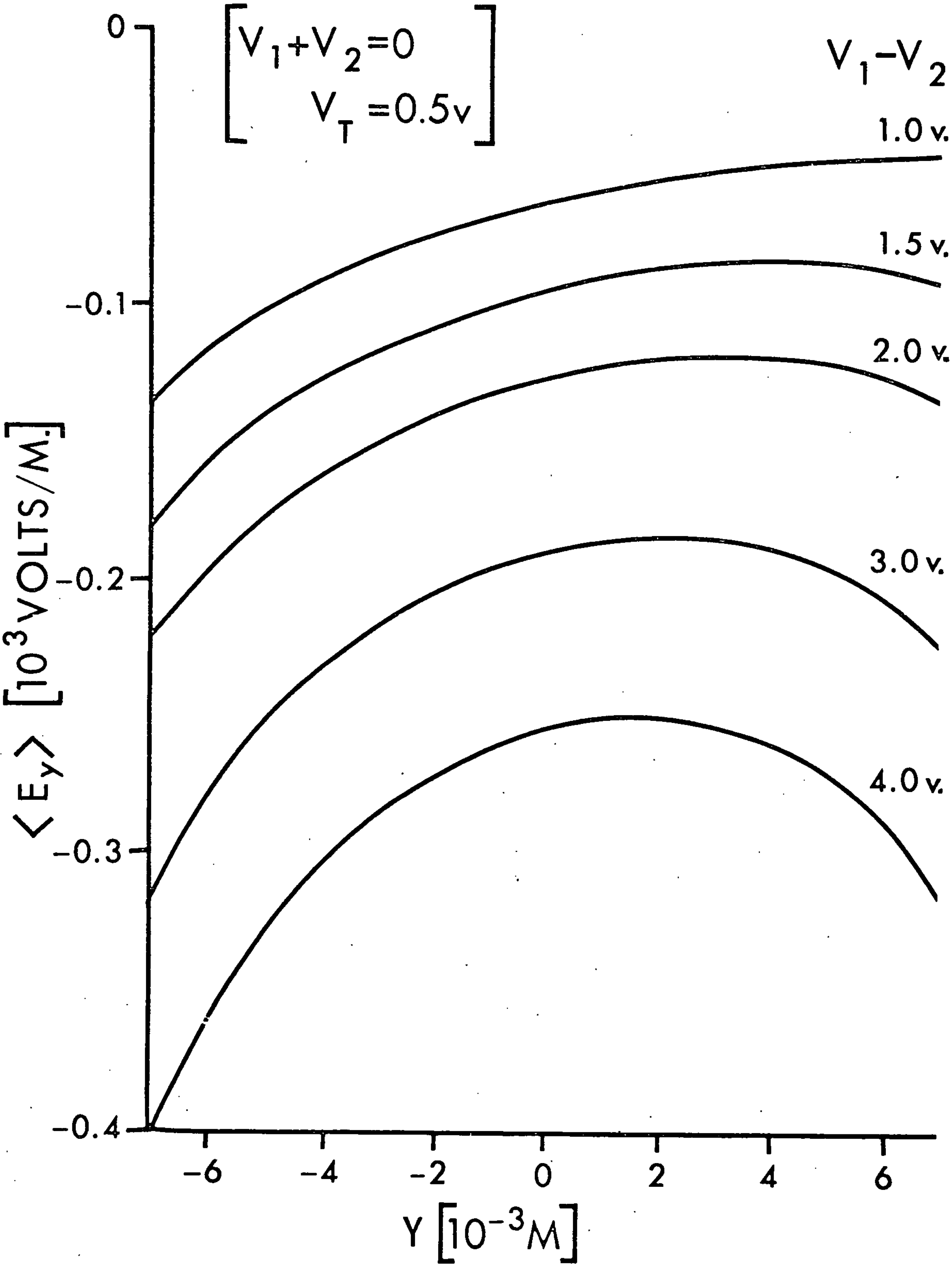
V_1+V_2=0
V_T =0.5v
V_1-V_2
1.0 v.
1.5 v.
2.0 v.
3.0 v.
4.0 v.
0
-0.1
-0.2
-0.3
-0.4
⟨E_y⟩ [10^3 VOLTS/M.]
-6
-4
-2
0
2
4
6
Y [10^-3 M]

of the ionising region by a constant amount Δ. Let y be the vertical position of the average ion in the resonance region. Since the ions drift along equipotentials between the source and resonance region we obtain the following relationship from [10.5].

$$[10.13] \qquad V_T + f_1(0)V_d + f_2(0)(V_T-V_a) + \Delta = V_T + f_1(y)V_d + f_2(y)(V_T-V_a)$$

This gives the result required to complete [10.12]

$$[10.14] \qquad \left(\frac{\partial y}{\partial V_T}\right)_{V_d,V_a} = \frac{f_2(0) - f_2(y)}{V_d \frac{df_1}{dy} + (V_T-V_a)\frac{df_2}{dy}}$$

Case 2. Suppose that the cell potentials in the resonance (V_T^r, V_d^r, V_a^r) and source (V_T^s, V_d^s, V_a^s) regions are independently controlled. Then, instead of [10.13], the drift along equipotentials gives the relation

$$[10.15] \qquad V_T^s + f_1(0)V_d^s + f_2(0)(V_T^s-V_a^s) + \Delta = V_T^r + f_1(y)V_d^r + f_2(y)(V_T^r-V_a^r)$$

Then, a variation of V_T^r with no change in any other of the cell potentials gives the result

$$[10.16] \qquad \left(\frac{\partial y}{\partial V_T^r}\right)_{\substack{V_d^r,V_a^r \\ V_T^s,V_d^s,V_a^s}} = - \frac{1 + f_2(y)}{V_d^r \frac{df_1}{dy} + (V_T^r-V_a^r)\frac{df_2}{dy}}$$

With the substitution of either [10.14] or [10.16], or an expression for $\left(\frac{\partial y}{\partial V_T}\right)$ appropriate for the ICR cell under consideration, we can interpret the variation of B_{eff} with V_T. Similar results are derived for the variation of B_{eff} or $\langle v_d \rangle$ with any of the cell voltages. The kind of behaviour predicted is illustrated below by substituting [10.14] into [10.12] (Case 1)

$$[10.16] \qquad \left(\frac{\partial B_{eff}}{\partial V_T}\right)_{V_d, V_a} = g_2(y) + \frac{V_d \dfrac{dg_1}{dy} + (V_T - V_a)\dfrac{dg_2}{dy}}{V_d \dfrac{df_1}{dy} + (V_T - V_a)\dfrac{df_2}{dy}} [f_2(0) - f_2(y)]$$

Therefore, the slope of a B_{eff} versus V_T plot is expected to be constant both for large and small V_T, but it should be different in each limit if $y \neq 0$.

11. Distribution of Ion Kinetic Energies in an ICR Cell

An important application of ICR is the study of the energy dependence of the scattering and charge exchange cross-sections for collisions between ions and neutral atoms or molecules. In order to interpret the ICR experiments, it is necessary to know the distribution of ion energies over which the theoretical, energy-dependent cross-sections must be averaged. The ions are produced with some sort of spatial and energy distribution both of which depend on the production mechanism. They then oscillate in the trap and drift from the source to the reaction and analyzer regions of the cell. During this drift interval, it is possible to change the ion energy by applying a resonant r-f electric field, both the time over which the ions are subject to ICR and the r-f electric field amplitude being controlled by the experimenter. In this section, we calculate the final distribution of ion kinetic energies resulting from trap oscillation and the application of an ICR r-f field under the following assumptions.

1. The ion motions along the z-axis and in the x-y plane are independent of one another.
2. The trap oscillations may be approximated by simple harmonic motion.
3. The r-f field, averaged over the trap oscillation, is uniform.
4. The initial distribution of ions is given by Maxwell-Boltzmann distribution functions for motions parallel and perpendicular to the z-axis.

In an experimental situation assumptions 1 to 3 are violated to a certain extent by the complicated potential structure of the ICR cell. Assumption 4 is violated when the ions are produced by molecular dissociation.

However, no discussion of the energy resolution of the ICR spectrometer is available in the literature for even the idealized case presented here.

We denote the kinetic energy associated with motion along the z-axis and perpendicular to it by $E_\parallel$ and $E_\perp$, respectively at a time t after the ions have been produced. The total time-dependent kinetic energy E_T is given by

$$[11.1] \qquad E_T = E_\parallel + E_\perp$$

Since the parallel and perpendicular motions are independent according to assumption 1, the distribution function for $E_\parallel$ and $E_\perp$ is the product of the individual distribution functions, i.e.

$$[11.2] \qquad P(E_\parallel, E_\perp)dE_\parallel\, dE_\perp = P_\parallel(E_\parallel)dE_\parallel\, P_\perp(E_\perp)dE_\perp$$

We wish to calculate the functions $P_\parallel(E_\parallel)$ and $P_\perp(E_\perp)$ given that the distributions of initial energies $\varepsilon_\parallel$ and $\varepsilon_\perp$ are Maxwellian, as stated in assumption 4. If the initial effective temperatures associated with $\varepsilon_\parallel$ and $\varepsilon_\perp$ are $T_\parallel$ and $T_\perp$, respectively, then

$$[11.3] \qquad P_{o\parallel}(\varepsilon_\parallel) = \left(\frac{1}{\pi\varepsilon_\parallel kT_\parallel}\right)^{\frac{1}{2}} e^{-\frac{\varepsilon_\parallel}{kT_\parallel}}$$

and

$$[11.4] \qquad P_{o\perp}(\varepsilon_\perp) = \frac{1}{kT_\perp} e^{-\frac{\varepsilon_\perp}{kT_\perp}}$$

where $P_{o\parallel}(\varepsilon_\parallel)$ and $P_{o\perp}(\varepsilon_\perp)$ are normalized distributions for one and two degrees of freedom, respectively.

Effect of ICR on the energy distribution:

We first consider the calculation of $P_\perp(E_\perp)$. Suppose that after the ions are produced they are subjected to ICR for a time t in an r-f electric field of amplitude E_1. Then, for ions having an initial momentum whose projection in the x-y plane makes an angle γ with the (rotating) r-f field (Butrill, 1969)

$$[11.5] \qquad E_\perp = E_m + 2(E_m\varepsilon_\perp)^{\frac{1}{2}}\mu + \varepsilon_\perp$$

where

$$[11.6] \qquad E_m = \frac{q^2E_1^2t^2}{8m}, \quad \text{and } \mu = \cos\gamma$$

We assume that γ is randomly distributed between 0 and π, from which it is easily shown that the distribution function for μ is given by

$$[11.7] \qquad p(\mu) = \frac{1}{\pi(1-\mu^2)^{\frac{1}{2}}} \qquad\qquad -1 \le \mu \le +1$$

Eqs. [11.5] and [11.7] enable us to define a distribution function $G(E_\perp,\varepsilon_\perp)$ such that $G(E_\perp,\varepsilon_\perp)dE_\perp$ is the fraction of ions having kinetic energies between $E_\perp$ and $E_\perp + dE_\perp$ for those ions having a given initial kinetic energy $\varepsilon_\perp$,

$$[11.8] \qquad G(E_\perp,\varepsilon_\perp) = \frac{P(\mu\{E_\perp,\varepsilon_\perp\})}{\left|\left(\frac{\partial E_\perp}{\partial\mu}\right)_{\varepsilon_\perp}\right|} = \frac{1}{\pi[4E_m\varepsilon_\perp-(E_\perp-E_m-\varepsilon_\perp)^2]^{\frac{1}{2}}}$$

from which $P_\perp(E_\perp)$ is calculated as follows.

$$[11.9] \qquad P_\perp(E_\perp) = \int_{\varepsilon_\perp^-}^{\varepsilon_\perp^+} G(E_\perp,\varepsilon_\perp)P_{o\perp}(\varepsilon_\perp)d\varepsilon_\perp$$

The lower and upper limits $\varepsilon_\perp^\pm$ arise from the limits on μ in [11.7] and are easily shown to be

[11.10] $$\varepsilon_\perp^\pm = E_\perp + E_m \pm 2(E_m E_\perp)^{\frac{1}{2}}$$

Making the substitution

[11.11] $$\varepsilon_\perp = 2(E_m E_\perp)^{\frac{1}{2}} w + E_\perp + E_m$$

Eqs. [11.4], [11.8] and [11.9] give the result

[11.12] $$P_\perp(E_\perp) = \frac{1}{kT_\perp} e^{-\frac{E_\perp + E_m}{kT_\perp}} I_o\left[\frac{2(E_m E_\perp)^{\frac{1}{2}}}{kT_\perp}\right]$$

where

[11.13] $$I_o(p) = J_o(ip) = \frac{1}{\pi} \int_{-1}^{+1} \frac{e^{-pw}}{(1-w^2)^{\frac{1}{2}}} dw$$

is the zero'th order Bessel function of imaginary argument. The distribution function $P_\perp(E_\perp)$ is plotted as a function of $E_\perp$ in Figure 15 for different values of $E_m/kT_\perp$. It reduces, as expected, to the form of $P_{o\perp}(E_\perp)$ for $E_m=0$, since $I_o(0) = 1$, while for the limit $E_m/kT_\perp >> 1$, the asymptotic form of $I_o(p)$ (see, e.g. Watson, 1962; page 204) may be used to obtain the result

[11.14] $$P_\perp(E_\perp) \simeq \left(\frac{1}{4\pi E_m kT_\perp}\right)^{\frac{1}{2}} e^{-\frac{(E_\perp - E_m)^2}{4E_m kT_\perp}} \quad , \quad E_m >> kT_\perp$$

This Gaussian function, peaked at $E_\perp = E_m$, has a relative full width

Fig. 15: Plots of the distribution function for the energy associated with the cyclotron motion for three values of the average energy imparted to the ions by the r-f electric field.

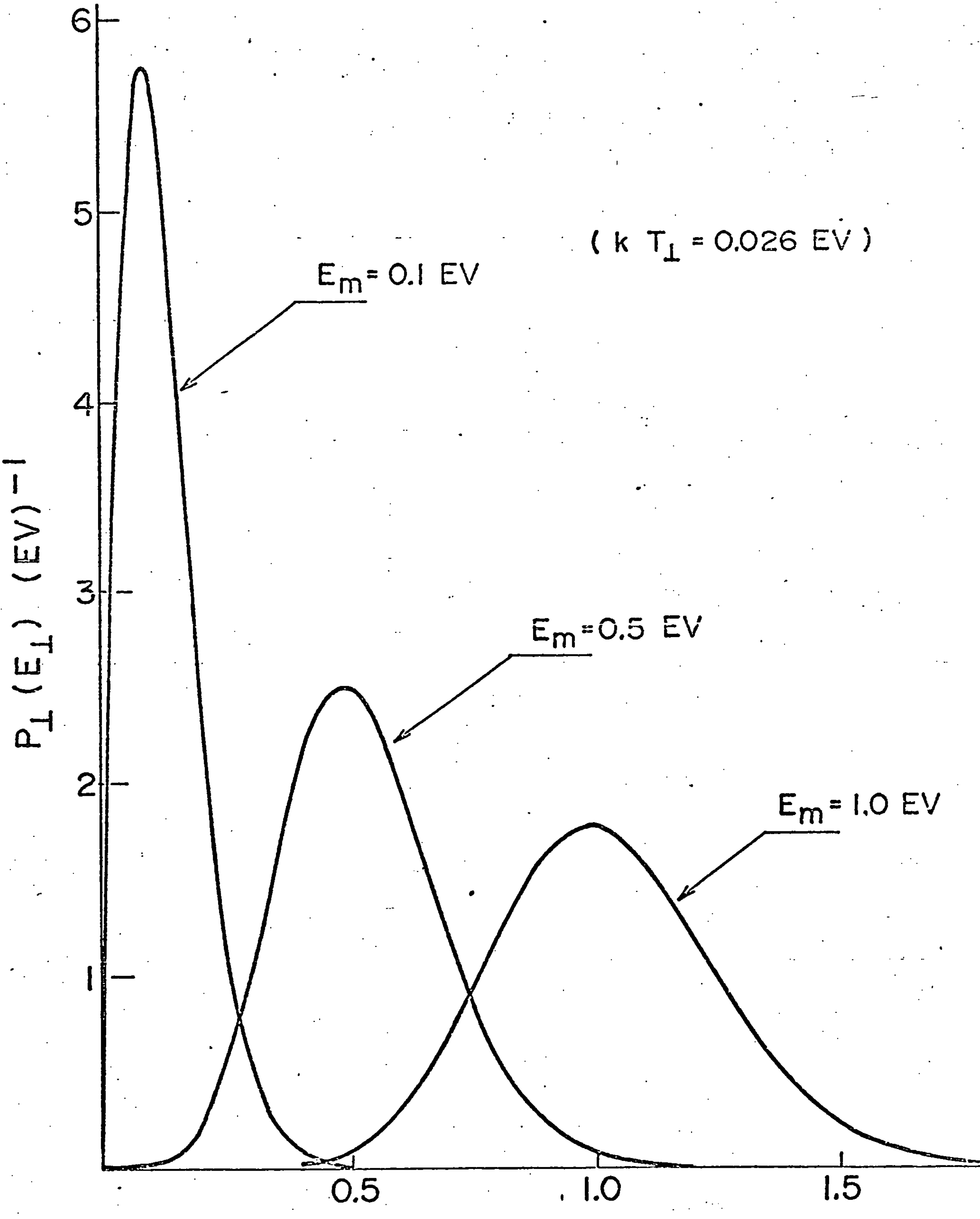

6
5
4
3
2
1
$P_\perp(E_\perp)$ (EV)$^{-1}$
(k $T_\perp$ = 0.026 EV)
E_m = 0.1 EV
E_m = 0.5 EV
E_m = 1.0 EV
0.5
1.0
1.5
$E_\perp$ (ev)

at half-maximum given by

$$[11.15] \qquad \frac{\Delta E_\perp}{E_m} = (8 \ln 2)^{\frac{1}{2}} \left(\frac{kT_\perp}{E_m}\right)^{\frac{1}{2}}$$

Thus, if an ensemble of ions is prepared with average energy E_m one hundred times greater than its initial energy spread $kT_\perp$, the fractional width of the final distribution is predicted to be $\simeq 0.235$, which is very high. We conclude that the standard method of exciting ions to higher energies in ICR spectrometers is not capable of giving good energy resolution on its own, even if the inhomogeneities in the r-f electric field are ignored. The reason for this is that ions produced with initial momentum components parallel to the r-f electric field are speeded up, while those with anti-parallel components are slowed down. Since the method of changing the ion energies involves the acceleration of the ions for a fixed time, the initial energy spread is amplified. By contrast, in those systems in which the change in ion energy is produced by passing the ions across a given potential difference, all the ions acquire the same change of energy regardless of the initial state.

Effect of trap oscillations:

An ion produced at position z in the trap with a momentum component P_z such that $P_z^2 = 2m\varepsilon_\parallel$ will oscillate between $\pm z_m$ given by

$$[11.16] \qquad V(z_m) = V(z) - V(0) + \varepsilon_\parallel \equiv V + \varepsilon_\parallel$$

In the harmonic approximation (Assumption 2), the kinetic energy of such an ion is given by

[11.17] $$E_{\parallel} = (V+\varepsilon_{\parallel})\sin^2\theta_o \quad , \theta_o = \omega_T t$$

Then, the kinetic energy distribution function for ions produced with given potential energy V and longitudinal kinetic energy $\varepsilon_{\parallel}$ is given by

[11.18] $$P(E_{\parallel},V,\varepsilon_{\parallel}) = \frac{P(\theta_o)}{\left|\left(\frac{\partial E_{\parallel}}{\partial \theta_o}\right)_{V,\varepsilon_{\parallel}}\right|} = \frac{1}{\pi(E_{\parallel})^{\frac{1}{2}}(V+\varepsilon_{\parallel}-E_{\parallel})^{\frac{1}{2}}}$$

where we have used the normalized distribution function for

[11.19] $$P(\theta_o) = \frac{2}{\pi} \qquad 0 \leq \theta_o \leq \frac{\pi}{2}$$

If the ions are produced with equal a priori probability in each interval dz, the probability g(V)dV that an ion is produced with potential energy between V and V + dV is given by

[11.20] $$g(V) = \frac{1}{2V_o^{\frac{1}{2}}V^{\frac{1}{2}}}$$

for the harmonic potential (Assumption 2)

[11.21] $$V(y,z) - V(y,o) = \left(\frac{2z}{a}\right)^2 V_o, \quad -\frac{a}{2} \leq z \leq \frac{a}{2}$$

where $V_o = V_T - V(y,o)$.

Averaging over all values of V in a manner which implicitly assumes that $\varepsilon_{\parallel} << V_o$, we obtain

$$[11.22] \qquad P(E_{\parallel},\varepsilon_{\parallel}) = \int_{V_1}^{V_o} P(E_{\parallel},V,\varepsilon_{\parallel})g(V)dV$$

$$= \frac{1}{\pi E^{\frac{1}{2}} V_o^{\frac{1}{2}}} \ln \left[\frac{V_o^{\frac{1}{2}} + (V_o + \varepsilon_{\parallel} - E_{\parallel})^{\frac{1}{2}}}{|E_{\parallel} - \varepsilon_{\parallel}|^{\frac{1}{2}}}\right] \quad , \quad E_{\parallel} \leq V_o$$

where $V_1 = 0$ if $E_{\parallel} \leq \varepsilon_{\parallel}$, and $V_1 = E_{\parallel} - \varepsilon_{\parallel}$ if $E_{\parallel} \geq \varepsilon_{\parallel}$.

Finally, the distribution function $P_{\parallel}(E_{\parallel})$ is obtained by averaging [11.22] over the initial energy distribution given by [11.3]. The result can be written in the form

$$[11.23] \qquad P_{\parallel}(E_{\parallel}) = \int_{0}^{\infty} P(E_{\parallel},\varepsilon_{\parallel})\, P_{o\parallel}(\varepsilon_{\parallel})\, d\varepsilon_{\parallel}$$

$$= \frac{1}{\pi^{3/2}(kT_{\parallel}V_o)^{\frac{1}{2}}} \int_{0}^{\infty} \frac{dv}{v^{\frac{1}{2}}}\, e^{-\frac{E_{\parallel}}{kT_{\parallel}}v} \ln \left[\frac{V_o^{\frac{1}{2}} + \{V_o + E_{\parallel}(v-1)\}^{\frac{1}{2}}}{E_{\parallel}^{\frac{1}{2}}|1-v|^{\frac{1}{2}}}\right]$$

One energy region of interest for the case $V_o >> kT_{\parallel}$ is the region $E_{\parallel} >> kT_{\parallel}$. For this case, Eq. [11.23] reduces, approximately, to [11.22] with $\varepsilon_{\parallel} = 0$. A plot of this distribution of energies is given in Figure 16 Although $P(E_{\parallel},0)$ diverges as $E_{\parallel} \rightarrow 0$, this logarithmic singularity is integrable and thus presents no problem when $P(E_{\parallel},\varepsilon_{\parallel})$ is used to calculate an ensemble average. Included in Fig. 17 as an insert is a plot of $f_3(E') = \int_0^{E'} P(E_{\parallel},0)dE_{\parallel}$, which is the fraction of ions having $E_{\parallel} \leq E'$.

In the first part of this section we have derived a result for the distribution of ion kinetic energies due to the influence of the r-f electric

Fig. 16: Plots of the distribution function $P(E_{\parallel},0)$ for two different values of the trapping well depth, V_o. The insert shows $f_3(E')$, the fraction of ions with energy $E \leq E'$.

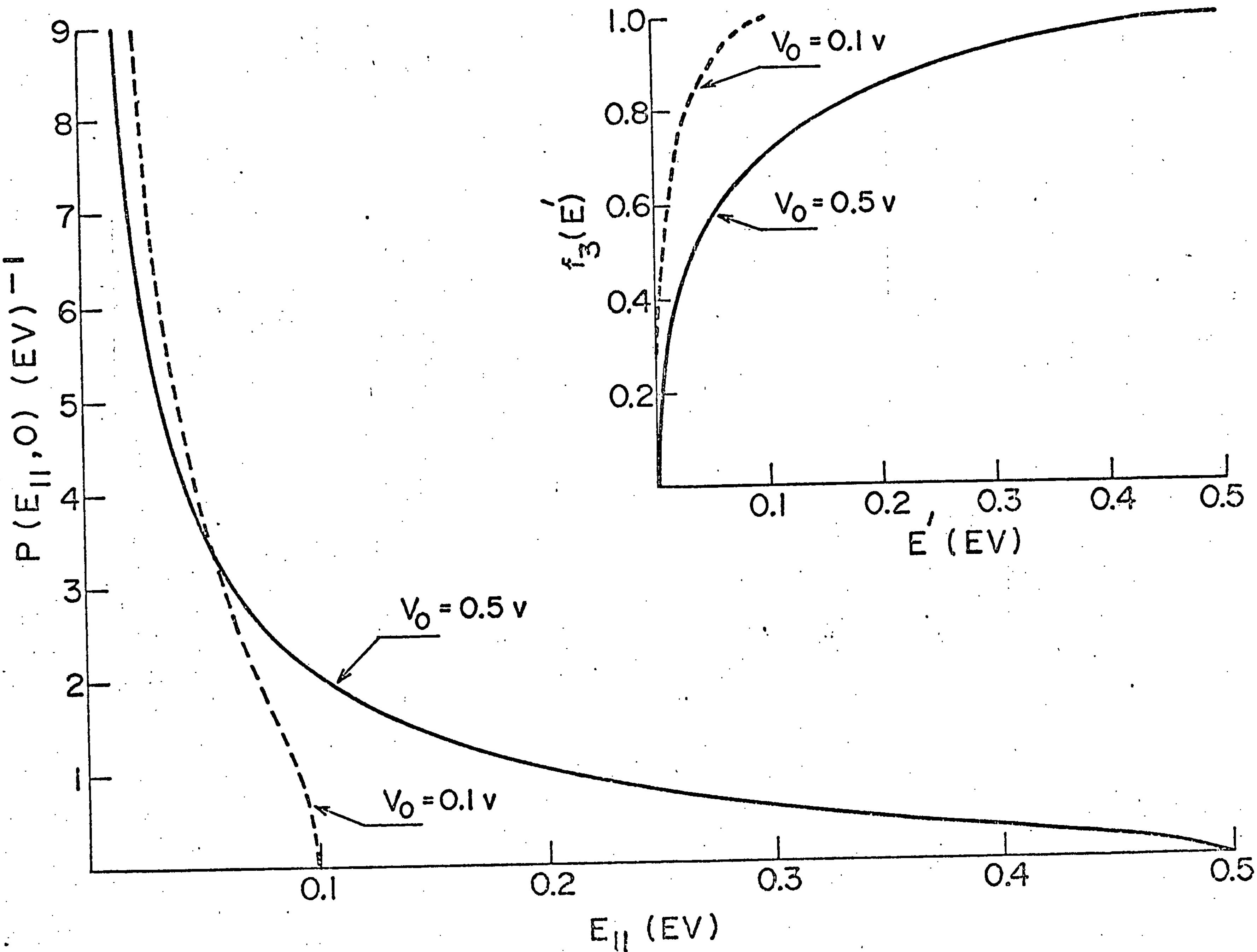
9
8
7
6
5
4
3
2
1
P (E₁₁,0) (EV)⁻¹
0.1
0.2
0.3
0.4
0.5
E₁₁ (EV)
V₀ = 0.5 v
V₀ = 0.1 v
1.0
0.8
0.6
0.4
0.2
f₃(E′)
0.1
0.2
0.3
0.4
0.5
E′ (EV)
V₀ = 0.1 v
V₀ = 0.5 v

field under resonant conditions, while in the second part the distribution of energies due to the trapping oscillations has been calculated when $kT_{\parallel} << V_o$. Often, the ions are produced with an average kinetic energy $\gtrsim V_o$. Under such conditions, it is clear that a certain fraction of the ions will escape from the trap. A calculation of this fraction is given in Section 15.

12. Experimental Apparatus: Ionisation by Electron Bombardment

The ICR device used in these experiments is divided into three separate drift regions as is common practice [Clow and Futrell, 1970]. Ions are produced in the source region by an electron beam which traverses the cell in the direction of the magnetic field (-z direction; see Fig. 1) after passing through a small hole, about 0.003 m. in diameter, situated in the centre of the source trapping plate. Next to the source region is a reaction region through which the ions drift unperturbed by the detection rf or the ionising electron beam. The purpose of this region is to decouple ion production in the source from the detection rf. In the third region, the analyser, ions are detected by rf excitation of their quasi-cyclotron oscillation using conventional resonance techniques [Robinson, 1958]. The drift plates in the analyser also serve as the tank circuit of a Robinson oscillator of standard design with rf level continuously variable over a range from 5 to 200 mv. peak to peak. Best ICR signals were obtained with the oscillator connected to the bottom drift plate, all other electrodes being at ac ground.

The drift and trapping plates are 0.014 m. and 0.025 m. apart, respectively, in all regions. The source, reaction, and analyser region are 0.025, 0.035 and 0.061 m long in the direction of the ions' drift (x-direction, see Fig. 1) and are electrically insulated from one another by thin mica strips. Likewise the trapping electrodes in the source are separated from the trapping plates which serve both the reaction and analyser regions, so that the source trapping potential may be varied independently of that in the other two regions. All electrodes are constructed of electropolished stainless steel about 0.001 m.thick and held in position by G.E. lucalox polycrystalline alumina rods.

The ionising electrons are produced by thermionic emission from a hot wire filament, mounted in a boron nitride holder, and are accelerated through a collimating grid and across the cell by negative biasing on the filament. The negatively biased grid is a thin plate, about 5×10^{-4} m. thick, having a 0.002 m.diameter hole through which the electrons pass before entering the cell. A schematic diagram of the filament mount and grid is shown in Fig. 17. A similarly constructed holder containing the electron collector is mounted on the trap opposite the filament mount. Both filament and collector mounts are supported on the lucalox rods which hold the cell electrodes in place. Wire mesh grids, 67% transparent, are spot welded across the holes in the trap, through which electrons enter and leave the cell, to prevent penetration of electric fields associated with the filament, grid and collector voltages. Tungsten, iridium, and rhenium wire filaments of varying diameters were used in the experiments reported here, and the results were found to be independent of the type of metal used.

The large static magnetic field B constrains electrons to small cyclotron radii at normal electron energies (15 to 100 ev). Furthermore B minimizes secondary electron emission due to electrons striking metal cell electrodes [Farnsworth, 1925] and therefore the electron beam should be relatively well defined spatially near $y = 0$ in the cell. From the dimensions of the filament and grid aperture, we expect the electron beam to be about 1×10^{-4}m. thick and about 0.002 m. wide initially and to diverge slightly due to coulombic repulsion as it crosses the cell.

Fig. 17: A schematic diagram, to scale, of the filament and its mount, with the grid plate not shown. Further construction details are given in the text. The electron beam is indicated by the arrow.

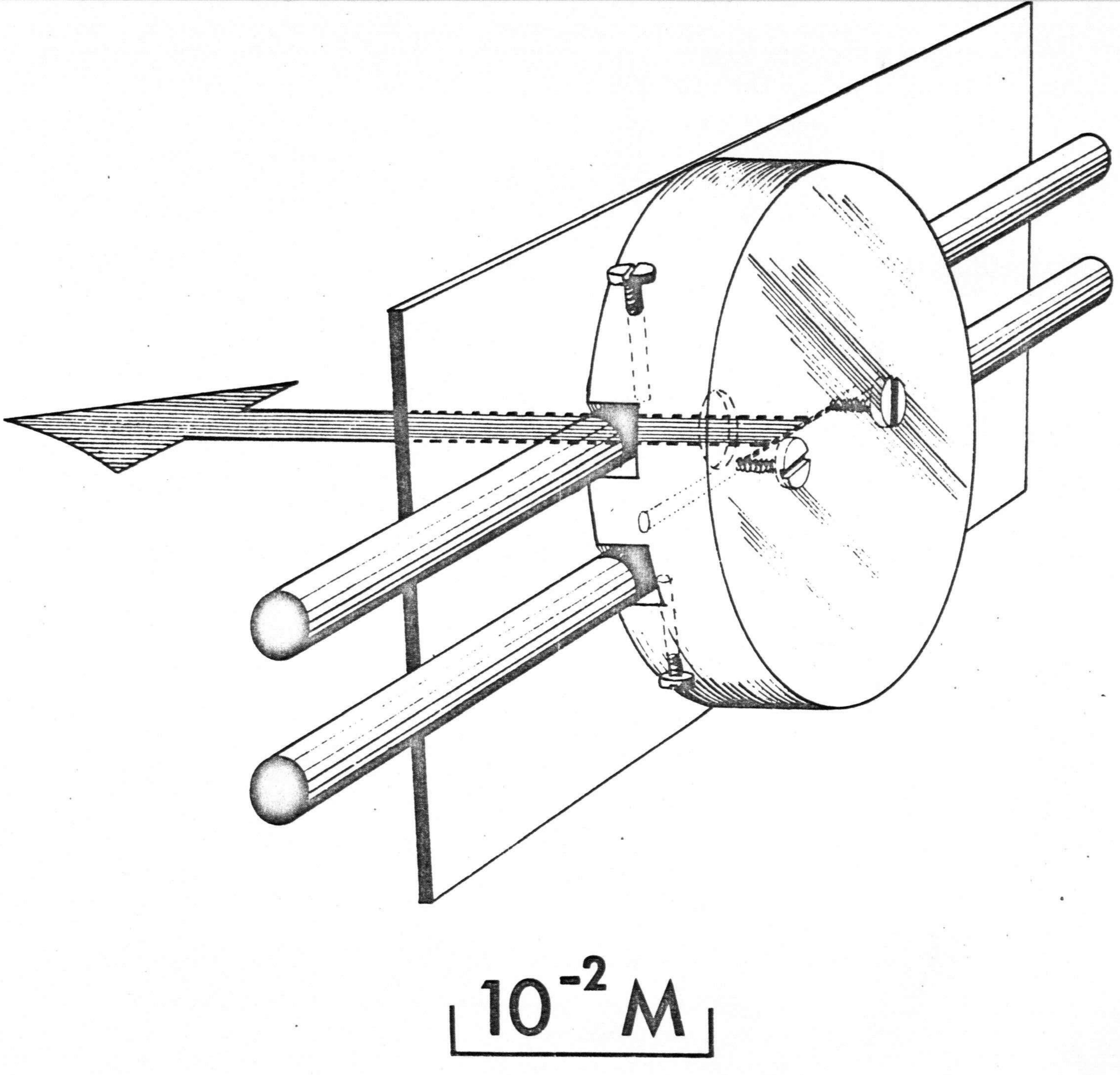
10^{-2} M

A 15-inch Magnion electromagnet with a 2¼ inch gap was used. At about 0.9 Tesla the magnetic field gradient across the ICR cell was less than 10^{-3} Tesla/m. With this homogeneity ICR line widths of about 8×10^{-5} Tesla were observable. B was measured with an NMR proton probe or a rotating coil calibrated by the NMR probe, whichever was convenient. The system was evacuated by a cold trapped CVC-PMCS-4 oil diffusion pump to about 3×10^{-8} torr. Normal operating pressures, controlled by a variable leak valve, were about 3×10^{-6} torr, well within the collisionless regime for the ions under consideration.

The ICR experiment offers many different parameters for modulation in a phase sensitive detection scheme. Magnetic field, source drift potential and source trapping potential were all modulated at various stages of this work. The results were found to be independent of these modes of operation.

13. Effect of Electron Beam on ICR

In these experiments ion cyclotron resonance is monitored by fixing the detection oscillator frequency and sweeping through the resonance with B. In practice the ICR absorption intensity, line width and magnetic field at maximum signal B_{eff} are dependent on the trapping and drift potentials in the source, reaction and analysing regions. To simplify quantitative analysis we first consider the case in which the same trapping potential, V_T, and drift voltages, V_1 and V_2, on the top and bottom plates respectively, are used in all regions of the cell. If the cell potentials are different in the various cell regions they will be denoted by $[V_1]_{source}$, $[V_1]_{analyser}$, $[V_1]_{reaction}$ etc., but when all regions have the same electrode voltages the notation V_1 etc. will be used. With this notation the drift electric field results from the potential V_1-V_2 while the average potential in the cell is mainly determined by V_T and the average potential of the drift plates, $(V_1+V_2)/2$.

In Figs. [18] and [19] we show the variation of B_{eff} with V_1-V_2 and V_T respectively, from which it is clear that B_{eff} for Ar^+ ions is dependent on the electron beam current, I_e. The line width also exhibits a dependence on I_e. This is in agreement with Smith and Futrell (1973) who find that the residence times of the ions in the source are strongly dependent on the electron beam current. No dependence of B_{eff} or the line width on the grid or collector potentials is observed although we detect a slight dependence on electron energy at high currents.

The electron beam can influence the ions detected in the analyser in several ways. First we will discuss the effects of electron space charge

Fig. 18: The variation of B_{eff}, the magnetic field at which ICR occurs, with V_1-V_2 for several different ionising currents. The oscillator frequency was 346.16 kHz while $V_1+V_2 = 0$ and $V_T = 0.5$ volt.

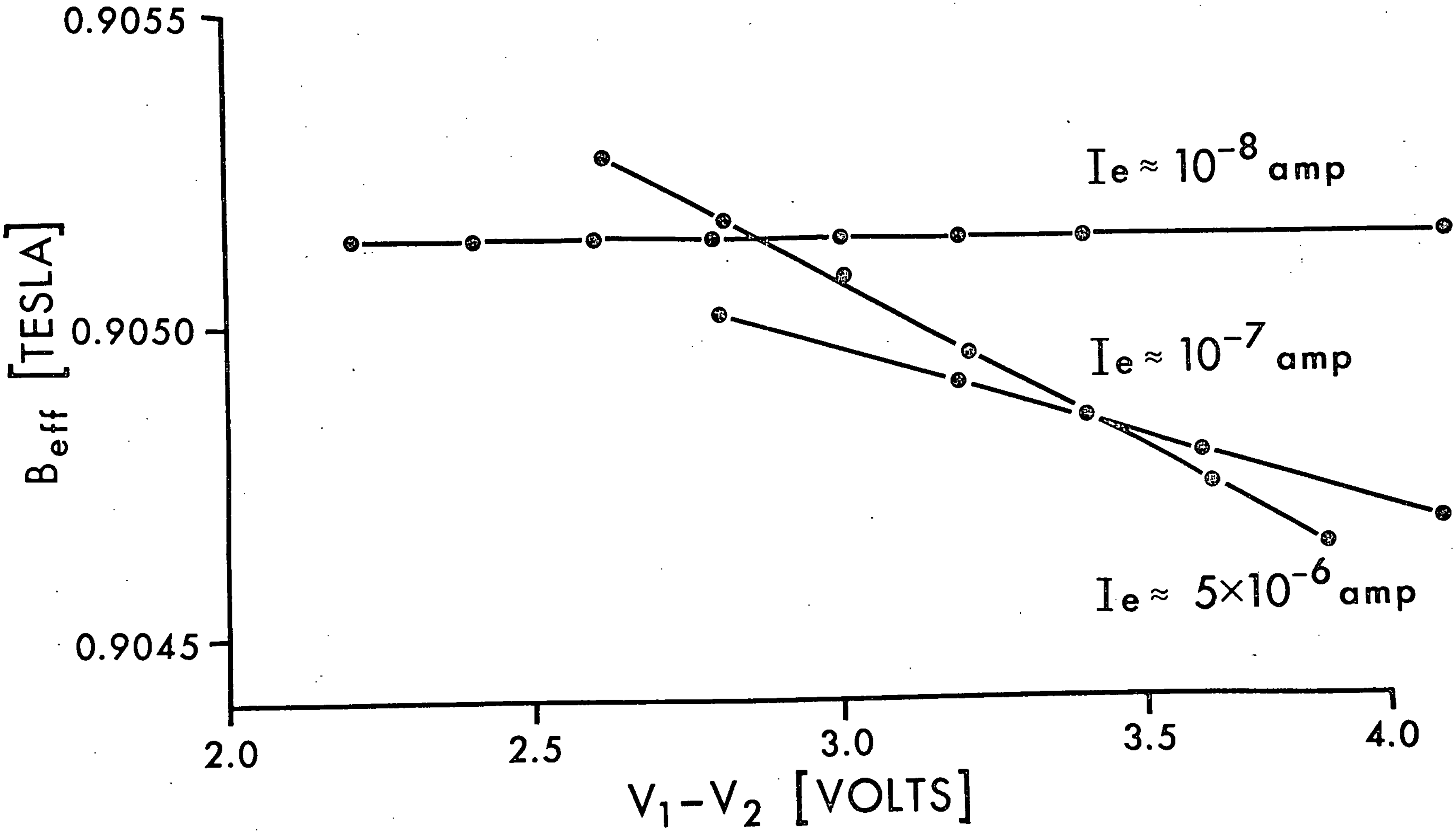
0.9055
0.9050
0.9045
B_{eff} [TESLA]
$I_e \approx 10^{-8}$ amp
$I_e \approx 10^{-7}$ amp
$I_e \approx 5\times10^{-6}$ amp
2.0
2.5
3.0
3.5
4.0
$V_1 - V_2$ [VOLTS]

Fig. 19: The variation of B_{eff} with V_T for several different electron beam currents. The oscillator frequency was 346.16 kHz, while $V_1+V_2 = 0$ and $V_1-V_2 = 1.0$ volt.

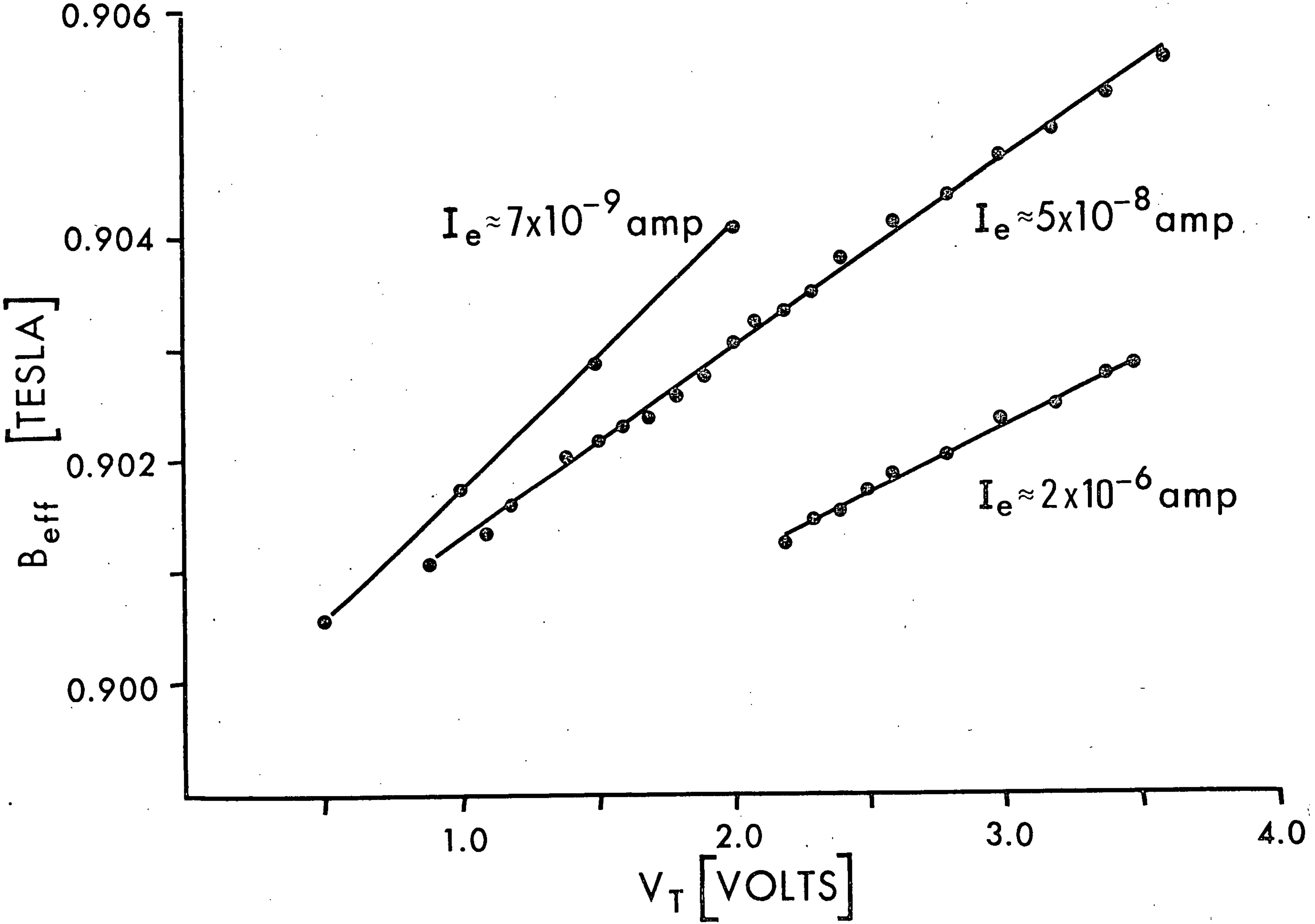
0.906
0.904
0.902
0.900
B_{eff} [TESLA]
1.0
2.0
3.0
4.0
V_T [VOLTS]
$I_e \approx 7\times10^{-9}$ amp
$I_e \approx 5\times10^{-8}$ amp
$I_e \approx 2\times10^{-6}$ amp

[Beauchamp, 1967; Woods et al, 1973]. Ions are produced uniformly across the z-axis of the cell near y = 0 (Fig. 1). The negative space charge depression due to the electron beam distorts the potential at which the ions are formed so that as positive ions leave the source where they are influenced by electrons they move downward in the cell in such a way as to conserve their average potential energy; that is, for our choice of coordinates positive ions move to negative values of y. In addition their amplitude of oscillation in the trap will be somewhat altered, but this will be discussed in Section 14. When the ions reach the analyser the effect of the electron beam is negligible but here instead of the ions being near y = 0, the centres of their quasi-cyclotron orbits are distributed about some average $\bar{y}$ satisfying the condition;

$$[13.1] \qquad [\langle V(\bar{y})\rangle]_{\text{analyser}} = [\langle V(0)\rangle]_{\text{source}} + \Delta$$

where Δ is the potential due to the electron beam and $\langle V(y)\rangle$ is the average potential energy of the ensemble, the average being performed first over one period of the trapping oscillation and then over all possible amplitudes of oscillation.

Thus the space charge of the electron beam alters the spatial distribution of ions which changes the average quasi-cyclotron frequency of the ions. If we interpret B_{eff} as corresponding to the average quasi-cyclotron frequency of the ion ensemble then

$$[13.2] \qquad B_{eff} = B + \frac{1}{2\omega_c} \left\langle \frac{\partial E_y}{\partial y} \right\rangle$$

as we have seen in Section 10. However in writing this equation, it must be emphasized that we

1) neglect the dependence of the line shape on the inhomogeneous rf electric field with which the ions are detected,
2) assume that the distribution of amplitudes z_m is not altered during the passage of the ions through the complicated potentials inside the cell,
3) assume that all ions have a common y coordinate,
4) assume that the quasi-cyclotron frequency and drift field of the average ion are equivalent to the ensemble average frequency and drift field respectively.

Equation [13.2] predicts a field dependent shift (to the first order) in the resonance field of the ion ensemble due to the electric field gradient inside the cell. The frequency of the tank circuit of the Robinson oscillator is also shifted by the dispersion which usually accompanies power absorption in these devices [Anders, 1967; Hughes and Smith, 1971]. This latter frequency shift varies rapidly in the vicinity of the ICR signal maximum, is a function of the number of ions in the cell and results in distorted line shapes. No such frequency pulling was observed in the experiments reported here, although shifts in the oscillator frequency as large as 15 hz have been detected in our laboratory and have been reported by others [Anders, 1967].

Because the spread in the ions' quasi-cyclotron frequencies due to their trapping oscillation is somewhat smaller than the width, in frequency units, of the ICR absorption as determined by the transit time of the ions through the analyser, it is often a good approximation to write,

$$B_{\frac{1}{2}} = \frac{5.566}{\omega_c \ell} |\langle E_y \rangle| \tag{13.3}$$

where $B_{\frac{1}{2}}$ is the full width at half maximum intensity of the absorption line. It is important to note that if we interpret the position y as the average y coordinate for the distribution of ions $y = \bar{y}$, then a knowledge of either B_{eff} or $B_{\frac{1}{2}}$ is sufficient to determine $\bar{y}$.

Eqs. [13.1], [13.2] and [13.3] may be used to discuss semi-quantitatively the dependence of B_{eff} on I_e shown in Figs. [18] and [19]. The space charge depression due to the electron beam has been estimated by Haeff [1939] as

$$[13.4] \qquad \Delta = -4.79 \times 10^4 \frac{I_e b}{W\sqrt{E_0}}$$

where W is the width of the beam, E_0 is the energy of the electrons in electron volts and Δ is the space charge potential in volts. Eq. [13.4] neglects complicated edge effects near the trapping electrodes [Morse and Feshbach, 1953; Pg. 1241] but is reasonably accurate near the cell centre. For cell potentials of $V_T = 0.5$v., $V_1 = 0.5$v. and $V_2 = -0.5$v. and an electron current $I_e \approx 5 \times 10^{-6}$amp. with $E_0 = 30$ev, Eqs. [13.1] and [13.4] give $\Delta \simeq 0.22$v., so that $\langle V(y=0)\rangle + \Delta = -0.09$v., taking $\langle V(0)\rangle$ from Fig. 12. This corresponds to a position $\bar{y} \approx -0.0033$m. in the analyser region of the cell and roughly accounts for the variation of B_{eff} with $V_1 - V_2$ and V_T of Figs. 18 and 19 respectively for $I_e = 5 \times 10^{-6}$ amp. Because of the approximate nature of Eq. [13.4] and uncertainties in measuring I_e, the space charge depression of the potential may be underestimated somewhat in the preceding discussion. However, with this qualification we see that the space charge depression can be neglected if $\Delta << \langle V(0) \rangle$ or when $I_e << 10^{-6}$ amp. for 30ev electrons. This means that B_{eff} should be independent of the electron current when I_e is less than about 10^{-7} amp. which is not normally the observed case with our system. The amplitude of oscillation in the trap z_m is also sensitive to the space charge through its dependence on z. This results in a non-uniform distribution of z_m's and y's for which the equations presented in this section are not precise. Also, stray electrons may be distributed over the electrodes if the cell surfaces are slightly dirty from pump oil vapour or similar residue. The potential inside the cell is then considerably distorted resulting in complicated non-uniform spatial distributions of the ions. We have, indeed, found that cleaning and baking the cell lessens the dependence of B_{eff} on I_e, but that precise agreement between experiment and the theory presented here occurs only at very low electron currents, even under best conditions.

As we have stated before, by measuring B_{eff} we are able to estimate $\bar{y}$ for the ion ensemble and since measurement of $B_{\frac{1}{2}}$ also yields $\bar{y}$, we have an independent check on the estimate obtained from B_{eff}. Fig. 20 shows $B_{\frac{1}{2}}$ as a function of V_1-V_2 with V_T and V_1+V_2 held constant. The solid curve is the variation of $B_{\frac{1}{2}}$ predicted by Eq.[13.3] using values of $\bar{y}$ obtained from the B_{eff} versus V_1-V_2 curve which is shown by the insert in the bottom right hand corner of the figure. The dashed curve is obtained from Eq.[13.3] assuming a constant electric field inside the cell; i.e., $\langle E_y \rangle = (V_1-V_2)/b$ [Beauchamp and Armstrong; 1969]. Fig. 21 exhibits the variation of B_{eff} with V_T when V_1 and V_2 are held constant. Here the solid line shows B_{eff} calculated from $B_{\frac{1}{2}}$ ($B_{\frac{1}{2}}$ is shown in the insert) and the dashed line is that predicted by Beauchamp and Armstrong [1969]. In both Figs.[20] and [21] the agreement between theory and

Fig. 20: The variation of the ICR line width, $B_{\frac{1}{2}}$, with V_1-V_2 for $V_T=0.5$ volt and $V_1+V_2 = 0$ in all regions of the cell. The solid line is the theoretical line width predicted by Eq. [3.6] while the dashed line is the line width predicted by assumption of a constant electric field, $E_y=(V_1-V_2)/b$. The insert shows the variation of B_{eff} with V_1-V_2 from which the solid line was obtained. In this experiment the electron current was 4.5×10^{-9} amp. with a mean electron energy of about 30 ev. and an oscillator frequency of 329.51 kHz.

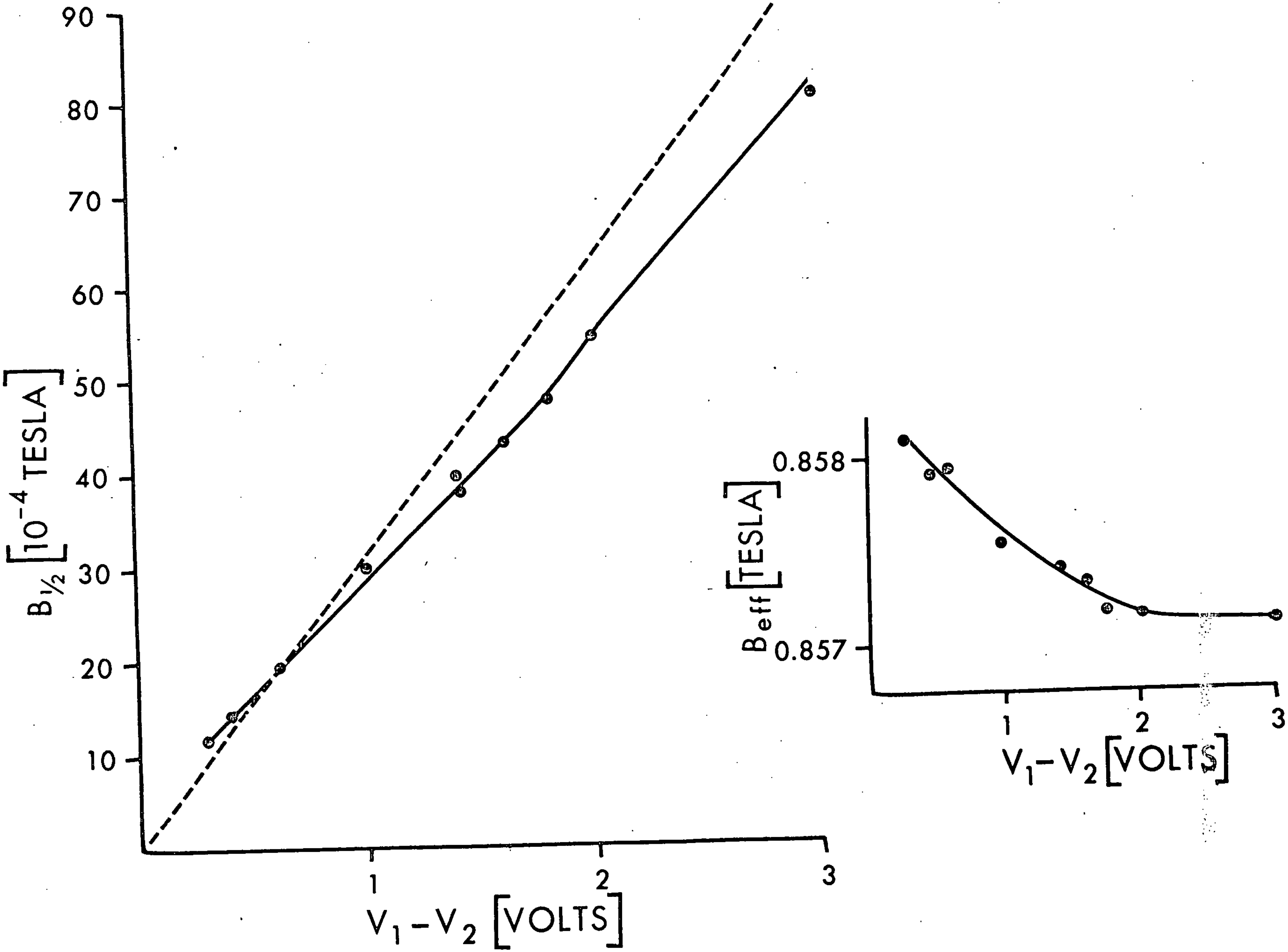
$B_{1/2}$ [10^{-4} TESLA]
90
80
70
60
50
40
30
20
10
1
2
3
$V_1 - V_2$ [VOLTS]
B_{eff} [TESLA]
0.858
0.857
1
2
3
$V_1 - V_2$ [VOLTS]

Fig. 21: The variation of B_{eff} with V_T showing the behavior predicted from measurement of the line width (solid curve) and that predicted by Beauchamp and Armstrong [1969] (dashed line). In this experiment the electron current was 2.3×10^{-8} amp. In all drift regions of the cell $V_1-V_2 = 1.0$ v. and $V_1+V_2 = 0$. The oscillator frequency was 329.54 kHz.

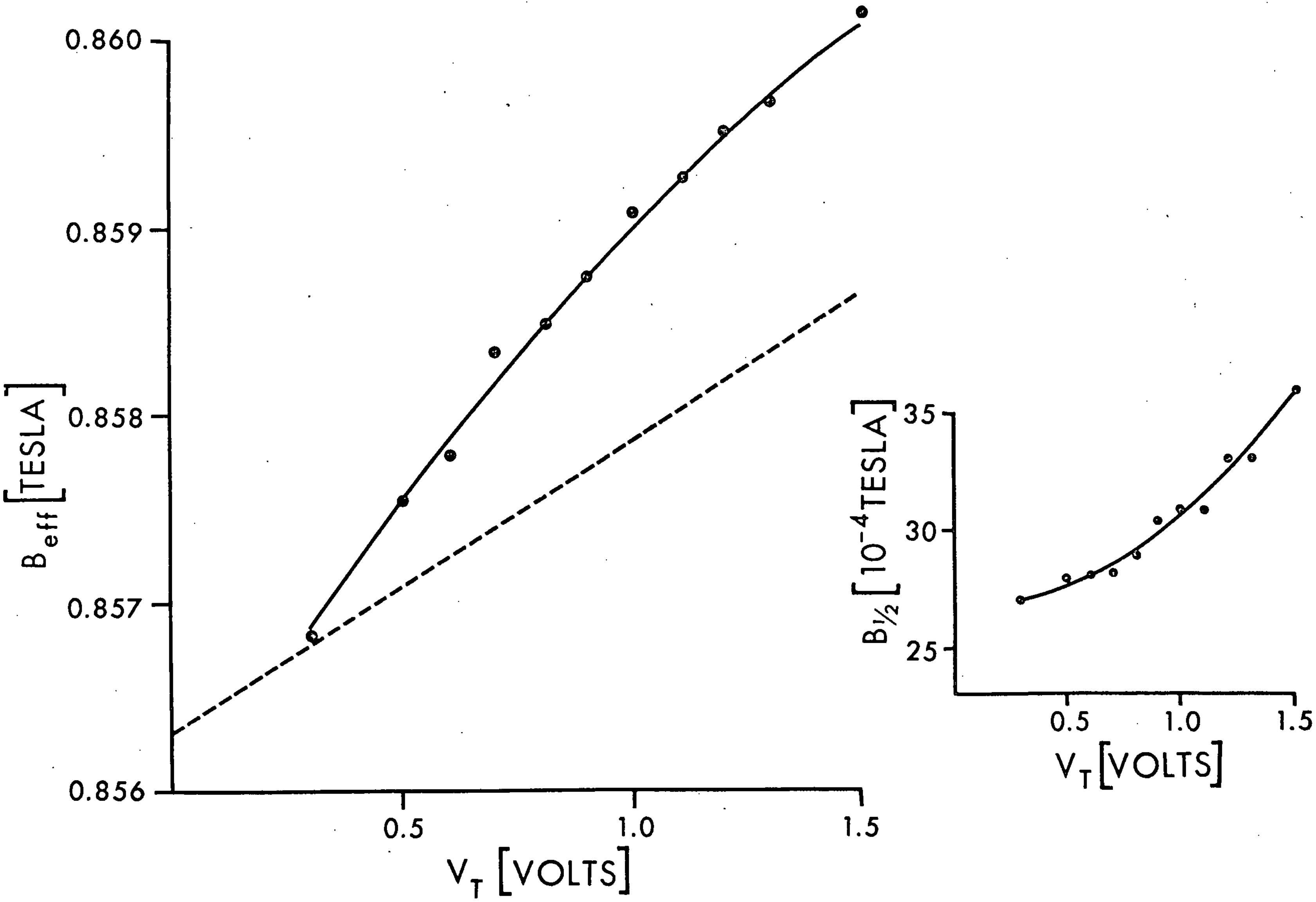
0.860
0.859
0.858
0.857
0.856
B_{eff} [TESLA]
0.5
1.0
1.5
V_T [VOLTS]
35
30
25
$B_{1/2}$ [10^{-4} TESLA]
0.5
1.0
1.5
V_T [VOLTS]

experiment is quite good. We have therefore demonstrated the validity of Eq. [13.2] and [13.3] in the low current regime when the harmonic approximation for the periodic trapping oscillation is used to obtain the motionally averaged electric field and its gradient with respect to y.

The spatial distribution of the ions in the ICR cell is altered by the electron beam, and this is manifested by a dependence of B_{eff} and $B_{\frac{1}{2}}$ on I_e. Measurement of B_{eff} as a function of V_1-V_2 and/or V_T may be used to estimate the spatial distribution of the ions. If there is no space charge depression of the potential in the source and $\bar{y} \simeq 0$, B_{eff} is independent of V_1-V_2 (Fig.13). For a cell with geometry a = 0.025 m. and b = 0.014 m., B_{eff} varies linearly with V_T having a slope of 0.5242 κ/ω_c (10^{-4} tesla/volt) when $\bar{y} \simeq 0$ in the analyser. These values differ somewhat from the results of Beauchamp and Armstrong [1969] since a realistic potential for the ICR geometry has been used to take account of the trapping oscillations.

14. Control of the Ions' Position in the Analyser

In the preceding section we considered the variation of $B_{\frac{1}{2}}$ and B_{eff} with V_T and V_1-V_2 when the potentials on the drift and trapping plates were the same in all three regions of the cell. In some experimental situations it may be advantageous to operate the ICR cell with different electrode potentials in the various cell regions. However, it is important to note that changing the cell potentials can alter the spatial distribution of the ions in the cell and thus alter their average drift time through the apparatus. In this section we wish to show how the position of the ions along the y-direction in the analyser can be controlled by adjustment of the drift and trapping potentials in the source. Once again $B_{\frac{1}{2}}$ and B_{eff} will be used to estimate the ions average position $\bar{y}$.

As mentioned previously the drift electric field results from V_1-V_2 while the average potential of the drift plates is $(V_1+V_2)/2$ so the average potential of the source region may be adjusted with either $[V_T]_{source}$ or $[V_1+V_2]_{source}$. When an ion moves from the source to an analyser with a different set of electrode potentials, its new amplitude of trapping oscillation and position y in the analyser depends on the nature of the transition between the two regions. There are two limiting cases, a sudden transition and an adiabatic one. In the sudden transition both z_m and the potential $V(y,z_m)$ remain constant, (see Eqs. [9.2] and [9.3]) but for most cases of interest in ICR, the transition between two regions of differing electrode potentials is nearly adiabatic; that is to say the ions undergo several trapping oscillations during the transition. For this case the ratio of the z_m's before and after the transition is equal to the fourth root of the ratio of the trapping well depth before and after the transition. This change in the amplitude of oscillation in the trap is not a particularly drastic one, being dependent on the fourth root of the cell potentials, so it is often a good approximation to ignore any change in the levels of oscillation and consider only the change in $\bar{y}$ via Eq.[13.1]. However we must proceed with caution in using this approach, since, for example, not only does $\bar{y}$ of the ion swarm change during a transition but so does the distribution of y's. In particular, ions with large levels of oscillation will undergo a larger change in y than those with small z_m's.

Ions are produced in the source region with $\bar{y} \approx 0$, where the amplitude averaged potential $\langle V(y)\rangle$ is independent of V_1-V_2 (Fig.12) and hence the spatial distribution of the ions should be independent of $[V_1-V_2]_{\text{source}}$ if the other cell potentials are not altered. Therefore, B_{eff} and $B_{\frac{1}{2}}$ will also be independent of $[V_1-V_2]_{\text{source}}$. This is verified in Fig. 22 where the upper curve shows B_{eff} versus $[V_1-V_2]_{\text{source}}$ with other cell potentials:

$$[V_1+V_2]_{\text{source}} = [V_1+V_2]_{\text{analyser}} = [V_1+V_2]_{\text{reaction}} = 0$$

$$[V_T]_{\text{source}} = [V_T]_{\text{reaction}} = [V_T]_{\text{analyser}} = 0.5 \text{ v}$$

and $$[V_1-V_2]_{\text{analyser}} = [V_1-V_2]_{\text{reaction}} = 1.0 \text{ v.}$$

Also shown in Fig. 22 is the result of varying V_1-V_2 in all regions of the cell for the same electron current. As in Figs. 18 and 20 the variation of B_{eff} with V_1-V_2 results from both a spatial rearrangement

Fig. 22: A comparison of B_{eff} versus $[V_1-V_2]_{source}$ and B_{eff} versus V_1-V_2.

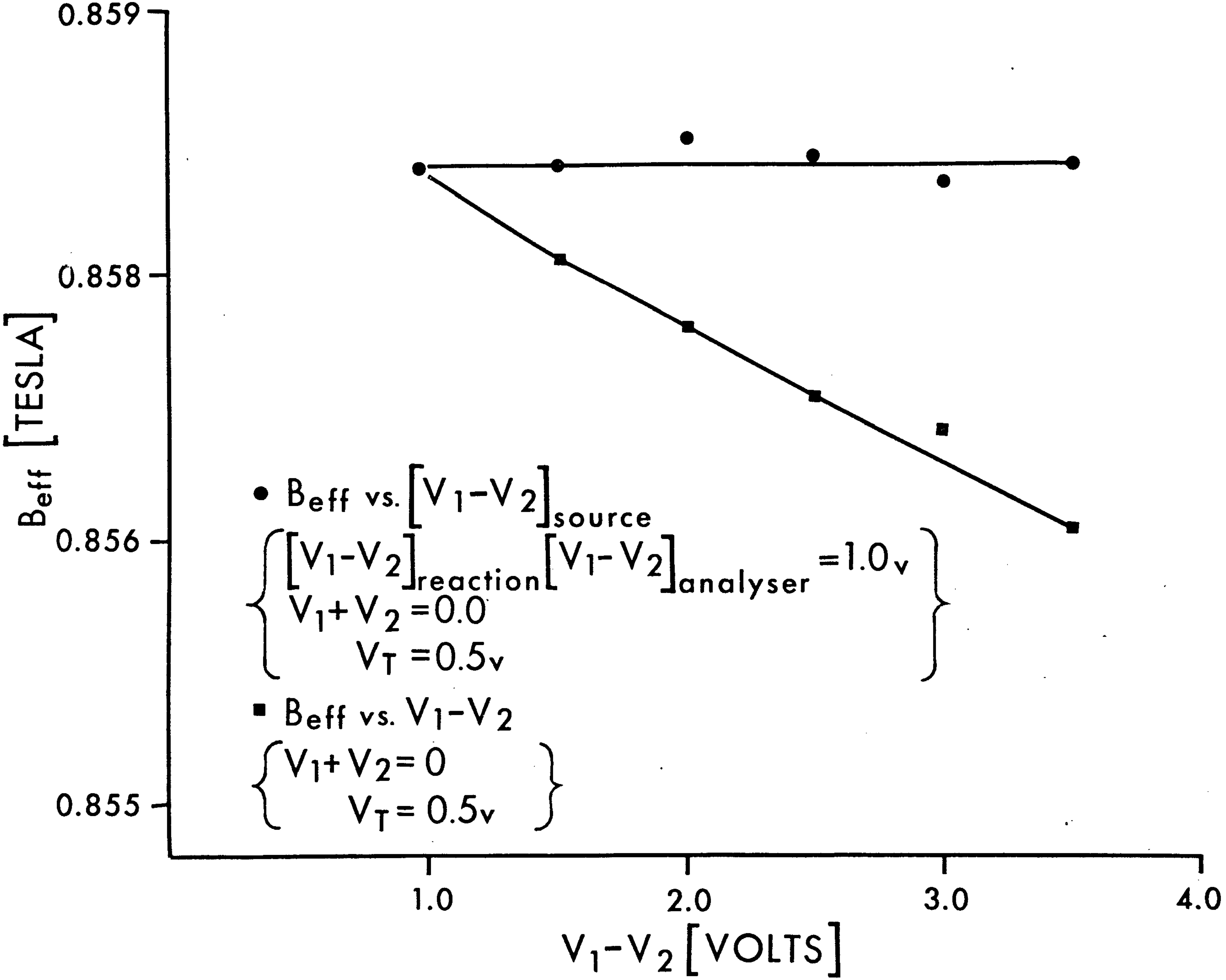
0.859
0.858
0.856
0.855
B_{eff} [TESLA]
1.0
2.0
3.0
4.0
V_1-V_2 [VOLTS]
● B_{eff} vs. $[V_1-V_2]_{source}$
$[V_1-V_2]_{reaction}[V_1-V_2]_{analyser}=1.0v$
$V_1+V_2=0.0$
$V_T=0.5v$
■ B_{eff} vs. V_1-V_2
$V_1+V_2=0$
$V_T=0.5v$

of the ions and a local variation of the motionally averaged electric field gradient with $[V_1-V_2]_{analyser}$ which causes a shift of the quasi-cyclotron frequency for off-centre ($y \neq 0$) ions.

Fig. 23 shows the dependence of B_{eff} on $[V_T]_{source}$ while the insert shows $B_{\frac{1}{2}}$ versus this potential. Increasing $[V_T]_{source}$ while keeping all other electrode potentials constant, forces the ions to more positive y's in the analyser hence decreasing both the amplitude averaged electric field and electric field gradient of the ensemble. This accounts for the decrease in both $B_{\frac{1}{2}}$ and B_{eff} with increasing $[V_T]_{source}$. Fig. 24 shows $\bar{y}$ versus $[V_T]_{source}$ estimated from B_{eff} in Fig. 23.

Fig. 25 shows $B_{\frac{1}{2}}$ versus $[V_1+V_2]_{source}$ and the insert shows B_{eff} versus this same parameter. Proceeding as in section 13 we use the measured values of B_{eff} to obtain an estimate of $\bar{y}$ from Eq. [13.2] and then use Eq. [13.3] to obtain $B_{\frac{1}{2}}$ shown by the solid line in the figure. Agreement between the measured and predicted values of $B_{\frac{1}{2}}$ is quite good at positive values of $[V_1+V_2]_{source}$ but is very poor for $[V_1+V_2]_{source}<0$. There are two possible explanations for this behavior. Firstly for negative $[V_1+V_2]_{source}$ the ions are forced to negative y's in the analyser where the potential is no longer harmonic and the approximation, $z(t) = z_m \cos\omega_T t$ is not a valid one. If this is the case then we cannot use the harmonic approximation to evaluate the averages required by Eqs. [13.2] and [13.3] and a tedious analysis of the line shape is required to obtain a reliable $\bar{y}$. A second possibility is that in moving towards the negative drift plates the ions undergo a transition to regions of higher trapping well depth. As we have already discussed this restricts their amplitude of oscillation in the trap since the well

Fig. 23: The effect of the source trapping potential on B_{eff} and $B_{\frac{1}{2}}$. The potentials in the other regions of the cell are given in the text. The solid curve shows B_{eff} calculated from $B_{\frac{1}{2}}$ which is shown in the insert. The electron current was 7.5×10^{-8} amp. while the oscillator frequency was 329.89 kHz.

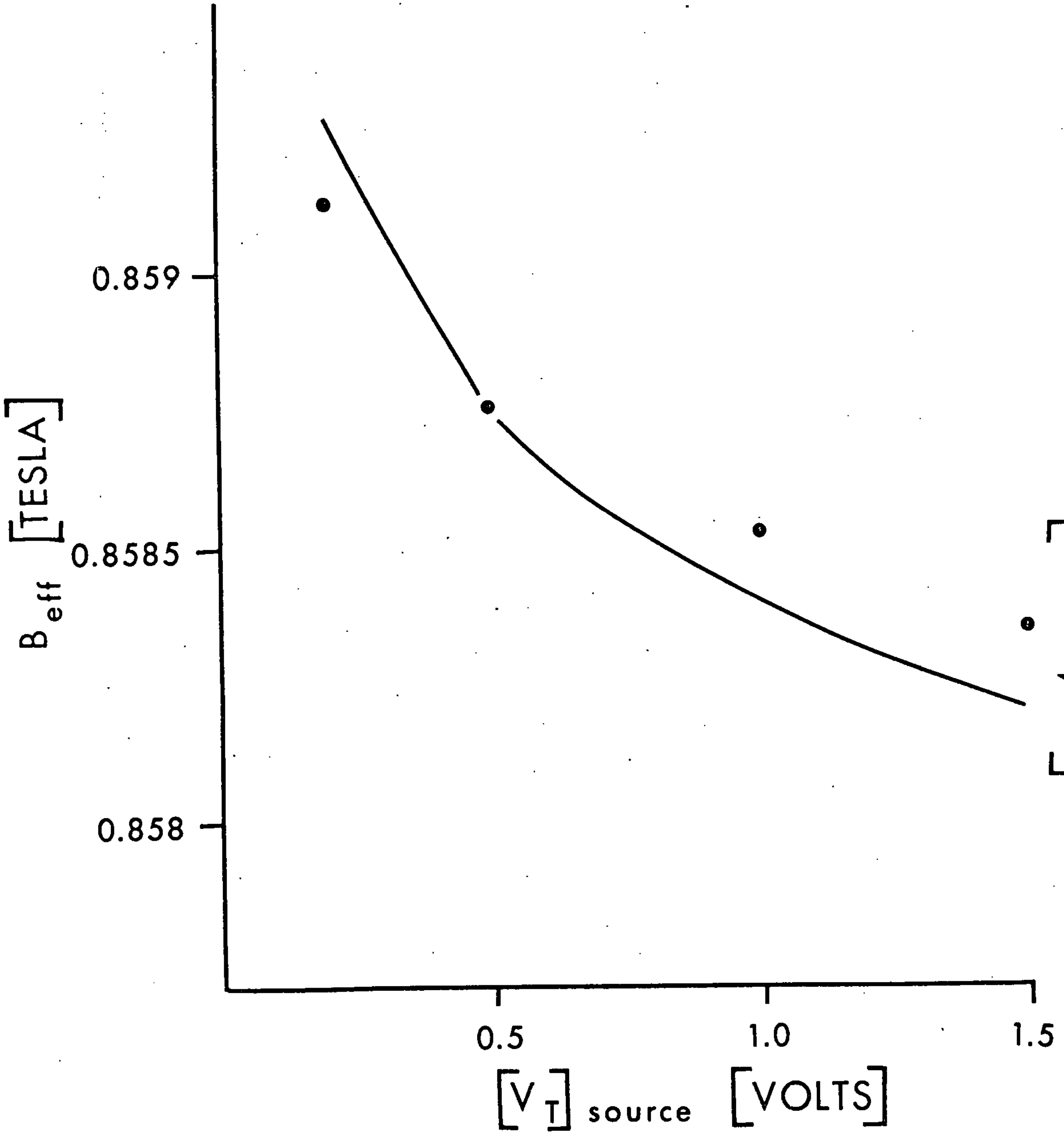
0.859
0.8585
0.858
B_{eff} [TESLA]
0.5
1.0
1.5
$[V_T]$ source [VOLTS]

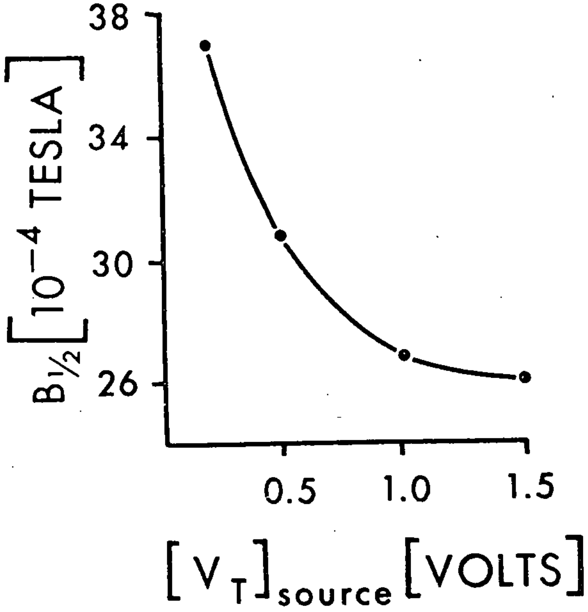
38
34
30
26
$B_{1/2}$ [10^{-4} TESLA]
0.5
1.0
1.5
$[V_T]_{source}$ [VOLTS]

Fig. 24: The variation of the average ion position in the analyser, $\bar{y}$, with the source trapping potential. In this case $\bar{y}$ was calculated from the line width, shown as a function of $[V_T]_{source}$ in Fig. 11.

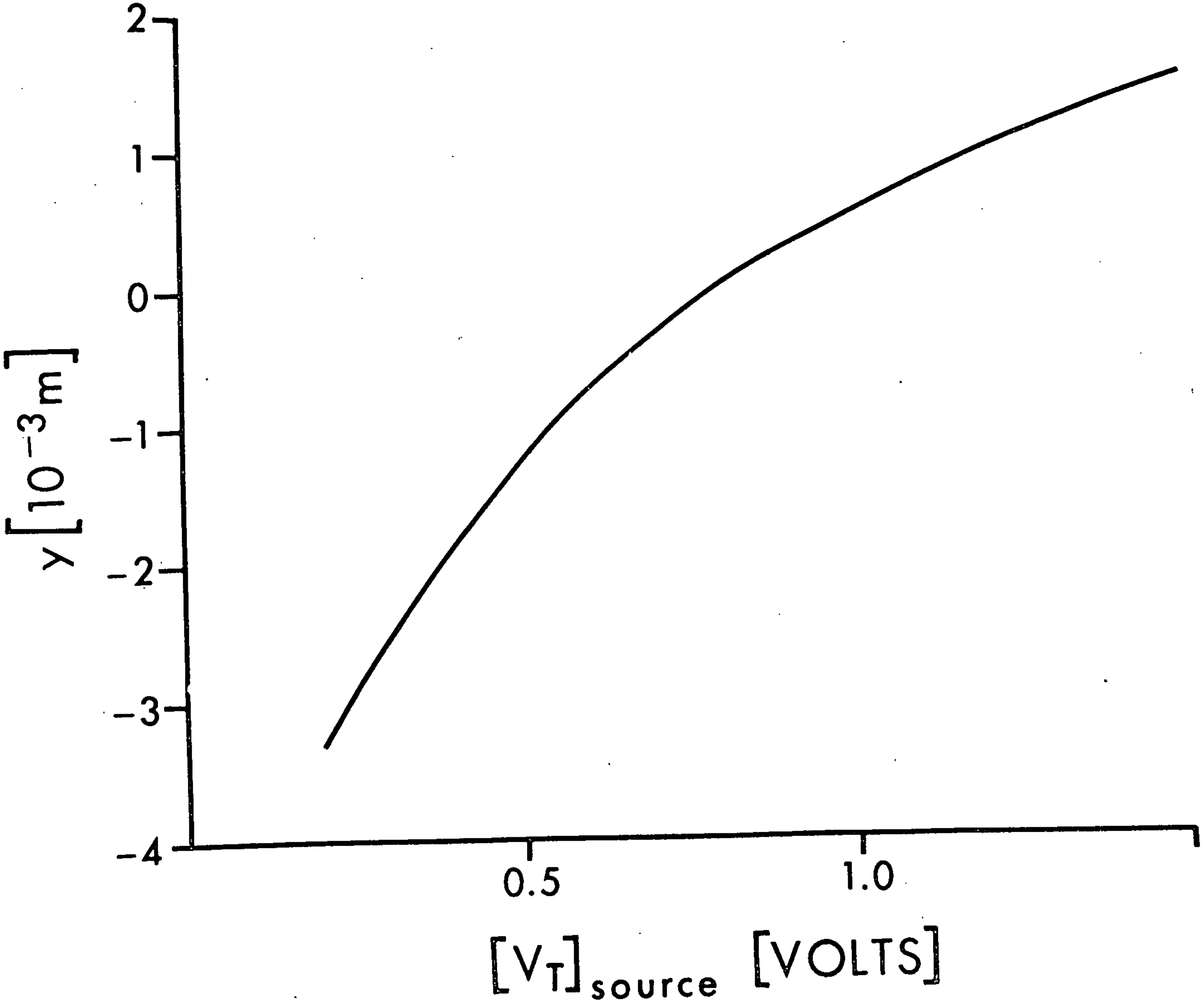
2
1
0
−1
−2
−3
−4
y [10⁻³m]
0.5
1.0
[V_T]_source [VOLTS]

Fig. 25: The dependence of $B_{\frac{1}{2}}$ and B_{eff} (insert) on $[V_1+V_2]_{source}$. The other cell potentials were:

$[V_1-V_2]_{analyser} = [V_1-V_2]_{reaction} = [V_1-V_2]_{source} = 1.0$ volt

$[V_1+V_2]_{analyser} = [V_1+V_2]_{reaction} = 0$

$[V_T]_{source} = [V_T]_{analyser} = [V_T]_{reaction} = 0.5$ volt.

The electron current was 7.5×10^{-8} amp. and the oscillator frequency was 329.89 kHz.

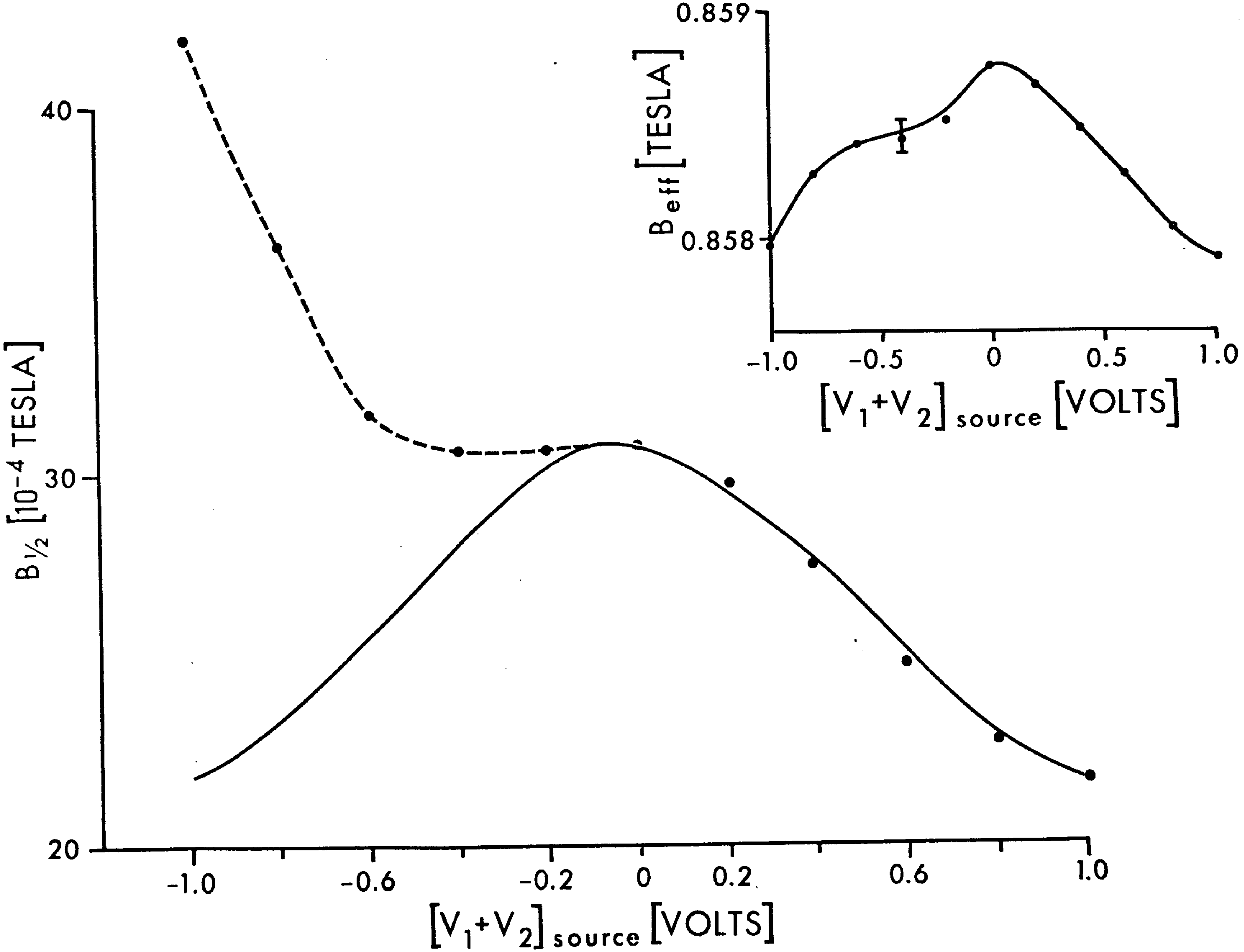
0.859
0.858
B_eff [TESLA]
-1.0
-0.5
0
0.5
1.0
[V_1+V_2]_source [VOLTS]
40
30
20
B_{1/2} [10^-4 TESLA]
-1.0
-0.6
-0.2
0
0.2
0.6
1.0
[V_1+V_2]_source [VOLTS]

depth increases with decreasing y. Indeed by restricting the range of averaging over z_m in Eqs. [13.2] and [13.3] we are able to obtain consistency between the measurements of B_{eff} and $B_{\frac{1}{2}}$ as shown by the dashed line in Fig. 13. However, in order to fit the measured values of $B_{\frac{1}{2}}$ and B_{eff} at $[V_1+V_2]_{source} = -1.0$v. we must choose $\bar{y} \simeq -0.0045$ m. and restrict z_m to values $\leq 0.1a$ which is considerably smaller than one would expect in the adiabatic transition limit. It is therefore likely that the agreement between the measurements of B_{eff} and $B_{\frac{1}{2}}$ implied by the dashed line is fortuitous and that the real truth of the matter lies in a combination of the two possibilities expressed above.

15. Determination of the Initial Distribution of Energy in the ICR System

The initial distribution of kinetic energies of ions formed by electron impact depends on the nature of the electronic transition from which the ions result. Ions formed by dissociation of molecules may have kinetic energies several hundreds of times greater than kT. This energy results from conversion of internal energy of the parent molecule into kinetic energy of the daughter particles. On the other hand ions formed by electrons from atoms or molecules without dissociation have kinetic energies very near to that of the corresponding neutral particles ($\simeq 3/2$ kT) due to the small ratio of the electron mass to the atomic mass. Those ions formed in the ICR cell with initial energies very much greater than the trapping well depth may escape from the system, but since the ions are formed with equal à priori probability in each dz in the range $-a/2 \leq z \leq a/2$ and the potential distribution inside the cell is known, the fraction of ions retained by the traps may be calculated. We now wish to calculate this fraction which we will denote by f.

An ion from a mono-energetic ensemble of ions whose initial velocity makes an angle θ with the z axis has an energy

$$[15.1] \qquad \varepsilon_{\parallel} = \frac{1}{2} m v_z^2 = E \cos^2\theta$$

associated with its z motion. We assume that the potential V(z) in the z direction is well represented by the approximation of Section 11

$$V(z) = V(0,0) + V_o(2 z/a)^2$$

where $V_o = V_T - V(0,0)$ is the trapping well depth. Further, if the first 3 assumptions outlined in Section 11 are valid, then those ions that are formed with $\varepsilon_{\parallel} \geq V_o - V(z)$ will hit the cell walls and presumably be lost from the system. It is therefore possible to define a cut-off angle by

$$[15.2] \qquad \cos\theta_c = \left(\frac{V_o - V(z)}{E}\right)^{\frac{1}{2}}$$

so that those ions with $\theta < \theta_c$ escape from the trap. Those ions with $\theta > \theta_c$ will remain in the cell if the magnetic field in the $-z$ direction is sufficiently large to ensure that the ions' cyclotron radii are much less than b/2. If the initial velocity distribution is isotropic, then the probability of having θ between θ and $\theta + d\theta$ in the interval $0 \leq \theta \leq \pi/2$ is $\sin\theta d\theta$. Note that since motion in the +z direction is equivalent to motion in the $-z$ direction insofar as kinetic energy is concerned, the intervals $0 \leq \theta \leq \pi/2$ and $\pi/2 \leq \theta \leq \pi$ are equivalent.

There are two regimes of V_o which we must consider for ions of energy E, $V_o \leq E$ and $V_o \geq E$. There is a θ_c for each value of V(z) so that the fraction of ions F(V), produced with potential V(z) = V which satisfies $V_o \leq E$ is given by

$$[15.3] \qquad F(V) = 1 - \int_o^{\theta_c} \sin\theta d\theta$$

$$= \left(\frac{V_o - V}{E}\right)^{\frac{1}{2}}$$

But in Section 11 the probability that an ion is formed with potential between V and V+dV is given by [Eq.11.20]. Thus the total fraction of ions collected for $V_o \leq E$ is

[15.4] $$f = \int_o^{V_o} F(V)g(V)dV$$

$$= \frac{\pi}{4}\left(\frac{V_o}{E}\right)^{\frac{1}{2}} \quad ; \qquad V_o \leq E$$

In the case that $V_o \geq E$ all ions formed at potentials $V \leq V_o - E$ are captured, $F(V) = 1$, and the fraction of mono-energic ions collected by the trap is

[15.5] $$f = \int_o^{V_o - E} g(V)dV + \int_{V_o - E}^{V_o} \left(\frac{V_o - V}{E}\right)^{\frac{1}{2}} g(V)dV$$

$$= \frac{1}{2}\left\{\left(\frac{V_o - E}{V_o}\right)^{\frac{1}{2}} + \left(\frac{V_o}{E}\right)^{\frac{1}{2}} \cos^{-1}\left(\frac{V_o - E}{V_o}\right)^{\frac{1}{2}}\right\}; \; V_o \geq E$$

It is now only necessary to average f over the distribution of initial energies, g(E), to obtain the total fraction of ions collected at a given V_o. When ions are formed by molecular fragmentation their distribution of kinetic energies depends on the nature of the electronic energy state of the molecule before and after the dissociative transition. For these ions a general g(E) cannot be defined. However, g(E) for ions formed without dissociation is well approximated by a Maxwell-Boltzman distribution

[15.6] $$g(E) = \sqrt{\frac{4E}{\pi}}\left(\frac{1}{kT}\right)^{3/2} e^{-E/kT}$$

where $\int_0^\infty g(E)dE = 1$. The total fraction of ions collected by the traps for this Maxwellian distribution of initial kinetic energies is therefore

$$[15.7] \qquad \langle f\rangle = \sqrt{\frac{4}{\pi}}\,(kT)^{-3/2} \int_0^{V_o} E^{\frac{1}{2}} e^{-E/kT}\, \frac{1}{2}\left[\sqrt{\frac{V_o - E}{V_o}} + \sqrt{\frac{V_o}{E}}\,\cos^{-1}\sqrt{\frac{V_o - E}{V_o}}\right] dE$$

$$+ \frac{\pi\sqrt{V_o}}{4} \int_{V_o}^{\infty} e^{-E/kT}\, dE$$

Making the substitution $\sqrt{E/V_o} = \sin\phi/2$ and using the relation

$$\int_0^\pi e^{\pm\beta\cos\phi} \sin^{2\nu}\phi\, d\phi = \sqrt{\pi}\,\left(\frac{2}{\beta}\right)^{\nu}\, \Gamma\!\left(\nu + \frac{1}{2}\right) I_\nu(\beta) \quad .$$

[Gradshteyn and Ryzhik, 1965; Pg. 482], Eq. [15.7] becomes, after some algebraic manipulation,

$$[15.8] \qquad \langle f\rangle = \left(\frac{\pi V_o}{4kT}\right)^{\frac{1}{2}} e^{-V_o/2kT} \left[I_1\left(\frac{V_o}{2kT}\right) + I_o\left(\frac{V_o}{2kT}\right)\right]$$

where I_o and I_1 are Bessel function with imaginary arguments.

Eq. [15.8] gives the dependence of <f> on the trapping well depth for a thermal population of ions. Since the ICR signal intensity is proportional to the number density of ions in the cell one can obtain information about the initial distribution of velocities from the dependence of the signal strength on V_o using relations such as [15.8].

The energy distribution for ions formed by dissociation of a molecule is usually discussed in terms of an energy level diagram of the type shown in Fig. 26. The energy distribution of the fragmented particles may be of two forms providing the transition of dissociation does not violate the Franck-Condon principle [Massey 1969; Chapter 12]. In Fig. 26 a transition of type A results from excitation to a repulsive state of the molecule possibly giving rise to fragments with large kinetic energies. Type B transitions occur upon excitation of the molecule to a bound state for which part of the Franck-Condon region of the ground state lies above the energy of infinite separation of the molecule's constitutents. The form of g(E) arising from these two types of transitions is shown at the right in Fig. 26. Dissociative transitions which violate the Franck-Condon principle are also possible [Massey, 1969; Chapter 12] resulting in a third type of energy distribution of the fragmented particles. This type of transition will not be considered here.

The ICR signal intensity is directly proportional to the number density of ions and thereby reflects their initial velocity distribution. Thus, to estimate this distribution we need only study the dependence of the ICR signal on the trapping well depth, or V_T. In order to avoid alteration of the cell potentials or the ionising electron beam the magnetic field was modulated for these experiments. In this case the observed signal is the derivative of the absorption and the strength of the

Fig. 26: Energy distribution of particles formed by molecular dissociation. The lined section shows the Franck-Condon region for the ground state of the molecule and two possible transitions leading to dissociation are indicated by the arrows marked A and B.

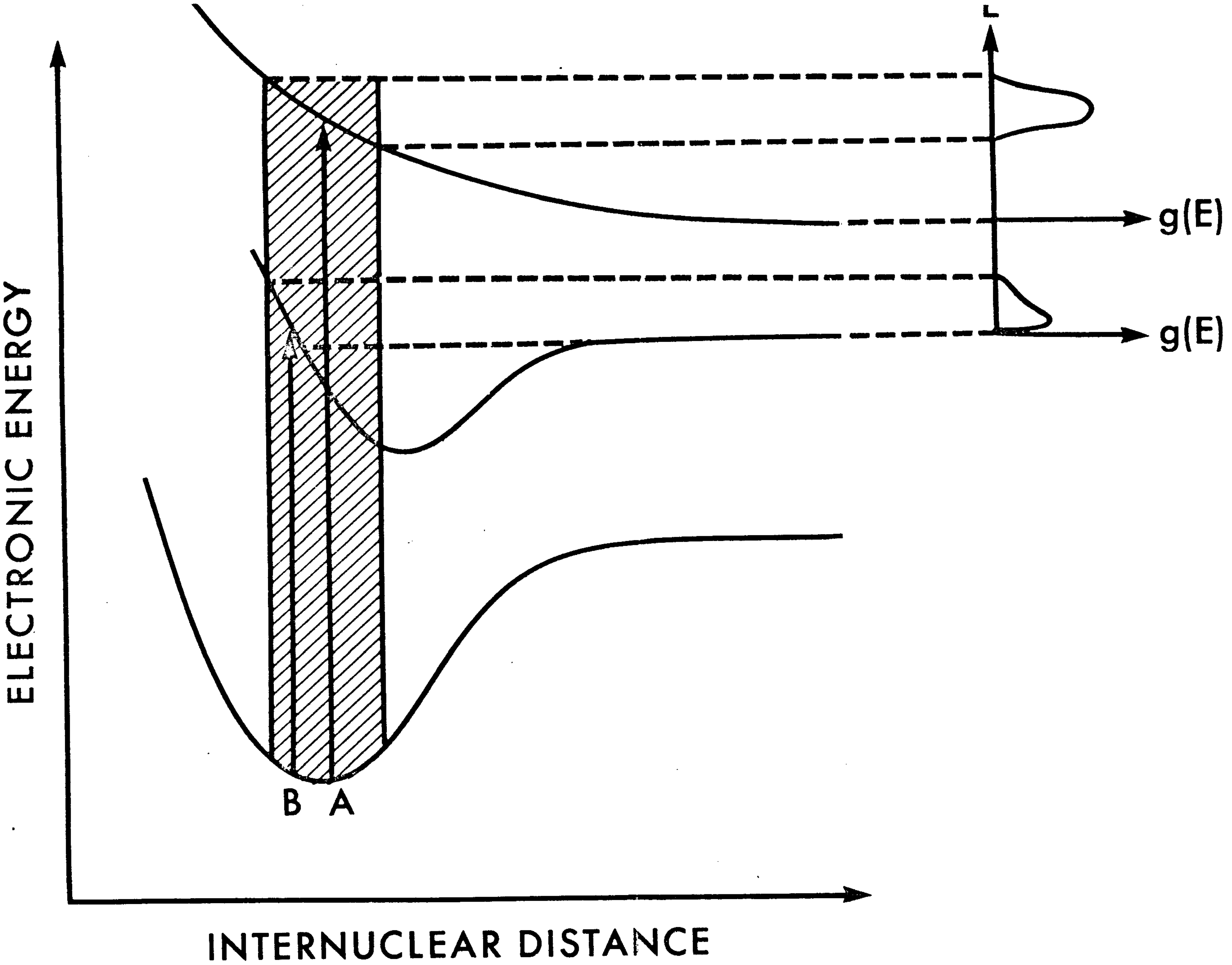
L
g(E)
g(E)
B
A
ELECTRONIC ENERGY
INTERNUCLEAR DISTANCE

line is best represented by the peak to peak intensity which we may write [Butrill, 1969]

[15.9] $$A_{pp} = C\tau^2 <f>$$

where τ is the average drift time of the ions through the analyser, and C is a constant depending on the ionic mass and the level of the rf electric field. Eq.[15.9] neglects the effect of rf inhomogenity and the complicated dependence of the ICR line shape, through τ and ω_{eff}, on the spatial distribution of the ions.

In changing the potentials of the ICR cell the spatial distribution of ions in the cell is altered as is the average drift time through the cell. Thus A_{pp} is a function of V_T through both τ and <f>. Also, as we show in Appendix 2 the line width and signal strength are dependent on $b_m/B_{\frac{1}{2}}$ where b_m is the field modulation amplitude and $B_{\frac{1}{2}}$ is the line width as defined previously in Eq. [13.3]. Since $B_{\frac{1}{2}}$ changes when τ varies it is necessary to correct the measured signal strengths for the effect of field modulation and we have,

[15.10] $$<f> \quad = \quad C' \, A_{pp} (B_{\frac{1}{2}})^2$$

where the dependence of A_{pp} on τ^2 is cancelled by multiplying by the experimentally determined $B_{\frac{1}{2}}$, and C' contains a normalizing factor to cancel the dependence of A_{pp} on $b_m/B_{\frac{1}{2}}$.

The solid lines in Fig. 27 shows <f> versus V_0 for a Maxwell-Boltzman distribution of initial velocities in the one case (Ar^+) and a gaussian distribution centred at 8.6 ev with 5.0 ev full width at half maximum.

Fig. 27: Theoretical calculation of the fraction of ions collected by the traps as a function of the well depth (solid line) together with normalized experimental results for argon ions (●) and protons from dissociation of H_2 (■).

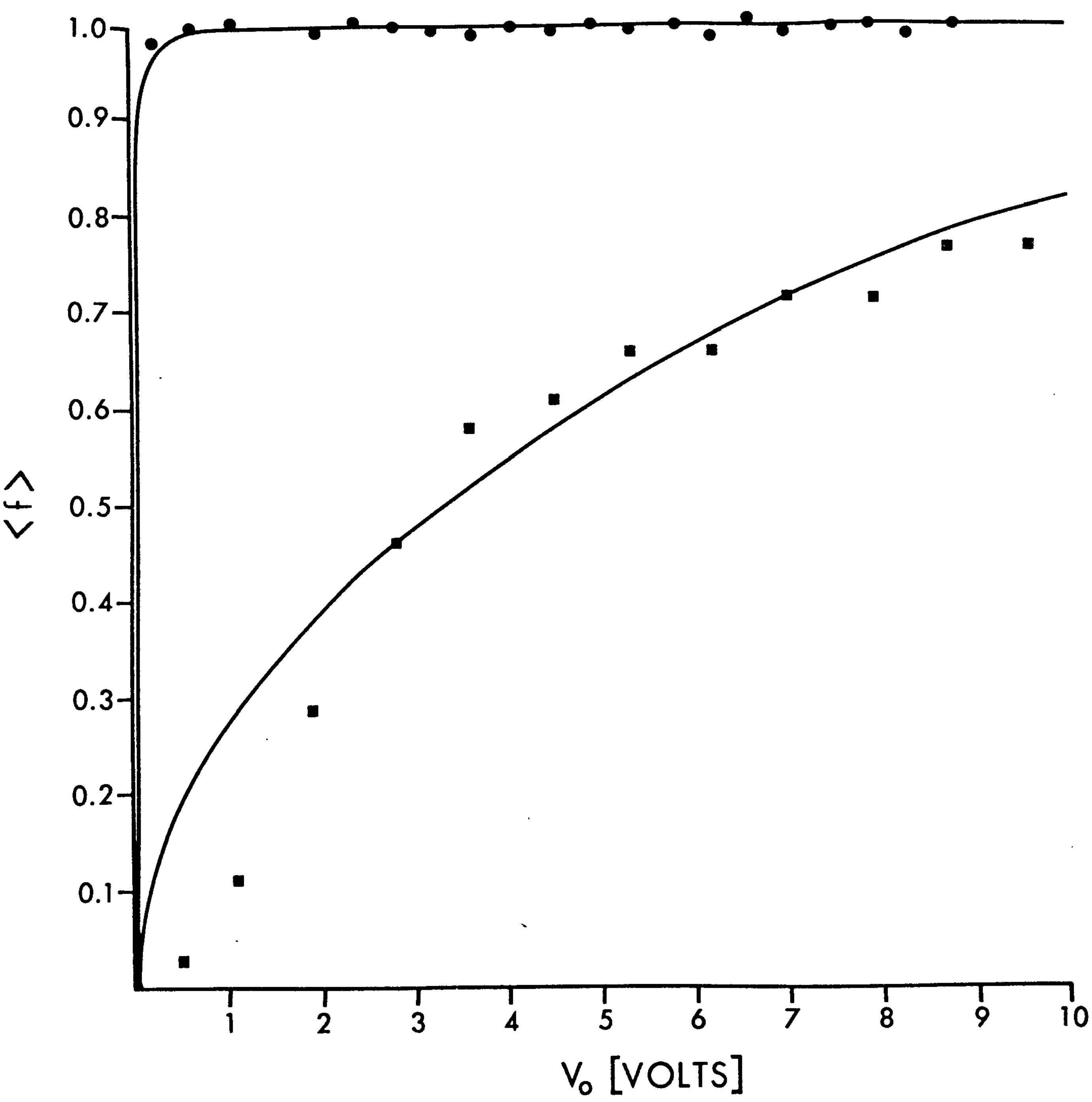

<f>
1.0
0.9
0.8
0.7
0.6
0.5
0.4
0.3
0.2
0.1
1
2
3
4
5
6
7
8
9
10
V$_o$ [VOLTS]

This latter case approximates the experimentally determined distribution of energies for protons formed by dissociation of molecular hydrogen by 75 ev. electrons [Dunn and Kieffer, 1963] but neglects the slight anisotropy of the real g(E) [Dunn, 1962]. Also shown in Fig. 27 are the experimental values of <f> found by further normalizing the ICR signal strength to one value of V_0 on the appropriate theoretical curve. The upper points are for Ar^+ ions and the bottom for protons.

Normally we find that Ar^+ and ions with similar velocity distributions are lost from our system at higher trapping potentials than is predicted by Eqs. [15.5] to [15.8]. However, this is not surprising in view of the complex dependence of the ICR signal on the electrostatic potentials, and other incalculable factors. But, at least a qualitative statement may be made. Ions from a thermal population are easily confined in the ICR cell at low trapping potentials while ions with large initial kinetic energies require larger values of V_T to trap an appreciable fraction of the originally formed ions. Using the technique outlined here, it is possible to obtain a qualitative understanding of the distribution of energies in the ICR apparatus.

16. Experimental Apparatus: Surface Ionisation

In the preceding sections we have shown that an ionising electron beam distorts the electrostatic potential of the ICR cell so that the spatial distribution of the ions becomes poorly defined. While the analysis used here yields estimates of the average position of the ions, there are obvious advantages to having the ions near the geometric centre of the cell. Since biasing the source trap greater than that in the analyser does not sufficiently restrict the maximum amplitude of trapping oscillation, it seems best to inject the ions into the ICR apparatus from an external source (e.g. a mass spectrometer), or to cross the ion beam with a well colliminated neutral beam of the particles being investigated, thereby selecting a relatively well defined energy range.

Experiments of this type using a hot wire ioniser for ion production have been performed in our laboratory. When a neutral atom or molecule with ionisation potential I strikes a surface with work function ϕ there is a very high probability that it will be re-emitted as a positive ion if $\phi > I$. If T_s is the temperature of the surface, then the ratio of positive ions to atoms re-emitted is [Zandberg and Ionov, 1959]

$$[16.1] \qquad \frac{n_+}{n_a} = A\, e^{(\phi - I)/kT_s}$$

where A is a dimensionless coefficient often set equal to one. Because of their high work function, hot tungsten or platinum filaments ($\phi \simeq 4.5$ and 4.1 ev, respectively) are ideally suited for surface ionisation of the alkali metals and a small class of molecules.

The cell used for experiments with a hot wire differed from that described in Section 12 only in that the source region and the electron beam were removed and replaced with a stainless steel oven. This is shown in Fig. 28 while a schematic side view of the oven and ICR cell is shown in Fig. 29. The oven is mounted on a stainless steel post attached to a rod which supports the ICR cell.

The receptacle of the alkali metal is 0.021 m. long and 0.005 m. in diameter. Upon heating, the atoms effuse from the oven through a channel 4×10^{-4} m. in diameter and 0.005 m. long. The heating filament was inductively wound from 3×10^{-4} m. (O.D.) tungsten wire and passed through two holes in a ceramic insulator which was inserted into a 0.003 m. diameter hole at the front of the oven, very near to the effusion channel. Thus the front was the hottest part of the oven to prevent pile-up of metal atoms at the effusion hole. Two straps were attached to the sides of the oven (Fig. 28), but insulated from it, to support a tungsten filament about 0.025 m. in front of the effusion channel. This filament (7×10^{-5} m. O.D.) is less than 5% of the width of the ICR cell in length (i.e. about 0.001 m.), so that ions are created very near to the geometric centre of the cell. The wire was biased slightly positive to cancel space charge due to electrons and prevent them from leaving the metal surface. The average position of the ions in the ICR cell is altered by this potential but its precise influence on the energy and spatial distribution is not yet known. In any case it has been experimentally demonstrated that the spread in energies of ions leaving a hot tungsten surface is about kT_s where T_s is the temperature of the surface [Zandberg and Ionov, 1959].

Fig. 28: The alkali oven and its mount together with the ionisation filament.

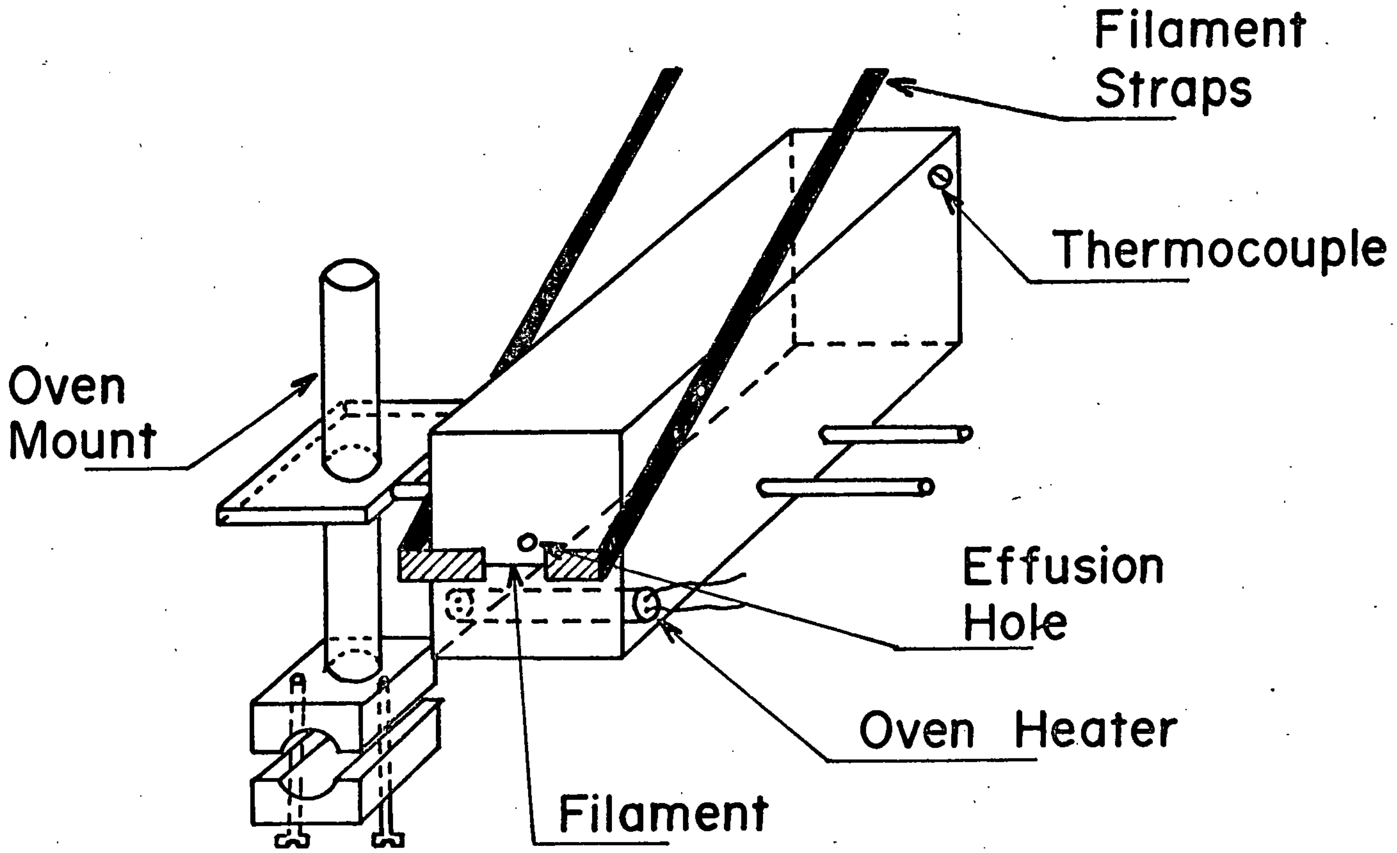
Filament Straps
Thermocouple
Oven Mount
Effusion Hole
Oven Heater
Filament

Fig. 29: A side view of the alkali oven and the ICR cell.

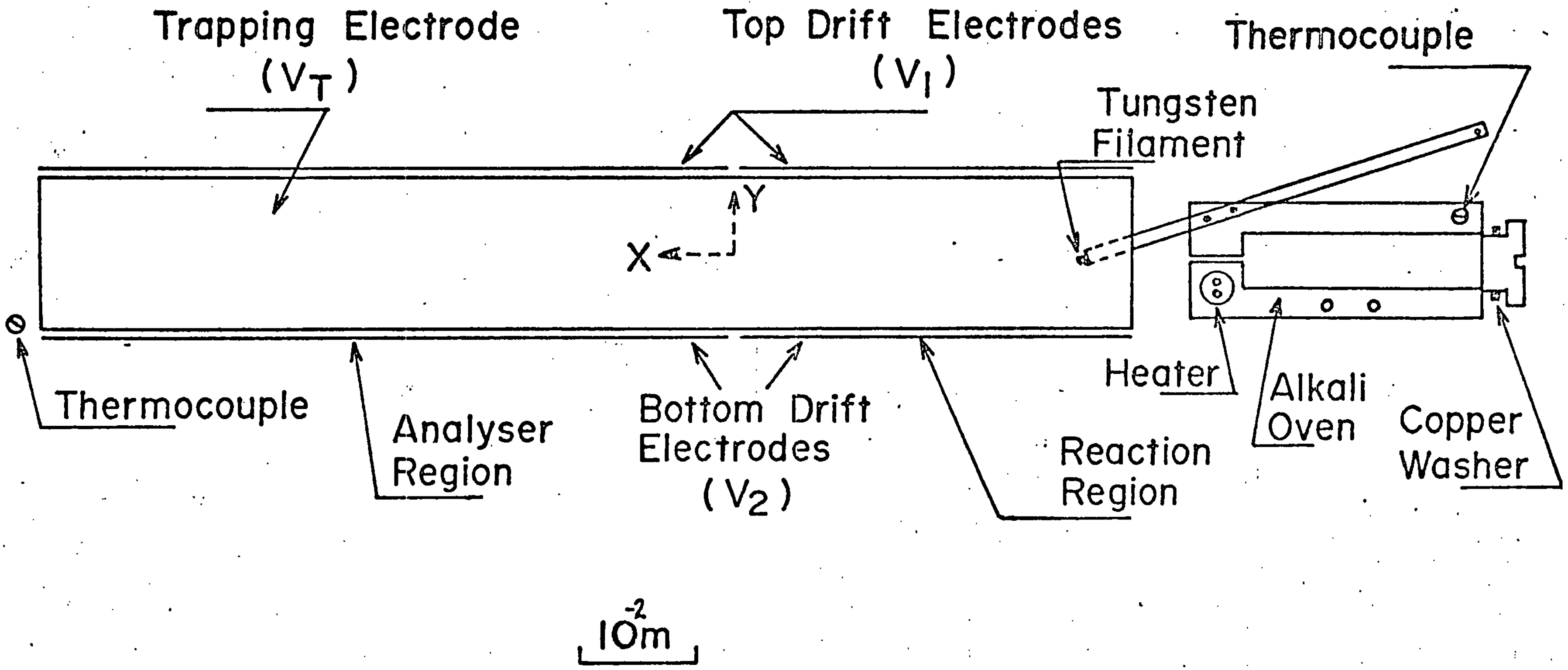
Trapping Electrode
(V_T)
Top Drift Electrodes
(V_1)
Thermocouple
Tungsten Filament
Y
X
Thermocouple
Analyser Region
Bottom Drift Electrodes
(V_2)
Reaction Region
Heater
Alkali Oven
Copper Washer
10^{-2}m

By varying the biasing on the filament the average energy of the ions formed there was changed. Thus both the amplitude of oscillation in the z-direction and the height of the ions in the y-direction will change with the filament biasing V_{fil} resulting in a variation of the averaged electric field that the ions experience in the analyser. Fig. 30 shows the dependence of line width on the potential of the hot wire. At higher potentials $B_{\frac{1}{2}}$ is smaller since the ions move to positive y's where their $<E_y>$ is smaller. The exact dependence of $B_{\frac{1}{2}}$ on V_{fil} is very complicated since the manner in which the ions' total average energy is shared between potential energy (y position in the cell) and kinetic energy (oscillation in the trap, cyclotron oscillation) is not yet completely known. For small biasing voltages, however, one expects low trapping oscillations and an ion beam that is relatively well defined spatially.

The temperature of the oven was measured with a copper-constantan thermocouple. Excellent ICR signals were obtained from $^{39}K^+$ ions at an oven temperature of about 70°C. corresponding to a potassium vapour pressure of about $4x10^{-6}$ torr. inside the oven with the filament a dull red in colour ($\approx$1400°K.). The efficiency of ionisation of sodium on tungsten is considerably smaller than that of potassium [Datz and Taylor, 1956], but adequate ICR signals of $^{23}Na^+$ were obtained with an oven temperature near 150°C. (the vapour pressure of sodium at 150°C. is approximately $7.9x10^{-6}$ torr. [Nesmeyanov, 1963]) and a slightly hotter filament. The temperature was also monitored at the end of the ICR cell near the detection region and was found to vary appreciably from room temperature only when the ion oven was heated above 300°C. Thus the experiments reported here were performed at about 293°K.

Fig. 30: The line width of $^{39}K^+$ ions formed by surface ionisation on a hot tungsten wire as a function of the biasing on the wire, V_{fil}. In this experiment the oscillator frequency was 404.34 kHz. and the ICR cell potentials were $V_1-V_2 = 1.0$ v., $V_1+V_2 = 0$ v., and $V_T = 0.2$ v. (●) and $V_T = 1.0$ v. (■).

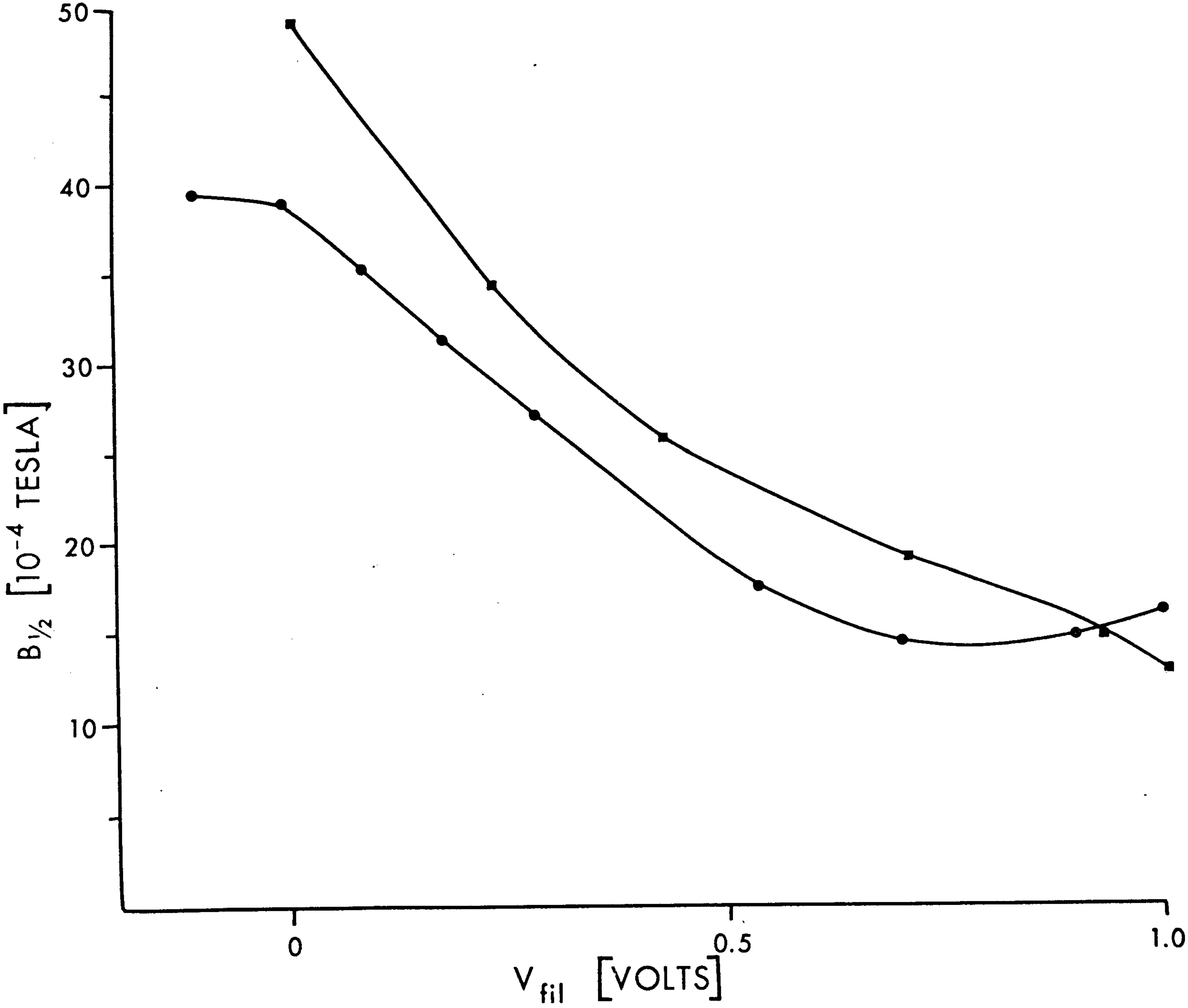
50
40
30
20
10
$B_{1/2}$ [10^{-4} TESLA]
0
0.5
1.0
V_{fil} [VOLTS]

As we have mentioned in Section 8, most ICR researchers find that the single resonance lines exhibit an asymmetry in which the side bands on the high field (low frequency) side of the maximum are suppressed. One possible explanation for this asymmetry was suggested in Section 8. The model, based on the position dependence of the quasi-cyclotron frequency, predicts that ICR lines should be nearly symmetric if $\bar{y} \gtrsim 0$ but should exhibit the experimentally observed asymmetry if $\bar{y} < 0$. Also, since the asymmetry is suggested to result from the rather large electric field gradients in the ICR cell, the asymmetry should be less prominent if the ions have, on average, small amplitudes of oscillation in the trap.

Therefore it is interesting to compare low pressure line shapes using a hot wire ioniser and an electron beam to the theory outlined in Section 8. However, such a comparison must necessarily be qualitative for several reasons. Firstly the theory of Section 8 assumes a single unique position along the y axis for all ions in the system, a uniform distribution of amplitudes of oscillation along the z axis, and the harmonic approximation for the ion motion in the trapping direction. All of these assumptions are certain to be violated in a real cell, so exact comparison between theory and experiment is unlikely. Secondly, extensive modifications of the spectrometer are required to convert from ionisation by a hot wire to ion production by electron bombardment, and since the spatial distribution of the ions in the cell is dependent on cell orientation and cleanliness, only qualitative comparisons between the line shapes of the two techniques can be expected.

In Fig. 31 (a) we show the $^{39}K^+$ resonance as a function of the biasing on the hot wire ioniser. The asymmetry of the lines is most prominent at low bias voltages for which the ions are expected to be in the lower part of the cell. As in Fig. 30 the lines at low V_{fil} are broader. In Fig. 31 (b) a typical $^{40}Ar^+$ resonance shows a more marked asymmetry than the $^{39}K^+$ lines in qualitative accordance with theory.

Fig. 31: A comparison of $^{39}K^+$ and $^{40}Ar^+$ resonances. The cell parameters were $V_T = 0.55$ v., $V_1 = -V_2 = 0.5$ v.

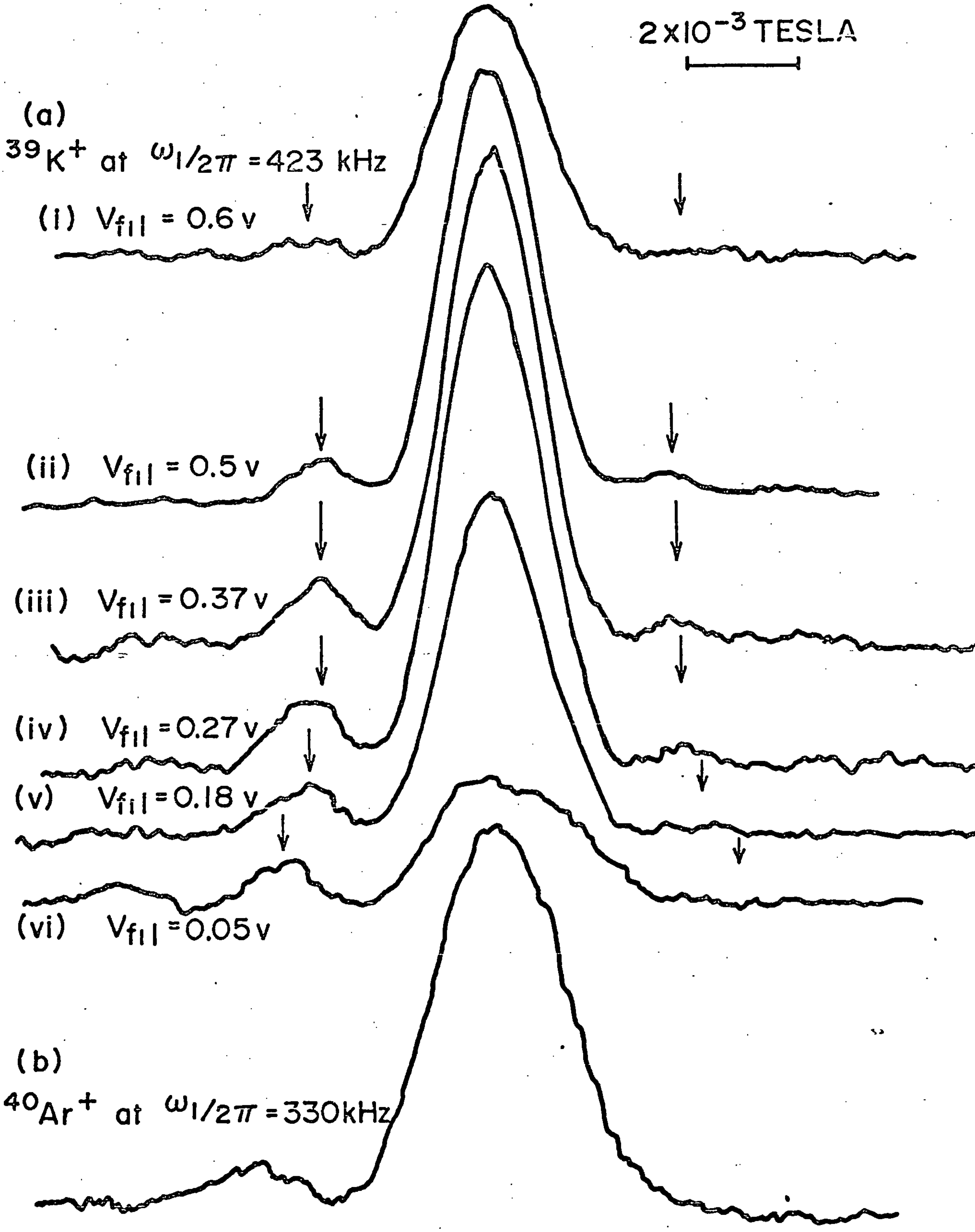
2×10⁻³ TESLA
(a)
³⁹K⁺ at ω₁/2π = 423 kHz
(i) V_f∥ = 0.6 v
(ii) V_f∥ = 0.5 v
(iii) V_f∥ = 0.37 v
(iv) V_f∥ = 0.27 v
(v) V_f∥ = 0.18 v
(vi) V_f∥ = 0.05 v
(b)
⁴⁰Ar⁺ at ω₁/2π = 330 kHz

17. Non-Reactive Collisions: Discussion of Collision Frequencies and Ionic Energy Distribution Functions

In the ICR spectrometer the free motion of the ions in the crossed electric and magnetic fields is interrupted by collisions with atoms or molecules in the background gas. This results in a pressure dependence of the ICR absorption spectra from which it is possible to determine the ion-neutral collision frequency defined by [Beauchamp, 1967]

[17.1] $$\xi = \frac{nM}{m+M} \langle \sigma_d v_o \rangle$$

where m and M are the ionic and neutral masses respectively, n is the neutral number density, σ_d is the momentum transfer cross section and v_o is the relative velocity of the colliding pair. The brackets in the above equation indicate an averaging of $\sigma_d v_o$ over the ion-atom relative velocity distribution function. In this section we report measurements of ξ for sodium and potassium ions in argon and helium gases. These systems are particularly simple since both the alkali ions and the inert gas atoms have closed electronic shells, hence charge exchange between ion and atom in the bi-particle collision is unlikely. At the end of this section the velocity dependence of ξ is discussed and a crude velocity distribution for ions undergoing elastic collisions with neutrals is derived.

However, first let us discuss the theoretical ICR line shape for ions undergoing non-reactive collisions. When the r-f electric field used to detect the ICR signal is uniform over the spatial distribution of the ions, Butrill [1969] has shown that the rate of change of energy at time t of an ion that has moved freely under the influence of the crossed electric and magnetic fields from t_o to t is

$$[17.2] \qquad \frac{dE_\perp}{dt} = \frac{E_1^2 q^2}{4m} \frac{\sin \delta\omega(t-t_o)}{\delta\omega}$$

where $\delta\omega = \omega_o - \omega_1$, ω_o is the frequency of the ion at maximum absorption intensity and ω_1 is the detector frequency. If the average ion undergoes no collision during the time that it is in the analyser then $t_o = 0$, but if the neutral particle density is such that collisions between ion and neutral are possible then t_o is the time of the last collision. At time t in the analyser there is a distribution of $\frac{dE_\perp}{dt}$'s associated with the distribution of t_o's resulting from collisions [Bloom, 1971]. The probability that an ion moves from t_o to t without collision is $e^{-(t-t_o)/\tau_c}$ while the fraction of ions that undergo collision in time dt_o is dt_o/τ_c. Therefore the instantaneous power absorption is

$$[17.3] \qquad \left<\frac{dE_\perp}{dt}\right>_{t_o} = n_o \int_o^t \frac{dE_\perp}{dt} \frac{e^{-(t-t_o)/\tau_c}}{\tau_c} dt_o + n_o e^{-t/\tau_c} \left[\frac{dE_\perp}{dt}\right]_{t_o=0}$$

where n_o is the number of ions in the analyser and $\tau_c(=\xi^{-1})$ is the mean time between collisions. The first term of Eq. [17.3] accounts for all those ions which undergo collisions between 0 and t, and the second those that move freely for this interval. Substituting Eq. [17.2] into [17.3] yields a well known expression for the instantaneous power absorption [Comisarow, 1971; Dunbar, 1971; Huntress, 1971];

$$[17.4] \qquad \left<\frac{dE_\perp}{dt}\right>_{t_o} = \frac{q^2 E_1^2 n_o}{4m(\delta\omega^2 + \tau_c^{-2})} \left[e^{-t/\tau_c}\left(\delta\omega \sin \delta\omega t - \frac{\cos \delta\omega t}{\tau_c}\right) + \tau_c^{-1}\right].$$

If we denote the average time which an ion spends in the analyser of the ICR cell by τ then the average power absorption is given by

$$[17.5] \qquad A(\delta\omega) = \frac{q^2 E_1^2}{4m(\tau_c^{-2}+\delta\omega^2)\tau} \{ [\frac{(\tau_c^{-2}-\delta\omega^2)\cos\delta\omega\tau}{\tau_c^{-2}+\delta\omega^2} - 2\,\frac{\tau_c^{-1}\,\delta\omega\sin\delta\omega\tau}{\tau_c^{-2}+\delta\omega^2}] e^{-\tau/\tau_c} + \frac{\delta\omega^2-\tau_c^{-2}}{\delta\omega^2+\tau_c^{-2}} + \frac{\tau}{\tau_c} \} .$$

The assumption of an average drift time of the ions through the analyser region is of course a crude one if there is a large dispersion of the positions of the ions in the ICR cell. However, the model has met with some success [Huntress, 1971] previously and should be a valid one, particularly for our geometry where the ions are produced with restricted amplitudes of oscillation in the trapping well. It therefore seems reasonable to estimate τ from the low pressure ICR absorption line, so that it is a simple matter to estimate τ_c for a given ion-atom pair from pressure broadened ICR lines.

The ICR collision frequencies ξ were obtained by a least squares fit of Eq. [17.5] to experimental spectra. Fig. 32 shows one of the best fits of experiment to theory while Figs. 33 and 34 show estimates of ξ for Na^+ and K^+, obtained with very low r-f electric fields, as functions of helium and argon pressures. When the average energy gained by an ion between collisions is very small the velocity distribution is nearly Maxwellian with the same temperature as the neutrals and the ICR collision frequency is simply related to the zero field d.c. mobility K(o) of the ions [Ridge and Beauchamp, 1971]

$$[17.6] \qquad \xi = \frac{q}{mK(o)} .$$

Fig. 32: A fit of an experimental $^{39}K^+$ resonance (0) to Eq. [17,5] (solid line). The average drift time was taken as 8.08×10^{-4} sec. and an argon pressure of 2.75×10^{-4} torr. was measured. The noise level of the Robinson oscillator was less than the size of the dots representing experiment on the diagram.

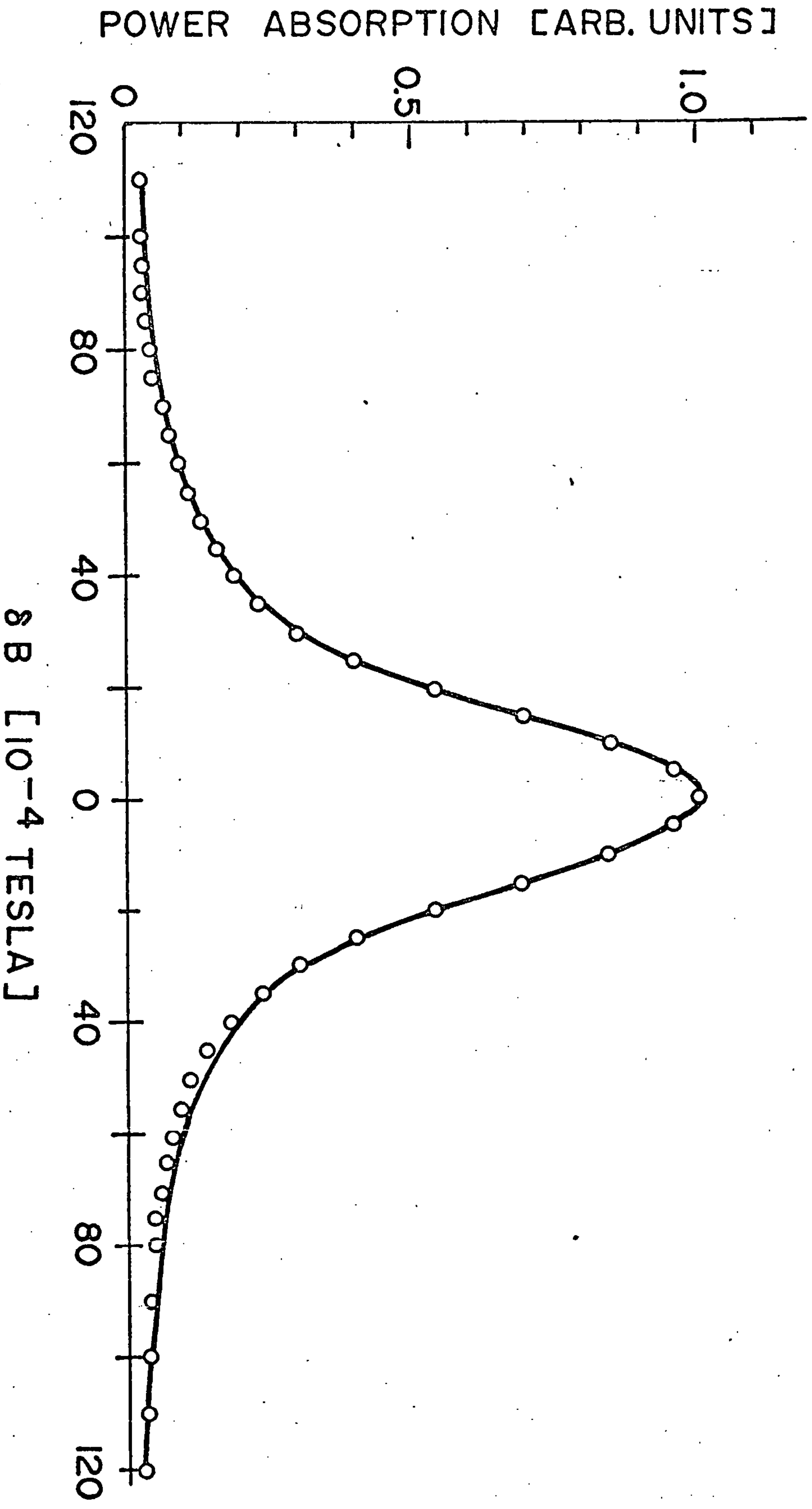
POWER ABSORPTION [ARB. UNITS]
0
0.5
1.0
120
80
40
0
40
80
120
δB [10⁻⁴ TESLA]

Fig. 33: The collision frequency $\xi = \tau_c^{-1}$ as a function of pressure for Na^+ and K^+ in helium gas. Typical ICR cell parameters are $V_1 = 0.5v$, $V_2 = -0.5v$, $V_T = 0.15$ to 0.5v with a bias on the ionization filament from 0.1v to 0.7v.

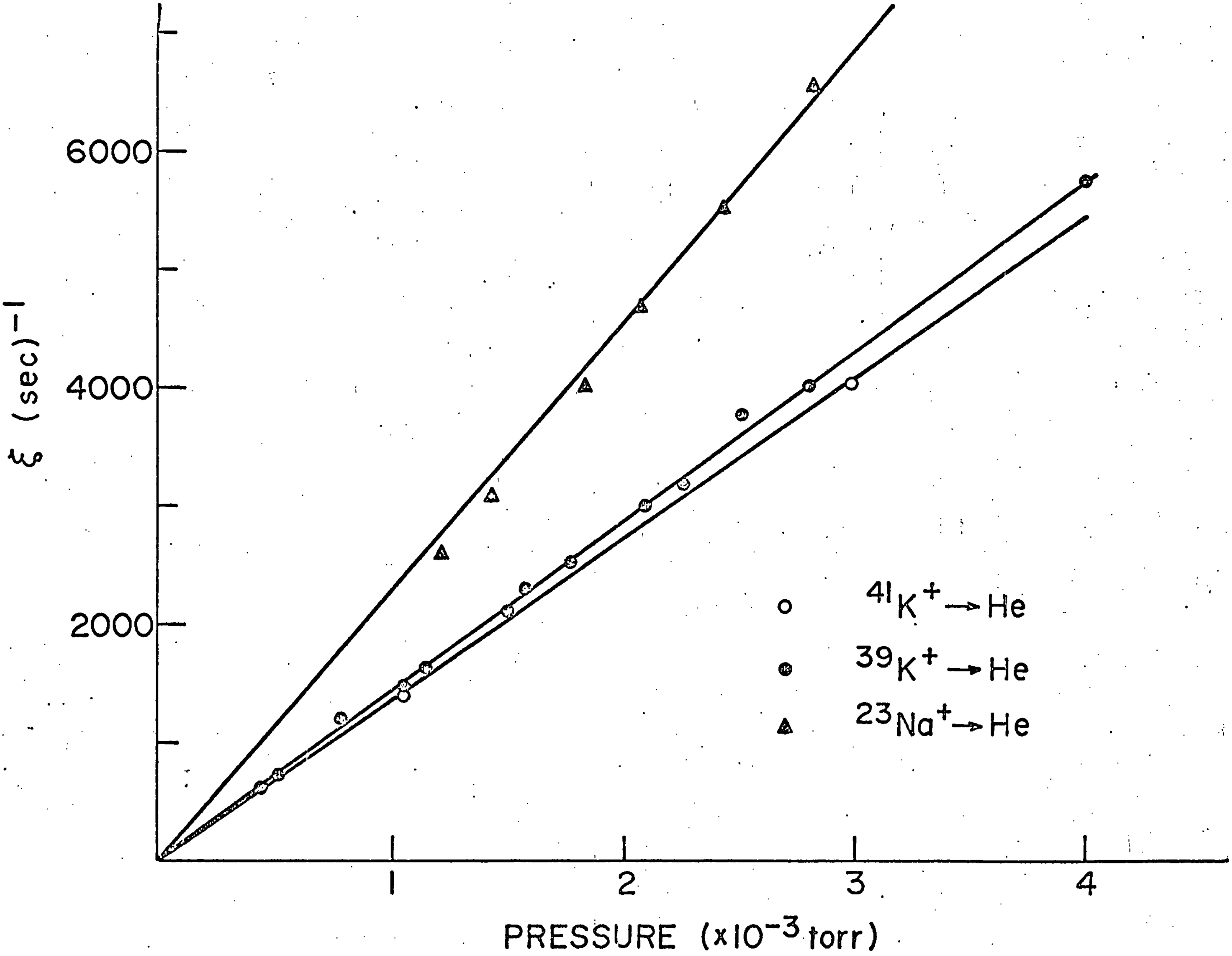
ξ (sec)$^{-1}$
6000
4000
2000
1
2
3
4
PRESSURE (x10^{-3} torr)
○ ^{41}K^{+} → He
● ^{39}K^{+} → He
▲ ^{23}Na^{+} → He

Fig. 34: The collision frequency of K^+ and Na^+ as a function of argon gas pressure. Experimental parameters are the same as for Fig. 33.

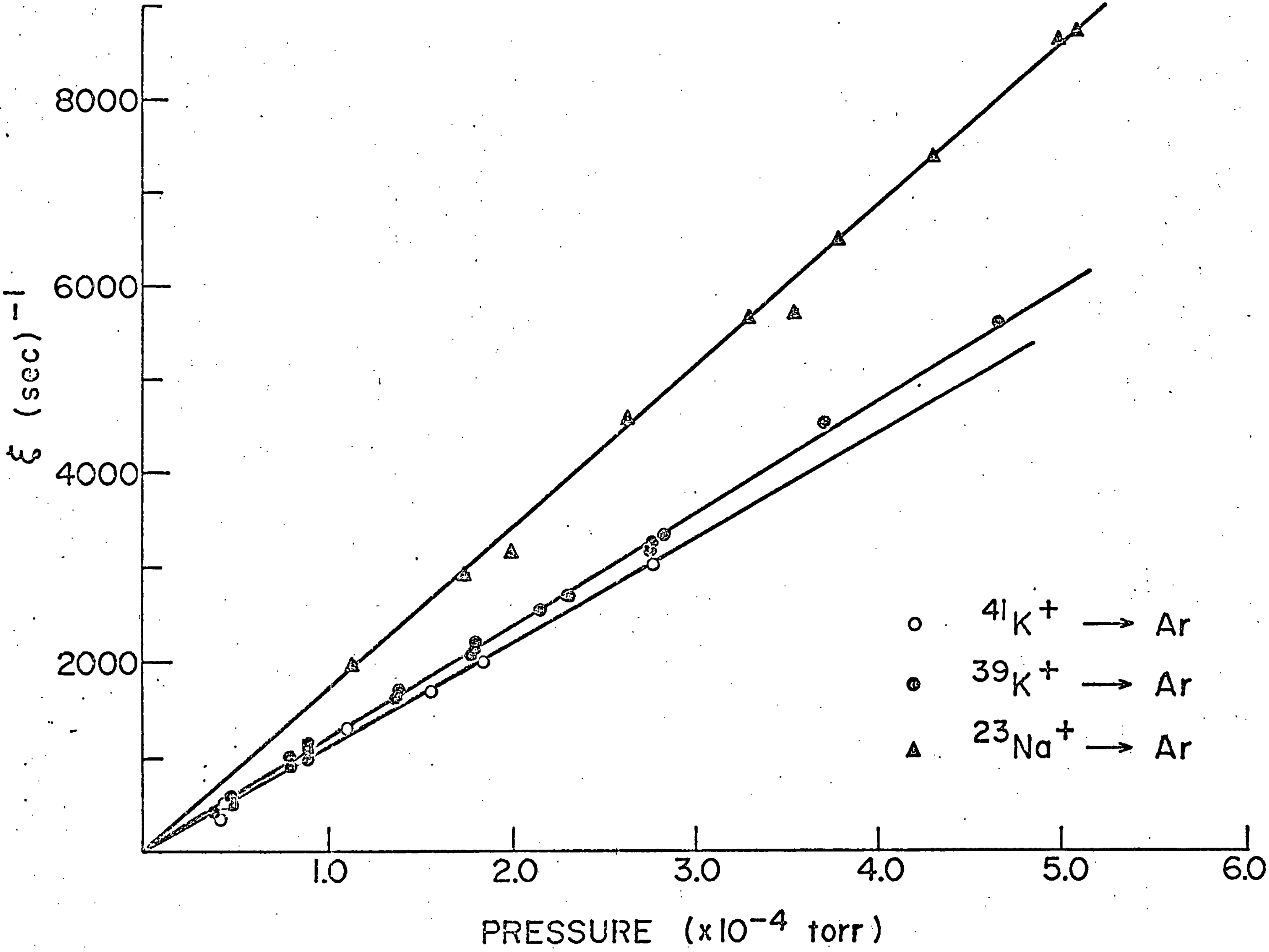

ξ (sec)$^{-1}$
8000
6000
4000
2000
1.0
2.0
3.0
4.0
5.0
6.0
PRESSURE (x10^{-4} torr)
○ $^{41}K^+ \rightarrow Ar$
● $^{39}K^+ \rightarrow Ar$
▲ $^{23}Na^+ \rightarrow Ar$

A theoretical discussion of the relations among ξ, K(o) and σ_d is given in Appendix 3 and the influence of various ion-atom interaction potentials on K(o) is discussed in Section 18. The solid lines in Fig. 33 and 34 were calculated from Eq. [17.6] using the experimental results of Tyndall et al. as given by Massey [1971]. Agreement between the ICR measurements and the d.c. mobility experiments are within the present errors in measurement of pressure [about 10%], which was measured with a Bendix G IC-017-2 ion tube on a CVC-GIC-111A control consul. Both ion tube and consul were calibrated using a McLeod gauge.

In this experiment the ion flux is independent of the pressure of the background gas unlike those experiments in which the ions are produced by electron bombardment of the neutrals. Thus it is a simple matter to compare the ICR signal amplitude as a function of pressure with the theoretical prediction of Eq. [17.5]. This is done in Fig. 35 were we plot the relative intensity of the $^{39}K^+$ signal at resonance versus argon pressure, the solid line being obtained from Eq. [17.5]. Measurement of the ICR signal intensity at resonance can, in principle, yield as much information as measurement of the line shape [Huntress, 1971] especially at high pressures where the analysis is particularly simple. Plots such as Fig. 35 give a useful check of our experimental determination of ξ from the line shape.

We now wish to extend the discussion of the ionic energy distribution given in Section 11 to include the effect of collisions. This is of interest since no such discussion is presently available in the literature nor is there available an expression for the average ion energy which adequately bridges the gap between the low pressure regime and the steady state limit where the average energy gained by the ion between collisions is equal to that lost to the neutrals through collisions.

Fig. 35: The relative intensity of the $^{39}K^+$ signal as a function of argon pressure. The solid line is obtained from Eq. [B.3].

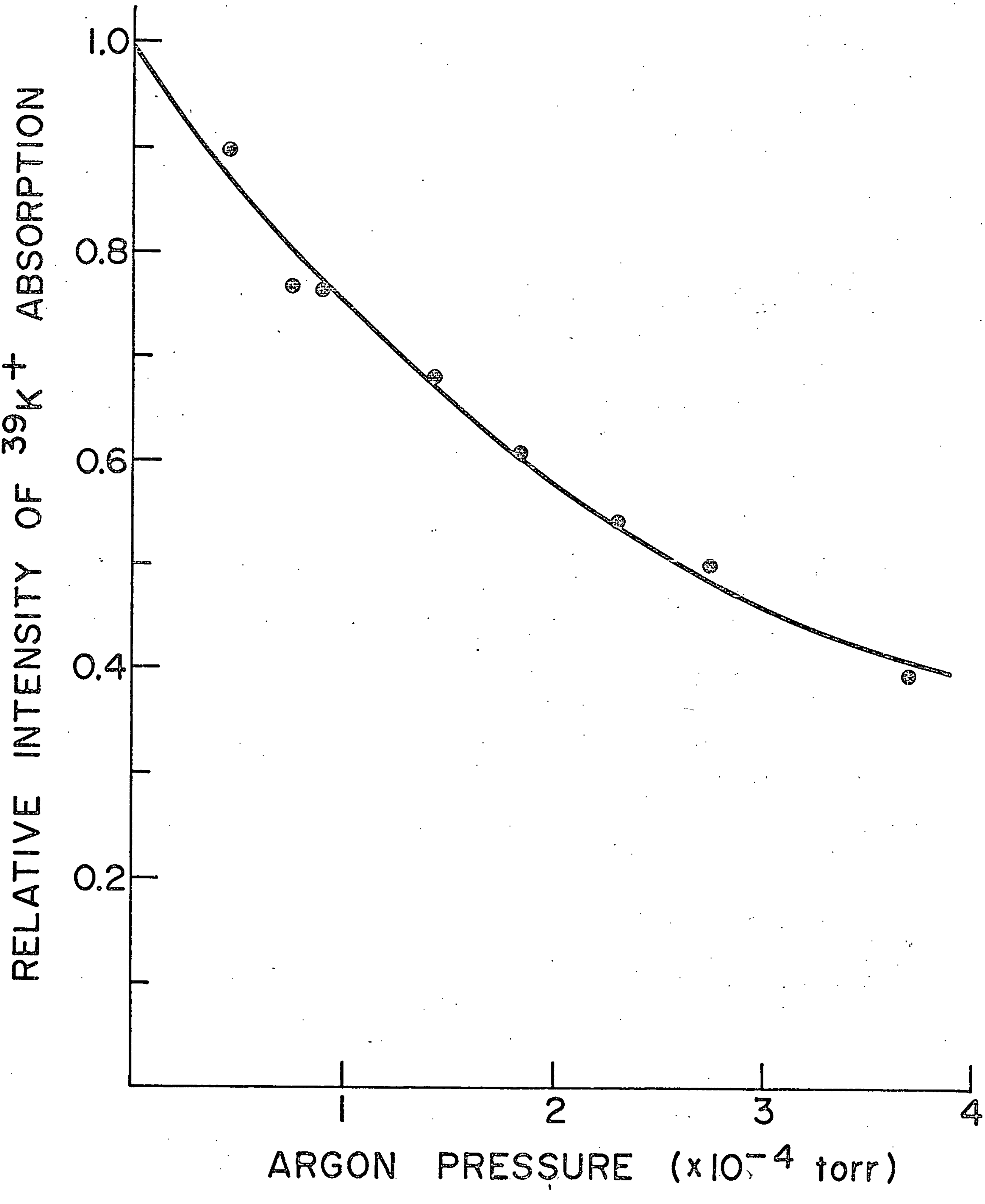
RELATIVE INTENSITY OF $^{39}K^+$ ABSORPTION
1.0
0.8
0.6
0.4
0.2
1
2
3
4
ARGON PRESSURE ($\times 10^{-4}$ torr)

If the initial energy distribution of the ions' motion in the x-y plane is represented by a two dimensional Maxwellian, with an initial temperature $T_\perp$, then as we have shown in Section 11, the energy distribution function after the ions have been subjected to ICR for a time $t-t_o$ during which no collisions occur is given by

$$[17.8] \qquad P_\perp(E_\perp) = \frac{e^{-(E_\perp+E_m')/kT_\perp}}{kT_\perp} \, I_o\left(\frac{2(E_m'E_\perp)^{\frac{1}{2}}}{kT_\perp}\right)$$

where I_o is the Bessel function with imaginary argument,

$$E_m' = \frac{q^2E_1^2}{8m}(t-t_o)^2 = \eta(t-t_o)^2, \quad 0 \le t_o \le t$$

and E_1 is the amplitude of the r-f electric field.

Now, assuming that the average time between collisions is τ_c, the fraction of ions per element of energy $dE_\perp$ that have undergone no collision at time t under resonant conditions is just $e^{-t/\tau_c}[P_\perp(E_\perp)]_{t_o=0}$. The probability that an ion which underwent a collision at t_o undergoes no collision between t_o and t is $e^{-(t-t_o)/\tau_c}$ while the fraction of ions which undergo collisions in time dt_o is dt_o/τ_c, so that at time t the fraction of ions per element of energy $dE_\perp$ whose last collision occured between t_o and t_o+dt_o is $e^{-(t-t_o)/\tau_c}[P_\perp(E_\perp)]_{t_o\neq 0}\frac{dt_o}{\tau_c}$. t_o may take on all values between and t, so a generalized distribution function for ions undergoing collisions may be written in the form,

$$[17.9] \quad P_\perp(E_\perp, \tau_c, t) = e^{-t/\tau_c} \frac{e^{-(E_m+E_\perp)/kT}}{kT_\perp} I_o\left(\frac{2(E_\perp E_m)^{\frac{1}{2}}}{kT}\right)$$
$$+ \frac{e^{-E_\perp/kT_g}}{kT_g} \frac{1}{\tau_c} \int_o^t dt_o \; e^{-(t-t_o)/\tau_c} \; e^{-\frac{(m+M)\eta}{2mkT_g}(t-t_o)^2} \; I_o\left(2\,\frac{\left(\frac{(M+m)}{2m}\,\eta E_\perp\right)^{\frac{1}{2}}}{kT_g}(t-t_o)\right)$$

where $E_m = \eta t^2$. The integral in the above expression may be evaluated in terms of Generalized Hypergeometric Series, but the result is not very tractable and will not be given here.

The first term in Eq. [17.9] represents the contribution to the distribution function of those ions which do not undergo collisions in time t while the second term accounts for those ions which do. In the steady state limit, where the average energy gained between collisions is equal to the average energy lost to the neutral particles, Huntress[1971] has shown that the average energy of an ion is different by a factor (m+M)/2m from the total energy gained between collisions. Thus in the second term of Eq. [17.9] E_m' is replaced by $(m+M)E_m'/2m$. Also, in the limit of $\tau_c^{-1} \rightarrow \infty$ the ions must come to equilibrium with the neutral gas so $T_\perp$, the initial ion temperature, is replaced by T_g, the gas temperature, for those ions undergoing collisions.

$P_\perp(E_\perp, \tau_c, t)dE_\perp$ is the fraction of ions whose cyclotron energy falls between $E_\perp$ and $E_\perp + dE_\perp$ after being subjected to a resonant r-f electric field for a time t in a medium where the average time between collisions with the background gas is τ_c. In this constant mean free time model $\tau_c^{-1} (= \xi)$ is assumed independent of the ion energy (i.e. τ_c is assumed independent of t and t_o). $P(E_\perp, \tau_c, t)$ is shown as a function of $E_\perp$ for several different values of t/τ_c in Fig. 36 for the special case m=M. As we would expect $P_\perp(E_\perp, \tau_c, t)$ reduces to $P_\perp(E_\perp)$ when $\tau_c^{-1} = 0$ and to a two dimensional Maxwellian when $\tau_c^{-1} \rightarrow \infty$. Also shown in the insert of Fig. 36 for $t/\tau_c = 2.5$ is $f(E') = \int_o^{E'} P_\perp(E_\perp, \tau_c, t)dE_\perp$, the fraction of ions whose energy $E_\perp \leq E'$.

Fig. 36: The ICR energy distribution function $P_\perp(E_\perp, \tau_c, t)$ versus $E_\perp$ for several different values of $\tau_c^{-1}t$. $P_\perp(E_\perp, \tau_c, t)$ was computed numerically from Eq. [17.9] with m=M, $E_m = \eta t^2 = 1.0$ ev and $kT_\perp = kT_g = 0.025$ ev. The insert shows the fraction of ions with $E_\perp \leq E'$ for the case $t/\tau_c = 2.5$.

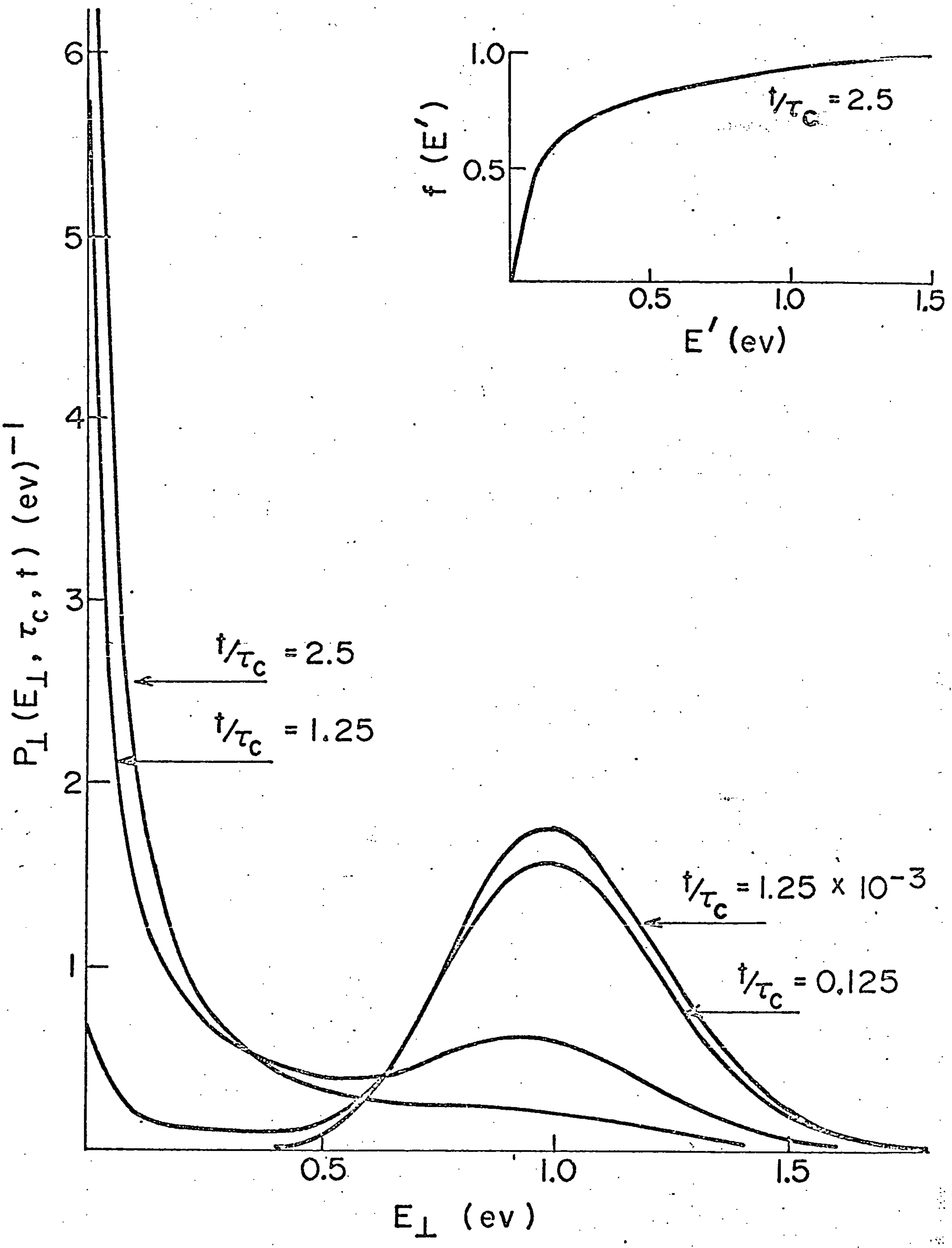
1.0
0.5
$f\,(E')$
0.5
1.0
1.5
E' (ev)
$t/\tau_c = 2.5$
6
5
4
3
2
1
$P_\perp(E_\perp, \tau_c, t)$ (ev)$^{-1}$
$t/\tau_c = 2.5$
$t/\tau_c = 1.25$
$t/\tau_c = 1.25 \times 10^{-3}$
$t/\tau_c = 0.125$
0.5
1.0
1.5
$E_\perp$ (ev)

In Appendix 4 the n^{th} moments of $P_{\perp}(E_{\perp}, \tau_c, t)$ are calculated. This is of interest for two reasons the first being that it gives insight into the effect of the energy distribution on measurements of energy dependent cross sections; i.e. it gives a feeling for $\overline{\sigma E_{\perp}}$ when σ is expanded in powers of $E_{\perp}$. Secondly, quantitative information on the spread of energies in the ICR apparatus is given by $(\overline{E_{\perp}^2} - (\overline{E_{\perp}})^2)^{\frac{1}{2}}/\overline{E_{\perp}}$ the fractional width of the distribution, which is shown by the solid lines in Fig. 37.

The distribution $P_{\perp}(E_{\perp}, \tau_c, t)$ which we have discussed above results when ions are prepared by subjecting them to resonant r-f for a fixed time t, such as in double resonance experiments [Clow and Futrell, 1970]. If after passing through a region of high r-f for a time t the ions enter a region in which they experience no cyclotron heating, they will evolve toward equilibrium with the gas and after a time t' in the new region the distribution function becomes

$$[17.10] \quad P_{\perp}(E_{\perp}, \tau_c, t, \tau_c', t') = e^{-t'/\tau_c'} P_{\perp}(E_{\perp}, \tau_c, t) + (1-e^{-t'/\tau_c'}) \frac{e^{-E_{\perp}/kT_g'}}{kT_g'}$$

where the primes indicate parameters in the region with no applied r-f. It is obvious from Eq. [17.10] that the ions very rapidly relax to thermal velocities if $(\tau_c')^{-1}$ is large.

Often the ions are detected and heated by the same oscillator, in which case the distribution function evolves, because it is a function of time, during the course of the measurement. In this circumstance a crude measure of the fractional spread in energies is given by $[\overline{\langle E_{\perp}^2\rangle_t} - (\overline{\langle E_{\perp}\rangle_t})^2]^{\frac{1}{2}}/\overline{\langle E_{\perp}\rangle_t}$ where the brackets $\langle\ \rangle_t$ indicate a time average over all t in the range $0 \leq t \leq \tau$, τ being the time that the average ion spends under the influence

Fig. 37: The fractional energy spreads of the distribution $P_\perp(E_\perp, \tau_c, t)$ as a function of pressure p, for $\tau_c^{-1}t = 1.25 \times 10^4 p$. The solid lines show $[\overline{E_\perp^2} - \overline{E_\perp}^2]^{\frac{1}{2}}/\overline{E_\perp}$ for two different values of $E_m = \eta t^2$ while the dashed lines show $[\overline{\langle E_\perp^2\rangle_t} - \overline{\langle E_\perp\rangle_t}^2]^{\frac{1}{2}}/\overline{\langle E_\perp\rangle_t}$ for values of $E_f = \eta\tau^2$.

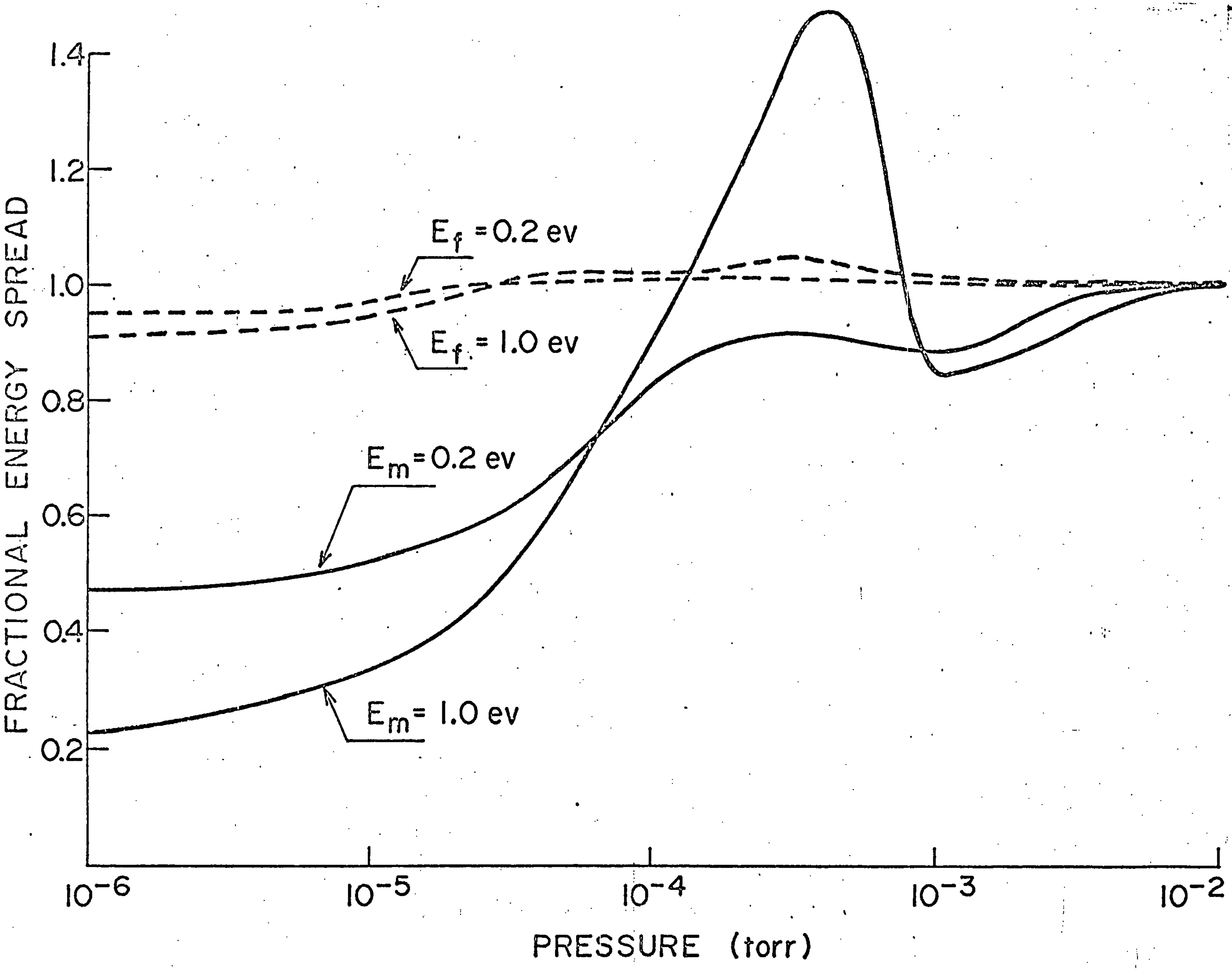
1.4
1.2
1.0
0.8
0.6
0.4
0.2
FRACTIONAL ENERGY SPREAD
$E_f = 0.2$ ev
$E_f = 1.0$ ev
$E_m = 0.2$ ev
$E_m = 1.0$ ev
10^{-6}
10^{-5}
10^{-4}
10^{-3}
10^{-2}
PRESSURE (torr)

of the heating r-f. From the dashed lines in Fig.37, this fractional spread in energies is seen to be considerably greater than the width of $P_\perp(E_\perp, \tau_c, t)$ at low pressures.

It should be emphasized that only the two-dimensional motion in the x-y plane has been considered here, neglecting the effect of the trapping oscillations in the z-direction. If the ions are produced with thermal energies at $z \simeq 0$ in the trap then $P_\parallel(E_\parallel)$ is initially a one-dimensional Maxwellian and $\overline{E}_T = \frac{1}{2} kT_g + \overline{E_\perp}$ if the temperature of the gas and the ions are the same. The effect of collisions is not only to damp out the trapping oscillations but also to initiate them in the presence of ICR by conversion of part of the energy gained from the r-f between collisions into motion in the z direction. A more realistic ICR energy distribution than that considered here must account for both of these effects. This has been done by Whealton and Woo [1971] for ions moving under the influence of a time independent electric field in the absence of a magnetic field.

Fig. 38 shows the collision frequency, at constant pressure, of Na^+ with argon neutrals as a function of $\langle\overline{E_\perp}\rangle_t$, which was altered by varying the r-f level of the detector oscillator and the value of τ_c used in Eq. [A4.5] was obtained from measurements made at small E_1. If the ions are produced by electron bombardment with all possible amplitudes of oscillation in the trapping potential, one whould use the amplitude averaged r-f electric field (Section 8) to calculate $\langle\overline{E_\perp}\rangle_t$. However in this experiment the ions are initially produced at the geometric centre of the cell and the spatial distribution of the ions can be controlled to a certain extent by the bias voltage of the filament, so that the r-f electric field amplitude at y=0, z=0 was used to estimate E_1. This of course is an over-simplification of the problem of calculating the average electric field strength.

From Fig. 38, τ_c^{-1} is seen to be independent of $\overline{\langle E_\perp \rangle}_t$ to about 1.0 ev (160 mv peak to peak r-f voltage; $E_f = 11.5$ ev) at which point a decrease in the total ion current collected at the end of the analyser was observed, indicating a loss of ions from the system. A similar decrease in the total ion current was noted at about the same r-f level in the collisionless regime. The total amount of r-f energy required to expand the ions cyclotron radii to a value b/2 is considerably larger than either $\langle E_\perp \rangle_t$ or $E_f = q^2 E_1^2 \tau^2/(8\ m)$ the latter being the average energy after a time τ of those ions undergoing no collisions. This phenomena has been observed by many other workers [Beauchamp and Ridge, 1971; Goode et al, 1971; Clow and Futrell, 1971]. Since under most experimental conditions there is a considerable spatial dispersion of the ions in the y-direction of the ICR cell and since in the collisionless regime half of the ions have energies greater than the average energy (Section 11), a loss of ions at energies less than $mb^2\omega_c^2/8$ is to be expected. This effect also could be a manifestation of the anharmonic nature of the electric fields inside the cell and may even be a result of coupling between the cyclotron and trapping oscillations at large cyclotron amplitudes.

The collision frequency of Na^+ in argon is seen to be relatively independent of average ion energy. Similar results were obtained for K^+ in helium and argon and Na^+ in helium. Because the ICR collision frequencies were obtained from a least squares fit of the central portion of the experimental absorption spectra, they are a weighted average of $\xi(E_\perp)$ over the off resonance energy distribution function and the effective energy of the ions for the measurements of Fig. 38 is lower than $\overline{\langle E_\perp \rangle}_t$ [Dunbar, 1971].

Fig. 38: The ICR collision frequency of Na^+ in argon as a function of $<\overline{E_\perp}>_t$ at two different gas pressures. The spread in energy at resonance with $<\overline{E_\perp}>_t$ = 0.61 ev for τ_c^{-1} = 3460 $sec.^{-1}$ is given by the solid bar at the bottom of the plot.

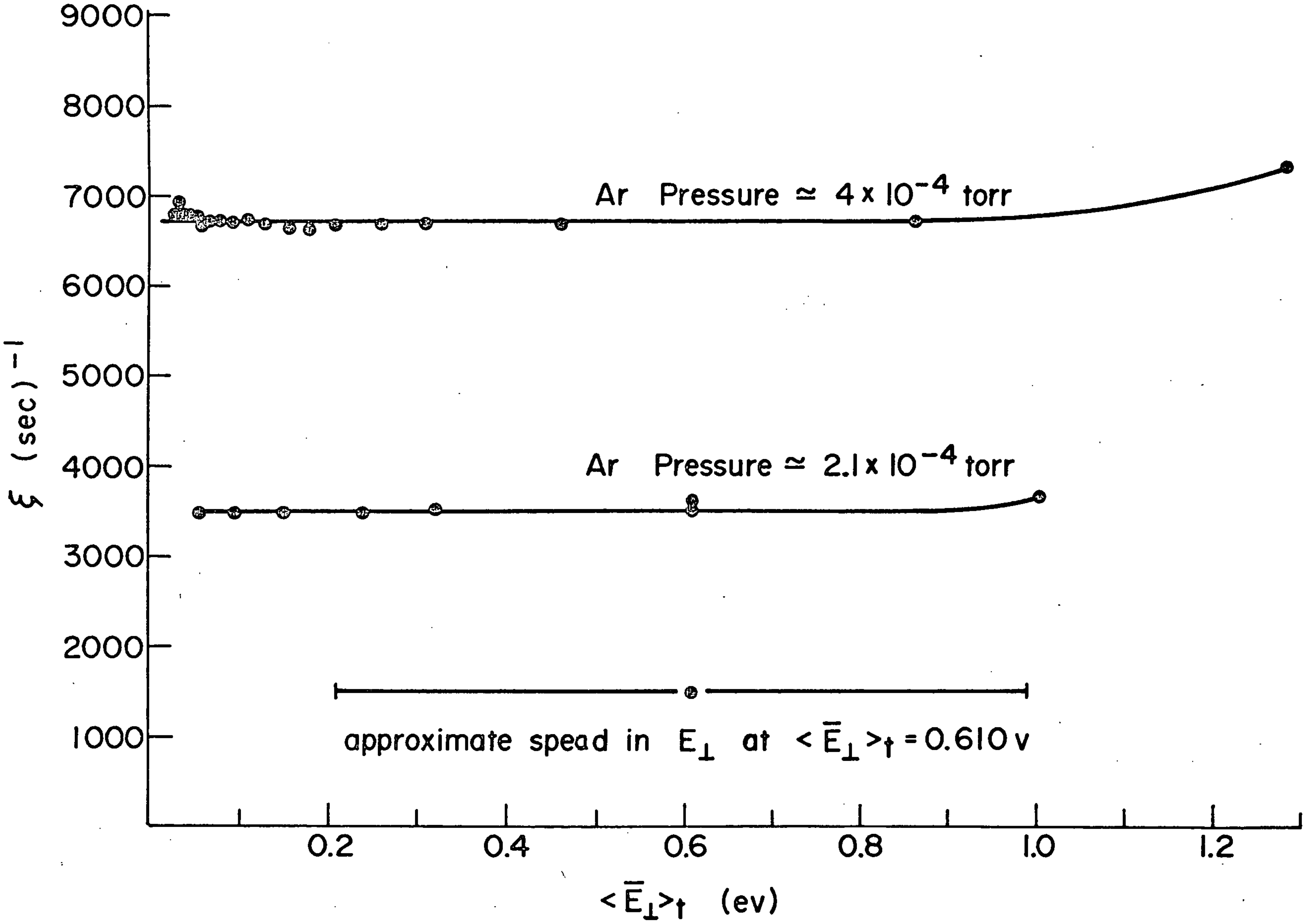
9000
8000
7000
6000
5000
4000
3000
2000
1000
ξ (sec)$^{-1}$
Ar Pressure ≃ 4 x 10^{-4} torr
Ar Pressure ≃ 2.1 x 10^{-4} torr
approximate spead in $E_\perp$ at $<\overline{E}_\perp>_t$ = 0.610 v
0.2
0.4
0.6
0.8
1.0
1.2
$<\overline{E}_\perp>_t$ (ev)

18. Discussion of Ion-Atom Interaction

At low energies the dominant interaction between an ion and a neutral arises from the well-known polarization attraction of the ion to the dipole induced on the atom by the ion itself. This interaction is described by the potential

$$[18.1] \qquad V(r) = -\frac{\alpha q^2}{2r^4}$$

where α is the polarizibility of the neutral atoms and r is the ion-atom separation. For the above potential $\sigma_d v_o$ is independent of v_o and the mobility takes a particularly simple form [Dalgarno, 1958]

$$[18.2] \qquad K' = \sqrt{\mu}\ \frac{K(0)N}{N_o} = \frac{35.9}{\sqrt{\alpha'}}$$

where μ is the reduced mass of the colliding pair, α' is the polarizibility expressed in a_o^3, N is the neutral gas density at atmospheric pressure at the temperature of measurement and N_o is Loschmidt's number. Thus K' is measured in $(\text{Volt sec.})^{-1}\text{cm.}^2(\text{PMU})^{\frac{1}{2}}$. In many systems Eq.[18.2] adequately accounts for the observed dc mobilities. However, for the alkali ion-inert gas case the experimental mobilities of Tyndall et al. [Massey, 1969] are consistently larger than indicated by a pure polarization attractive force and therefore other forms of the potential will be discussed. The effect of short range repulsion on the mobility has been approximated by assuming a purely hard sphere collision and also by combining the polarization attraction and the hard sphere repulsion in the following manner [Langevin, 1905]

$$[18.3] \qquad V(r) = -\frac{\alpha q^2}{2r} \qquad r > D$$
$$= \infty \qquad r \leq D$$

where D, the collision diameter is the sum of the atomic and ionic radii. Hassé and Cook [1931] have included a r^{-8} repulsive term in the potential but usually both models fail to account for observed dc mobilities.

More recently Mason and Schamp [1958] have calculated collision integrals of the form $<\sigma_d v_o^n>$ using a potential which includes a r^{-6} attractive term and a r^{-12} repulsion as well as the polarization attraction. They write

$$[18.4] \quad V(r) = \frac{1}{2}\,\varepsilon\left[(1+\gamma)\left(\frac{r_m}{r}\right)^{12} - 4\gamma\left(\frac{r_m}{r}\right)^{6} - 3(1-\gamma)\left(\frac{r_m}{r}\right)^{4}\right]$$

where $3(1-\gamma)\varepsilon r_m^4 = e^2\alpha$, r_m is the value of r at minimum V(r) and γ is an adjustable parameter which determines the importance of the r^{-6} term relative to the r^{-4} attraction. The r^{-6} term in Eq. [18.4] accounts for a charge induced quadrupole attraction and the London dispersion energy while the short range repulsion is entirely represented by the r^{-12} term.

By varying the two adjustable parameters in Eq. [18.4] Mason and Schamp [1958] were able to fit their derivation of K' to the temperature dependence of the experimental mobilities and obtain values of r_m, ε and γ. On the other hand Patterson [1972] defined the collision diameter D to be the value of r for which the interaction potential is zero. Thus using an experimental D the parameters r_m and ε, and hence K' may be calculated for any γ. Dymerski et al. have used Patterson's technique to estimate the Mason-Schamp potential parameters for anions in numerous molecular gases. We have also used this procedure to calculate theoretical K''s for the Mason-Schamp potential with $\gamma=0$, 0.25 as well as for the Hassé-Cook potential. Table 3 compares experimental and theoretical drift mobilities for these different models of the interaction potential. Table 4 gives the parameters of Eq. [18.4] which lead to the best agreement between theory and experiment.

On the basis of these ICR experiments there seems no reason to suspect systematic errors in the measurements of Tyndall et al. as suggested by Dalgarno et al. [1958] and an ion-atom interaction potential like that of Mason and Schamp is required to account for the mobilities of the alkali ions in inert gases. Poor energy resolution of the ICR spectrometer as well as lack of precise theoretical information on the effect of a velocity dependent $\sigma_d v_o$ on the ICR line shape prevents a detailed study of the energy dependence of the ICR collision frequencies. Nevertheless a first order energy distribution for ions at resonance with an applied r-f electric field was derived and the average ion energy obtained for all regimes of pressure. It is hoped that the treatment of the ICR line shape given in this section will lead to a better understanding of the influence of velocity dependent rate constants on the ICR line shape.

Table 3. A comparison of the effect of different ion-atom interaction potentials on the d.c. drift mobility.

TABLE 3

	EXPERIMENTAL		THEORETICAL[h]				
	DC Drift Mobility	ICR[c]	Polarization[d] 4-Power	Hard Sphere[e]	Lanagevin[f]	Mason-Schamp[g] 4-12 Power	Hassé-Cook[g] 4-8 Power
$^{39}K^+$ In Argon	11.7[a], 11.8[b]	11.4	10.8	49.6	12.2	12.9	14.4
$^{39}K^+$ In Helium	41.0[a]	40.7	30.5	58.7	34.7	46.8	58.4
$^{23}Na^+$ In Argon	11.5[a]	11.6	10.8	66.6	12.1	11.6	13.2
$^{23}Na^+$ In Helium	41.9[a]	42.8	30.5	80.9	35.1	45.4	57.5

a Tyndall et al. as recorded by Massey [1969]

b James et al. [1973]

c This work

d Dalgarno et al. [1958]

e Patterson [1972]

f Lanagevin [1905], Hassé and Cook [1931]

g Coefficient of the higher power obtained by setting V(D) = 0

h α given by Landolt-Barnstein [1950], ionic radii from Seitz [1940, Pg.93] atomic diameters of helium and argon taken as 2.18 Å and 2.6 Å respectively [Mason and Schamp, 1958]

Table 4. Values of the parameters in the Schamp-Mason potential that lead to best agreement between theory and measured d.c. mobilities.

TABLE 4

	γ	r_m(Å)	D(Å)	ε(ev)	K'($cm^2(PMU)^{\frac{1}{2}}/v.s$)
$^{39}K^+$ In Argon	0.25	3.0	2.63	0.13	11.8
$^{39}K^+$ In Helium	0.25	2.76	2.42	0.02	41.0
$^{23}Na^+$ In Argon	0	2.6	2.27	0.14	11.6
$^{23}Na^+$ In Helium	0.25	2,35	2.06	0.04	40.7

19. A Crossed Beam Experiment

As we have already mentioned, an important application of ICR involves the study of rate constants for charge exchange or ion-molecule reactions. The measurement of the cross section $\sigma(v_0)$ as a function of average velocity of the ions is of particular interest, but for such investigations it is necessary to use as well-defined an ion velocity as possible. In ICR we measure not a cross section but a rate constant $\langle\sigma(v_0)v_0\rangle$, so in order to extract information about σ it is necessary to have a thorough knowledge of the relative velocity distribution of the interacting particles. Unfortunately we saw in Sect. 10 that the ensemble of ions is quite complicated since it involves a large distribution of trapping oscillation amplitudes. Furthermore, the result of resonant r-f is to amplify the initial spread of ion velocities. In Sect. 16 a possible method of restricting the trapping oscillation amplitudes was proposed, but there appears to be no obvious method for eliminating the large spread in energy of the ion beam when ion cyclotron heating in the manner of double resonance experiments is used. However using a background gas seems not to be the best means of introducing a target for the ion beam. Somewhat better energy selection might be achieved by intersecting the ion beam at a well-defined height in the cell with a secondary neutral atom beam. After traversing the cell the neutral beam could be removed from the system by a suitable cold trap, and since the beam need not be confined in the magnetic field, the total atom flux could easily be monitored. In our laboratory we have started such a project, and although not complete, we will present preliminary measurements here.

Fig. 39. The secondary alkali oven and its mounting collar

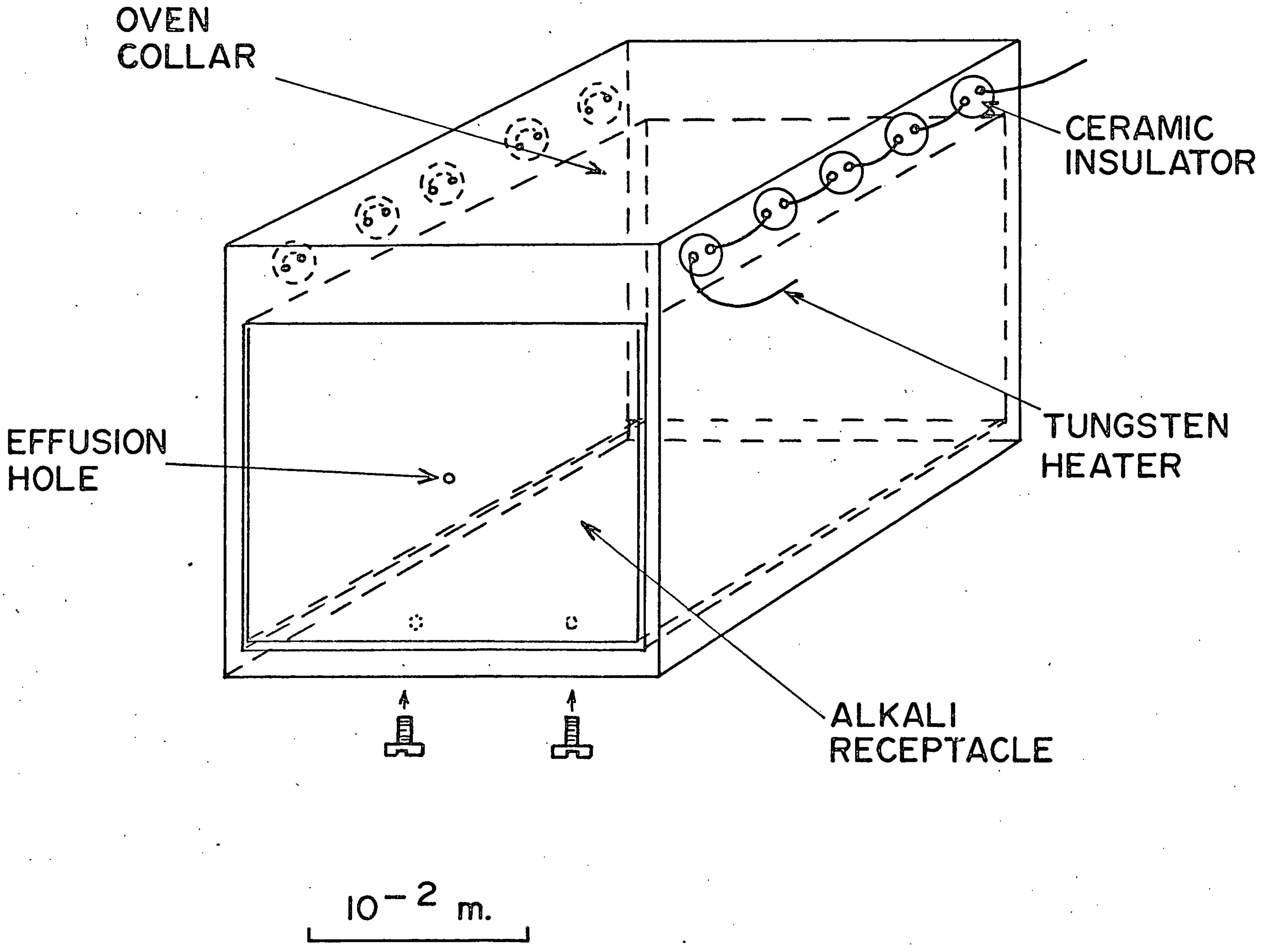
OVEN
COLLAR
CERAMIC
INSULATOR
EFFUSION
HOLE
TUNGSTEN
HEATER
ALKALI
RECEPTACLE
10⁻² m.

A second alkali oven (secondary oven, Fig. 39) was mounted at the end of the cell opposite the oven (primary oven, Fig. 28) used to generate the ion beam. To facilate its removal the secondary oven was mounted in a collar which contained the heating elements. Four screws in the bottom of the collar forced the oven into thermal contact with the heaters. The collar was mounted in the same manner as the primary oven. In these preliminary experiments charge exchange rate constants of alkali metal ions with alkali atoms in the secondary atom beam were estimated from collision broadening of single resonance absorption lines. In order to obtain a relatively intense atom beam a large effusion orifice (3.5×10^{-4}m radius and about 5×10^{-4}m long) was used. Two systems were studied; one in which both secondary and primary ovens were charged with potassium and the other in which the primary oven contained sodium and the secondary potassium.

Rate Equations and Method of Analysis:

Before we specialize to the particular cases mentioned above let us consider the reactions;

[19.1] $$A^+ + B \xrightarrow{k'} A + B^+$$

$$B^+ + A \xrightarrow{k''} B + A^+$$

which are characterized by rate constants $k'(=\langle\sigma' v_o\rangle)$ and $k''(=\langle\sigma'' v_o\rangle)$. The number densities of atoms A and B are n_A and n_B respectively and the corresponding ion currents are N_A and N_B. The rate equations for these reactions are,

[19.2] $$\frac{dN_A}{dt} = - n_B\, k'\, N_A + N_B\, n_A\, k''$$

and

[19.3] $$\frac{dN_A}{dt} = - \frac{dN_B}{dt}$$

The first term on the right hand side of Eq.[19.2] accounts for a loss of A^+ ions due to charge transfer to B atoms and the second represents a gain of A^+ ions from collisions of B^+ ions with neutral A atoms. The solution of Eq. [19.2] is

$$N_A(t) = [N_A(o) - \frac{Nn_A\ k''}{n_B\ k' + n_A\ k''}]\ e^{-(k'\ n_A \pm k''\ n_B)\ t} + \frac{Nn_A\ k''}{n_B\ k' + n_A\ k''} \quad [19.4]$$

where $N_A(o)$ is the value of $N_A(t)$ at $t = 0$ and $N\ (= N_A(o) + N_B(o))$ is the current of ions. $N_B(t)$ may be obtained from Eq.[19.4] by interchanging A and B, and k' and k''.

To calculate the instantaneous power absorption at time t we follow the procedure outlined briefly in Sect. 17, bearing in mind that for reactions [19.1] the ion populations change with time in accordance with Eq.[19.4]. Consider ion A^+, for which the collision frequency (i.e. the inverse of the mean time between collisions) for momentum transfer to both atoms A and B is ξ, and the collision frequency for charge exchange with atom B is ξ'. The fraction of A^+ ions that undergo charge exchange between t_o and $t_o + d\ t_o$ is $\xi'\ d\ t_o$ and the fraction of B^+ ions that convert to A^+ ions in this time interval is $\xi''\ d\ t_o$ where ξ'' is the collision frequency for charge transfer between B^+ and A. At time t_o the total number of A^+ ions that have their momentum randomized in $d\ t_o$ is

$$\tau\ N_A\ (t_o)\ \xi\ d\ t_o + \tau\ N_B\ (t_o)\ \xi''\ d\ t_o \quad [19.5]$$

τ again being the average drift time in the x- direction. Note that $\tau\ N_A$ is a number of particles since N_A is a current. The probability that an ion A^+ moves without collision for a time $t - t_o$ is $e^{-(t - t_o)(\xi + \xi')}$, so at time t the total contribution to the instantaneous absorption by those ions that have undergone collisions in the time interval $0 \leq t_o \leq t$ is

$$[19.6] \qquad \tau \int_0^t \frac{dE_\perp}{dt} \left(N_A(t_o)\,\xi + N_B\,(t_o)\,\xi''\right) e^{-\,(t-t_o)(\xi+\xi')} d\,t_o$$

where $\frac{dE_\perp}{dt}$ is given by Eq. [17.2]. To obtain the total instantaneous power absorbed at time t, $A(t, \delta\omega)$, we must add to Eq. [19.6] the power absorbed by that fraction f_o of A^+ ions that move without collision from time $t_o = 0$, so that

$$[19.7] \qquad A(t,\,\delta\omega) = \tau \int_0^t \frac{dE_\perp}{dt} \left(N_A\,(t_o)\,\xi + N_B\,(t_o)\,\xi''\right) e^{-\,(t-t_o)(\xi+\xi')} d\,t_o$$

$$+ \,\tau\, f_o\, N_A(o)\, \left[\frac{dE_\perp}{dt}\right]_{t_o=o}$$

where the zero of time is the time at which an ion enters the analyser. Further, note that the integration over t_o in the above is equivalent to integration over x_r, the distance along the axis of the analyser, since $x_r = V_D\, t_o$ where V_D, the drift velocity, is assumed constant for all ions and independent of the collision frequencies. Eq. [19.7] may be used to obtain the total power absorption,

$$[19.8] \qquad A\;(\delta\omega) = \frac{1}{\tau} \int_0^\tau A(t,\delta\omega)\; dt.$$

To proceed further in our analysis it is necessary to specialize to the processes (Eq. [19.9] to [19.12]) which we wish to investigate here,

$$[19.9] \qquad {}^{39}K^+ + {}^{41}K \xrightarrow{k_1} {}^{39}K + {}^{41}K^+$$

$$[19.10] \qquad {}^{41}K^+ + {}^{39}K \xrightarrow{k_2} {}^{41}K + {}^{39}K^+$$

$$[19.11] \qquad {}^{23}Na^+ + {}^{39}K \xrightarrow{k_3} {}^{23}Na + {}^{39}K^+$$

$$[19.12] \qquad {}^{39}K^+ + {}^{23}Na \xrightarrow{k_4} {}^{39}K + {}^{23}Na^+$$

We will also study charge exchange between like isotopes of ^{39}K. These reactions may be written in the form

$$A^+ + (B^+ + e^-) \rightarrow (A^+ + e^-) + B^+.$$

That is, we picture a single electron which may be on either nucleus A^+ or B^+ and neglect all other electrons in the atoms. This model is particularly applicable to Eqs. [19.9] - [19.2] since the alkali atoms have a single s-electron in their outer shell, and the corresponding ions have closed shell configurations. Symmetric resonant charge transfer occurs when A and B are identical and the energy of the transferred electron is the same in both atoms. Thus, reactions [19.9] and [19.10] are equivalent to symmetric resonant charge transfer only if the ionisation potentials of the ^{41}K and ^{39}K atoms are identical. There are two main isotope shifts [Stacey, 1966] resulting from the finite mass of the nucleus and the overlap of the wave function of an s-electron with the nucleus. Neither of these effects have been completely investigated either theoretically or experimentally for elemental masses less than 60 A.M.U, but they are presumably very small. To a first approximation the ionisation potentials of ^{39}K and ^{41}K are equal (4.339 ev), so at the typical thermal velocities considered here, the rate constants k_1 and k_2 associated with processes [19.9] and [19.10] are the same. With $k_1 = k_2$ the current of both $^{39}K^+$ and $^{41}K^+$ ions is independent of the time spent in the ICR cell and Eq. [19.7] takes the form,

$$[19.13] \qquad A\,(t,\delta\omega) = N_A(o)\ \tau\Big[\int_o^t \frac{dE_\perp}{dt}\,(\xi+\xi')\ e^{-(t-t_o)(\xi+\xi')}\ d\,t_o + e^{-\,t(\xi+\xi')}\Big[\frac{dE_\perp}{dt}\Big]_{t_o\,=\,o}\Big]$$

Using Eq. [19.8] we get

$$[19.14] \qquad A\,(\delta\omega) = \frac{q^2 E_1^{\,2} N_A(o)}{4m(\xi_c^{\,2}+\delta\omega^2)} \left\{ \left[\frac{(\xi_c^{\,2}-\delta\omega^2)\cos\delta\omega\tau}{\xi_c^{\,2}+\delta\omega^2} - 2\,\frac{\xi_c\delta\omega\,\sin\delta\omega\tau}{\xi_c^{\,2}+\delta\omega^2} \right] e^{-\tau\xi_c} + \frac{\delta\omega^2-\xi_c^{\,2}}{\xi_c^{\,2}+\delta\omega^2} + \xi_c\tau \right\}$$

where $\xi_c = \xi + \xi'$. Eq. [19.14] is identical to Eq. [17.5] with τ_c^{-1} $(=\xi)$ replaced by ξ_c. This equation gives the ICR line shape for $^{41}K^+$ ions moving through a vapour primarily composed of ^{39}K atoms. We can neglect charge exchange and momentum transfer between $^{39}K^+$ and the ^{41}K atomic isotope since it comprises less than 7% of the total natural abundance by mass of potassium. If we make this approximation Eq. [19.14] also gives the ICR line shape of $^{39}K^+$ ions with ξ and ξ_c appropriately redefined.

In addition to $N_A(o)$ Eq. [19.14] contains only two unknown parameters τ and ξ_c which must be determined from experiment. On the basis of a single experiment the relative contributions of ξ and ξ' to ξ_c cannot be estimated. As in Sect. 17 we choose to estimate τ from the ICR line shape in the collisionless regime, $\xi_c = 0$ and then to use this value of τ in Eq. [19.14] to fit theoretical and experimental lines at higher neutral particle densities, thereby obtaining an estimate of ξ_c. A typical fit of a pressure broadened $^{39}K^+$ resonance to Eq. [19.14] is shown in Fig. 40. Fig. 41 shows ξ_c for $^{41}K^+$ and $^{39}K^+$ ($^{41}\xi_c$ and $^{39}\xi_c$ respectively) as a function of the square root of the number density, $n_s^{1/2}$ of potassium atoms inside the secondary alkali oven. The significance of the dependence of ξ_c on $n_s^{1/2}$ will be discussed after a discussion of the experimental and theoretical line shapes for Na^+ ions colliding with ^{39}K atoms.

Fig. 40. A typical fit of the theoretical (solid line) and experimental (points) ICR absorption line shapes for $^{39}K^{+}$ ions colliding with a beam of potassium atoms. The number density inside the secondary oven was 4.2×10^{21} m^{-3}, with an average drift time of 1.0×10^{-3} sec. The Robinson oscillator frequency was 420.15 kHz and the r-f level in this and subsequent experiments was such that $E_f < 0.1$ ev.

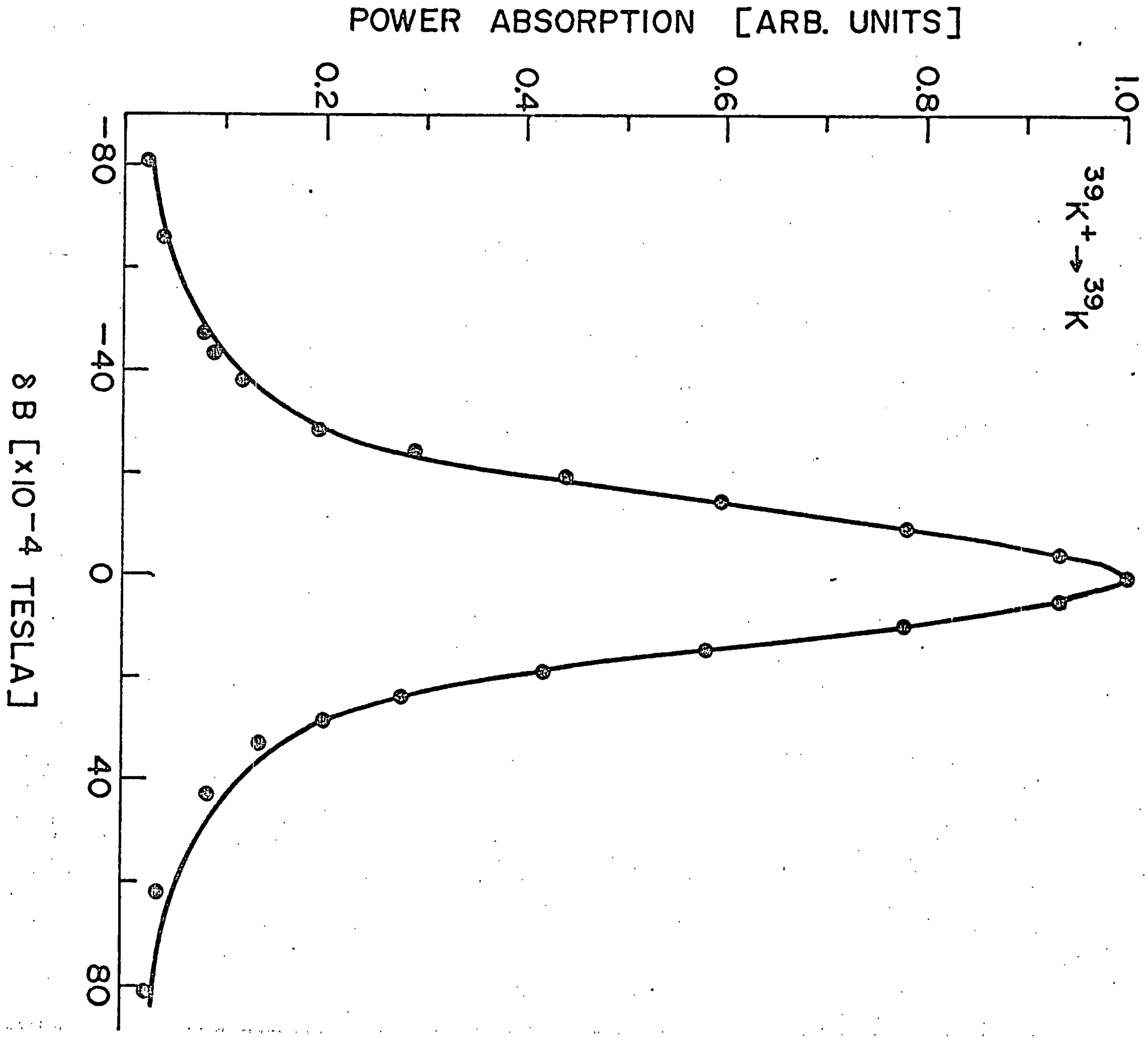
POWER ABSORPTION [ARB. UNITS]
0.2
0.4
0.6
0.8
1.0
$^{39}K^+ \rightarrow {}^{39}K$
-80
-40
0
40
80
δB [x10^{-4} TESLA]

Fig. 41. The ICR collision frequency ξ_c of $^{41}K^+$ and $^{39}K^+$ ions plotted as a function of the square root of the number density inside the secondary oven, n_s.

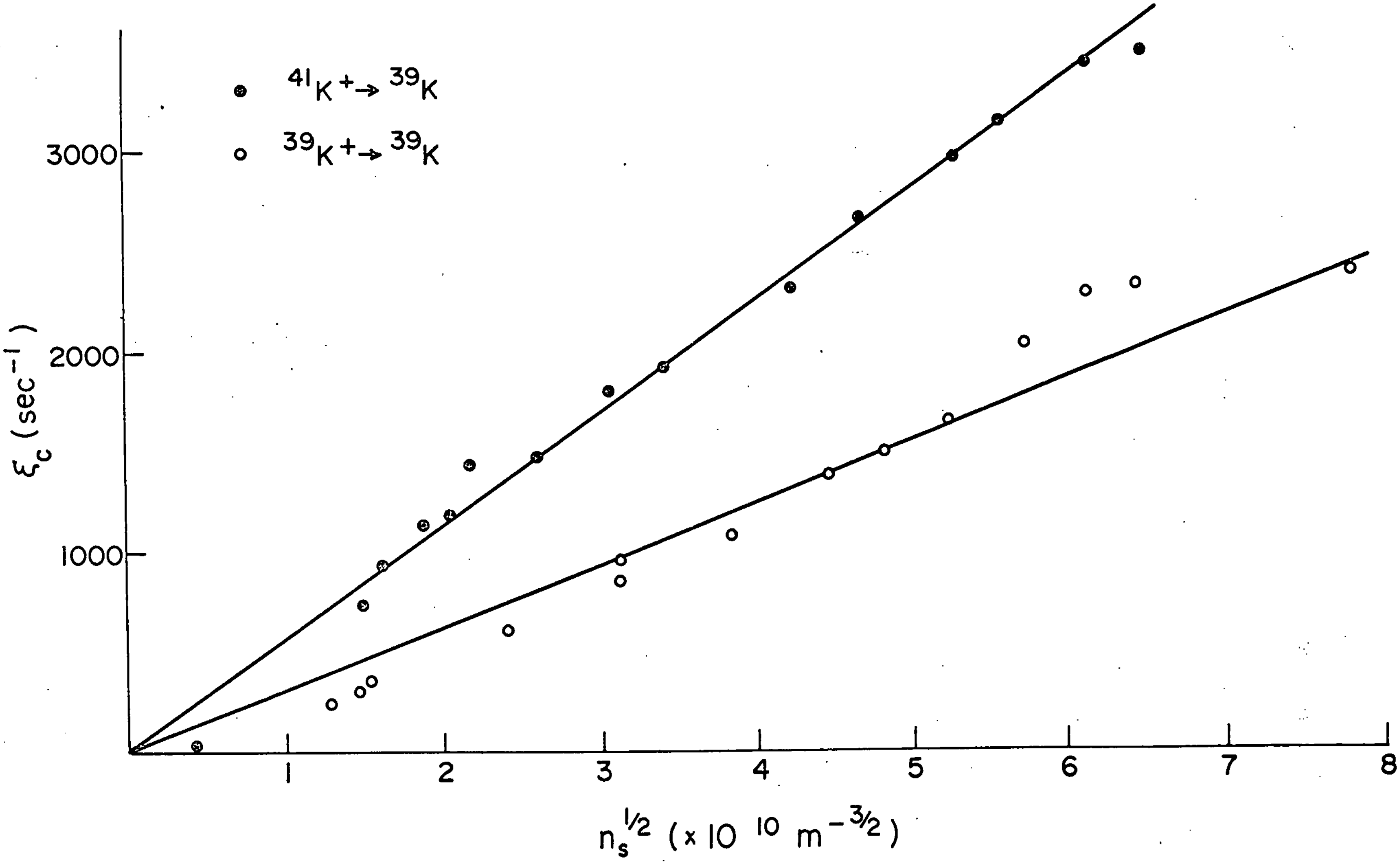
$^{41}K^+ \rightarrow {}^{39}K$
$^{39}K^+ \rightarrow {}^{39}K$
3000
2000
1000
ε_c (sec^{-1})
1
2
3
4
5
6
7
8
$n_s^{1/2}$ ($\times 10^{10}$ m$^{-3/2}$)

Consider Eqs. [19.11] and [19.12]. In this case there is an energy defect between the systems $^{23}Na^{+}\ ^{39}K$ and $^{23}Na\ ^{39}K^{+}$ of 0.8 ev since the ionisation potential of ^{23}Na (5.138 ev) is greater than that of ^{39}K. Hence for reaction [19.12] to take place 0.8 ev must be transfered to the system (i.e. reaction [19.12] is endothermic) from the relative translational motion of the colliding particles, and for thermal velocities $k_4 = 0$. Sodium ions moving at thermal velocities in potassium metal vapour give rise to $^{39}K^{+}$ ions since reaction [19.11] is exothermic and k_3 is non-zero. With $k_4 = k'' = 0$ Eqs. [19.4] and [19.7] yield,

$$[19.15] \qquad A(t,\delta\omega) = N_A(o)\tau \left\{ \int_o^t \frac{dE_\perp}{dt}\xi e^{-\xi' t_o} e^{-(\xi+\xi')(t-t_o)} dt_o + e^{-(\xi+\xi')t} \left(\frac{dE}{dt}\right)_{t_o = o} \right\}$$

Substituting Eqs. [19.15] and [17.2] into Eq. [19.8] we get,

$$[19.16] \qquad A(\delta\omega) = \frac{N_A(o)q^2E_1^{\ 2}}{4m\ (\delta\omega^2+\xi^2)} \left\{ F_1\ (\xi; \xi') + \frac{\xi}{\xi'}(1-e^{-\xi'\tau}) \right\}$$

where

$$F_1(\xi,\xi') = \left[\frac{e^{-(\xi+\xi')t}}{(\xi+\xi')^2 + \delta\omega^2} \left((\xi(\xi+\xi') - \delta\omega^2)\cos \delta\omega t - \delta\omega(2\xi+\xi') \sin \delta\omega t \right) \right]_o^\tau$$

$N_A(o)$ is now the current of sodium ions at t = 0.

Single resonance line shapes of Na^{+} ions (from the primary oven) were measured as a function of the vapour pressure of potassium inside the secondary oven. The best least squares fits of the experimental lines to Eq. [19.16] were obtained with $\xi \sim \xi'$. These collision frequencies ξ' are shown as a function of $n_s^{\frac{1}{2}}$ in Fig. 42.

Fig. 42. The collision frequency ${}^{23}\xi'$ for sodium ions as a function of the square root the number density of potassium atoms inside the secondary oven. The two sets of points represent different experimental runs.

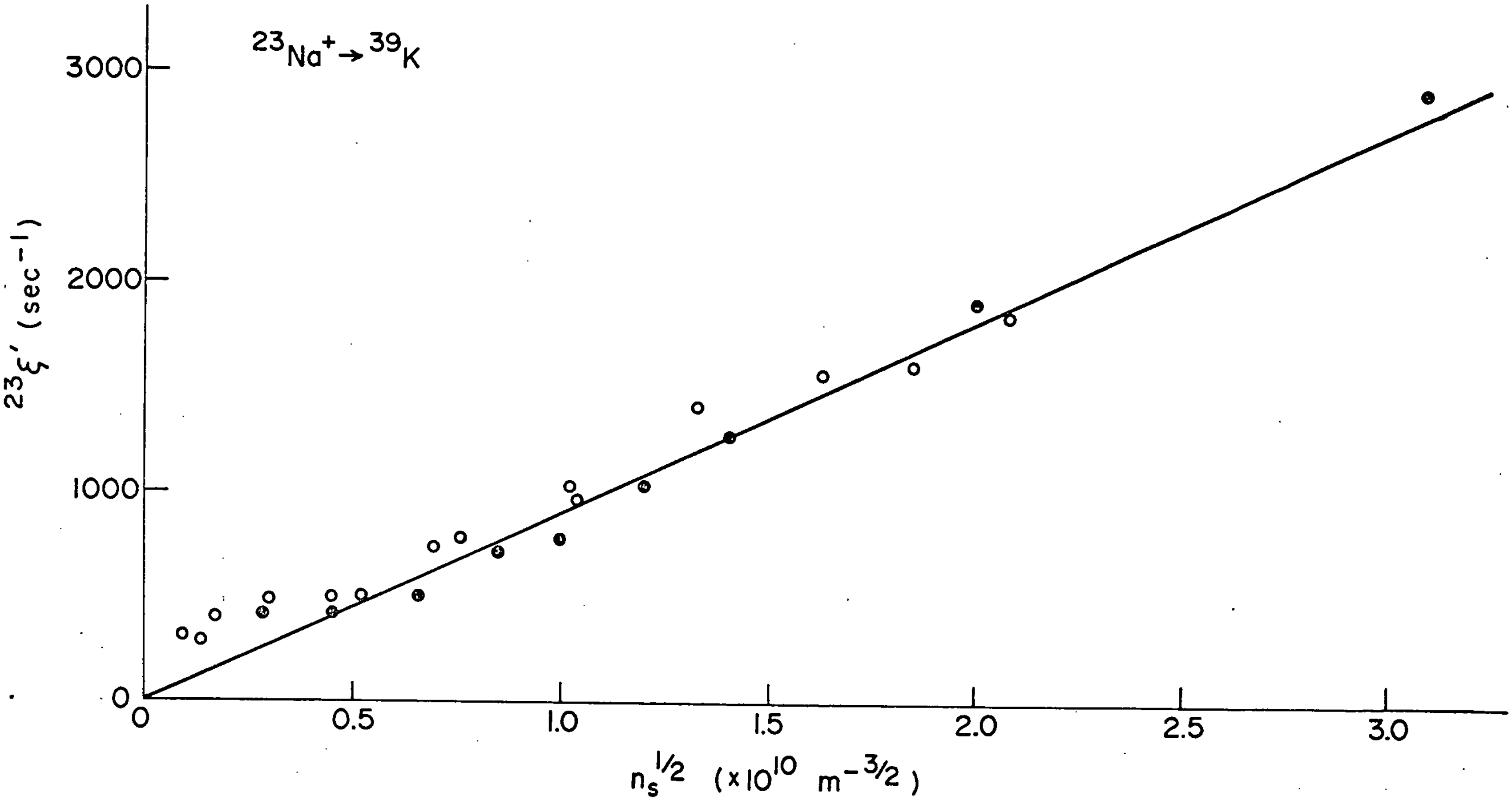
$^{23}Na^+ \rightarrow {}^{39}K$
$^{23}\xi'$ (sec^{-1})
3000
2000
1000
0
0
0.5
1.0
1.5
2.0
2.5
3.0
$n_s^{1/2}$ ($\times 10^{10}$ m$^{-3/2}$)

The area, $C(n_s, n_p)$ under an ICR absorption line is,

$$[19.17] \qquad C(n_s, n_p) = \int_{-\infty}^{\infty} A(\delta\omega)\, d\,(\delta\omega)$$

which using Eq. [19.15] becomes

$$[19.18] \qquad C(n_s, n_p) = \frac{q^2 E_1^{\,2} \Pi}{4m} N_A(-\tau') e^{-{}^{23}\xi'\tau'} \left[\frac{1 - e^{-{}^{23}\xi'\tau}}{{}^{23}\xi'}\right]$$

where τ' is the average drift time between the ioniser and the analyser region. $N_A(-\tau')$ is the current of sodium ions formed at the ioniser and is dependent on n_p, the number density in the primary oven. In Fig. 43 $C(n_s, n_p)$ is shown for $^{23}Na^+$ ions as a function of $n_s^{1/2}$ obtained by numerical integration of the experimental lines. The solid line in Fig. 43 is obtained from Eq. [19.18] using the experimental values of $^{23}\xi'$ shown in Fig. 42. The agreement between theory and experiment gives an independent check on the values of $^{23}\xi'$ obtained from the analysis of the line shape and also indicates that there are no other ion loss mechanisms for $^{23}Na^+$ in addition to that represented by $^{23}\xi'$ over the range of n_s used here. The area under the $^{39}K^+$ and $^{41}K^+$ resonances will be dealt with later in this section.

In order to investigate our experimental results more fully we will use the formalism of the Boltzman equation [Beauchamp, 1967]. If we neglect momentum transfer and charge exchange of $^{41}K^+$ with ^{41}K then we need only consider momentum and charge transfer between $^{41}K^+$ and ^{39}K, and the collision term of the Boltzman transport equation [Appendix 3] is

$$[19.19] \qquad \left(\frac{\partial \underline{v}_1}{\partial t}\right)_{coll} = \frac{1}{(n_+)_1}\Big\{ \int (\underline{v}_1' - \underline{v}_1)(1 - P_{12}) f_1(\underline{v}_1) F(\underline{V}_2) V_{12}\, b\,db\,d\varepsilon\, d\underline{v}_1 d\underline{V}_2$$

$$d\underline{v}_1 d\underline{V}_2 - \int \underline{v}_1 P_{12}\, f(\underline{v}_1)\, F(\underline{V}_2)\, v_{12}\, b\,db\,d\varepsilon\, d\underline{v}_1 d\underline{V}_2 \Big\}$$

Fig. 43. The area $C(n_s, n_p)$ of the $^{23}Na^+$ absorption as a function of the square root of the number density of potassium in the secondary oven. $C(n_s, n_p)$ is a function of n_s through $^{23}\xi'$ and of n_p through $N_A(-\tau')$. The significance of the theoretical curve is discussed in the text.

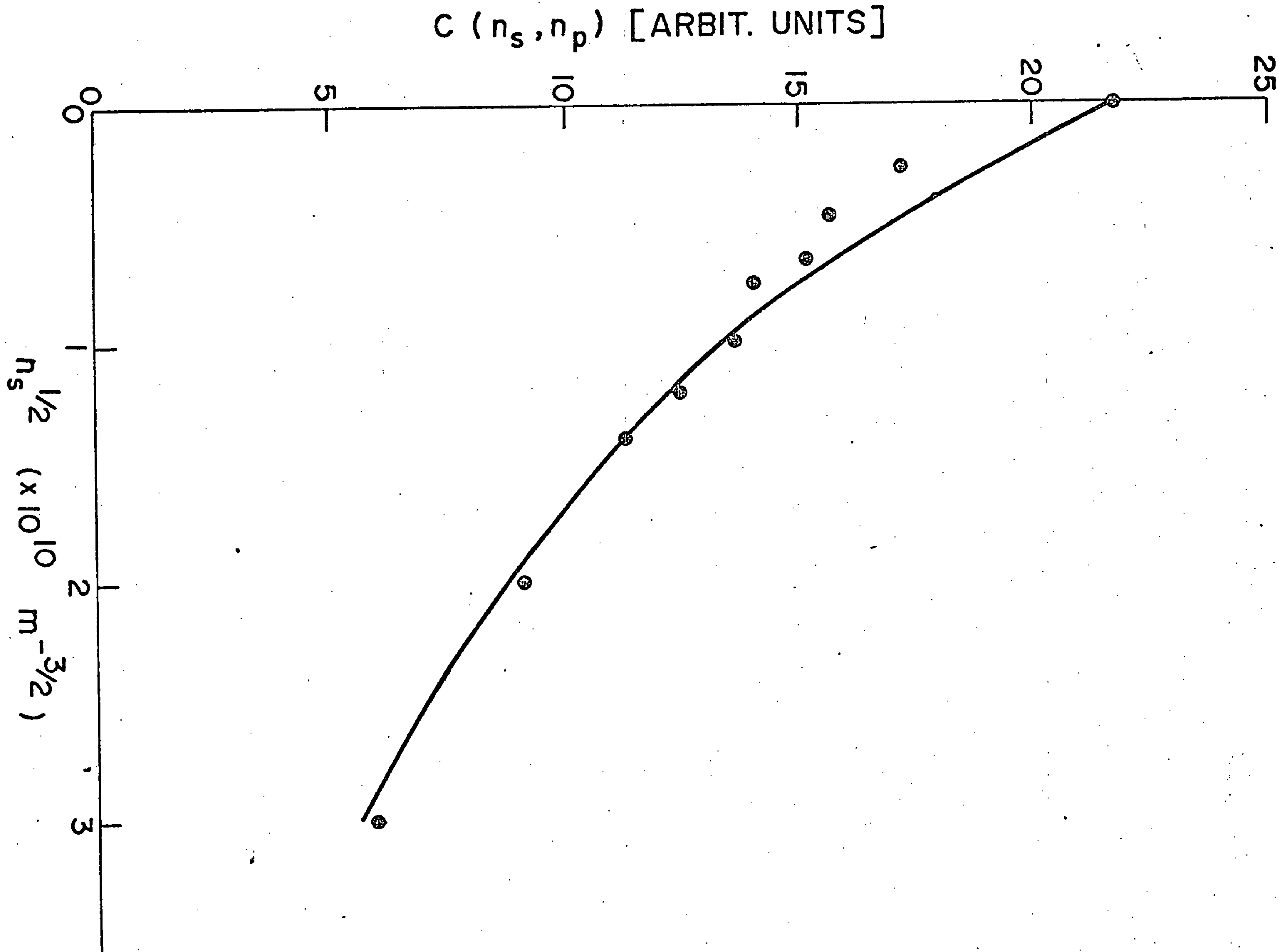
C (n_s , n_p) [ARBIT. UNITS]
0
5
10
15
20
25
0
1
2
3
n_s^1/2 (x 10^10 m^-3/2)

where the subscript 1, refers to the ${}^{41}K$ isotope, 2 to ${}^{39}K$ and v_{12} is the relative velocity of the ion atom pair. All parameters in Eq. [19.19] are defined in Appendix 3. The first term represents elastic collisions and the second charge transfer. Using the factorization procedure outlined in Appendix 3 for simple elastic collisions allows us to re-write Eq. [19.19] as;

[19.20] $$\left(\frac{\partial \underline{v}_1}{\partial t}\right)_{coll} = -{}^{41}\xi < \underline{v}_1 >_f - {}^{41}\xi' < \underline{v}_1 >_f$$

where

[19.21] $${}^{41}\xi = (n_+)_1^{-1} \left(\frac{m_2}{m_1+m_2}\right) \int (1-P_{12})\ (1-\cos\theta)\ bdb) v_{12} f\ (\underline{v}_1)\ F\ (\underline{v}_2) d\underline{v}_1 d\underline{V}_2$$

$$= \left(\frac{m_2}{m_1+m_2}\right) < v_{12}\ 2\Pi \int_0^\infty (1-P_{12})\ (1-\cos\theta)\ bdb > n_{39}$$

and

[19.22] $${}^{41}\xi' = \frac{1}{(n_+)_1} \int P_{12}\ f\ (\underline{v}_1)\ F\ (\underline{V}_2)\ v_{12}\ bdbd\varepsilon d\underline{v}_1 d\underline{V}_2$$

$$= < v_{12}\ 2\Pi \int_0^\infty P_{12}\ bdb > n_{39}$$

n_{39} is the number density of potassium -39 atoms seen by the ions. The brackets < > again indicate an average over the relative velocity distribution of the ion-atom pairs. This distribution is discussed in Appendix 5. Eq. [19.22] defines the collision frequency for charge exchange between ${}^{41}K^+$ and ${}^{39}K$, so Eq. [19.21] and [19.22] together give a formal definition of ${}^{41}\xi_c$ appearing in Eq. [19.13]. An analogous equation to [19.22] defines the collision frequency ${}^{23}\xi'$ for charge transfer from ${}^{23}Na^+$ to ${}^{39}K$ which appears in Eq. [19.16].

The collision term for ${}^{39}K^+$ moving in ${}^{39}K$ is

[19.23] $$\left(\frac{\partial \underline{v}_2}{\partial t}\right)_{coll} = \frac{1}{(n_+)_2} \left\{ \int (1-P_{22})(\underline{v}_2' - \underline{v}_2) v_{22} f(\underline{v}_2) F(\underline{V}_2) bdbd\varepsilon d\underline{v}_2 d\underline{V}_2 \right.$$

$$\left. + \int ((\underline{v}_2')_c - \underline{v}_2)\ P_{22}\ v_{22} f(\underline{v}_2) F(\underline{V}_2) bdbd\varepsilon d\underline{v}_2 d\underline{V}_2 \right\}$$

where $(v_2')_c$ is the velocity of $^{39}K^+$ following charge exchange. When charge transfer occurs between an ion and its parent atom the ion appears to be scattered through an angle $\Pi-\theta$ (see Fig. A3.1) and integrating $(\underline{v}_2')_c - \underline{v}_2$ over ξ gives [Beauchamp, 1967]

$$[19.24] \qquad \int_0^{2\Pi} ((\underline{v}_2')_c - \underline{v}_2)\, d\varepsilon = -\Pi(1 + \cos\theta)(\underline{v}_2 - \underline{V}_2)$$

and this leads directly to

$$[19.25] \qquad {}^{39}\xi_c = {}^{39}\xi + {}^{39}\xi'$$

$$= n_{39} \{ <v_{22} (\Pi \int_0^\infty (1-P_{22})(1-\cos\theta) bdb)>$$

$$+ < v_{22} (\Pi \int_0^\infty P_{22} (1+\cos\theta) bdb)$$

$$= n_{39}\, \Pi \{<v_{22} (\int_0^\infty (1-\cos\theta)\, bdb + 2 \int P_{22} \cos\theta\, bdb)>\}$$

Eq. [19.25] defines the collision frequency ξ_c appearing in Eq. [19.16] for $^{39}K^+$ moving in its parent gas.

$^{41}\xi_c$ and $^{39}\xi_c$ from Eq. [19.21], [19.22] and [19.25] differ because when different isotopes collide the momentum of the final ion is uncorrelated with the orientation of the rotating electric field associated with its ICR since the momentum of the initial ion has no such correlation. This is not true for collisions between like isotopes. Thus there is a persistence of momentum in the $^{39}K^+$ ^{39}K system that results in $^{39}\xi_c$ being somewhat smaller than $^{41}\xi_c$, as will be shown using a well known model of symmetric resonant charge transfer

The collision frequencies in the above expressions are expressed in terms of P_{ij}, the probability of charge transfer from ion i to atom j, which in general depends on the impact parameter b and the relative velocity v_{ij}. The cross section for charge exchange then is [Rapp and Francis, 1962].

$$[19.26] \qquad \sigma_c(v) = 2\,\Pi \int_0^\infty P_{ij}\, (b, v_{ij})\, bdb$$

For symmetric resonant charge transfer ($A^+ + A \rightarrow A + A^+$) an expression for P_{ij} may be derived from an analysis of the collision complex AA^+ treated as a one electron problem [Firsov, 1951]. The non-stationary state describing the collision can be expressed in terms of the symmetric and antisymmetric stationary states of the single electron orbitals. The difference in energies of these anti-symmetric and symmetric states depends only on the separation r of A and $A^+ + e$ where $r^2 = b^2 + v_{ij}^2 t^2$, t being the time measured from $-\infty$ to ∞. By choosing a semi-empirical wave function for $A^+ + e^-$ Rapp and Francis [1962] find that P_{ij} oscillates rapidly between 0 and 1 for $b < b_1$ and is small for $b > b_1$ so replacing P_{ij} by ½ for $b \leq b_1$ yields

[19.27] $$\sigma_c^{\frac{1}{2}} = \sqrt{\frac{\pi}{2}}\ b_1$$

where

$$\left(\frac{2^{\circ}\pi}{\gamma a_o}\right) \left(\frac{I}{v_{ij}}\right) b_1^{3/2} \left(1 + \frac{a_o}{\gamma b_1}\right) e^{-\gamma b_1/a_o} = \frac{\pi}{6}$$

I is the ionisation potential of the atom and $\gamma = I/13.6$. This theory assumes rectilinear motion of the ions and is valid only at fairly high velocities. At low velocities the ionic orbits are not rectilinear but an ad hoc model of the charge exchange may be used to calculate σ_c. At large impact parameters and low velocities the potential between the ion and atom is dominated by the polarization attraction and one speaks of two types of collisions; orbiting collisions in which the incident ion orbits the target atom and grazing collisions. The critical impact parameters b_o such that all collisions with $b < b_o$ result in orbiting is [Gioumousis and Stevenson, 1958]

[19.28] $$b_o = \left(\frac{4\ q^2\ \alpha}{\mu_{ij}\ v_{ij}^2}\right)^{1/4}$$

where μ_{ij} and v_{ij} are the reduced mass and relative velocity of the colliding pair and a pure polarization attraction has been assumed.

If $b_o > b_1$ it is customary [Beauchamp, 1967] to take

[19.29] $$P_{12} = P_{22} = \frac{1}{2}, \quad b \leq b_o$$
$$= 0 \qquad b \geq b_o$$

Substituting Eq. [19.29] into Eqs. [19.21], [19.22] and [19.25] gives

[19.30] $${}^{39}\xi_c \approx n_{39}\ \Pi(\frac{q^2\alpha}{\mu_{22}})^{\frac{1}{2}}$$

and

[19.31] $${}^{41}\xi_c \approx n_{39}\ (\Pi(\frac{q^2\alpha}{\mu_{12}})^{\frac{1}{2}} + 2.21\ \Pi\ \frac{m_2}{m_1+m_2}\ \ (\frac{q^2\alpha}{\mu_{12}})^{\frac{1}{2}})$$

α being the polarizability of the neutral potassium atom. The first term in Eq. [19.31] is the collision frequency for charge exchange ${}^{41}\xi'$ and the second is ${}^{41}\xi$ for the pure polarization potential [Dalgarno et al, 1958]. This crude theory indicates that ${}^{41}\xi_c$, ${}^{41}\xi_c - {}^{39}\xi_c$ and ${}^{39}\xi_c$ are in the ratios 2.1 : 1.1 : 1.0, to be compared with experimental ratios of about 1.9 : 0.9 : 1.0 obtained from Fig. 41. In view of the crude nature of the theory and the accuracy of this experiment the agreement seems quite good.

For the case of asymetric charge transfer from ${}^{23}Na^+$ to ${}^{39}K$ we might assume that the cross section is the same as the cross section for orbiting collisions [McDaniel, 1969, Pg. 72; Gioumousis and Stevenson, 1958] and calculate that

]19.32] $${}^{23}\xi' = n_{39}\ \ 2\Pi\ (\frac{q^2\alpha}{\mu_{23}})^{\frac{1}{2}}$$

where μ_{23} is the reduced mass of the ${}^{23}Na^+\ {}^{39}K$ system. We thus expect ${}^{23}\xi'$ and ${}^{39}\xi_c$ to be in the ratio of 2.3 : 1.0 but experimentally find that ${}^{23}\xi'/{}^{39}\xi_c \approx 2.9$. The reason for this rather poor agreement of experiment with Eq. [19.31] is not known, but may lie in the experiment. Nevertheless, it is significant that ${}^{23}\xi' > {}^{39}\xi_c$.

Effusion:

To this point we have not attempted to make a quantitative estimate of the rate constants for the two processes studied here, since this requires knowledge of the neutral particle number density. The rather striking dependence of the collision frequencies on the square root of the number density inside the secondary oven also requires some discussion. Atoms from the secondary oven traverse the cell, and a certain fraction are ionised on the hot wire placed in front of the primary oven. The ICR signal strengths are a measure of the total flux of atoms falling on the ioniser. It is easy to show that the area of the ${}^{41}K^+$ resonance is given by

[19.33] $$\mathcal{C}(n_s, n_p) = \frac{q^2 E_1^2}{4m_1} \bar{\Pi} \; N_A(o) \, \tau$$

which is independent of the collision frequency ${}^{41}\xi_c$ since the total number of ${}^{41}K^+$ ions does not change with position in the cell at thermal velocities when both secondary and primary ovens are charged with potassium. Thus $N_A(o)\tau$, the number ${}^{41}K^+$ ions formed at the ioniser is dependent on both n_s and n_p. But, the quantity

[19.34] $$R(n_s) = \mathcal{C}(n_s, n_p) - C(0, n_p)$$

where $C(0, n_p)$ is the contribution to the area of the ${}^{41}K^+$ resonance of the primary beam, is proportional to the flux of atoms from the secondary oven. Fig. 44 shows that $R(n_s)$ is linear with $n_s^{1/2}$, a strong indication that the atomic number density seen by the ioniser is proportional to $n_s^{1/2}$. While this behavior of $R(n_s)$ indicates why the experimentally determined collision frequencies are proportional to $n_s^{1/2}$, it does not yield an absolute number density inside the cell. It is therefore necessary to investigate the process

Fig. 44. $R(n_s)$ as a function of the square root of the number density inside the secondary alkali oven. $R(n_s)$ is proportional to the flux of atoms from the secondary oven as explained in the text.

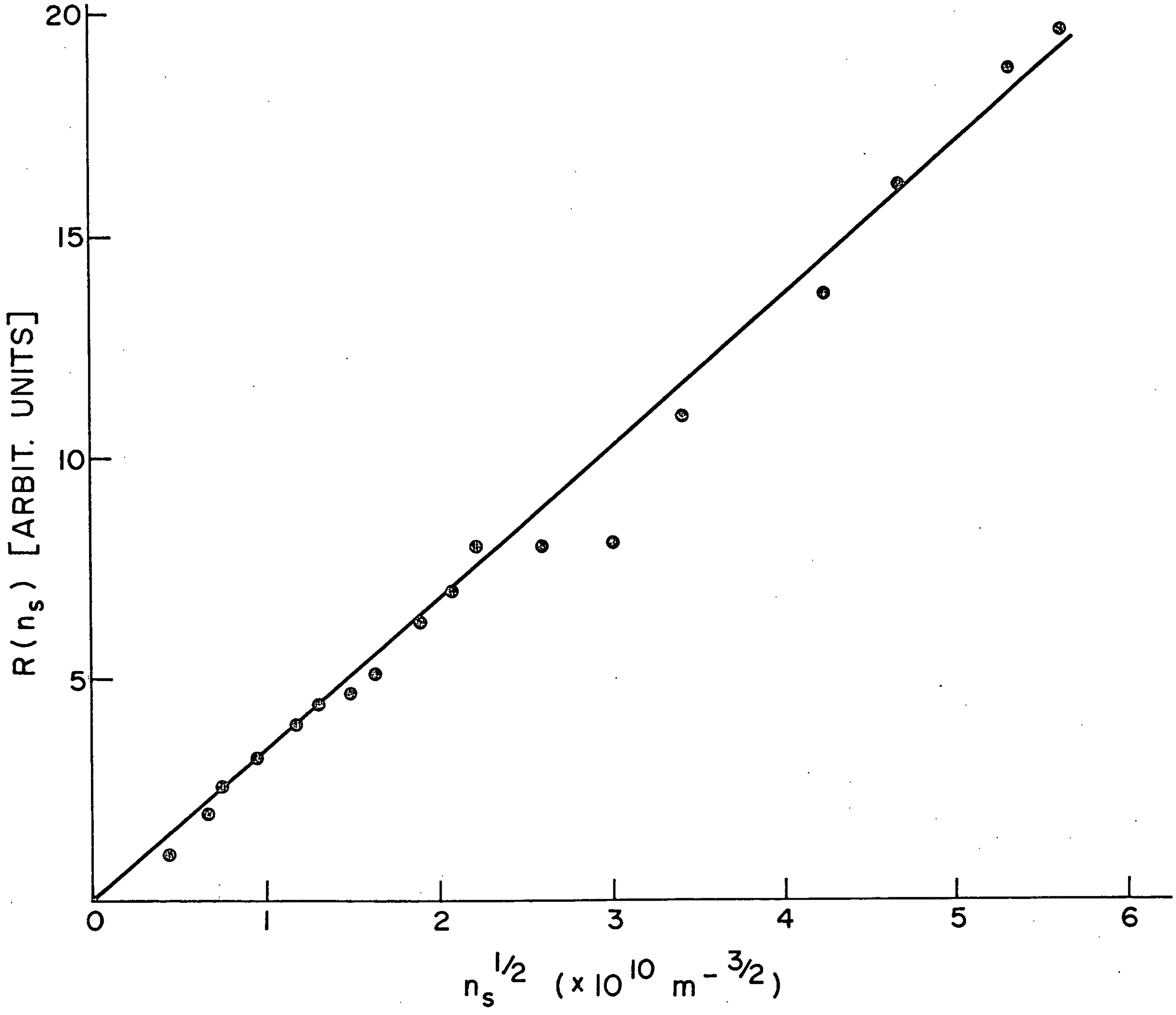
R(n_s) [ARBIT. UNITS]
20
15
10
5
0
1
2
3
4
5
6
n_s^{1/2} (x 10^{10} m^{-3/2})

of effusion of atoms through an oven orifice.

Depending on the ratio of the mean free path λ of the atoms in a tube to the dimensions of the orifice, several different types of molecular flow can be distinguished. For a cylindrical tube of length L_o and radius c, true effusion occurs only if $\lambda >> L_o > c$ [Lew, 1967], and in this case the peak intensity and total flow rate are proportional to the pressure behind the source. When λ is comparable with the length of the tube the peak intensity of the beam is not proportional to the pressure behind the source since collisions between atoms in the beam are then important. The atomic diameter d of potassium is 4.76 Å indicating a mean free path $\lambda \approx 10^{18} n_s^{-1}$ $(= 1/(\sqrt{2}\, \Pi\, d^2 n_s))$. This means that for at least a portion of the density range spanned in these experiments collisions between atoms in the source played a role in defining the emergent atomic beam.

Giordmaine and Wang [1960] have studied molecular flow through tubes both experimentally and theoretically. They find that the peak beam intensity is

$$[19.35] \qquad I(o) = \frac{2^{1/4} c^2 \bar{v}_a}{8\, d\, L_o^{1/2}}\; n_s^{1/2}$$

while the total flow rate from the source is proportional to n_s. In Eq.[19.35] $\bar{v}_a$ is the average velocity inside the oven source not in the beam. Since the ioniser is aligned with the secondary oven's effusion tube, the dependence of the area of the ICR lines on $n_s^{1/2}$ (see Fig. 43) is probably explained by Eq. [19.35]. Furthermore if the ions in the primary beam are relatively well defined spatially near the centre of the cell, they will see a secondary atom flux that is proportional to $n_s^{1/2}$. This might explain why the collision frequencies are dependent on $n_s^{1/2}$ also. It should be noted, however, that the half width of the angular distribution of particles in the collisiondispersed atomic beam is also proportional to $n_s^{1/2}$ (recall that the total flow rate is proportional to n_s) and if the ions are distributed over a considerable fraction of the atomic beam they will see an average atom flux that is proportional to n_s. One further cautionary note is that the theory of Giordmaine and Wang is usually only applied to very long tubes (i.e. $L_o \gg c$) while for the oven used in these experiments L_o is about a factor of 2 larger than c.

We assume that the ion beam is homogeneous having a circular cross section of area A_p. At large densities in the source the angular distribution of the atomic beam may be approximated by [Giordmaine and Wang, 1960].

[19.36] $$I(\Theta) \approx I(0) \cos^{3/2} \Theta$$

and for small A_p the atom flux across A_p is

A

$$I_a = 2\Pi \int_o^{\Theta_1} \sin \Theta \, I(\Theta) \, d\Theta$$

$$\approx 2\Pi \, \Theta_1^2 \, I(\Theta)$$

where
Θhis Oann angle measured from the axis of the effusion tube and Θ_1 is the half angle subtended by A_p. Θ_1 is assumed small. The number density at a distance L from the source oven is now just

[19.37] $$n(L) = \frac{I_a}{A_p \bar{v}_a}$$

$$= \frac{2}{L^2} \left(\frac{2^{1/4} \bar{c}^2}{8d \, L_o^{1/2}} \right) n_s^{1/2}$$

The number density obviously varies with distance from the source so we replace L^{-2} in Eq. [19.37] by $(L' \, L'')^{-1}$ where L' is the distance from the effusion tube to the ICR cell and L'' is the distance to the end of the analyser. Substituting for values of the parameters in Eq. [19.36] we obtain $n_{39} \approx 4.31 \times 10^{-6}\ n_s^{\frac{1}{2}}$. for potassium atoms. Since the slope of ${}^{39}\xi_c$ versus $n_s^{\frac{1}{2}}$ plot in Fig. 41 is $3.1 \times 10^{-8}\ m^{3/2}$/sec. we obtain a rate constant of $7 \times 10^{-15}\ m^3$/sec. ($7 \times 10^{-9}\ cm^3$/sec.) for symmetric resonant charge transfer between ${}^{39}K^+$ ions and ${}^{39}K$ atoms. In Fig. 45 this rate constant is compared with other measurements by Kushnir et al [1959] who measured the attenuation of a potassium ion beam in a neutral potassium background. The solid line in Fig. 44 shows the theoretical prediction [Rapp and Francis 1962] of Eq. [19.27]. This line differs slightly from that published by Rapp and Francis, due to the use of a slightly different ionisation potentials. Also shown by the dashed lines in Fig. 45 is the value of $\sigma_c\ \bar{v}_{22}$ obtained from Eq. [19.30] using two different values of the polarizability [Landolt-Bornstein, 1953]. The error bars on the point represent estimates, of the errors in measurement of $\bar{c}^2/L_o^{\frac{1}{2}}$ in the one case, and the kinetic temperature of the ions in the other.

Double Resonance

Double resonance experiments were also performed on the two alkali ion-atom systems using the crossed beam arrangement, but these did not meet with much success. In order to selectively heat either ionic species (${}^{41}K^+$ or ${}^{39}K^+$ in this case), a secondary oscillator (Wavetek Model 114) was connected to the positive drift electrode in the reaction region. The double resonance experiments consisted of fixing the magnetic field and monitoring the single resonance signal of ${}^{41}K^+$ with the fixed frequency Robinson oscillator attached to the bottom plate of the analyser region. When the secondary oscillator was swept through the cyclotron frequency of

Fig. 45. Dependence of the rate constant for charge exchange between $^{39}K^+$ and ^{39}K on relative velocity.

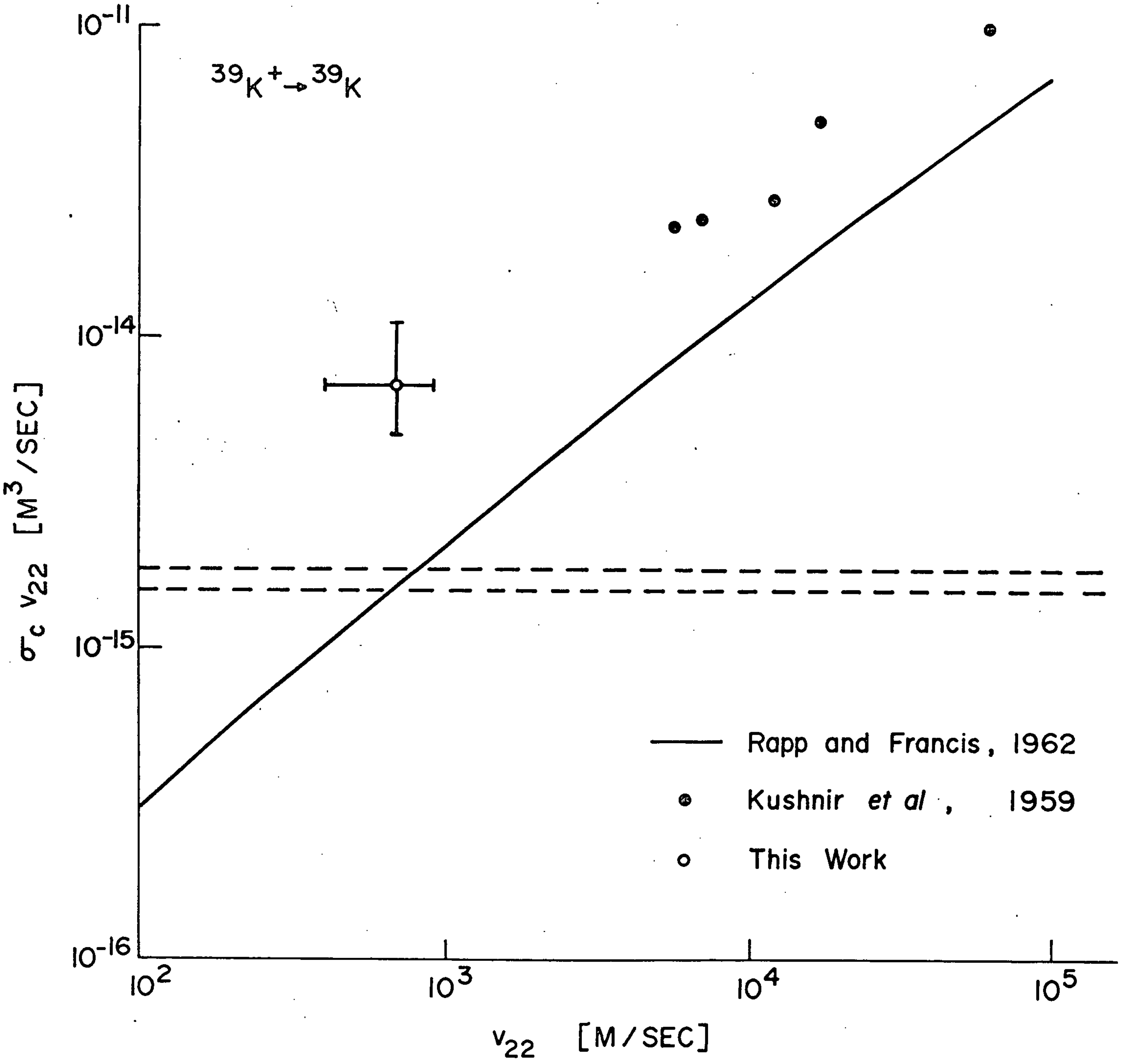
$^{39}K^+ \rightarrow {}^{39}K$
10^{-11}
10^{-14}
10^{-15}
10^{-16}
$\sigma_c v_{22}$ [M^3/SEC]
10^2
10^3
10^4
10^5
v_{22} [M/SEC]
Rapp and Francis, 1962
Kushnir et al, 1959
This Work

$^{39}K^+$ ions a change in the $^{41}K^+$ ICR signal was detected due to the coupling of $^{39}K^+$ to $^{41}K^+$ via reaction [19.9]. However we found that both the sign and magnitude of this double resonance signal werea functions of the magnetic field as indicated in Fig. 46 which shows the change in the ICR single resonance signal of $^{41}K^+$ as a function of the secondary oscillator frequency ω_2 for several different values of the magnetic field.

A qualitative explanation of the above phenomena might be as follows. In cyclotron heating the $^{39}K^+$ ions we change both their average energy and spatial distribution. Changing the average energy of $^{39}K^+$ increases the rate constant k_1 hence increasing the number of $^{41}K^+$ ions which leads to an increase in the $^{41}K^+$ signal. On the other hand changing the spatial distribution of the $^{39}K^+$ ions changes the spatial distribution of the $^{41}K^+$ ions due to charge exchange reactions, resulting in a change in their average quasi-cyclotron frequency. This shift of the resonance condition of $^{41}K^+$ also leads to a change in the $^{41}K^+$ signal if the magnetic field is constant, but does not reflect a change in the net number of $^{41}K^+$ ions detected. To pursue this matter somewhat more quantitively let us assume that the $^{41}K^+$ ICR line shape is the same when $^{39}K^+$ are irradiated as when they are not. Then in the absence of $^{39}K^+$ cyclotron heating the $^{41}K^+$ signal S_1 is

[19.38] $$S_1 = Q_1\, G(B - B_{eff})$$

where B is the magnetic field, B_{eff} the magnetic field at maximum intensity and $G(B - B_{eff})$ is a shape factor so that $G(0) = 1$. When $^{39}K^+$ is irradiated the $^{41}K^+$ signal strength S_2 is

[19.39] $$S_2 = Q_2\, G(B - B'_{eff})$$

where B'_{eff}, the field at maximum intensity, is different from B_{eff} because of the spatial rearrangement of the $^{41}K^+$ ions. The ICR double resonance signal is just the difference between S_2 and S_1,

Fig. 46 The double resonance signal ΔS for reaction [19.9] plotted as a function of B and $\omega_2/2\Pi$. The $^{41}K^+$ resonance S_1 was monitored with the Robinson oscillator and is indicated as a function of $B_1 - B_{eff}$ by the base line of the double resonance signals. ΔS was obtained by sweeping a heating oscillator (frequency denoted by $\omega_2/2\Pi$) through resonance with $^{39}K^+$. The Robinson oscillator frequency was 420.15 kHz. and the number density inside the secondary alkali oven was 6.2×10^{20} m^{-3}. The final energy of the $^{39}K^+$ ions was about $E_f = 0.7$ ev.

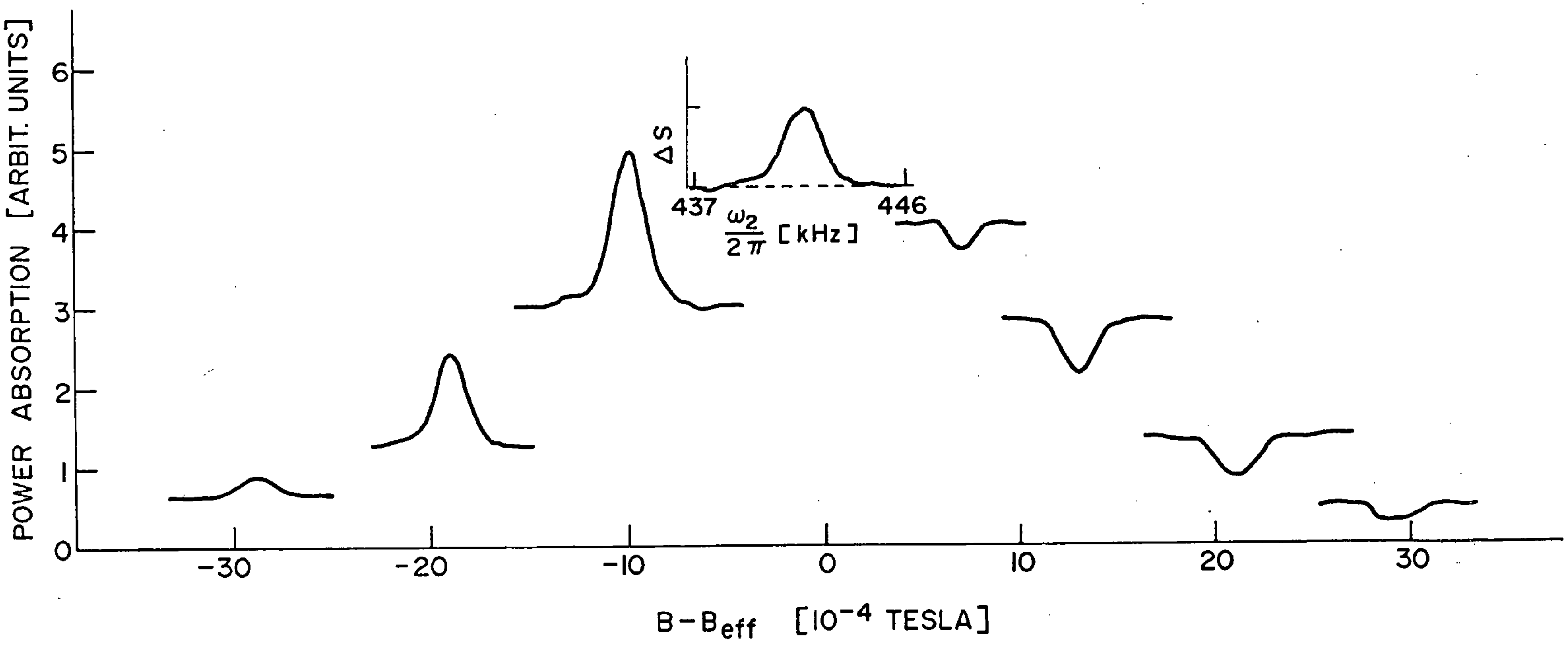
POWER ABSORPTION [ARBIT. UNITS]
0
1
2
3
4
5
6
B−B$_{eff}$ [10^{-4} TESLA]
−30
−20
−10
0
10
20
30
ΔS
437
446
$\frac{\omega_2}{2\pi}$ [kHz]

[19.40]
$$S_2 - S_1 = Q_2\, G(B - B'_{eff}) - Q_1\, G(B - B_{eff})$$

Expanding $G(B - B'_{eff})$ in a Taylor's series about $B - B_{eff}$ we obtain,

[19.41]
$$\begin{aligned} S_2 - S_1 &= Q_2\, [G(B - B_{eff}) + (B_{eff} - B'_{eff})\, G'(B - B_{eff}) \\ &\qquad + \left(\frac{B_{eff} - B'_{eff}}{2!}\right)^2 G''(B - B_{eff}) + \ldots.] \\ &\quad - Q_1\, G(B - B_{eff}) \\ &\simeq (Q_2 - Q_1) G(B - B_{eff}) + Q_2\, (B_{eff} - B'_{eff}) G'(B - B_{eff}) + \text{--} \end{aligned}$$

If we now normalize S_1 to 1 then $Q_1 = 1$ and

[19.42]
$$\frac{S_2 - S_1}{S_1} = \Delta S = Q\, G(B - B_{eff}) + (B_{eff} - B'_{eff})(1 + Q)\, g'(B - B_{eff})$$

where $Q = (Q_2 - Q_1)/Q_1$. This expresses the double resonance intensity in terms of the single resonance signal and its derivative, $G'(B - B_{eff}) = dG/dB$, higher derivatives having been neglected. Q and $(B_{eff} - B'_{eff})(1 + Q)$ are parameters which contain information on the variation of the rate constant k_1 with the average energy of $^{39}K^+$ as well as the spatial rearrangement of the ions by the secondary oscillator. Fig. 47 shows a fit of ΔS versus $B - B_{eff}$ (Eq. [19.42]) to the experimental results. Similar results were obtained at higher irradiating amplitudes where fits of the experiment to theory require higher derivatives of G.

Using the theory developed in this section and plots such as Fig. 47 it should be possible to extract the dependence of k_1 on $^{39}K^+$ average velocity, provided that the r-f level of the secondary oscillator is maintained below the ejection threshold of $^{39}K^+$ and if the higher derivatives in Eq. [19.41] are small. We will not attempt this analysis here, but these results on the energy dependence of reactions [19.9] to [19.12] will be reported at a later date.

Fig. 47. A fit of the experimental double resonance signal ΔS (●) for reaction [19.10] to Eq. [19.42] represented by the solid line. The line shape factors $G(B - B_{eff})$ and $G'(B - B_{eff})$ were obtained directly from the $^{41}K^+$ single resonance line shape indicated in the previous figure. The analysis yields the parameters $Q = 0.187$ and $B_{eff} - B'_{eff} = 1.96 \times 10^{-4}$ Tesla.

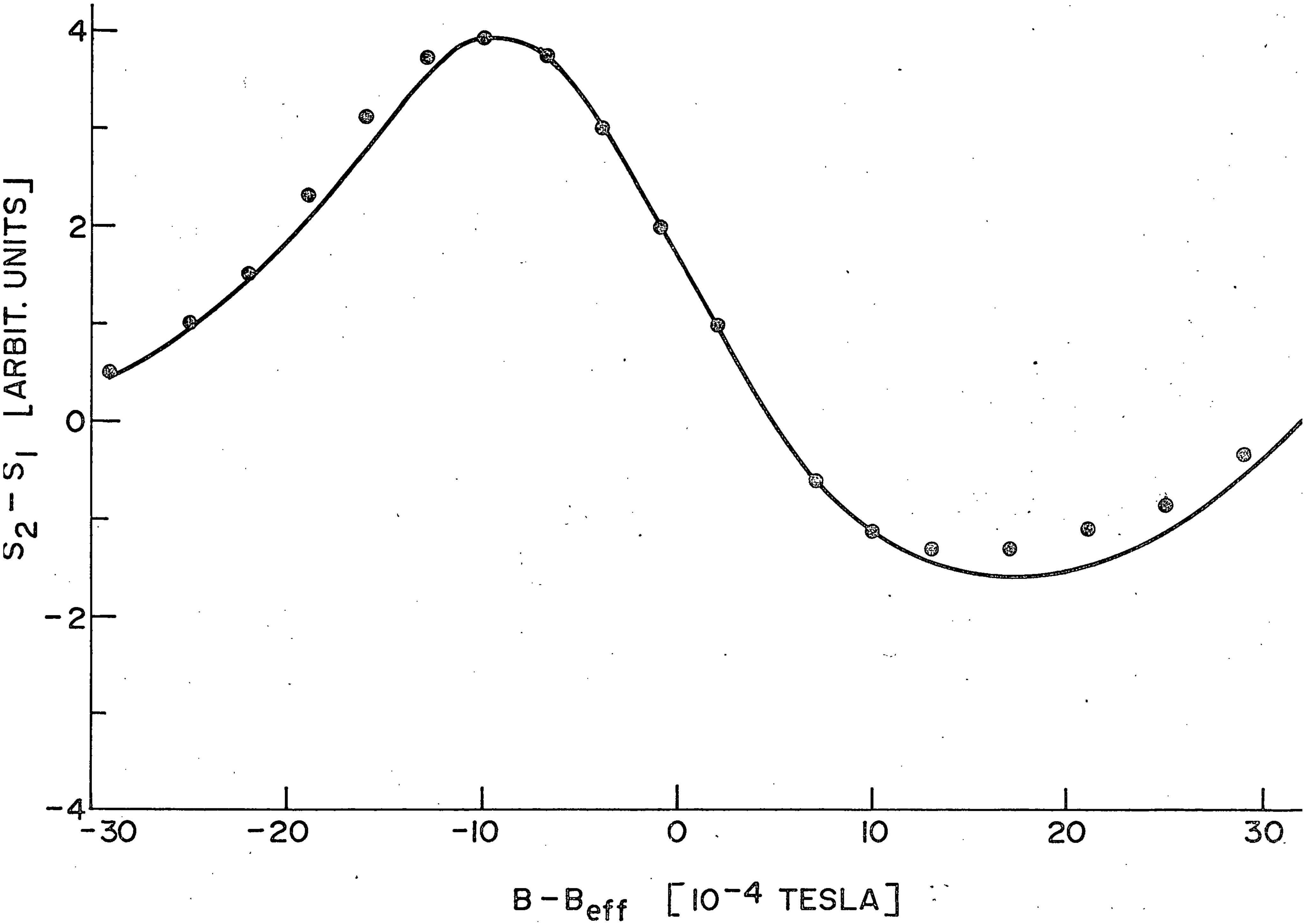
4
2
0
-2
-4
$S_2 - S_1$ [ARBIT. UNITS]
-30
-20
-10
0
10
20
30
$B - B_{eff}$ [10^{-4} TESLA]

A dependence of the sign ΔS on B has not been reported in the literature and appears to be unique to our apparatus. Similar results were obtained in the sodium-potassium system with the same Robinson oscillator, and the large separation between ω_1 and ω_2 ($\approx$ 200 kHz) in this case seems to eliminate the possibility of beating between the oscillators. The same effect was noted when the secondary oscillator was applied to the top electrode of the analyser region, quite far removed from the ioniser. It is thus quite probable that the explanation offered here is the correct one, and the phenomena reflects the non-uniform number density in the beams.

The analysis of this section has neglected spatial variation of the atomic flux from the secondary oven, so the results are admittedly crude ones. Furthermore estimation of the number density inside the ICR cell is based on a theoretical calculation, not on an absolute calibration, although the theory was crudely tested by weighingg the amount of metal plated out on a target. However, it seems reasonable to expect more reliable results after the effusion from the ovens is studied more thoroughly. This may be done using spectroscopic techniques.

20. Summary

In this thesis we have developed a theory of Ion Cyclotron Resonance for typical cells of rectangular cross section. The effect of inhomogeneous electrostatic fields on the dynamical motions of the ions was investigated in some detail using an expansion of the electric field to the third power of the y co-ordinate. An ensemble to specify the spatial distribution of the ions as they drift through the complicated fields was developed.

An explicit energy distribution function was derived for ions at resonance with a uniform r-f electric field. It was found that the initial spread in energy of the ions was amplified by such resonant r-f fields. The ionic energy distribution is also broadened by the large distribution of trapping oscillation amplitudes. Production of the ions with small amplitudes of oscillation at the bottom of the trapping well has obvious advantages, and we have investigated one possible method of doing this. The hot wire ioniser is relatively easy to operate but can only be used for a very small class of molecules. However, there seems no reason why the ions cannot be produced from a well collimated molecular beam which is made to cross an electron beam at the geometric centre of the cell. Better energy selection might also be expected if a second molecular beam crosses the ion beam at a well defined cyclotron radius. This secondary beam might be incident along the x-axis as in the experiments reported here or along the z direction in which case the particles need not be neutral. We believe that the experiments performed here, although in a preliminary stage of development, indicate that such techniques are feasible. It should be emphasized however that the theory of ICR presented here is based on a linearized model of the ionic motions in which the cyclotron motion is rigorously decoupled from the trapping oscillation. At high r-f levels when the ion cyclotron radius becomes an appreciable fraction of the cell dimensions, this is no longer true, and the ionic motions and the manner in which energy is shared between the trapping and cyclotron amplitudes are probably quite complex.

Of course the study of the energy dependence of cross sections for charge transfer and ion molecule reactions is not the only application of the ICR device. Its most attractive feature is its ability to guide an ion beam at very near thermal energies in a well defined direction. Thus its major use is in the determination of thermal energy rate constants for ion molecule reactions. It is probably more reliable to determine the short range part of the interaction which determine these rate constants by temperature dependent studies rather than by their dependence on average ion energy.

At near thermal energies the precision with which rate constants may be determined is dependent on the accuracy with which the pressure and average drift time are measured. It is hoped that the calculation of the average drift velocity and the treatment of the ICR line shape given here will be of use to workers in this field.

Appendix 1 Drift of Ions Between Different Regions of an ICR Cell

Consider two regions 1 and 2 of an ICR cell of the type shown in Figure 1, which are characterized by cell parameters a_1, b_1 and a_2, b_2 and voltages $V^{(1)}(y_1,z_1)$, $V_T^{(1)}$ and $V^{(2)}(y_2,z_2)$, $V_T^{(2)}$, respectively. Suppose that an ion has a vertical position y_1 and a reduced trap oscillation amplitude $\rho_1 = 2z_{m1}/a_1$. After drifting from 1 to 2, the ion has a vertical position y_2 and reduced trap oscillation amplitude $\rho_2 = 2z_{m2}/a_2$. As has been shown in Section 4, the values of y_2 and ρ_2 can be obtained in a straightforward way in terms of y_1, ρ_1 and the cell dimensions and voltage parameters for the limiting cases of fast drift and adiabatic drift. In this Appendix we derive explicit expressions for y_2 and ρ_2 in the adiabatic drift limit for potentials in regions 1 and 2 given by the harmonic approximation, i.e.

[A1.1] $$V^{(i)}(y_i,\rho_i') = V^{(i)}(y_i) + [V_T^{(i)}-V^{(i)}(y_i)]\rho_i'^2$$

where

[A1.2] $$V^{(i)}(y_i) = V^{(i)}(y_i,0)$$

and

[A1.3] $$\rho_i' = \frac{z_i}{\frac{a_i}{2}}$$ (Note that $0 \le \rho_i' \le 1$)

Then, Eqs. [9.3] and [9.5] for the adiabatic drift limit may be written for this case as

[A1.4] $$V^{(1)}(y_1,\rho_1) = V^{(2)}(y_2,\rho_2)$$

and

[A1.5] $$[V_T^{(1)}-V^{(1)}(y_1)]^{\frac{1}{2}}\rho_1^2 = [V_T^{(2)}-V^{(2)}(y_2)]^{\frac{1}{2}}\rho_2^2$$

respectively. Substituting for ρ_1^2 from [A1.5] into [A1.4] and [A1.1] gives the equation

[A1.6] $$u_2^2 - u_1\rho_1^2u_2 + (u_1^2\rho_1^2-u_1^2-\Delta) = 0$$

where

[A1.7] $$u_i^2 = V_T^{(i)} - V^{(i)}(y_i)$$

and

[A1.8] $$\Delta = V_T^{(2)} - V_T^{(1)}$$

The only physically allowed solution to [A1.6] is

[A1.9] $$u_2 = \frac{1}{2}u_1\rho_1^2 + [u_1^2(1-\frac{1}{2}\rho_1^2)^2 + \Delta]^{\frac{1}{2}}$$

By squaring [A1.9] and using [A1.7], this solution may be written in the form

[A1.10] $$V^{(2)}(y_2) = V^{(1)}(y_1) + u_1^2\rho_1^2(1-\frac{1}{2}\rho_1^2)\{1 - [1 + \frac{\Delta}{u_1^2(1-\frac{1}{2}\rho_1^2)^2}]^{\frac{1}{2}}\}.$$

Special Case: $\Delta \ll u_1^2 = V_T^{(1)} - V^{(1)}(y_1)$.

For this case of a small difference between the trap voltages of 1 and 2, expansion of [A1.10] in powers of Δ/u_1^2 gives the result

$$[\mathrm{A1.11}]\qquad V^{(2)}(y_2) \simeq V^{(1)}(y_1) - \frac{\Delta\rho_1^2}{2(1-\frac{1}{2}\rho_1^2)}$$

It may be seen from calculations such as these that the influence of different potentials in different regions of the cell can give a substantial dispersion of the beam in the y-direction. For example, if one identifies Δ in [A1.11] and [A1.8] with the effect of the ionising electron beam on the cell potential and if its effect is to displace the potential near y_1 by a constant amount Δ, so that

$$[\mathrm{A1.12}]\qquad V_T^{(2)}-V_T^{(1)} \simeq V^{(2)}(y_1) - V^{(1)}(y_1) \simeq \Delta \quad ,$$

then the approximately linear variation of $V^{(i)}(y)$ for small changes in y, i.e.

$$[\mathrm{A1.13}]\qquad \begin{aligned} V^{(2)}(y_2) &\simeq V^{(2)}(y_1) + A(y_2-y_1) + - - \\ &\simeq V^{(1)}(y_1) + \Delta + A(y_2-y_1) + - - \end{aligned}$$

taken together with [A1.11] gives

$$[\mathrm{A1.14}]\qquad y_2-y_1 \quad - \frac{\Delta/A}{(1-\frac{1}{2}\rho_1^2)}$$

This result predicts a large dispersion of the beam $[(\Delta y)_{max}/(\Delta y)_{min} \simeq 2]$, since ions are produced with uniform probability in the range $0 \leq \rho_1 \leq +1$. Note that since ρ_2/ρ_1 is proportional to the fourth root of the ratio of potential well depths in regions 1 and 2 (see Eq. [A1.5]), the dispersion in the reduced maximum trapping oscillation amplitude produced by adiabatic drift is not expected to be as large as the dispersion in y.

Appendix 2: Effect of Magnetic Field Modulation On ICR Signals

In the constant electric field approximation the low pressure ICR line shape is given by [Butrill, 1969]

$$[A2.1] \qquad A(B) = \frac{2.783}{\pi B_{\frac{1}{2}}} \; \frac{\sin^2 \delta B \dfrac{2.783}{B_{\frac{1}{2}}}}{(2.783 \; \delta B / B_{\frac{1}{2}})^2}$$

where $B_{\frac{1}{2}}$ is the absorption line width defined by Eq.[13.3] and $\delta B(= B - B_{eff})$ is the distance along the magnetic field axis from the centre of the line. The line shape in Eq.[A2.1] has been normalized to unity,

$$[A2.2] \qquad \int_{-\infty}^{\infty} A(B) \; dB = 1$$

If we modulate the magnetic field with a small periodic field, $b_m \cos \omega_m t$ and sweep through the resonance at B_{eff} then

$$[A2.3] \qquad B(t) = B'(t) + b_m \cos \omega_m t$$

where $B'(t)$ is the slowly varying applied magnetic field.

Under these conditions the output of a phase sensitive detector is proportional to the coefficient of the first harmonic term in the Fourier expansion of the resonance line shape [Smith, 1964]. Therefore rewriting Eq.[A2.1]

$$[A2.4] \qquad A(B) = \frac{2.783}{\pi B_{\frac{1}{2}}} \; \frac{\sin^2 \dfrac{2.783}{B_{\frac{1}{2}}} (\delta B' + b_m \cos \omega_m t)}{\left(\dfrac{2.783}{B_{\frac{1}{2}}} (\delta B' +- b_m \cos \omega_m t) \right)^2}$$

$$= \frac{2.783}{\pi B_{\frac{1}{2}}} \sum_{n=0}^{\infty} a_n \cos n\omega_m t$$

where $\delta B' = B'(t) - B_{eff}$. We thus see that the quantity of interest is

$$[A2.5] \qquad a_1 = \frac{1}{\pi}\int_{-\pi}^{\pi} \frac{\sin^2(\beta + \alpha\cos\theta)}{(\beta + \alpha\cos\theta)^2}\cos\theta d\theta$$

In the above equation

$$\beta = 2.783\,\frac{\delta B'}{B_{\frac{1}{2}}},$$

$$\alpha = 2.783\, b_m/B_{\frac{1}{2}}$$

and

$$\theta = \omega_m t$$

As is well known a_1, the output of the p.s.d., is an approximation to the derivative of the absorption line, but the nearness of a_1 to the real derivative depends on the amplitude of the magnetic field modulation. At very low values of b_m, a_1 is a quite adequate representation of the derivative of the true line shape but when b_m is large the observed signal may be much broader than the real line. In Ion Cyclotron Resonance experiments the signal intensity is often of interest and this too is a function of the modulation amplitude. Thus there are two parameters that must be examined as a function of b_m. The first is the observed peak to peak line width B_{pp}, or the separation between the extrema of a_1, and the other is the value of a_1 at its maximum $(a_1)_p$.

In Fig.[A2.1] we show $B_{pp}/B_{\frac{1}{2}}$ versus $b_m/B_{\frac{1}{2}}$ obtained numerically from Eq.[A2.5] while Fig.[A2.2] shows $(a_1)_p$, normalized to its maximum value, as a function of $b_m/B_{\frac{1}{2}}$. It is interesting to note that maximum signal intensity is obtained for $b_m/B_{\frac{1}{2}} \simeq 0.68$ but undistorted line shapes occur only for $b_m/B_{\frac{1}{2}} \leq 0.2$.

Fig. A2.1: The effect of magnetic field modulation amplitude b_m on the apparent line width B_{pp} of the low pressure ICR absorption derivative.

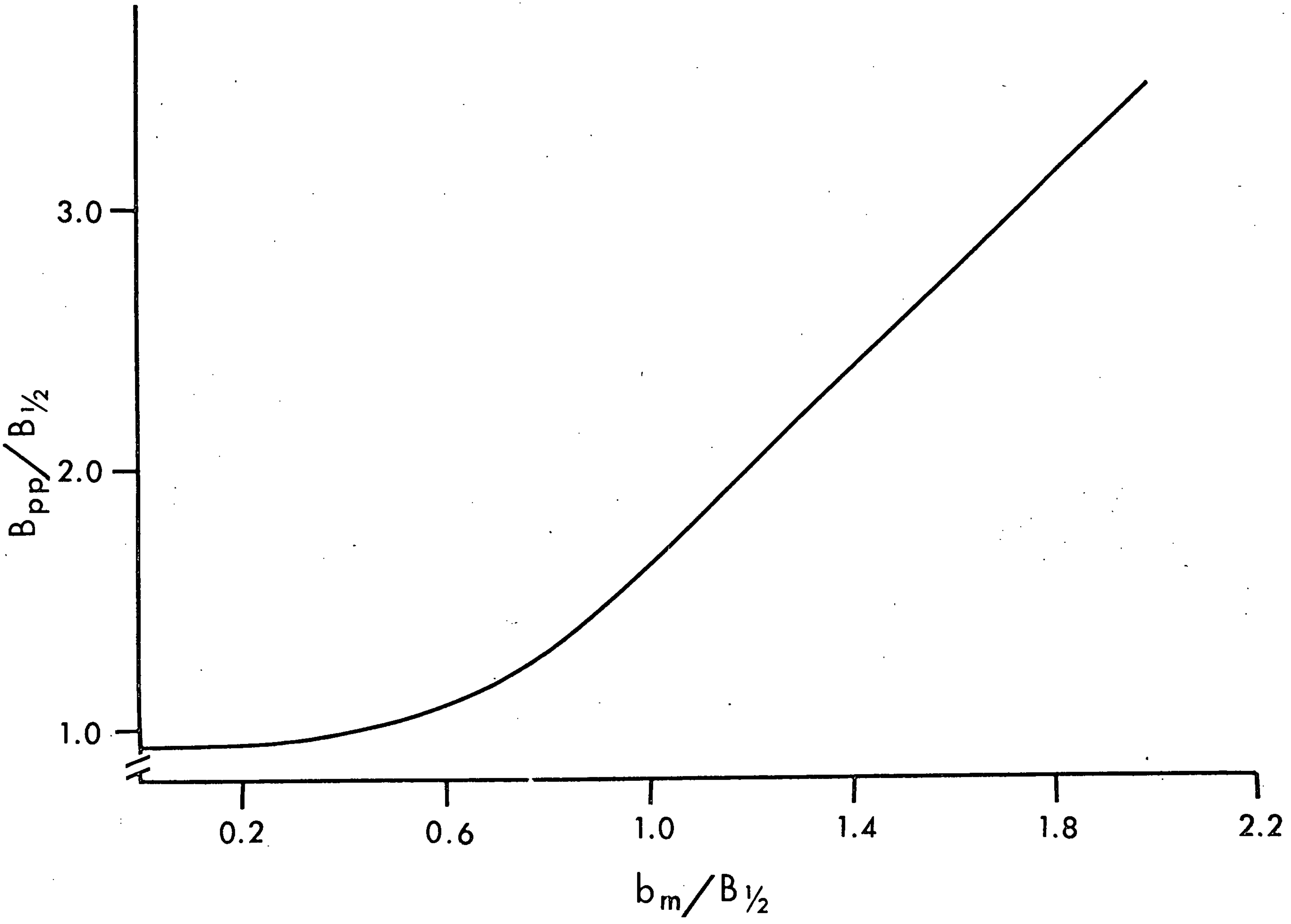
3.0
2.0
1.0
$B_{pp}/B_{1/2}$
0.2
0.6
1.0
1.4
1.8
2.2
$b_m/B_{1/2}$

Fig. A2.2: The effect of magnetic field modulation amplitude on the ICR signal intensity.

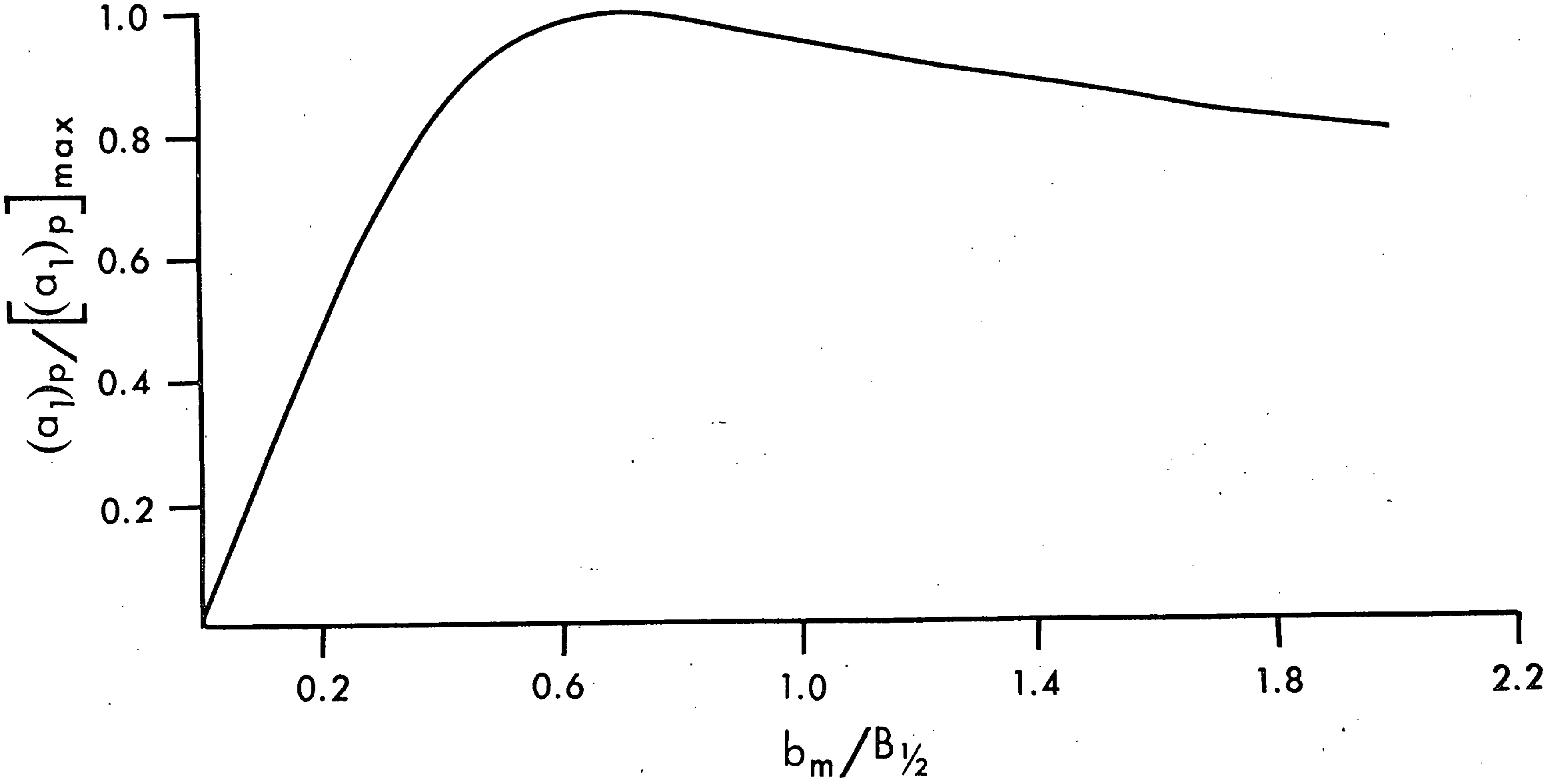
$(a_1)_p/\left[(a_1)_p\right]_{max}$
1.0
0.8
0.6
0.4
0.2
0.2
0.6
1.0
1.4
1.8
2.2
$b_m/B_{1/2}$

Appendix 3: Bi-Particle Collisions

The effects of collisions on the motions of ions through a gas of uniform density are treated in this appendix. We discuss both elastic collisions and resonant charge exchange and in the case of simple elastic collisions establish a formal relationship between ξ, the collision frequency, and K(o), the dc mobility. The influence of the ion-atom interaction potential on the momentum transfer cross-section and the transport properties of gases is also discussed. The outline presented here follows closely that of Beauchamp [1967].

From the Boltzmann equation it has been shown that the time rate of change of some property $x(\underline{v}_i)$ of ions moving under the influence of external forces in a neutral gas is given by [Allis, 1956]

$$[A3.1] \quad \frac{\partial}{\partial t}[(n_+)_i \langle x(v_i)\rangle_f] = \frac{q(n_+)_i}{m_i} \left\langle (\underline{E}(t) + \underline{v}_i \times \underline{B}) \cdot \frac{\partial x(\underline{v}_i)}{\partial \underline{v}_i} \right\rangle_f$$

$$+ \sum_j \int [x(\underline{v}_i') - x(\underline{v}_i)] \; f(\underline{v}_i) F(\underline{V}_j) v_{ij} \; b\,db\,d\varepsilon\,d\underline{v}\,d\underline{V}$$

where $\underline{V}_j$ is the velocity of neutral atom j, $\underline{v}_i$ the velocity of ion i, v_{ij} the magnitude of $\underline{v}_i - \underline{V}_j$ and $F(\underline{V}_j)$ the three dimensional Maxwellian velocity distribution characterizing the neutrals j. $f(\underline{v}_i)$ is the velocity distribution of ion i and is normalized to $(n_+)_i$, the ion number density. In terms of the velocity distribution discussed in Section 17,

$$f(E_i) = (n_+)_i \int_0^{E_i} P\;(E_i - E_\parallel)\; P_\parallel(E_\parallel) dE_\parallel$$

where $E_i = \frac{1}{2} m_i v_i^2$ and $P_\parallel(E_\parallel)$ must include the effects of energy transfer, via collisions between the cyclotron and trapping oscillations. The brackets $< >_f$ in Eq. [A3.1] indicate an average over $f(\underline{v}_i)$.

In a collision the ion interacts with a neutral, their velocities changing from $\underline{v}_i$ and $\underline{V}_j$ to $\underline{v}_i'$ and $\underline{V}_j'$ respectively. The scattering parameters are b, the initial impact parameter, $\bar{\varepsilon}$ the scattering azimuth and θ, the angle through which the relative velocity vector $\underline{v}_i-\underline{V}_j$ rotates on collision. Thus the first term on the right hand side of Eq. [A3.1] accounts for the rate of change of $(n_+)_i\ x(\underline{v}_i)$ due to externally applied electric and magnetic fields while the second term represents the rate of change of $(n_+)_i\ x(\underline{v}_i)$ due to collisions.

The equation of motion of the average ion i is found by setting $x(\underline{v}_i) = \underline{v}_i$ and, if $\partial(n_+)_i/\partial t = 0$

$$\text{[A3.2]} \qquad \frac{\partial\langle\underline{v}\rangle_f}{\partial t} = \frac{q}{m_i}\,\underline{E}(t) + \frac{q}{m_i}\,\langle\underline{v}_i\rangle_f \times \underline{B} + \left(\frac{\partial\underline{v}_i}{\partial t}\right)_{coll}$$

where $\left(\frac{\partial\underline{v}_i}{\partial t}\right)_{coll}$ accounts for the effect of collisions on $\langle\underline{v}_i\rangle_f$. For ions i colliding with neutrals i and j there are five elastic or charge exchange reactions which alter $\langle\underline{v}_i\rangle_f$. These are

(1) elastic collisions and charge exchange between ions i and their atomic parents,

$$i^+ + i \rightarrow i^+ + i$$
$$\rightarrow i + i^+$$

(2) the above two processes for i^+ ions with neutrals j,

$$i^+ + j \rightarrow i^+ + j$$
$$i^+ + j \rightarrow i + j^+$$

(3) charge transfer between ions j and neutrals i

$$j^+ + i \rightarrow j + j^+$$

Fig. A3.1: A collision in velocity space. $\underline{V}_c$ and v_o are not changed by an elastic collision.

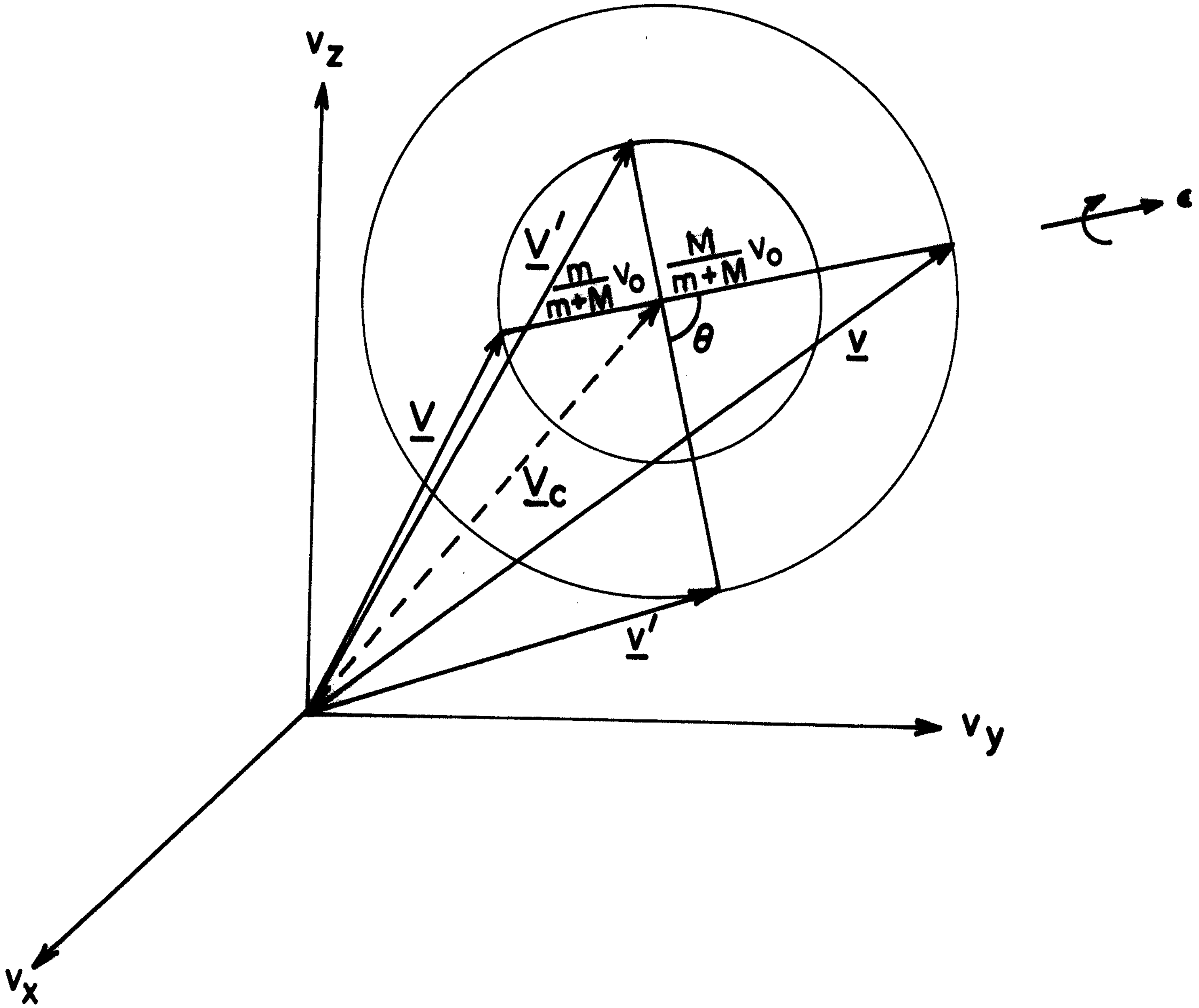
v_z
V′
m/(m+M) v_o
M/(m+M) v_o
θ
v
V
V_c
v′
v_y
v_x

The two processes in (1) above cannot be experimentally distinguished from one another. The second of (2) results in a decrease and (3) an increase in the population of ions i. If P_{ij} is the probability of charge exchange between ion i and neutral j on collision then [Beauchamp, 1967]

$$[A3.3] \qquad \left(\frac{\partial \underline{v}_i}{\partial t}\right)_{coll} = \frac{1}{(n_+)_i}\Bigg[\int (\underline{v}_i' - \underline{v}_i)(1-P_{ii}) f(\underline{v}_i) F(\underline{V}_i) v_{ii}\ bdbd\varepsilon d\underline{v}_i d\underline{V}_i$$

$$+ \int [(\underline{v}_i')_c - \underline{v}_i]\ P_{ii}\ f(\underline{v}_i)\ F(\underline{V}_i)\ v_{ii}\ bdbd\varepsilon d\underline{v}_i d\underline{V}_i$$

$$+ \sum_{j \neq i} \int (\underline{v}_i - \underline{v}_i)(1-P_{ij}) f(\underline{v}_i) F(\underline{V}_j)\ v_{ij}\ bdbd\varepsilon d\underline{v}_i d\underline{V}_j$$

$$- \sum_{j \neq 1} \int \underline{v}_i\ P_{ij}\ f(\underline{v}_i)\ F(\underline{V}_j)\ v_{ij}\ bdbd\varepsilon d\underline{v}_i d\underline{V}_j$$

$$+ \sum_{j \neq i} \int (\underline{v}_i')_c\ P_{ji}\ \lambda_{ji}\ f(\underline{v}_j)\ F(\underline{V}_i)\ v_{ji}\ bdbd\varepsilon d\underline{v}_j d\underline{V}_i\Bigg]$$

where $(\underline{v}_i')_c$ is the value of $\underline{v}_i$ following charge exchange and the reactions listed above correspond to sucessive terms in Eq. [A3.3].

For elastic collisions ($P_{ii}=0$) between ions of mass m with neutrals of mass M Eq. [A3.3] becomes (dropping the subscripts i and j)

$$[A3.4] \qquad \left(\frac{\partial \underline{v}}{\partial t}\right)_{coll} = \frac{1}{n_+} \int (\underline{v}' - v)\ f(\underline{v})\ F(\underline{v})\ v_o\ bdbd\varepsilon d\underline{v} d\underline{V}$$

where $v_o = |\underline{v} - \underline{V}|$. $\underline{v}$, $\underline{V}$, v_o, θ and V_c(= $[m\underline{v} + M\underline{V}]/[m+M]$), the velocity of the centre of mass are indicated by Fig. A3.1 from which it is seen that

$$[A3.5] \qquad \int_o^{2\pi} (\underline{v}' - \underline{v})\ d\varepsilon = -\ 2\pi \frac{M}{m+M} (1 - \cos\theta)(\underline{v} - \underline{V})$$

The momentum transfer cross section is defined as [McDaniel, 1964]

[A3.6] $$\sigma_d = 2\pi \int_o^\infty (1 - \cos\theta)\ b\,db$$

and the collision term becomes

[A3.7] $$\left(\frac{\partial \underline{v}}{\partial t}\right)_{coll} = \frac{-M}{n_+(m+M)} \int \underline{v}\ f(\underline{v})\ F(\underline{v})\ \sigma_d v_o d\underline{v} d\underline{V}$$

since the average of $\underline{V}$ in Eqs. [A3.5] and [A3.4] over $F(\underline{V})$ vanishes. We cannot evaluate $\left(\frac{\partial \underline{v}}{\partial t}\right)_{coll}$ unless the velocity dependence of $\sigma_d v_o$ is known, but fortunately the momentum transfer cross section is inversely proportional to v_o if the interaction potential between ion and atom depends on the inverse fourth power of the distance between their centres. For this polarization potential and others that are not strongly velocity dependent we may write,

[A3.8] $$\left(\frac{\partial \underline{v}}{\partial t}\right)_{coll} \simeq \frac{-M}{(m+M)n_+} \left(\frac{\int \underline{v}\ f(\underline{v})\ d\underline{v}}{n_+}\right) \int \sigma_d v_o f(\underline{v})\ F(\underline{V})\ d\underline{v} d\underline{V}$$

$$= \frac{-M\ n}{(m+M)} <\underline{v}>_f\ <\sigma_d v_o>$$

$$= -\ \xi <\underline{v}>_f$$

where the dependence of f and F on n_+ and n respectively has been extracted from the average over $<\sigma_d v_o>$. The effect of elastic collisions is therefore to introduce a damping term into the equation of motion for the average ion,

[A3.9] $$\frac{\partial <\underline{v}>_f}{\partial t} = \frac{q}{m} [\underline{E}(t) + <\underline{v}>_f \times \underline{B}] - \xi <\underline{v}>_f$$

This equation has been solved for the ICR field configuration to yield precisely the same line shape as derived in Section 17. The analysis of that section requires that ξ(or $\sigma_d v_o$) be independent of v_o. This is true only when the polarization force dominates the ion-atom interaction. Terms other than the r^{-4} term in the interaction potential result in a velocity dependence of $\sigma_d v_o$ and become more important as the average velocity of the ions with respect to the neutrals becomes large. Alternately, we may say that the polarization force dominates the ion-atom interaction at low ion velocities. Therefore, the approximation in Eq.[A3.8] is best satisfied when low rf levels are used to detect the ions or when the neutral gas density is sufficiently high that the average energy gained by an ion between collisions is small. We have already seen that under these conditions

$$[A3.10] \qquad f(\underline{v}) = \left(\frac{m}{2\pi kT}\right)^{3/2} e^{-mv^2/2kT}$$

and substituting into $<\sigma_d v_o>$ we obtain

$$[A3.11] \qquad \xi = \left(\frac{Mn}{m+M}\right) \left(\frac{(mM)^{\frac{1}{2}}}{2\pi kT}\right)^3 \iint e^{-\frac{(mv^2+MV^2)}{2kT}} \sigma_d v_o \, d\underline{v}d\underline{V}$$

which reduces to

$$[A3.12] \qquad \xi = \left(\frac{Mn}{m+M}\right) \left(\frac{32}{\pi}\right)^{\frac{1}{2}} \left(\frac{kT}{\mu}\right)^{\frac{1}{2}} \int_o^{\infty} g^3 \sigma_d \, e^{-g^2} dg$$

with $g = \left(\frac{\mu}{2kT}\right)^{\frac{1}{2}} v_o$.

In drift tube experiments the dc mobility is measured directly from the time of flight of a pulse of ions across a region of constant electric field and pressure [Albritton et al, 1967]. From analysis of the shape of the arrival times of the ions at a suitable counter, the longitudinal and transverse diffusion constants of the ions under study may be determined. Experiments such as these have been extensively investigated theoretically so that to date they provide the most reliable estimates of the ion-atom interaction. Kihara [1953] calculates that at low electric field strengths the average component of ionic velocity in the direction of the applied electric field is

$$[A3.13] \qquad \langle v_z \rangle = \frac{3}{16} \frac{q}{n \mu \Omega} E_{dc} = K(o) E_{dc}$$

where E_{dc} is the electric field and Ω is a collision integral with form;

$$[A3.14] \qquad \Omega = \left(\frac{kT}{2\pi\mu}\right)^{\frac{1}{2}} \int_o^\infty \sigma_d \, g^5 \, q^{-g^2} \, dg$$

The dc mobility in the limit of zero field is thus

$$[A3.15] \qquad K(o) = \frac{3}{16} \frac{q}{n \mu \Omega}$$

It is clear that the dc mobility is simply related to the ICR collision frequency only if $\sigma_d v_o$ is relatively constant and may be taken outside the integrals in Eqs. [A3.12] and [A3.14]. The relation

$$[A3.16] \qquad K'(o) = \frac{q}{m\xi_c}$$

is therefore seen to apply only at very low ionic velocities. When the ionic velocity is not well approximated by a Maxwellian Eq. [A3.16] is not valid since the operational definition of ξ (Eq. [A3.8]) requires modification. The extension of ICR measurements to high rf electric field strengths therefore requires further theoretical development. Now let us consider a single elastic collision in detail.

A two body collision is dynamically equivalent to the one-body collision problem in which a hypothetical particle of mass $\mu = mM/m+M$ approaches a fixed scattering centre with impact parameter b and velocity $\underline{v}_o$ equal to the relative velocity of the two interacting particles. The one body collision is illustrated in Fig. A3.2. The distance from the hypothetical particle μ to the scattering center is r and the force field of the scatterer is represented by a potential V(r). The effect of V(r) on μ is to change its direction by an angle θ.

Far from the scattering center μ has energy $\frac{1}{2}\mu v_o^2$ so conservation of energy requires that

$$[A3.17] \qquad \frac{1}{2}\mu v_o^2 = \frac{1}{2}\mu \dot{r}^2 + \frac{J^2}{2\mu r^2} + V(r)$$

where the right hand side of the equation is the energy of μ in the presence of V(r). The term $J^2/2\mu r^2$ in the above expression represents the rotational kinetic energy of the system. Since $\underline{J} = m\underline{r} \times \dot{\underline{r}}$ we may rewrite Eq. [A3.17]

$$[A3.18] \qquad \frac{1}{2}m v_o^2 = \frac{1}{2}\mu \dot{r}^2 + \mu v_o^2 b^2/2r^2 + V(r)$$

The angle ϕ gives the orientation of $\underline{r}$ with respect to $\underline{v}_o$ and the value of ϕ for which r is a minimum is denoted by Φ. From Fig. A3.2 it is clear that the trajectory of μ is symmetric about Φ and that

[A3.19] $$\theta = \pi - 2\Phi$$

The angle through which the relative velocity v_o is rotated during a collision is completely specified by Φ, a quantity that is easily calculated by noting that $\dot{\phi} = \frac{d\phi}{dt} = bv_o/r^2$, from the constancy of angular momentum, and

[A3.20] $$\frac{dr}{d\phi} = \frac{\dot{r}}{\dot{\phi}} = \pm \frac{r^2}{b} [1 - \frac{2V(r)}{\mu v_o^2} - \frac{b^2}{r^2}]^{\frac{1}{2}}$$

At the angle of closest approach $\frac{dr}{d\phi} = 0$, $r = r_a$ and Φ is given by

[A3.21] $$\Phi = - \int_{\infty}^{r_a} \frac{d\phi}{dr}\, dr = - \int_{\infty}^{r_a} \frac{(b/r^2)\, dr}{[1 - \frac{2V(r)}{\mu v_o^2} - \frac{b^2}{r^2}]^{\frac{1}{2}}}$$

Eqs. [A3.12], [A3.15] and [A3.21] relate K(o), ξ and σ_d. For a given interaction potential the distance of closest approach r_a and Φ may be calculated as functions of v_o and b. The average of 1-cosθ over all possible impact parameters then yields σ_d as a function of v_o. The appropriate average over the relative velocity distribution finally yields the desired transport properties. Although this procedure is purely classical, Vogt and Wannier [1954] have shown that a quantum mechanical description of the polarization potential is similar in most respects.

Fig. A3.2: The one body equivalent of a bi-particle collision.

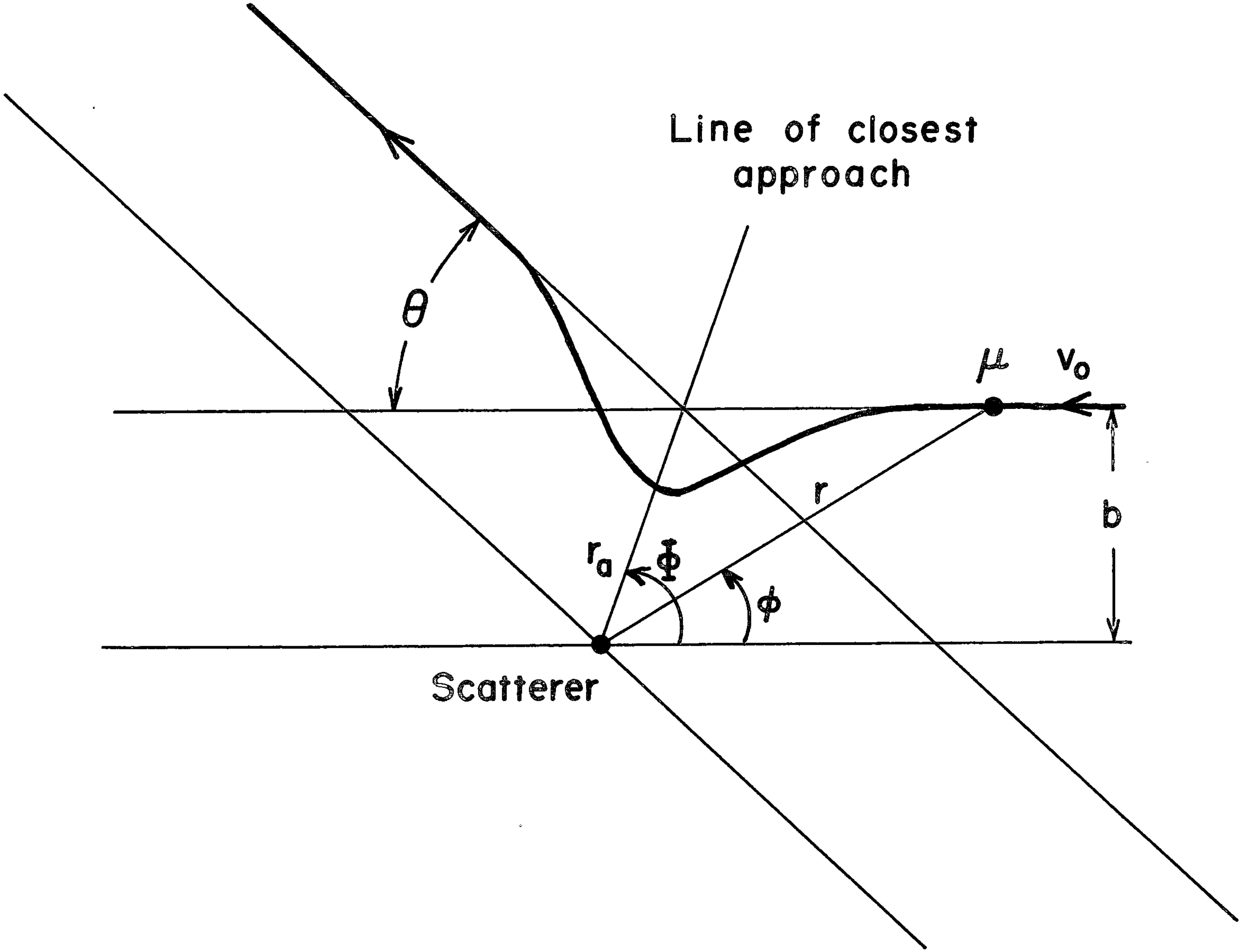
Line of closest approach
θ
μ
v_o
b
r
r_a
Φ
ϕ
Scatterer

Appendix 4 : Moments of the Energy Distribution Function

In section 17 an approximate energy distribution for ions subjected to resonant r-f for a time t was derived in which the possibility of collisions of the ions with a background gas was included. The n^{th} moment of this energy distribution may easily be calculated in the following manner;

$$[A4.1]\quad \overline{E_\perp^n} = \int_o^\infty E_\perp^n P_\perp(E_\perp, \tau_c, t)dE_\perp$$

$$= \frac{e^{-t/\tau_c} e^{-E_m/kT}}{kT} \int_o^\infty e^{-E_\perp/kT_\perp} E_\perp^n I_o\left(\frac{2(E_m E_\perp)^{\frac{1}{2}}}{kT_\perp}\right)dE_\perp +$$

$$\frac{1}{kT_g} \int_o^1 dp\, e^{-P} e^{-\frac{\eta(m+M}{2mkT_g} \tau_c^2 p^2} \left[\int_o^\infty dE_\perp E_\perp^n e^{-E_\perp/kT_g} I_o\left(\frac{2\sqrt{\frac{\eta(m+M)}{2m} \tau_c^2}}{kT_g} E_\perp^{\frac{1}{2}} P\right)\right]$$

The integrals over $E_\perp$ in the above expression may be expressed in terms of Whittaker function $M_{\mu,\nu}$ using the standard form [Gradshteyn and Ryzhik, 1965; Pg. 720]

$$[A4.2]\quad \int_o^\infty s^{\mu-\frac{1}{2}} e^{-\rho s} I_{2\nu}(2\beta\sqrt{s})ds = \frac{\Gamma(\mu+\nu+\frac{1}{2})}{\Gamma(2\nu+1)} \beta^{-1} e^{\beta^2/2\rho}(\rho)^{-\mu} M_{-\mu,\nu}\left(\frac{\beta^2}{\rho}\right)$$

where $\Gamma(k)$ is the Gamma function. The Whittaker functions resulting from substitution of Eq. [A4.2] into Eq. [A4.1] are transformed to degenerate hypergeometric functions Φ;

$$[A4.3]\quad M_{-\mu,o}\left(\frac{\beta^2}{\rho}\right) = \left(\frac{\beta^2}{\rho}\right)^{\frac{1}{2}} e^{-\frac{\beta^2}{2\rho}} \Phi\left(\mu + \frac{1}{2}, 1; \frac{\beta^2}{\rho}\right)$$

so that for n=0,1,2 Eq.[A4.1] takes the following simple forms

[A4.4]
$$n=0 : \quad \overline{E_\perp^o} = \int_o^\infty P_\perp(E_\perp,\ \tau_c,\ t)\,dE_\perp = 1$$

$$n=1 : \quad \overline{E_\perp} = (kT_\perp+E_m)e^{-t/\tau_c} + kT_g(1-e^{-t/\tau_c}) + \frac{(m+M)}{2m}\eta\tau_c^2\,\gamma(3,\ t/\tau_c)$$

$$\begin{aligned} n=2 : \quad \overline{E_\perp^2} = {} & e^{-t/\tau_c}(kT_\perp)^2\left[\left(\frac{E_m}{kT_\perp}\right)^2 + 4\left(\frac{E_m}{kT_\perp}\right) + 2\right] \\ & + (kT_g)^2\left[\left(\frac{(m+M)\,\eta\tau_c^2}{2m\ \ kT_g}\right)^2\gamma(5,\ t/\tau_c)\right. \\ & \left. + 4\left(\frac{(m+M)\,\eta\tau_c^2}{2m\ kT_g}\right)\gamma(3,\ t/\tau_c) + 2(1 - e^{-t/\tau_c})\right] \end{aligned}$$

where $\gamma(k,\ t/\tau_c)$ is an incomplete Gamma function.

When the same oscillator is used to both heat and detect the ions, the experiment is actually performed over a time τ where τ is the total time the ions remain in the resonant r-f. Thus the time average of $\overline{E_\perp}$ is

[A4.5]
$$\begin{aligned} \langle\overline{E_\perp}\rangle_t &= \frac{1}{\tau}\int_o^\tau \overline{E_\perp}\,dt \\ &= kT_g + kT_g(e^{-\tau/\tau_c} - 1)\,\frac{\tau_c}{\tau} \\ &\quad + kT\ (1 - e^{-\tau/\tau_c})\,\frac{\tau_c}{\tau} + \frac{\eta\tau_c^3}{\tau}\ \gamma(3,\ \tau/\tau_c) \\ &\quad + \frac{\eta(m+M)\ \tau_c^2}{2m\ \tau}\int_o^\tau \gamma(3,\ t/\tau_c)\,dt \end{aligned}$$

and $\langle\overline{E_\perp^2}\rangle_t$ is similarly obtained from $\overline{E_\perp^2}$.

Appendix 5 : The Relative Velocity Distribution

In this appendix we wish to calculate the relative velocity distribution for ion-atom pairs over which the rate constants measured in ICR experiments are averaged. As in Appendix 3 the ion velocity is denoted by $\underline{v}_i$, that of the atom by $\underline{V}_j$ and the relative velocity by $\underline{v}_{ij} = \underline{v}_i - \underline{V}_j$. Angles $(\theta_i, \varepsilon_i)$ and $(\theta_j, \varepsilon_j)$ define the orientation of $\underline{v}_i$ and $\underline{V}_j$ with respect of an arbitrary co-ordinate system and angles θ' and ε' give the orientation of $\underline{v}_i$ with respect to $\underline{V}_j - \underline{v}_{ij}$ as shown in Fig. A5.1. The relative velocity distribution $H(\underline{v}_{ij})$ is given in general form by [M. Bloom, private communication].

[A5.1]
$$H(\underline{v}_{ij}) = \frac{1}{4\Pi} \int_0^\infty \sin\theta' d\theta' \int_0^{2\Pi} d\varepsilon' \int_0^\infty F(V_j) V_j^2 dV_j \int_{\Omega_i}^{d} \frac{d\Omega_i}{4\Pi} \int v_i^2 f(v_i) \delta(\underline{v}_i - \underline{V}_i - \underline{v}_{ij})\, d\underline{v}_i$$

The ionic distribution of speeds is assumed to be Maxwellian.

[A5.2]
$$f(v_i) = A_i\, e^{-\alpha_i v_i^2} \quad \text{with } A_i = 4(\Pi\alpha_i^3) \text{ and } \alpha_i = \frac{m_i}{2kT_i}$$

subject to the restrictions which are discussed in previous sections. It is further assumed that $f(v_i)$ is independent of $(\theta_j, \varepsilon_j)$ for any $(\theta_i, \varepsilon_i)$. From Fig. [A5.1] the relation

[A5.3]
$$(\underline{V}_j + \underline{v}_{ij})^2 = V_j^2 + v_{ij}^2 - v_{ij} V_j \cos\theta'$$

is easily obtained and substituting into Eq. [A5.1] yields

[A5.4]
$$H(v_{ij}) = \frac{A_i}{2} \int_0^\Pi \sin\theta d\theta \int_0^\infty V_j^2 F(V_j)\, e^{-\alpha_i (V_j^2 + v_{ij}^2 - 2V_j v_{ij} \cos\theta')} dV_j$$

$$= \frac{A_i}{2v_{ij}\alpha_i} \int_0^\infty F(V_j)\, V_j\, e^{-\alpha_i (v_{ij}^2 + V_j^2)} \sinh(2V_i v_{ij} \alpha_i) dV_j$$

Fig. A5.1 The relative velocity vector

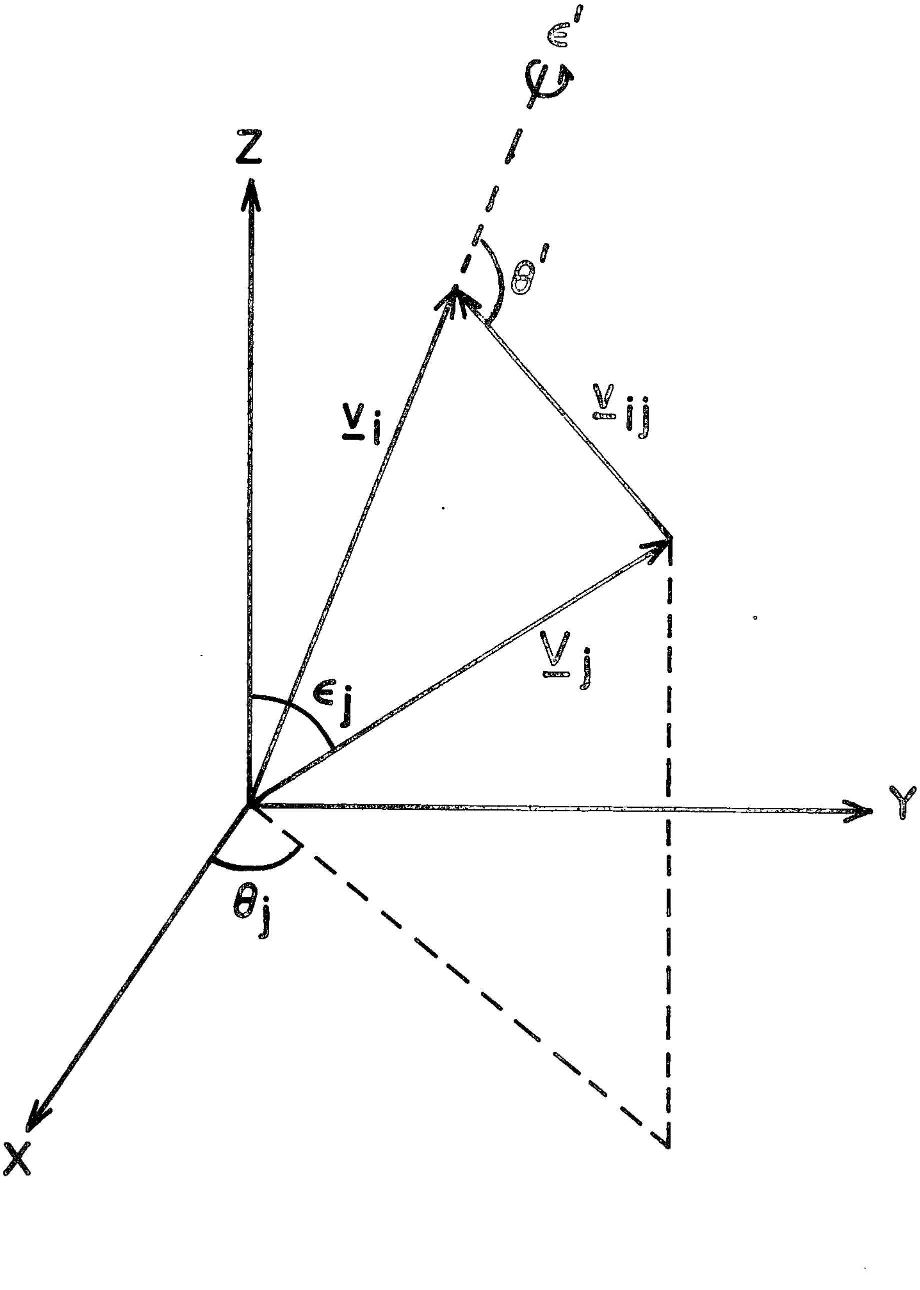
ε'
φ
Z
θ'
$\underline{v}_i$
$\underline{v}_{ij}$
$\underline{V}_j$
ϵ_j
Y
θ_j
X

There are two types of distributions $F(V_j)$ that are of interest here.

Case 1. If the atomic distribution function is Maxwellian, analogous to Eq. A5.2, then

[A5.5] $$H(v_{ij}) = 4 \left(\frac{\Pi\, \alpha_i\, \alpha_j}{\alpha_i + \alpha_j}\right)^{3/2} e^{-v_{ij}^{2} \left(\frac{\alpha_i\, \alpha_j}{\alpha_i + \alpha_j}\right)}$$

This distribution function describes the relative speeds when the target of the ion beam fills a well defined spatial region. It has been used in Appendix 3 to obtain Eq. [A3.11] from [A3.10]..

Case 2. The velocity distribution in a molecular beam is not Maxwellian. The probability of an atom emerging from an oriface in an oven is proportional to its velocity, and as a result the velocity distribution inside a beam is [Ramsey, 1969].

[A5.6] $$F(V_j) = A_j^{!}\, V_j\, e^{-\alpha_j V_j}$$

where

$$A_j^{!} = 2\, \alpha_j^{2} \text{ and } \alpha_j = M_j/2kT_j .$$

Now, the relative velocity distribution becomes

[A5.7] $$H(v_{ij}) = \frac{A_i A_j^{!}}{2\alpha_i} \frac{e^{-\alpha_i v_{ij}^{2}}}{v_{ij}} \int_0^{\infty} V_j^{2}\, e^{-(\alpha_i+\alpha_j)V_j^{2}} \sinh(2\alpha_i V_j v_{ij})\, dV_j$$

In the crossed beam experiment reported in Sect. 19, the number density inside the ICR cell was controlled by varying the temperature of the secondary ion oven, thus changing the velocity distribution in the atomic beam. It is therefore important to understand the dependence of measured collision frequencies on α_j, and since these collision frequencies are averages of a rate constant $v_{ij}\, \sigma$ over $H(v_{ij})$ the moments of $H(v_{ij})$ are of interest.

If a cross section σ is proportional to v_{ij}^{n} then the corresponding collision frequency is proportional to $\int_0^{\infty} H(v_{ij})\, v_{ij}^{n+3} dv_{ij}$. Calculation of the

$(n + 1)^{th}$ moment of $H(v_{ij})$ is tedious and will not be given here. However it is a simple matter to show from Eq. [A5.7] that the $(n + 1)^{th}$ moment is proportional to $T_j^{(n + 1)/2}$ if $\alpha_i = \alpha_j$.

REFERENCES

Abragam, A. 1961. The principles of Nuclear Magnetism, Oxford University Press, London.

Albritton, D.L., Martin, D.W., McDaniel, E.H., Miller, T.M., and Moseley, J.T., Technical Report, School of Physics, Georgia Institute of Technology, Atlanta, Georgia.

Allis, W.P. 1956. Handbuch der Physik (S. Flügge, ed) Springer-Verlag 21, 383.

Anders, L.R. 1967. Ph.D. Thesis (unpublished), Harvard University.

Baldeschwieler, J.D. 1968. Science 159, 263.

Beauchamp, J.L. 1967. Jour. Chem. Phys. 46, 1231.

——— 1967. Ph.D. Thesis (unpublished), Harvard University.

Beauchamp, J.L., and Armstrong, J.T. 1969. Rev. Sci. Instrum. 40, 123.

Beauchamp, J.L. 1971. Ann. Rev. Phys. Chem. 22, 527.

Bloom, M. 1971 Proceedings of Second Annual Conference on Atomic Physics, Plenum Press, London.

Born, M. 1969. Atomic Physics, 8th Edition, Blackie and Son Ltd. London.

Butrill, S.E. 1969. J. Chem. Phys. 50, 4125.

Churchill, R.V. 1941. Fourier Series and Boundary Value Problems, (McGraw-Hill, New York).

Clow, R.P. and Futrell, J.H. 1970. Int. J. Mass Spect. Ion Phys. 4, 165.

Comisarow, M.B. 1971. Jour. Chem. Phys. 55, 205.

Dalgarno, A. McDowell, M.R.C. and Williams, A. 1958. Proc. Roy. Soc. 250, 51.

Datz, S. and Taylor, E.H. 1956. Jour. Chem. Phys. 25, 389.

Dunbar, R.C. 1971. Jour. Chem. Phys. 54, 711.

——— 1971. J. Amer. Chem. Soc. 93, 4354.

Dunbar, R.C., and Kramer, J.M. 1973. J. Chem. Phys. 58, 1266.

Dunn, G.H., and Kieffer, L.J. 1963. Phys. Rev. 132, 2109.

Dunn, G.H., 1963. Phys. Rev. Lett. 8, 62.

Dymerski, P.P., Dunbar, R.C. and Dugan, J.V. (to be published, private communication from Paul Dynerski).

Farnsworth, H.E. 1925. Phys. Rev. 25, 41.

Firsov, O.B. 1951. Zh. Eksperim i Teo. Fiz. 21, 1001.

Giordmaine, J.A. and Wang, T.C. 1960. J. Appl. Phys. 31, 458.

Gioumousis, G. and Stevenson, D.P. 1958. J. Chem. Phys. 29, 294.

Goode, G.C., Ferrer-Correia, A.J. and Jennings, K.R., 1970. Int. J. Mass. Spectrom. Ion Phys. 5, 229.

Gradshteyn, I.S. and Ryzhik, I.M. 1965. Tables of Integrals, Series and Products. Academic Press. New York.

Haeff, A.V. 1939. Proc. I.R.E. 27, 586.

Hassé, H.R. and Cook, W.R. 1931. Phil. Mag. 12, 554.

Huntress, W.T. 1971. Jour. Chem. Phys. 55, 2146.

Hughes, D.G., and Smith, M.R. 1971. Jour. Phys. E (U.K) 4, 13.

James, I.R. Graham, E., Thomson, G.M., Gatland, I.R. and McDaniel, E.W. 1973. Jour. Chem. Phys. 58, 3653.

Kihara, T. 195. Revs. Mod. Phys. 25, 844.

Kushnir, R.M., Palyukh, B.M., Sena, L.A. 1959. Bull. Acad. Sci. U.S.S.R., Phys. Ser. 23, 1161.

Landolt, H. and Bornstein, R. 1950. Atom. und Molekularphysik, pt. I, Springer, Berlin.

Langevin, P. 1905 Annls. Chem. Phys. 5, 245.

Lew, H. 1967. Methods of Experimental Physics. (Hughes, V.W. and Schultz, H.L.; eds.).

McDaniel, E.W. 1964. Collision Phenomena in Ionized Gases, (John Wiley & Sons. Inc. New York).

McIver, R.T. 1970. Rev. Sci. Instrum. 41, 555.

McMahon, T.B. and Beauchamp, J.L. 1971. Rev. Sci. Instr. 42, 1632 (1971).

Mason, E.A. and Schamp, H.W. 1958. Ann. Phys. (New York), 4, 233.

Massey, H.S.W. 1969. Electronic and Ionic Impact and Collision Phenomena, Vol. 3, Oxford University Press, London.

Morse, P.M., and Feshbach, H. 1953. Methods of Theoretical Physics,(McGraw-Hill, New York).

Nermeyanov, A.N. 1963. Vapour Pressure of the Chemical Elements, Elsvier Publishing Co., Amsterdam.

Patterson,P.L. 1972. Jour. Chem. Phys. 56, 3943.

Ramsey, N.E. 1969. Molecular Beams, (Oxford University Press, London).

Rapp, D. and Francis, W.E. 1962. J. Chem. Phys. 11, 2631.

Ridge, D.P. and Beauchamp, J.L. 1969. Jour. Chem. Phys. 51, 470.

Robinson, F.N.H. 1959. J. Sci. Instrum. 36, 481.

Seitz, F. 1940. Modern Theory of Solids,(McGraw-Hill, New York).

Sharp, T.E., Eyler, J.R. and Li, E. 1972. Inter. J. Mass Spectrom. Ion Phys., 9, 421 (1972).

Smith, D.L., and Futrell, J.H. 1973. Int. J. Mass Spectrom. Ion Phys. 10, 405.

Smith, G.W. 1964. J. Appl. Phys. 35, 1217.

Smyth, K.C. and Brauman, J.L. 1972. J. Chem. Phys. 56, 1132.

Southard, T.H. 1969. In Handbook of Mathematical Functions, edited by M. Abramowitz and I.A. Stegun (N.B.S. U.S. Gov't Printing Office, Washington).

Stacey, D.N. 1966. Rep. Prog. Phys. 29, 171.

Tyndall, A.M. 1938. Mobilities of Positive Ions in Gases, (Cambridge University Press, London).

Vogt, E. and Wannier, G.H. 1954. Phys. Rev. 95, 1190.

Watson, G.N. 1962. Theory of Bessel Functions, 2nd Edition, (Cambridge University Press, London).

Whealton, J.H. and Woo, S.B. 1971. Phys. Rev. A6, 2319.

Whittaker, E.T. and Watson, G.N. 1927. A Course of Modern Analysis, 4th ed. (Cambridge University Press, London).

Wobschall, D., Graham, J.R., Malone, D.F. 1963. Phys. Rev. 131, 1565.

Woods, I.B., Riggin, M., Knott, T.F.m and Bloom, M. 1973. Int. J. Mass Spectrom. Ion Phys. 12, 341.

Zandberg, E.,Ya., and Ionov, N.I. 1959. Soviet Phys. - Uspekhi (English Transl.) 2, 255.

GLOSSARY OF SYMBOLS

Symbol	Definition	Page
a	Distance between trapping electrodes.	3
(a_o,a_1,a_2,a_3,a_4)	Coefficients of quantic in Weierstrauss calculation.	22
$(a_1)_p$	Maximum of field modulated ICR absorption derivative.	221
$A(\delta\omega)$, $A(\delta B)$	ICR absorption signal assuming uniform electric field.	149
$A(t, \delta\omega)$	Instantaneous power absorption.	181
$A_k\ (y)$	y dependent term in the expansion of $V(y, z)$	47
A_i	A convenience parameter; the normalization constant of the velocity distribution function of the i^{th} component in the system.	240
A_p	Area over which ions are distributed.	203
A_{pp}	Distance between extrema of the ICR absorption derivative.	130
$Ar(\xi,\xi')$	Argon Atom. [illegible]tion, used [illegible] convenience	
b	Distance between drift electrodes in the ICR cell.	3
b_i	Distance between drift electrodes in the i^{th} cell region.	216
b	Impact parameter in a two particle collision.	227
b_o	Impact parameter for orbiting collisions.	197
b_1	Impact parameter such that $P_{ij} = 0$ for all $b>b_1$ in Firsov theory of resonant charge exchange.	197
b_m	Field modulation amplitude.	220
B	Static Magnetic Field.	3
B_{eff}	Magnetic field at maximum power absorption.	72

Symbol	Definition	Page
B'_{eff}	B_{eff} in the presence of an irradiating r-f electric field.	207
$B_{\frac{1}{2}}$	Half width at half height (in magnetic field units). of the low pressure ICR absorption.	103
B_{pp}	Line width of the absorption derivative.	130
c	Radius of effusion aperature.	202
cn (u)	See Abramowitz and Stegun [1969, pg. 587].	
$C(n_s, n_p)$	Area under the ICR absorption line.	192
(c, c')	Strengths of the derivative of the ICR absorption.	130
d	Atomic diameter.	202
D	Collision diameter; sum of atomic and ionic radii.	171
$\hat{e}_{m,n}$	Expansion coefficient of the electric field.	8
e_m	Sum of Z^{2n} $e_{m,n}$ over n.	20
E	Initial kinetic energy of an ion.	123
E_i	Total kinetic energy of ion species i.	226
$\underline{E}$	Static electric field vector.	8
E_{dc}	Static electric field in d.c. mobility experiments.	233
E_f	Energy gained by an ion from resonant r-f in a time τ.	164
E_m	Energy gained by an ion from resonant r-f. in a time t.	82
E'_m	Energy gained by an ion from resonant r-f in a time $t-t_o$.	159
E_T	Total time dependent kinetic energy.	81
E_y (y, z)	y component of two dimensional $\underline{E}$.	8
E_z (y, z)	Z component of two dimensional $\underline{E}$.	8
E_z	Initial kinetic energy in the Z direction	

Symbol	Definition	Page
$\langle E_y \rangle$	Amplitude (Z_m) averaged E_y (y, z).	75
$\langle E'_y \rangle$	Amplitude (Z_m) averaged electric field gradient.	72
$E_\perp$	Kinetic energy associated with the cyclotron motion.	81
$E_\parallel$	Kinetic energy associated with the trapping oscillation.	81
E'	An energy such that $E_\parallel$, $E_\perp \leq E'$.	89
$\overline{E}_\perp$	Average of $E_\perp$ at time t.	239
$\langle E_\perp \rangle_t$	Time average of $\overline{E}_\perp$.	239
E_o	Average electron energy.	104
E_1, (E_{rf})	r-f electric field amplitude.	57
f	Fraction of monoenergic ions collected by the trap.	125
f_o	Fraction of ions that have moved for time t without collision.	181
f(s)	A quartic polynominal in s.	22
$\langle f \rangle$	f averaged over all initial ionic energies.	126
$f_1(y)$, $f_2(y)$	Parts of A_k (y); convenience functions.	72
f (v_i)	Distribution of velocities v_i of ion species i.	226
F (V_j)	Distribution of velocities V_j of neutral species j.	226
F (V)	Fraction of ions with potential V collected by the traps.	124
F_1 (ξ,ξ')	Part of the ICR absorption, used for convenience only.	189
g	Reduced relative velocity (dimensionless).	232
g (E)	Maxwell-Boltzmann distribution of ionic energies.	125
g (V)	Distribution of ionic potentials in the trapping well.	87
g_2, g_3	Invarients of the quartic f(s).	23
$g_1(y)$, $g_2(y)$	Convenience function; $g_i(y) = (2\omega_c)^{-1} f''_i(y)$.	72

Symbol	Definition	Page
G $(\delta\omega)$, G (δB)	Unnormalized line shape function.	57
H (v_{ij})	Distribution of relative velocities.	240
i	A subscript only.	72
I	Ionisation potential	134
I_a	Atomic flux through area A_p.	203
I_e	Ionising electron current.	104
I_o, I_1	Bessel functions with imaginary argument.	83
$I(\delta\hat{\omega}')$	ICR ensemble averaged power absorption.	60
I (Θ)	Atomic flux as a function of angle.	202
j	A subscript only.	226
J	Angular momentum in relative coordinate system.	234
J_n (P)	n^{th} order Bessel function with real argument.	49
k	A subscript only.	47
$\binom{k,\ k',\ k''}{k_1\ k_2\ k_3\ k_4}$	Rate constants.	179
K	Symbol for potassium atom.	150
K (0)	D.C. drift mobility at zero field.	149
K'	Reduced zero field d.c. drift mobility.	170
ℓ (	Length of analyser region.	46
L	Distance from the source of atomic beam.	203
L', L"	Distances to the ends of the analyser from the atom source.	203
L_o	Length of the effusion tube.	202
m	A subscript.	8
(m, m_i)	Ionic masses.	1
m_e	Electronic mass.	

Symbol	Definition	Page
(M, M_j, m_j)	Neutral masses.	147
$M_{\mu,\nu}(p)$	Whittaker function.	238
n	A subscript.	8
$(n, n_j, n_A, n_B, n_{39})$	Neutral number density.	147
n_o	Number of ions in the analyser.	148
$(n_+)_i$	Number density of ion species i.	226
n_p	Number density inside the primary oven.	192
n_s	Number density inside the secondary oven.	184
n_+	Positive ions emitted by surface ioniser.	134
n_a	Atoms emitted by surface ioniser.	134
(N, N_A, N_B)	Ion current.	60
Na	Sodium atom.	152
$\underline{p}$	Ion momentum.	10
p	Neutral gas pressure.	164
$p\ (y, Z_m)$	General spatial distribution of ions.	56
$p_o\ (y, Z_m)$	A special case of $p\ (y, Z_m)$	60
P_{ij}	Probability of charge transfer between ion i and neutral j.	230
$P\ (E_T)$	Distribution function of E_T.	81
$P_{\parallel}\ (E_{\parallel})$	Distribution function of $E_{\parallel}$	81
$P_{\parallel}(E_{\parallel}, 0)$	Special case of $P_{\parallel}\ (E_{\parallel})$	89
$P_{\perp}\ (E_{\perp})$	Distribution function of $E_{\perp}$ in the limit of zero pressures.	81
$P_{\perp}(E_{\perp}, \tau_c, t)$	$P_{\perp}(E_{\perp})$ generalized to include the effect of non-reactive collisions.	159

Symbol	Definition	Page
q	Ionic charge, equal in magnitude to the electronic charge in this thesis.	1
Q_1, Q_2, Q	Intensity of ICR signals with and without irradating oscillator.	207
r	Ion-atom separation.	170
r_a	Distance of closest approach of reduced mass to scattering centre in a bi-particle collision.	237
r_m	Value of r at the minimum of the ion-atom interaction potential.	171
R_o	Cyclotron radius.	26
$R(n_s)$	Contribution to the area of the ICR resonance of the secondary oven.	199
s	The argument of f(s) the quartic polynominal.	22
s	Separation between two cell regions.	65
S_1, S_2	ICR absorption with and without irradition by the secondary oscillator.	207
t	Time.	24
t_o	Time of a momentum randomizing collision.	148
t_n	Sum of $\langle y^m \rangle c_{m+1,n}$ (m+1) over m; used for convenience.	
T_i, T_j	Temperature of ion component i and neutral component j.	240
T_g	Neutral gas temperature.	160
T_s	Temperature of an ionising surface.	134
$T_\perp$	Temperature associated with the two dimensional cyclotron motion.	81
$T_\parallel$	Temperature associated with the one dimensional trapping motion.	81
	$(= \omega t+\phi)$ Argument of cn term in $y(\tau)$.	

Symbol	Definition	Page
v_D	Ion drift speed in the x direction.	34
$\underline{v}_{ij}$	Relative velocity of ion i and neutral j.	229
$\bar{v}_a$	Average velocity of an atom in a gas.	202
$\underline{v}_i$	Velocity of ion i before collision.	229
$(\underline{v}_i')_c$	Velocity of ion i after a collision resulting in charge exchange.	230
$\underline{v}_i'$	Velocity of ion i after an elastic collision.	229
v_o	Relative velocity in a system of one neutral and one ionic component.	147
$\langle v_z \rangle$	Average velocity in the direction of the electric field in the d.c. mobility experiment.	233
V (y, z), V	Two dimension potential at (y, z) inside the ICR cell.	8
$\underline{V}_j$	Velocity of neutral j before collision.	229
$\underline{V}_j'$	Velocity of neutral j after collision.	229
V_o	Trapping well depth.	124
V_1	Positive drift potential.	1
V_2	Negative drift potential.	1
V_T	Trapping potential.	1
V_{fil}	Bias potential on the surface ioniser.	140
V_d	$(V_1 - V_2)/2$	8
V_t	$V_T - (V_1 + V_2)/2$	8
V_c	Potential at the centre of the cell.	9
$\langle V \rangle$	Amplitude (z_m) averaged potential.	69
V_a	$(V_1 + V_2)/2$ average potential of the drift plates.	69
$V(r)$	Ion-atom interaction potential.	170

Symbol	Definition	Page
w	An arbitrary parameter.	22
W	Width of the electron beam.	104
(x, y, z)	Spatial coordinates inside the ICR cell.	2
$x(t), y(t), z(t)$	Spatial coordinates of an ion as a function of time.	31
(X_o, y_o, z_o)	Initial coordinates.	19
$(\dot{X}, \dot{y}, \dot{z})$	Components of velocity of an ion in the ICR cell.	10
$(\dot{X}_o, \dot{y}_o, \dot{z}_o)$	Initial velocities	19
$(\ddot{X}, \ddot{y}, \ddot{z})$	Components of acceleration of an ion.	10
y_a	Amplitude of y(t).	47
Y_o	Initial amplitude of y(t).	25
$\bar{y}$	Average of y position of the ion ensemble.	102
Z_m	Amplitude of oscillation in the trap.	49
α	Zero of the quartic f(y).	31
α	Atomic Polarizability	170
α_{ii}	Inverse temperature parameter in distribution of velocities.	240
α_k	Integral over Bessel function, may be expressed in terms of Strauve functions.	69
γ	Ratio of r^{-4} to r^{-6} term in V(r).	171
γ	Angle between r-f electric field and initial velocity.	82
$\gamma\ (n, t)$	Incomplete Gamma function.	239
$\Gamma(n)$	Gamma function.	238
$\delta\omega$	Distance along the frequency axis from the maximum of an an absorption line.	57
$\delta(y-y')$	Dirac delta function.	60
Δ	Discriminant of the quartic f(s).	25

Symbol	Definition	Page
Δ	Space charge depression	104
ΔB	Shift of an ion's cyclotron frequency (expressed at a magnetic field) due to the electric field gradients.	27
$\Delta\omega$	Spread in quasi cyclotron frequency resulting from the modulation of ω by the trapping oscillation.	42
ε	Deviation of y_o from α the zero of (y).	31
$(\varepsilon, \varepsilon', \varepsilon_i)$	Azimuthal angles.	241
$\varepsilon(w_1; y, Z_m)$	Power absorbed by an ion at y with trapping amplitude Z_m.	56
$\varepsilon_{res}(y, z_m)$	Energy absorbed at resonance by an ion at y with trapping amplitude Z_m.	56
$\varepsilon_{\pm 1}$	Energy associated with $T_{\pm 1}$.	81
$\varepsilon_{\parallel}$	Energy associated with $T_{\parallel}$	81
$\varepsilon_{\perp}^{\pm}$	Limits on $E_{\perp}$ due to γ.	82
ξ	Collision frequency associated with the momentum transfer cross section.	147
ξ'', ξ'	Collision frequencies for charge transfer.	180
κ	Charge to mass ratio, q/m.	19
ϕ	Phase angle of y(t).	24
ϕ	Orientation of $\underline{r}$ with respect to $\underline{v}_o$.	237
Φ	The value of ϕ at the position of closest approach of μ to the scattering centre in a bi-particle collision.	237
$\Phi(\mu, \nu, z)$	Degenerate Hypergeometric Function.	238

Symbol	Definition	Page
μ_{ij}	Reduced mass of particles i and j.	198
μ	Reduced mass in an elastic collision.	170
μ	(= cos γ) used for convenience only.	82
(μ,μ',μ'')	Moduli of Jacobi Elliptic function used in Weierstrauss calculation.	25
$\hat{\eta}$	$q^2\ E_1^2/8\ m$.	159
$\wp$	Weierstrauss Elliptic function.	23
$(\rho_i,\ \rho')$	Reduced trapping amplitude and z coordinate respectively.	216
$\sigma_{\underline{d}}$	Momentum transfer cross section.	147
σ_c	Charge exchange cross section.	196
σ	An arbitrary cross section.	147
Ω_{2m}	A parameter used for convenience of notation in the expansion of $\omega(y,z)$.	49
Ω	Solid angle.	240
θ	Angle between the initial velocity of an ion and the z axis.	123
θ_c	Cut off angle for θ such that all particles with $\theta \geq \theta_c$ are trapped in the cell.	124
θ	Angle through which the relative velocity vector is rotated in velocity space by an elastic collision.	229
$(\theta_i,\ \theta')$	Angles specifying orientation of $\underline{v}_i$ and $\underline{v}_{ij}$ respectively.	242
Θ	Angle of a particle in a beam with respect to the axis of the effusion orifice.	203
Θ_1	Half angle subtended by A_p a distance c from the effusion source.	203

Symbol	Definition	Page
τ	Mean drift time of the ions through the analyser.	149
τ'	Mean drift time of the ions from the ioniser to the analyser.	192
τ_c	Mean time between collisions.	148
$\omega(y, z)$	Instantaneous quasi cyclotron frequency of an ion.	26
$\omega_o (y, Z_m)$	Quasi-cyclotron frequency of an ion at y with trapping oscillation amplitude Z_m.	50
ω_c	Cyclotron frequency of an ion in a uniform electric and magnetic field.	1
ω_1	Detector oscillator frequency.	57
ω_2	Secondary oscillator frequency.	208
ω_T	Trapping oscillation frequency.	20
ω_n	Frequency of modulation.	220
ω_2	Half period of the Weierstrauss Elliptic function.	24
$\omega_{\frac{1}{2}}$	ICR line width (in frequency units) at half maximum in the collisionless regime of pressure.	46
ω_i	Frequency o[illegible] ICR absorption	